Proceedings of the Workshop on Sputtering Caused by Plasma (Neutral Beam) Surface Interaction

Argonne National Laboratory
July 9-10, 1979

Planned By
The Plasma/Materials Interaction
Task Group
Office of Fusion Energy, ER

U.S. Department of Energy
Office of Fusion Energy, ER
Division of Development & Technology
Materials & Radiation Effects Branch

DISCLAIMER

NOTICE

Printed in the United States of America
Available from
National Technical Information Service
U. S. Department of Commerce
5285 Port Royal Road
Springfield, VA 22161

NTIS price codes
Printed copy: A10
Microfiche copy: A01

CONF-790775

UC-20c, -20f

Proceedings of the Workshop on Sputtering Caused by Plasma (Neutral Beam) Surface Interaction

Argonne National Laboratory
July 9-10, 1979

Published April 1980

Planned By
The Plasma/Materials Interaction
Task Group
Office of Fusion Energy, ER

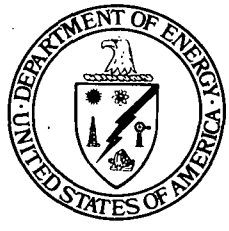

Sponsored By

U.S. Department of Energy
Office of Fusion Energy, ER 950 7528
Division of Development & Technology
Materials & Radiation Effects Branch
Washington, D.C. 20585

044 8000
FUSION POWER PROGRAM
Argonne National Laboratory
9700 South Cass Avenue
Argonne, Illinois 60439

THIS PAGE

WAS INTENTIONALLY

LEFT BLANK

Proceedings of the Workshop on Sputtering Caused by Plasma (Neutral Beam)-Surface Interaction

Argonne National Laboratory

July 9-10, 1979

List of Contents

WORKSHOP ON SPUTTERING CAUSED BY PLASMA (NEUTRAL BEAM) SURFACE INTERACTIONS

Argonne National Laboratory
July 9-10, 1979

INTRODUCTORY REMARKS

Charles R. Finfgeld
U.S. Department of Energy

During the past few years, there has been a very significant expansion of the existing data on sputtering as it relates to first wall problems in thermonuclear fusion devices. This has resulted both from identification of the problem by program management with corresponding funding emphasis, and through intensified effort on the part of investigators in the field. Simultaneously, through the application of diagnostics in confinement experiments as well as calculations in design studies, we have obtained a much better appreciation of the fluxes to be expected from plasmas. The rapid growth in this body of information makes it essential to draw together all of the existing data in one place.

The data should be compared with the data needs derived from our knowledge of fluxes to first walls, followed by identification of areas which should receive further study in order to round out the necessary data base for fusion applications. Simultaneously, this data compilation should be very useful to those conducting confinement experiments and design studies. It is my hope that those of you participating in this Workshop will succeed in doing these tasks.

FOREWORD

The Workshop on Sputtering Caused by Plasma (Neutral Beam)-Surface Interactions is one of a series of workshops which was planned by the Plasma Interaction Task Group and conducted under the auspices of the Materials and Radiation Effects Branch, Office of Fusion Energy, U.S. Department of Energy. The sputtering phenomenon had been identified in the Fusion Reactor Materials Program Plan, Section III, Plasma Material Interaction (DOE/ET-0032/3-July 1978) as a process which contributes to plasma contaminant release and to surface erosion of irradiated components. It was decided not to include in this workshop an extensive review of the blistering phenomenon, a process which can contribute significantly to surface erosion under certain irradiation conditions. In view of the large amount of data available on blistering relevant to fusion, a separate workshop on this topic may be organized in the future. This workshop was held to review the existing data base (experimental and theoretical) for sputtering relevant to plasma-wall interactions, to identify existing gaps in the data needed for the fusion program, and to discuss priorities of the work which needs to be done.

These workshop notes consist of an introduction by Dr. Charles Finfgeld, U.S. DOE, a statement of the objectives of the workshop, a brief summary of the work which needs to be done for the fusion program, together with an indication of the priorities. The major part of these notes consists of summaries of the existing data base prepared by individual authors who are expert in the field.

We would like to thank the following authors for preparing summary notes:

J. Biersack, Hahn-Meitner Institute, Berlin, Germany and
A. Riccato and W. Kaczerowski, Techn. Univ., Berlin, Germany

J. L. Cecchi, Princeton Plasma Physics Laboratory

S. Devoto, Lawrence Livermore Laboratory

F. Dylla, Princeton Plasma Physics Laboratory

G. Emmert, University of Wisconsin-Madison

L. G. Haggmark, Sandia Laboratories-Livermore

J. T. Hogan, Oak Ridge National Laboratory

A. Krauss and R. B. Wright, Argonne National Laboratory

J. B. Roberto, Oak Ridge National Laboratory

R. R. Rye, Sandia Laboratory-Albuquerque

C. Singer and D. Post, Princeton Plasma Physics Laboratory

D. Smith, Argonne National Laboratory

K. Wilson and W. Bauer, Sandia Laboratories-Livermore

In addition, we would also like to acknowledge gratefully the valuable verbal contributions made by the following workshop attendees not listed above:

J. Bohdansky, Max Planck Institute, Garching, Germany

C. Finfgeld, U.S. Department of Energy

T. Kammash, University of Michigan-Ann Arbor

J. Khan, Lawrence Livermore Laboratory

R. Langley, Oak Ridge National Laboratory

D. Mattox, Sandia Laboratories-Albuquerque

G. M. McCracken, Princeton Plasma Physics Laboratory
(visiting from Culham Laboratory UKAEA Research Group)

M. T. Robinson, Oak Ridge National Laboratory

The workshop was preceded by an information meeting held at General Atomic, San Diego, California, April 30-May 1, 1979. This meeting was attended by many of the authors listed above, and it was held to plan the agenda for the workshop, to identify the people to be invited to the workshop, and to discuss the scope of the subtasks to be handled by the individual authors.

The workshop summary notes of individual authors were collated by C. Finfgeld and M. Kaminsky. The summary of the workshop disucssion was prepared by M. Kaminsky, who also prepared the final version of the proceedings for publication.

It is with pleasure that we thank Mrs. Lee Northcutt, Mrs. Laura Hins and Mrs. Connie Bury, all at Argonne National Laboratory, for their secretarial assistance.

Joe N. Smith, Jr.
General Atomic
Co-Chairman

Manfred Kaminsky
Argonne National Laboratory
Co-Chairman

WORKSHOP OBJECTIVES

(1) Assessment of the needs for sputtering data by those who develop plasma impurity codes and provide estimates of surface erosion rates in existing plasma devices, near-term devices, and future fusion reactors.

(2) Assessment of the available data base on sputtering relevant to plasma-wall interactions. Assessment of the status of different theoretical approaches for sputtering calculations.

(3) Assessment of the gaps in the data base which need to be filled for the fusion program. Assessment of the required improvements in the theoretical approaches for sputtering calculations. Discussion of priorities for the work to be done in the future.

(4) Prepare a workshop report which will include the assessments mentioned above under (1)-(3) and the supporting documentation used for the presentation of subtasks during the time of the workshop and given earlier at the time of the information meeting on Sputtering, San Diego, April 30, May 1, 1979.

SUMMARY OF WORKSHOP DISCUSSIONS

A review of the workshop discussions on the needs for sputtering data and for improvements of the theoretical approaches for sputtering calculations relevant to the fusion program will be given first. This will be followed by a discussion of the priorities for the experimental and theoretical work which needs to be done in the future. Finally, these proceedings contain the contributions of authors who had been invited to assess (1) the available data base on sputtering relevant to plasma-wall interactions and (2) the status of different theoretical approaches for sputtering calculations.

Needs for Sputtering Data Relevant to the Fusion Program

The importance of a comprehensive data base for physical sputtering relevant to the fusion program was stressed during the discussions. During the last few years significant advances have been made in gathering relevant sputtering data and in improving theoretical approaches for sputtering calculations. More detailed descriptions of the present status of the available data base are given in the reports of individual coordinators, and are included in these proceedings. In turn, a list of high priority experiments which need to be performed is given on pages 7 to 8. Several attendees, some of whom are working on the development of codes for plasma impurity transport, prepared a comprehensive list of the important types of information on physical sputtering which one would like to have for the fusion program. The list is given in Table 1.

Several attendees pointed out that at the present the state of plasma theoretical models is such that it would not be necessary to know the sputtering yield values better than within a factor of two in the near future. One exception to this is the sputtering yield for 20-100 keV/amu H and D on metals (C, Fe, Ti, Mo, W). The flux of these neutrals which come from the portion of the neutral beam which was not stopped by the plasma, can be estimated quite accurately, and thus accurate sputtering rates can be used. Furthermore, it was stressed that it would be desirable to determine yield values for a selected number of materials (some of those listed in Table 1) which have received different surface treatments, for example, such as (1) plasma cleaning, (2) degreasing (without plasma cleaning), (3) coating under in-situ conditions. Finally, for the determination of sputter yields of first wall materials under plasma radiations the use of in-situ detection techniques (e.g. laser fluorescence spectroscopy) was recommended.

Table 1. Experimental Data on Physical Sputtering Needed for Fusion Applications

Energy Range for Incident Projectiles	Incident Projectile Species	Target Materials	Quantities to be Determined
0.1 to 1.0 keV/amu (including plasma radiations with broader energy spectra)	Plasma Fuel Projectiles: (e.g. H, D) Fusion Reaction Products: (e.g. He) Plasma Impurity Projectiles: (e.g. Li, B, C, O, Ti, V, Fe, Ni, Cu, Mo, W)	Elemental Materials: (e.g. Li, B, C, Al, Ti, V, Cr, Fe, Ni, Cu, W) Alloys: [e.g. steels, V(Ti), V(Ti,Cr)] Compounds: (e.g. TiB_2, TiC, B_4C)	(1) Total Yield Values for Elemental Materials. (2) Differential Yield Values for the Constituents of Alloys and Compounds. (3) Angular Distribution of Sputtered Species [(i) for normal incidence, (ii) for near-grazing angle of incidence]. (4) Energy Distribution of Sputtered Species [(i) peak region of distribution, (ii) width of distribution at half maximum]. The items listed under (1) to (4) should be determined as a function of dose (particularly for "gas loaded surface regions") angle of incidence, and surface microstructure.
1.0 to 100 keV/amu	H, D, He	Same as above.	Same as above.
0.1 to 1 MeV/amu	H, He	Same as above.	Same as above

Gaps in the Data Base on Chemical Surface Effects Relevant to the Fusion Program

Major gaps in the existing data base, which were identified by attendees, are listed below:

(1) Establish if chemical reactions between active forms of hydrogen isotopes (e.g. H^0, H^+) and surface atoms (molecules) are assisted by different types of radiation (e.g. α-particles, electrons, γ-rays). For example, determine if the reduction of oxided surfaces by active forms of hydrogen isotopes is enhanced (or diminished) by coincident radiations.

(2) Establish if the simultaneous interaction of different types of plasma radiations will affect the kind of chemical reactions mentioned above under (1).

(3) Establish if the erosion of first wall surfaces under plasma irradiation (and injected neutral beams) is affected by chemical surface reactions (e.g. determine erosion yields).

(4) Establish if the release of plasma contaminants from first wall surfaces is affected by chemical surface reactions (e.g. determine yields, species of released particles, energy and angular distributions of released particles).

(5) Establish if changes in the chemical composition of first wall surfaces (particularly for low-Z coatings, such as C, B_4C, B) occur under irradiations with hydrogenic plasmas or simulated plasmas or neutral deuterium beams.

Gaps in the Theoretical Approaches for Sputtering Calculations and for the Modeling of Plasma-Wall Interactions

The following major improvements needed in existing theoretical approaches were identified:

(1) Incorporate more adequately the angular-energy distributions of sputtered particles. The influence of the angle of incidence and of the incident particle energy on these distributions should be included.

(2) Provide improvements to make the approaches more applicable to technological surfaces which can be found in existing devices and will exist in future fusion reactors.

(3) Incorporate chemical surface effects.

(4) Assess through sensitivity studies the relative importance of chemical surface composition and of physical surface heterogeneities (e.g. roughness, grain size) for sputtering calculations and the modeling of plasma-wall interactions.

Priorities for the Experimental and Theoretical Sputtering Work to be Done

Discussions of priorities for the experimental and theoretical sputtering work to be done in the near future concluded the workshop discussions. It should be pointed out that the discussions of the priorities for studies of chemical surface effects were cut short for lack of time.

The following major priority items were identified:

(1) Determine total yield values for a limited number of elemental materials and, in addition, differential yield values for the constituents of selected alloys and compounds (e.g. coatings and claddings materials) under energetic light ion bombardment (1.0 to 100 keV/amu for H and D, and 1.0 to 1 MeV/amu for ^{4}He). The experimentally determined yield values should help to establish scaling laws and be useful for plasma-wall interaction modeling.

(2) Determine both total and differential yield values for low energy ions (0.1 to 1 keV/amu for H, D, He, B, C, O) for selected special materials such as coatings and claddings.

(3) For a limited number of elemental materials and of alloys and compounds (e.g. coatings, claddings) determine for the irradiation conditions listed above under (1) and (2) the following parameters and/or quantities:

(a) The angular and energy distribution of sputtered species as a function of the angle of incidence and of the primary ion energy (at least for normal incidence and for an angle between 70° and 80° with respect to normal). It was felt that in the determination of the energy distribution the accuracy for the measurement of the peak intensity and for the intensities of the high energy tail would not have to be better than a factor of two.

(b) The different types of sputtered species released (both charged and uncharged, atomic and molecular).

(c) The effect of surface roughness on total yields, differential yields, and the angular distribution of sputtered species (for example, use polished surfaces and "technological" surfaces which are characteristic of those used in plasma devices).

(d) The effect of gas loading of materials (e.g. gas trapping of incident H, D, He ions) on yield values and energy distributions.

(4) Determine for a very limited number of materials selfsputtering yields for the energy region of 0.1 to 1.0 keV/amu.

(5) Determine for a selected number of materials the yields and velocity distributions of particles sputtered by plasma radiations in existing devices. For these measurements the use of in-situ techniques is recommended.

(6) Determine the overall surface erosion yields (caused by the simultaneous occurence of sputtering, blistering, flaking) for the selected systems and conditions described above under (1), (2) and (3).

(7) Establish if the erosion yields of first wall component surfaces under either ion beam and/or plasma irradiations are affected by chemical surface reactions. Some of these studies should be conducted in the presence of hydrogen gas and with in-situ monitoring devices.

(8) Incorporate more adequately the angular-energy distributions of sputtered particles into existing theoretical approaches. Improve the modeling of plasma-wall interactions by incorporating more adequately the angular and energy distributions of species sputtered from "technological" surfaces.

SPUTTERING DATA REQUIREMENTS FOR TOKAMAK TRANSPORT CODES

C. E. Singer and D. E. Post

Princeton University Plasma Physics Laboratory

Princeton, N.J. 08544

I. INTRODUCTION

The requirements of tokamak transport codes for sputtering data can be summarized as follows. Sputtering data must be provided which are relevant to working tokamak environments. In order of decreasing importance, the required data are total sputtering yields for a variety of materials bombarded by hydrogenic ions and typical tokamak impurities with energies from 0.1 to 1 keV, and possibly for hydrogenic ions from 20 to 100 keV/amu, energy distribution of sputtered atoms, angular distribution of sputtered atoms, and species composition in any rare case where neutral atoms are not the dominant species sputtered.

This data is used to analyze and predict impurity behavior in current and future large tokamaks, and to try to find ways to minimize the impurity levels in the discharge. Sputtering of the wall and limiter by charge-exchanged neutrals, untrapped beam ions and neutrals, and ions at the plasma edge is a real and potentially lethal source of impurities. Accurate sputtering data will assist in the quantitative understanding of impurity source mechanisms.

II. RELEVANCE TO TOKAMAK ENVIRONMENT

Sputtering measurements must, of course, pertain to surface and plasma conditions which are actually obtained in a tokamak environment in order to be useful for transport simulation codes. Ideally this means *in situ* measurements with simultaneous diagnostics of the plasma edge region conditions. At the very least it means surface and bombardment conditions which approximate or lend understanding to those which occur in a tokamak environment. For example, the BALDUR one dimensional transport code has concentrated on modelling of sputtering by charge exchange neutrals incident on the plasma wall, with the result that comparison of the code with PLT results indicates that this mechanism is not an important problem for the generation of high impurity levels in PLT. On the other hand, variation of the metal target or wall potential in small tokamaks has indicated that sputtering by charged ions accelerated through a plasma sheath is important in such devices [1,2]. These results, together with a wide variety of surface analysis data, indicate that low accuracy *in situ* estimates of sputtering (preferably in combination with comprehensive diagnosis of the plasma edge conditions) may be much more useful than higher accuracy sputtering measurements which are not directly relevant to impurity generation mechanisms *in situ*.

An addition, a variety of dramatic changes in surface conditions have been shown to occur during tokamak operation. Therefore, a detailed study of materials which have been exposed to a tokamak environment or prepared in a way which allows sputtering measurements to give insight into the sputtering mechanisms which occur in situ would be more valuable at this point than higher accuracy measurements of sputtering on simpler surfaces.

III. DATA REQUIREMENTS

In discussing data requirements for tokamak simulation codes, one must differentiate between the rather rudimentary needs of present codes and the somewhat more comprehensive needs of codes which may be developed in the future. Present codes give a crude estimate of the actual production of sputtered materials but are potentially useful for surveying the wide variety of materials which have been used or proposed for use in tokamaks. For example, one of the main effects of impurities is to radiate power, and the BALDUR code includes relevant atomic physics for 48 different elements [3]. There is thus a need for developing (and documenting the limitations of) general sputtering models such as that of Bodhansky [4]. The immediate need for more detailed sputtering tables, at least at PPPL, is concentrated on materials which are being considered for use in TFTR, including graphite, niobium, molybdenum, titanium carbide, titanium diboride, boron carbide, titanium, vanadium, and zirconium.

The accuracy required in these general sputtering models and in tabulated data is determined by the detail which can be sensibly included in the transport code. Ideally, the inaccuracies in the input data are sufficiently small that they do not add noticeable uncertainty beyond that inherent in the limitations imposed by other data and the assumptions used in the modelling theory. For present models of the tokamak edge region this probably requires only on the order of a factor of two accuracy in the overall sputtering yields; the tolerable inaccuracy in the sputtering data can be expected to decrease very slowly as transport models are improved.

Thus given the wide variety of materials which may be used in tokamaks, sputtering models which summarize results for a variety of materials are useful. For existing, rather unsophisticated, edge models, generality may be more useful than extreme accuracy in energy or angular distributions of the sputtered atoms.

To summarize, the primary immediate need for transport modelling is the total yield (for realistic surface conditions) for sputtering by hydrogenic ions, a representative highly stripped low-Z ion, and an ion representative of self-sputtering, with energies in the 0.1 to 1 keV/amu range typical of tokamak edge conditions for existing devices and projected reactors.

There is also interest in sputtering by beam-injected hydrogen and deuterium near 20-40 keV/amu may be of interest in existing tokamaks. There may also be conditions where sputtering by 120 to 160 keV deuterium ions injected into advanced tokamaks may be important. At neutral injection energies, particular attention should be paid to the low angles of incidence typical of unconfined beam particles incident on toroidally extended surfaces. Since the flux of high energy neutrals from the beam "shine-through" can be more accurately calculated and measured than the other neutral fluxes, accuracies better than a factor of two (~30-50%) would be useful.

A moderate resolution of the energy spectrum of sputtered neutral atoms is useful for modelling their penetration into the plasma. The tokamak geometry and source distribution of sputtered neutrals are not sufficiently well defined in existing codes to make more than a minimum of energy resolution sensibly usable, however.

The angular distribution of sputtered neutrals is only of interest in transport modelling insofar as it deviates markedly from a 'cosine' distribition. Requirements for yield as a function of incidence are similarly limited to a need for a rough measure of this effect. An exception to this is the yield as a function of the angle of incidence for high energy neutrals from the neutral beam "shine-through".

The composition of sputtered particles is only of significant interest for transport modelling if there is not a single neutral species which is the dominant component of the sputtered material.

The problem of developing a truly guantitative code for modelling the edge region in a tokamak is complicated by the need for two or three dimensional geometry including complicated magnetic geometries and rapid spatial variations in plasma parameters, the existence of plasma flows and sheath potentials, and the need for an accurate treatment of multispecies transport in this environment including all of the relevant atomic physics. Only when these problems have been solved would detailed energy and angular distributions (e. g., ± 20%) be of use in sputtering measurements (and, of course only if the measurements referred to realistic surface conditions). It should therefore be evident that less detailed sputtering data will suffice for some time to come. In particular, the main item of interest for global transport codes is the depth of penetration of impurities into the plasma, which is dominated by the energy distribution of the neutral sputtering products. The angular distribution of the sputtered neutrals also influences the penetration depth. But the angular distribution will only have a significant effect if it differs markedly from distributions known to be typical of sputtering. Also, the location and geometry of the most important sputtered surfaces must be reasonably accurately modelled before information about angular distributions is useful. The one exception is the sputtering yield from the high energy neutral beam atoms which are not stopped by the plasma and strike the opposite wall, in which case the neutral flux and wall geometry can be fairly accurately determined.

ACKNOWLEDGEMENT

Work supported by U.S. Department of Energy Contract No. EY-76-C-02-3073.

REFERENCES

(1) Ohasa, K., et al., Nucl. Fusion 18 (1978) 872.

(2) Taylor, R. J. and Oren, L., Phys. Rev. Lett. 42 (1979) 446.

(3) Post, D. E., Jensen, R. V., Tarter, C. B., Grasberger, W. H., and Lokke, W. A., Atomic Data and Nuclear Data Tables, 20, 397-439 (1977)

(4) Bodhansky, J., Roth, J., and Vernickel, H., in Tenth Symp. on Fusion Technology (Padova, Italy, Sept. 1978) to be published.

SPUTTERING DATA NEEDS FOR MODELLING TOKAMAK TRANSPORT IN HIGH BETA EXPERIMENTS

J. T. Hogan
Oak Ridge National Laboratory, Oak Ridge, Tennessee

1. General Remarks

Sputtering of the first wall by hot charge exchange neutrals has been recognized for many years as potentially a fundamental barrier to long pulse operation of a fusion reactor. The source of this energetic flux of neutrals is unavoidable, at least in designs without a divertor, but the remedy for dealing with it is also well known: lower the edge temperature of the plasma. By lowering the temperature of the plasma in the region where the bulk of the charge exchange emission is formed, one may hope to decrease the resulting sputtered flux of impurities to the plasma and even eradicate this source, if the neutrals' energy can be kept below the sputtering threshold of the first wall/limiter material.

This is the "conventional wisdom" for dealing with sputtering as a source of impurities, but recent trends in reactor designs may force a reassessment, and a greater urgency for needed information on sputterng. It has become apparent that the highest possible $\beta(\equiv 2\mu_o \int dv \frac{3}{2} nT/B_T^2)$ (n, T plasma density, temperature) must be attained in reactor designs. While present experiments are focussed on maximizing T(0), $\beta(0)$, (i.e., peak values in the core) the long term trend must be to improve bulk plasma confinement. This means that there is an inevitable pressure, for economic reasons, toward raising the edge temperature and densities. The point at which it is no longer beneficial to raise $\overline{\beta}$ will probably be determined by the balance between the incremental neutron production resulting from higher $\overline{T}$, on the one hand, and the plasma degradation (shorter pulse, lower confienment time,...) resulting from the incremental rise in sputtered impurities. The sputtering mechanism is not drastically visible in present-day experiments, which are limited by short pulse neutral beam technology. It is, however, an ingredient in one of the fundamental tradeoffs $\overline{\beta}$ vs Z_{eff}) which will determine the operating characteristics of a fusion reactor.

2. Data Needs

Sputtering data for the wall materials typical of present and planned experiments, resolved in energy and angle, has been obtained by many workers. Much of this data is not useful for transport modelling,

however, because it has been obtained by using large bombardment doses. Thus, processes such as flaking, blistering and exfoliation of surfaces may be contributing to the measured yield. Transport calculations require knowing the prompt response to an incremental fast neutral flux. While high bombardment dose sputtering experiments provide useful data for reactor-life erosion rates, they cannot be used in transport models in a meaningful way.

Hence, information needed for transport modelling on light ion (H, D, T, H_e) sputtering rates as a function of energy and angle of incidence, and energy and angle of reflux, seem to be lacking for almost all materials of interest. Again, we emphasize that high dose experiments give only a rough guide.

This data is expected to be critical in the next year or two, when high-power injection experiments on ISX-B, PDX, PLT and Doublet III produce results. Even with relatively short beam pulse lengths, the high power (6 MW in the PDX case, 8 MW of beam + RF for PLT) should produce a detectable effect. The interpretation of these results will be difficult, if not impossible, if the sputtering yields are not known to within $\sim$ 20% for laboratory surfaces, and with some estimate of the changes to be expected in dealing with the real engineering surface of the experiments.

The prompt emission of charge exchange neutrals which are produced by trapping incident injected beam atoms will generate a sizable number of impurity atoms by sputtering of the wall. This charge exchange efflux can be measured, and if the sputtering yields are known only to within a factor 2, then this prompt flux contribution will be wrongly identified and will be combined with the thermal and arcing contributions. This problem is important for the PDX 6-MW injection experiment and the ISX-B 3 MW experiment. It is crucial for the Doublet III 80 kV injection experiments if densities above $10^{14}/cm^{-3}$ cannot be obtained.

The energy and angle ranges of interest are, of course, well known. However, for neutral beam injection experiments special attention should be paid to near-grazing incidence in the 10-40 keV (H^o) energy range. Particles injected against the plasma current direction are often trapped in the plasma on orbits which lead quickly to the wall and grazing collisions may contribute substantially to the observed lack of efficacy of counter injected beams.

Plasma Impurity and Buildup in Mirror Devices

R. S. DeVoto
Lawrence Livermore Laboratory, Livermore, California 94550

Two types of mirror devices are currently under intensive study in fusion laboratories: the field-reversed mirror and the tandem mirror. Currently, the largest effort is devoted to the tandem mirror, and the emphasis in this report will be on that device. Some preliminary considerations for the field-reversed mirror are covered in Reference 12.

The effects of impurities are much different in the end plugs and central cell of the tandem mirror. The end-plugs are much like the standard minimum-B mirror.[7] Only those ions with energy

$$E > 2Z\,\phi/(R-1)$$

are confined. ϕ is the ambipolar potential, R is the mirror ratio and Ze is the ion charge. For typical conditions we have $\phi \gtrsim 5\ T_e$ and $R \gtrsim 2$ so only very high-energy impurities will be confined in the plugs, the remainder being swept out the end in a transit time. Even high-energy impurities will not build-up but will be lost in the time it takes to drag down to the loss boundary. It is easy to show that fully stripped carbon and titanium will be confined for approximately 0.2 and 0.02 times as long as deuterium in the end plugs. A sketch of the loss region in velocity space is shown in Figure 1.

The situation for the central-cell is much different. In this case all low-energy ions are confined; only those ions with

$$E'' \gtrsim Z\ \phi_i$$

being swept out. In this case, the ion containing potential ϕ_i is approximately T_e. The loss region is shown in Fig. 2. The ion confinement time out the open end scales as (Pastukhov)

$$n\tau_p \propto \frac{m^{1/2} T_i^{3/2} Z\phi_i \exp(Z\phi_i/T_i)}{Z^2 T_i}$$

where m is the ion mass and the ion temperature $T_i \gtrsim 2T_e$. We thus find the ratio of confinement times of an impurity to a deuteron is

$$\frac{\tau_p(Z,m)}{\tau_p(1,2)} = \frac{1}{Z}\left(\frac{m}{2}\right)^{1/2} \exp[2(Z-1)]$$

with the results for C $\approx$ 9000 and Ti $\approx$ 4 x 10^{17}. Clearly, impurities must find their way out radially or be diverted before reaching the main central-cell plasma.

Because of the poor confinement of high Z ions in standard mirrors, few studies have been made of impurities. In recently completed work, Drake[13] found O, N, C and Ti in the 2XIIB plasma. The O and N evidently comes from the neutral beams, the C from the getter wires and the Ti from sputtering of the titanium evaporated onto the wall during gettering operations. A calculation by Rognlien of the effect of the same amount of Ti on TMX operations shows that T_e could be reduced from 200 to 100 eV. No other code results are yet available for the effect of impurities on mirror plasma.

In lieu of further code results and/or experimental results on tandem mirrors, needs can be estimated from references 1-11 and unpublished material at Lawrence Livermore Laboratory. The TMX[1] has just begun operation with neutral beams accelerated to 20 keV(D^+) and soon will use beams to 40 keV. MFTF[2-6] will begin operation in the early 1980's, initially with neutral beam potentials to 80 keV (D^+) and later, with longer pulse beams to 150 keV (D^+) or perhaps, 200 keV (D^-). Reactor studies indicate the need for beam energies to 500 keV (D^-). We thus project the need for sputtering data on neutral-beam dump materials, such as stainless steel or titanium, to energies of 500 keV. Data for charge-exchange neutral energies to 500 keV off typical wall materials is also desirable.

REFERENCES

TMX

1. "TMX Major Project Proposal," F. H. Coensgen, Lawrence Livermore Laboratory Prop-148 (1977)

MFTF

2. "MX Major Project Proposal," F. H. Coensgen, Lawrence Livermore Laboratory Prop-142 (1976).

3. "Neutral-Beam Current Requirements for MX," B. W. Stallard and M. E. Rensink, Lawrence Livermore Laboratory UCRL-52205 (1977).

4. "The Effect of Extended Pulse Length on the Mirror Fusion Test Facility," G. D. Porter et al., Lawrence Livermore Laboratory UCRL-52294 (1977)

5. "Review of the Neutral-Beam Current Requirements for the Mirror Fusion Test Facility," G. D. Porter et al., Lawrence Livermore Laboratory UCRL-52517 (1978).

6. Additional information is contained in unpublished memoranda at Lawrence Livermore Laboratory.

Reactors

7. "Plasma Models for Standard Mirror Reactors," R. S. Devoto and D. Bender, Nucl. Fusion 19, (1979).

8. "Preliminary Design Study of the Tandem Mirror Reactor (TMR)," R. M. Moir et al., Lawrence Livermore Laboratory UCRL-52302.

9. "Status Report on Tandem Mirror Fusion Reactor Studies," G. A. Carlson et al., Lawrence Livermore Laboratory UCID-17990 (1978).

10. "Tandem Mirror Reactors," B. G. Logan et al., Proceedings Seventh International Conference Plasma Physics Contr. Nuc. Fusion, Insbruck, IAEA (1978).

11. "An Improved Tandem Mirror Reactor," D. E. Baldwin, B. G. Logan and T. K. Fowler, Lawrence Livermore Laboratory UCID-18158 (1979).

Reversed Field Devices

12. "Conceptual Design of the Field-Reversed Mirror Reactor," G. A. Carlson et al., Lawrence Livermore Laboratory UCRL-52467 (1978)

13. P. Drake, Ph.D Dissertation, Johns Hopkins University (1979).

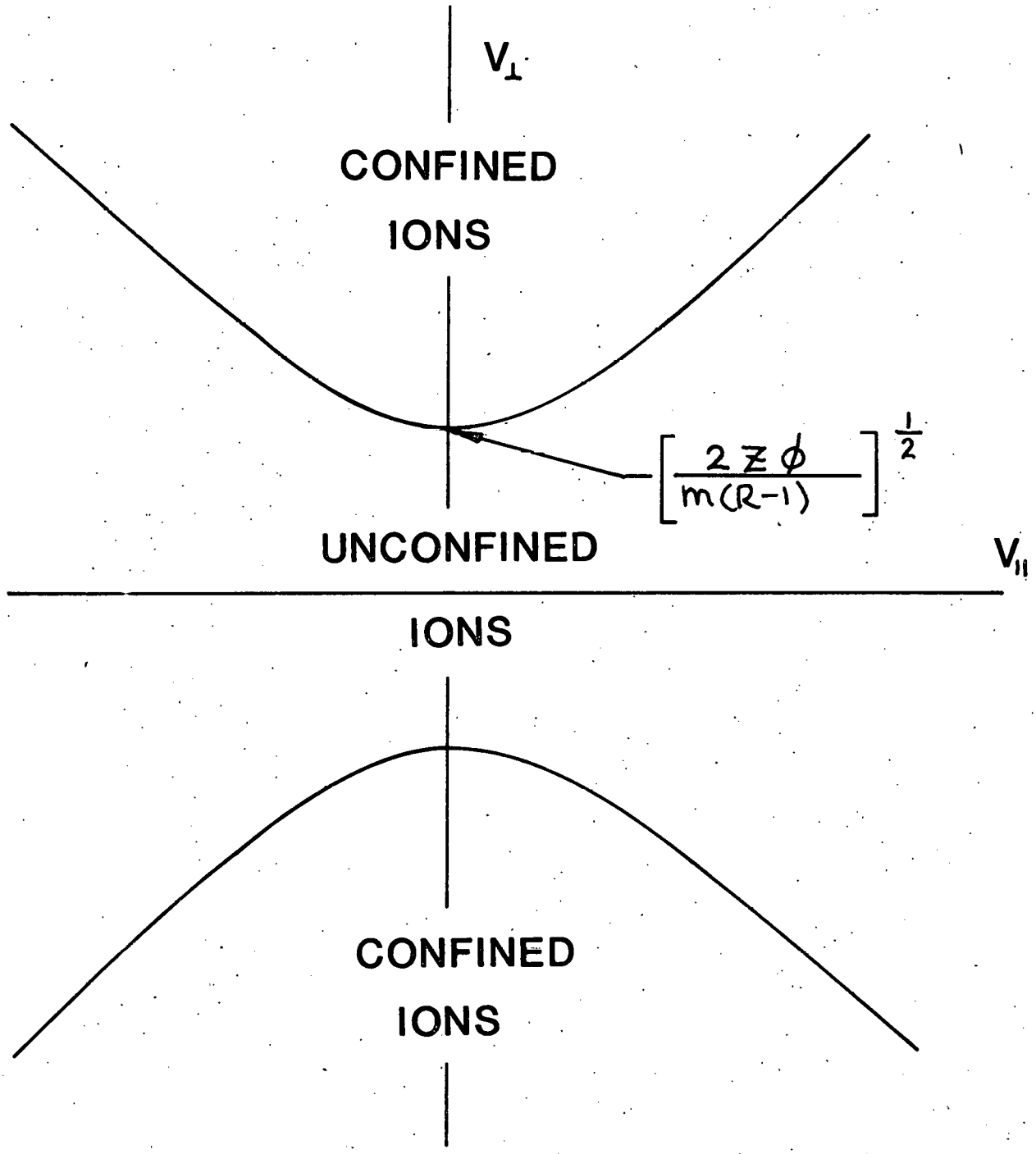
$V_\perp$
CONFINED
IONS
$\left[\frac{2Z\phi}{m(R-1)}\right]^{\frac{1}{2}}$
UNCONFINED
IONS
$V_{||}$
CONFINED
IONS

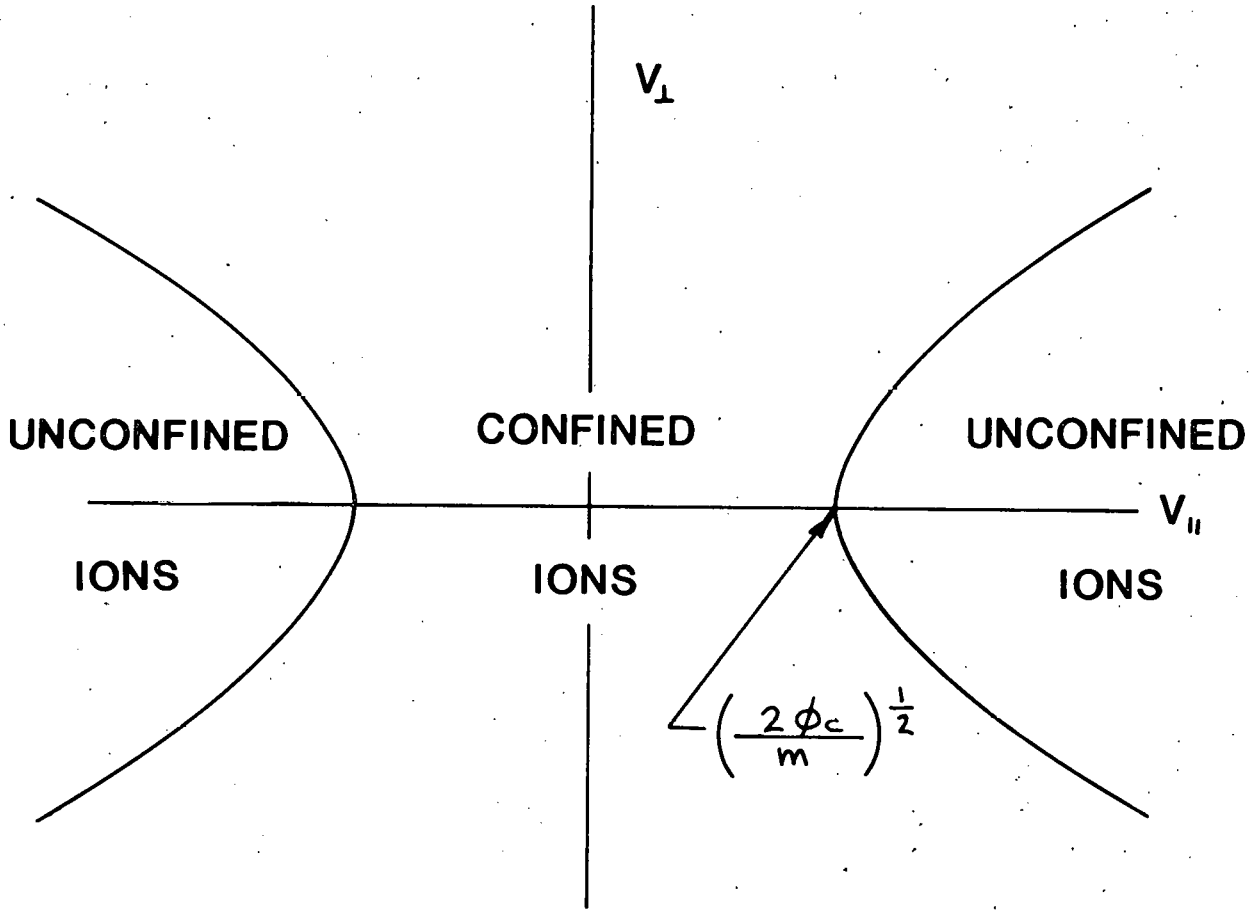

Figure 1 - Sketch of loss boundary for ions contained in tandem-mirror end plugs. The asymmetry due to the presense of the central cell is ignored.

Needs for Sputtering Data in Fusion Reactor Design

G.A. Emmert

Summary

1. The liner of a toroidal reactor is bombarded by charge exchange neutrals with a broad energy spectrum covering the range from the sputtering threshold to roughly 10 keV. The incident angular distribution is also rather broad (0 to ~ 60° from the normal).

2. The limiter or target plate of a divertor is bombarded by fuel ions, alpha particles, and impurity ions. These particles hit the surface primarily at normal incidence with a fairly monoenergetic distribution. The energy can range from ~ 500 eV to ~ 10 keV for singly ionized ions depending on whether the device has a limiter or a divertor and the degree of recycling and radiation at the edge of the plasma. Multiply charged ions have correspondingly higher energy because of acceleration across the sheath at the surface of the limiter or target plate.

3. Determination of the extent to which impurity atoms get into the major plasma depends primarily on the energy distribution of the sputtered atoms and secondarily on their angular distribution. In addition, one needs, of course, the sputtering yield as a function of the incident energy and angle for various reactor candidate materials.

Supporting Material

Sputtering in fusion reactors is a source of concern primarily because it contributes to the production of impurity atoms and, secondarily, because of erosion of wall material. In toroidal devices, the primary surfaces undergoing sputtering are the liner, which sees the charge exchange neutral flux from the plasma, and the limiter or divertor target plate, which is bombarded by hydrogenic ions, alpha particles, and impurity ions. In addition, because of toroidal field ripple, suprathermal alpha particles can bombard the liner in localized zones. It is difficult to be very quantitative about the energy spectrum and magnitude of the fluxes bombarding the surfaces; they are sensitive to both uncertainties in plasma transport coefficients and design options, such as shallow versus deep pellet refuelling or gas refuelling, impurity concentration, type of divertor (if any), possibilities for enhancing recycling in the boundary zone, etc. The numbers given here are meant to be "ball park" estimates typical of current power reactor designs.[1-3]

Figure 1 shows the energy spectrum of the charge exchange neutral atoms reaching the liner for various refuelling profiles in a tokamak reactor with a poloidal divertor.[4] Large δ corresponds to shallow refuelling; this increases the neutral flux to the liner but also cools the edge of the plasma and thereby causes the energy spectrum to be colder. The total charge exchange flux to the liner is ~ 10^{16} cm^{-2} sec^{-1} in these calculations. The angular distribution of the charge exchange flux originating at a given

optical depth and reaching the liner is shown in Fig. 2. These results indicate that sputtering yields are required for a broad energy spectrum (threshold to ~ 10 keV) and a broad incident angular distribution in order to determine the impurity generation and erosion rates. The divertorless tokamak[2] would have a colder charge exchange spectrum and hence is contained as a subset in the above energy range.

In addition to the charge exchange neutral flux, the liner can be bombarded by suprathermal alpha particles,[5,6] which in the course of their slowing down from 3.5 MeV can be trapped in the toroidal field ripple and drift to the liner before scattering onto confined drift surfaces. It has been estimated that as much as 50% could escape in this way with a typical energy of several hundred keV.[6] Careful magnetic field design can reduce this effect, but localized bombardment by high energy alpha particles is always a possibility. Such particles are likely to bombard the liner at grazing incidence.

The bombardment conditions at the surface of the limiter or divertor target plate are rather different from those at the liner. In front of this surface, there is a plasma sheath with a potential drop of the order of $(3\text{-}4)kT_e/e$. The ions are accelerated across this sheath and become fairly monoenergetic in the forward direction (Fig. 3), although they can still be Maxwellian in the transverse direction. In order to reduce the surface heat flux, it is customary to incline the surface at an angle to the magnetic field; this spreads the total heat load over a greater area. Consequently, the ions can approach the sheath with grazing incidence; acceleration across the sheath, however, turns the ion trajectories so that they hit the surface with essentially normal incidence, assuming $T_i \simeq T_e$. The dominant part of the energy spectrum of the ions hitting the surface can range from ~ 10 keV[3,7] (with an unload divertor) down to ~ 500 eV (divertorless machine with a lot of recycling and/or impurity radiation at the edge) for singly ionized ions. Impurity ions with a charge Ze have an energy Z times higher and consequently can play a substantial role in sputtering of the surface when the plasma edge is colder. Secondary electron emission[7,9,10] can reduce the sheath potential and hence the energy at which the ions hit the surface (Fig. 4).

The determination of the impurity concentration in the main plasma depends not only on the total sputtering yield, but also on the angular and energy distribution of the sputtered atoms as they leave the surface. A divertor or limiter can shield the main plasma from impurities to the extent that the impurities are ionized in the scrape-off zone (or limiter shadow) and flow parallel to the magnetic field to a target surface. (This also promotes high Z sputtering of the target). The probability of an impurity atom passing through the scrape-off zone without ionization is given in Fig. 5 for various angular distributions of the sputtered atoms as a function of the optical depth, μ. The kinetic energy of the atom enters into μ, which is inversely proportional to its velocity. As shown in Fig. 5, the surviving neutral atom flux is exponentially dependent on the velocity of the atoms, but is not so sensitive to their angular distribution.

To the extent that a fraction of the sputtered atoms leave the surface as positive ions, the rate of erosion and impurity production is correspondingly reduced. This is because the ionized atoms can be turned back to the surface by the electrostatic sheath or by the magnetic field. The charged fractions are worthy of consideration only when they get close to unity.

The above considerations are based upon conceptual tokamak reactor design experience. Similar considerations apply to other toroidal devices without substantial change. These considerations also apply qualitatively to mirror reactors, except that the bombarding energies are potentially much higher and the ambipolar potential in a mirror excludes impurities from the plasma. Accumulation can occur in the central cell of a tandem mirror, but this requires that the impurities enter across the magnetic field, as in a toroidal device, since the ambipolar potential of the plug excludes their entry parallel to the magnetic field. These effects have been reviewed by Post.[11]

References

1. B. Badger, et al., "UWMAK-III, A Higher Performance, Noncircular Tokamak Power Reactor Design", UWFDM-150, University of Wisconsin Nuclear Engineering Dept. (1975).

2. B. Badger, et al., "NUWMAK - A Tokamak Reactor Design Study", UWFDM-330, University of Wisconsin Nuclear Engineering Dept. (1979).

3. A.T. Mense and G.A. Emmert, Nuclear Fusion 19, 361 (1979).

4. G.A. Emmert, "Effect of Refuelling Profile on the Performance of Divertor Tokamaks", IPP4/175, Max-Planck-Institut für Plasmaphysik (1979).

5. T.F. Yang and G.A. Emmert, "Analysis of α-Particle Loss Due to Toroidal Field Ripple and Determination of the Number of TF Coils", UWFDM-121, University of Wisconsin Nuclear Engineering Dept. (1974).

6. J.D. Callen, R.H. Fowler, and J.A. Rome, "Alpha Particle 'Pumping' in a Toroidal Fusion Reactor by Magnetic Ripple Effects", Sherwood Theory Mtg. Mt. Pocono, Pennsylvania (1979).

7. P.J. Harbour and M.F.A. Harrison, Nuclear Fusion 19, 695 (1979).

8. R.W. Conn, et al.,"Impurity Control, Refuelling, and Exhaust in INTOR," Intor Internal Rept. #4 (1979).

9. G.D. Hobbs and J.A. Wesson, Culham Rept. CLM-R61 (1966).

10. J.N. Davidson, G.A. Emmert, A.T. Mense, R.M. Wieland, Trans. ANS 32, 75 (1979).

11. R.F. Post, J. Nuclear Materials 76 & 77, 112 (1978).

Other Useful Sources of Information are:

1. R.W. Conn, J. Nucl. Materials 76 & 77, 103 (1978).

2. W.M. Stacey, et al., "Impurity Control in Tokamak Reactors", ANL/FPP/TM-91, Argonne National Laboratory (1977).

3. H. Vernickel, et al., "Relative Importance of Different Impurity Sources in Tokamak Reactors as Estimated From Particle Balance Equations", Proc. Int. Symp. on Plasma Wall Interaction (Jülich, FRG), pg. 209 (1976).

4. G.M. McCracken and P.E. Stott, "Plasma-Surface Interactions in Tokamaks", Culham Rept. CLM-P573 (1979).

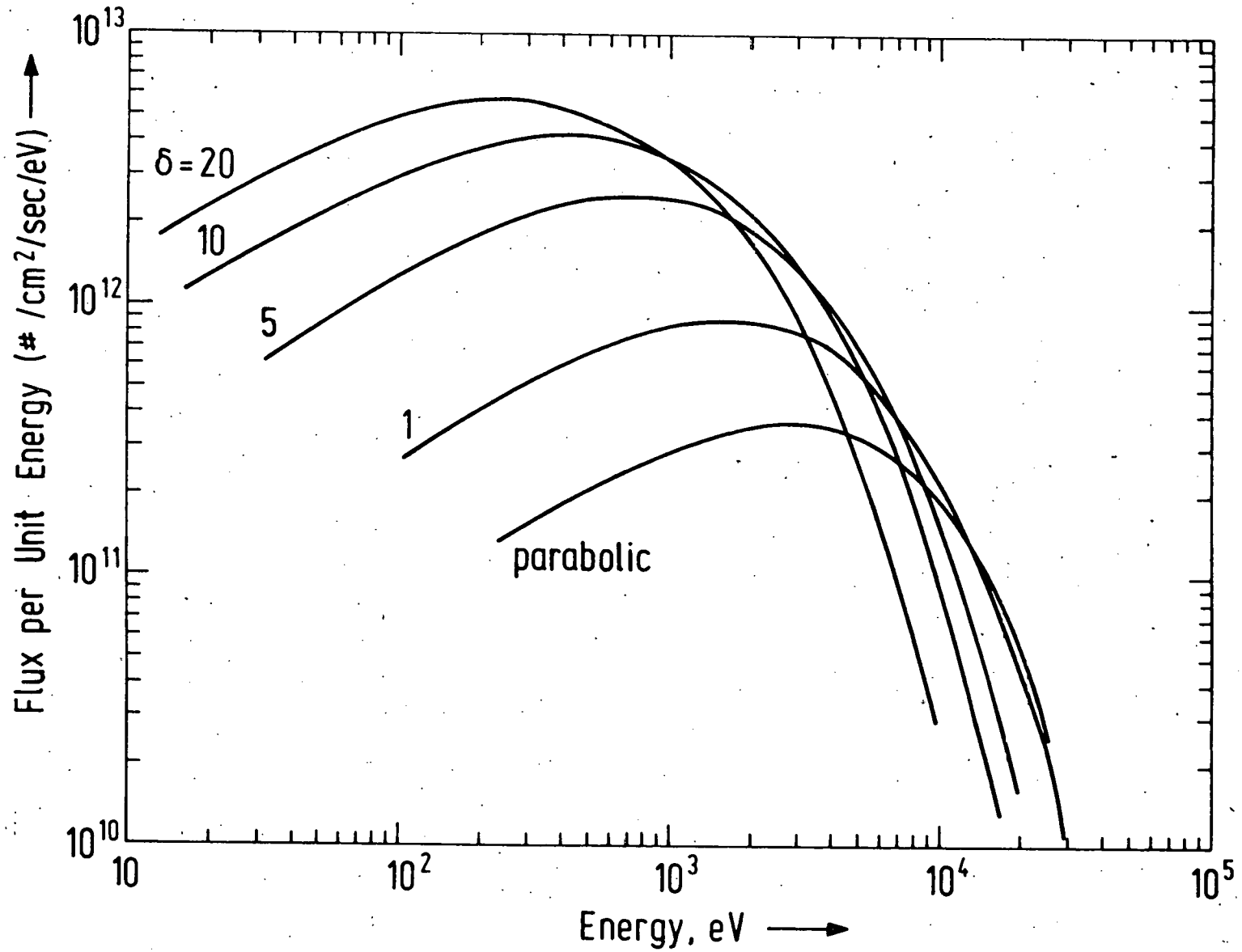

Fig. 1 ENERGY DISTRIBUTION NEUTRAL PARTICLE FLUX (REACTOR SIZE)

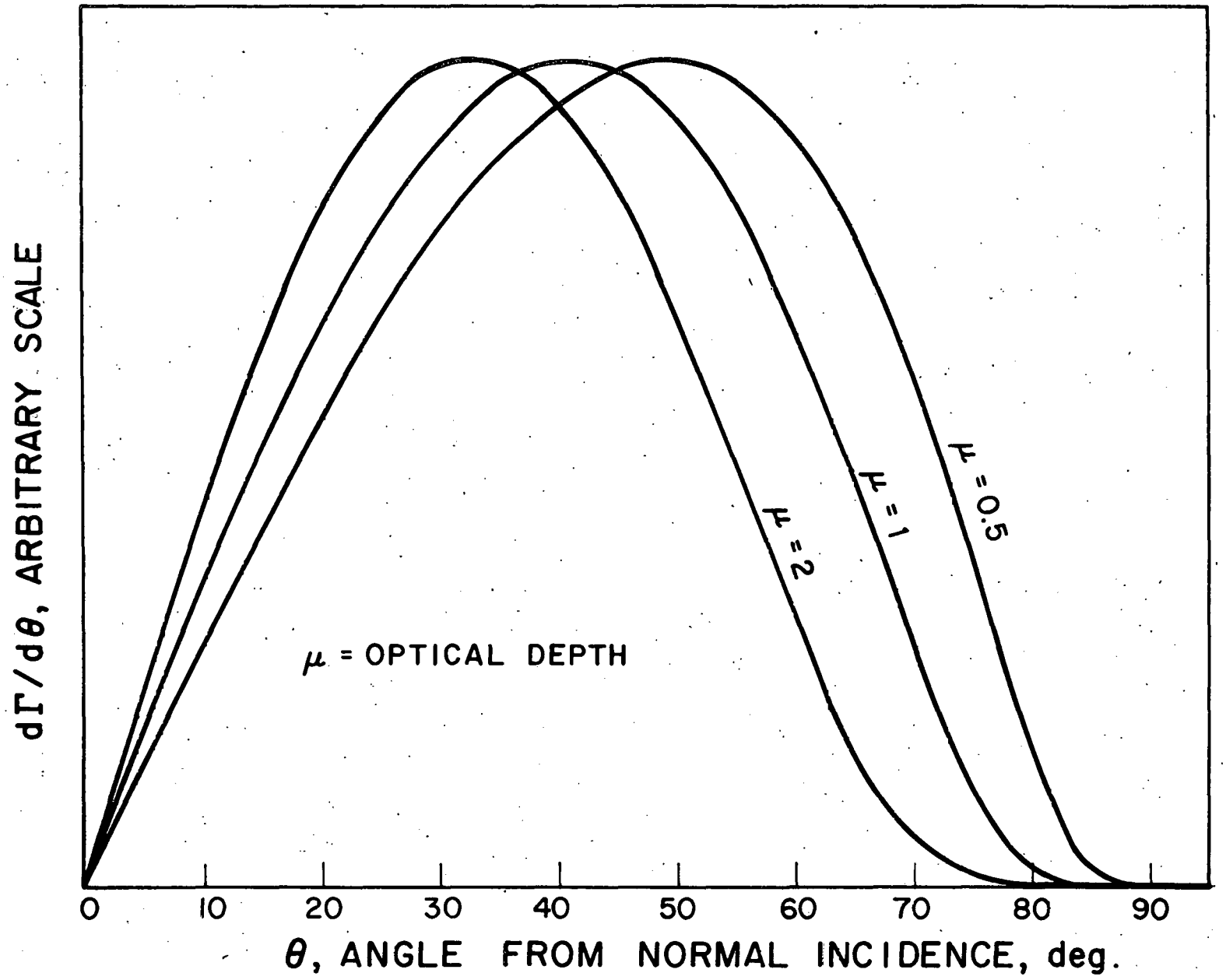

FIG. 2. Angular distribution of the charge exchange flux incident on the wall coming from a given optical depth μ.

FIGURE 3

Ion Distribution Function Approaching a Wall

($T_i = T_e$, Hydrogen)

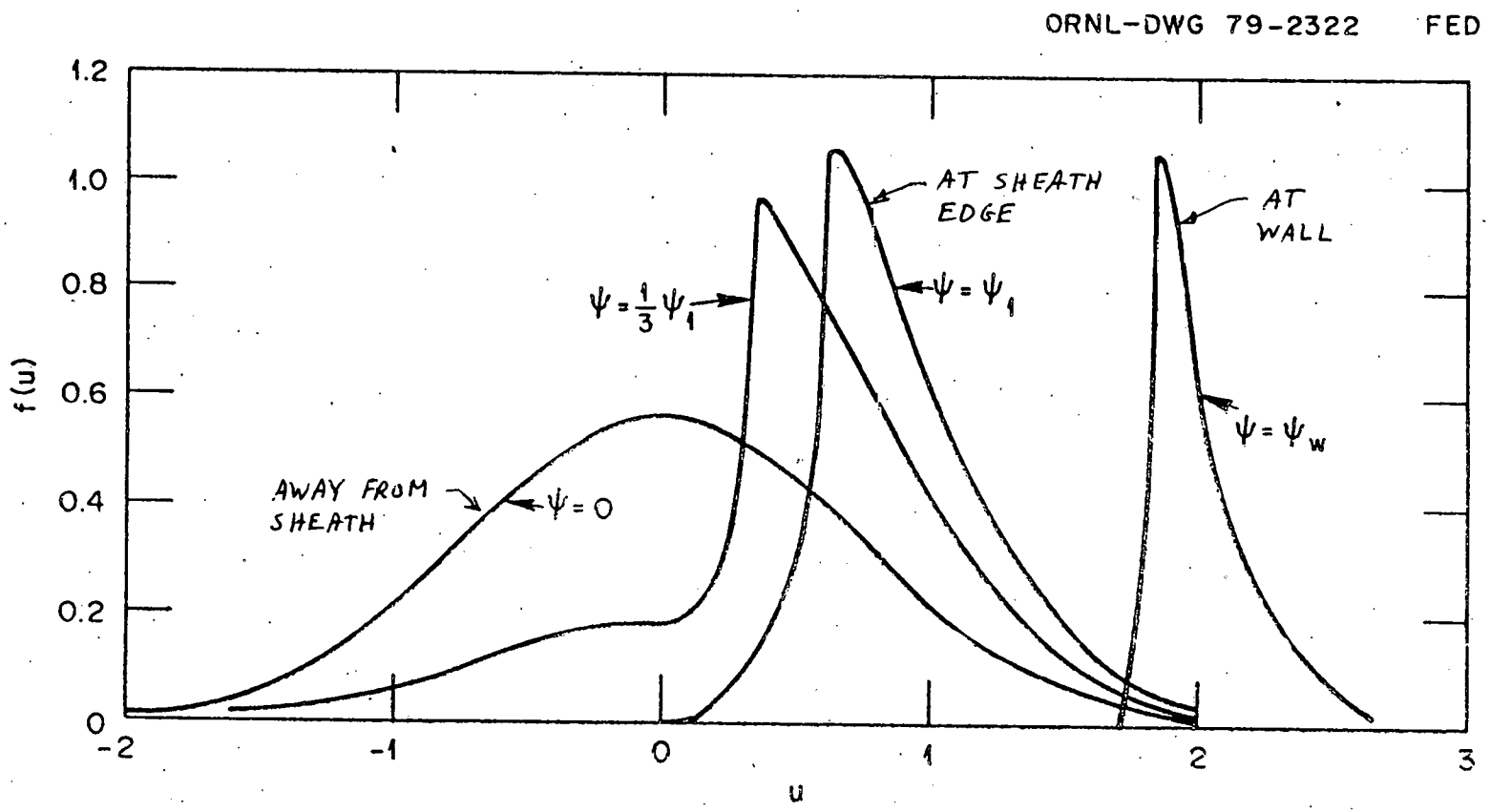

FIGURE 4

Effect of secondary electron emission on the wall potential.

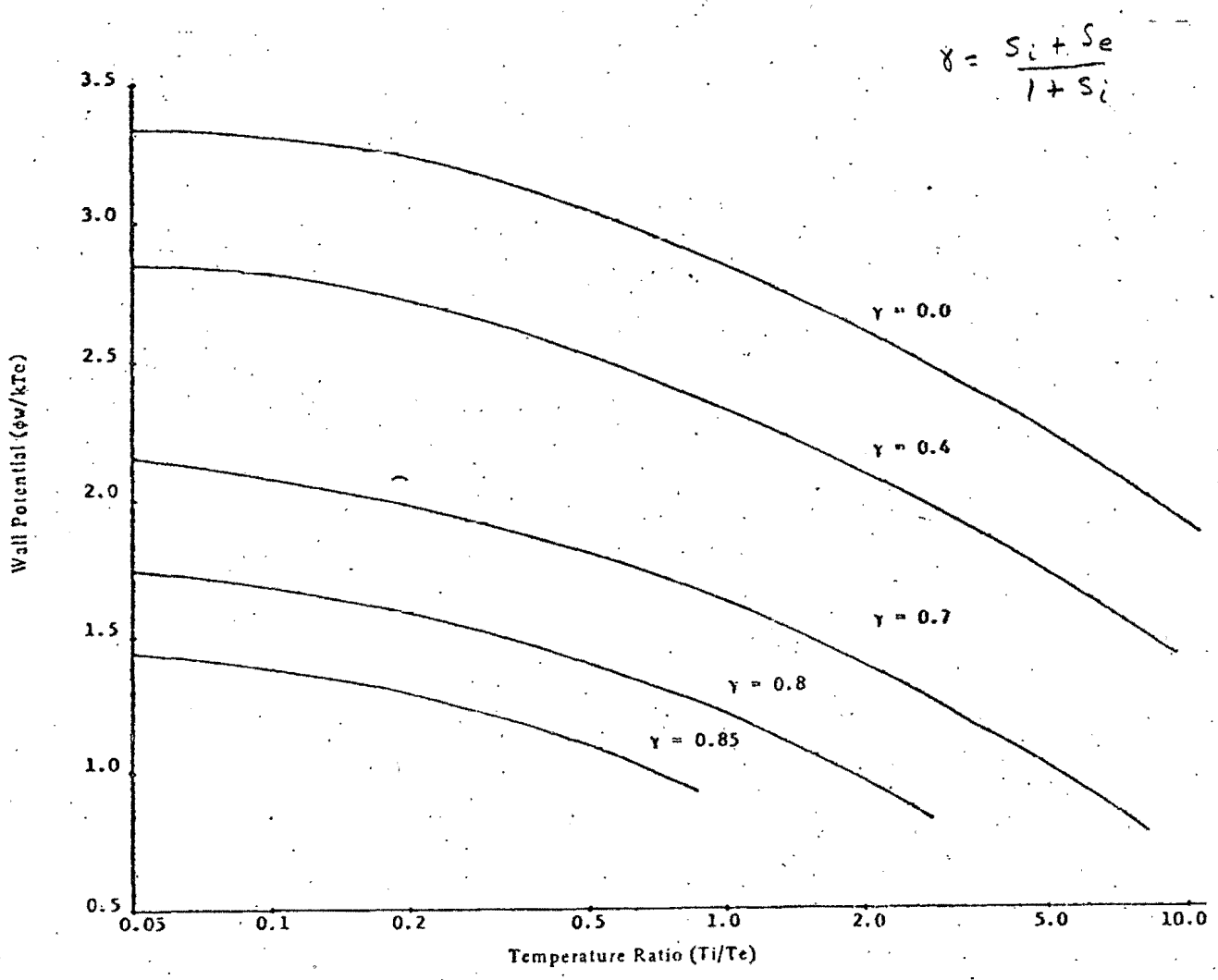

$S_{e(i)}$ = secondary electron emission coefficient due to electron (ion) impact

FIGURE 5
SURVIVING IMPURITY FLUX FOR DIFFERENT ANGULAR DISTRIBUTIONS

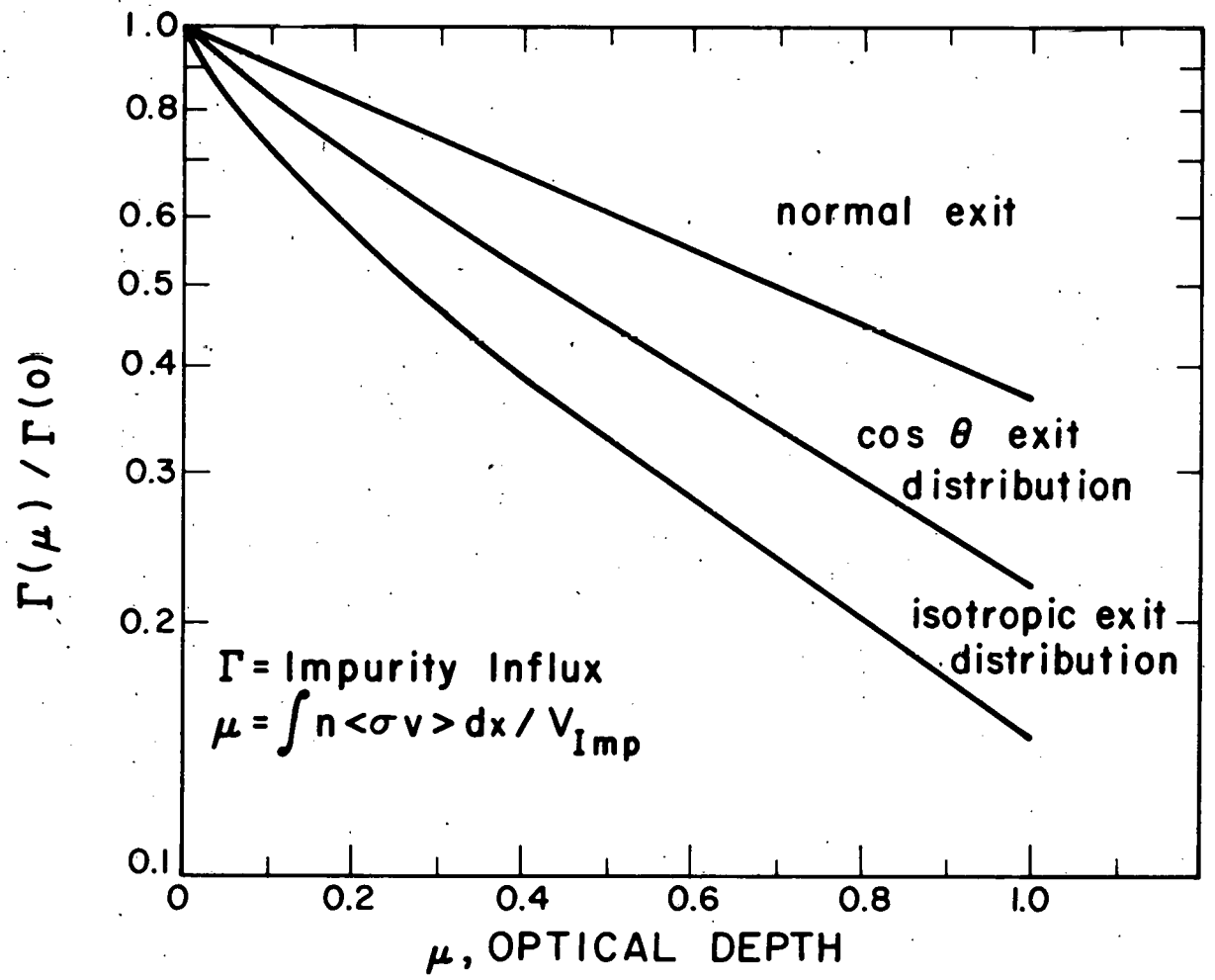

EXPERIMENTAL OBSERVATIONS OF SPUTTERING IN TOKAMAKS

H. F. Dylla

Princeton Plasma Physics Laboratory

ASSESSMENT

There is qualitative evidence to indicate that ion sputtering within the scrape-off plasma and, to a lesser extent, charge exchange sputtering of the vacuum vessel wall are significant mechanisms for high Z impurity contamination of plasmas in present generation tokamaks. A quantitative correlation of tokamak impurities with sputtering effects will require more extensive impurity studies of the edge plasma.

High power neutral beam injection will enhance a number of sputtering effects within the bulk plasma. Intrinsic neutral beam impurities are most likely the result of sputtering effects within the ion source. Detailed experimental measurements of these effects remain to be done.

INTRODUCTION

Although sputtering is assumed to be an important impurity generation mechanism in tokamak fusion devices, there is a lack of experimental evidence for the existence and relative importance of sputtering in present-generation tokamaks.[1,2] One reason for this anomaly is the small number of published impurity studies. Secondly, post-operative analyses of tokamak components which could be expected to exhibit the most obvious effects of sputtering, such as limiter and neutral beam armor, are often obscured by melting and ablation. Thirdly, ion temperatures and pulse lengths of existing tokamaks have not been of sufficient magnitude for charge-exchange neutral sputtering of wall components to be definitely identified. This report briefly reviews the available experimental evidence for sputtering in tokamaks by dividing the observations into three categories: (1) ion sputtering of limiters, divertor plates, and probes introduced into the edge (or "scrape-off") plasma; (2) charge-exchange neutral sputtering of wall components; and (3) neutral beam effects which include lost orbit effects, increased charge exchange sputtering, direct beam sputtering on armor plate, and sputtering in the ion source and optics.

I. ION SPUTTERING IN THE EDGE PLASMA

A tokamak limiter or divertor plate, by definition, is a surface that is introduced into the plasma at radii smaller than the wall radius to intercept plasma flux. This interruption of the flux lines usually results in an exponential decrease in plasma density across the radial projection of the surface, (the "scrape-off" layer). For this reason limiter and divertor plates and any probes introduced within the plasma scrape-off layer are exposed to 10^3-10^4 larger ion fluxes than the vacuum vessel wall. Thus, ion sputtering effects should be proportionally larger on such surfaces.

Recent measurements in PLT[3] have obtained the mean energy and flux of incident deuterium which impacted a carbon probe introduced within the edge plasma (Figs. 1-4). The mean D^+ energies fall from ~600 eV at the poloidal ring limiter radius to 100-200 eV at the normal wall position. The measured flux falls by two orders of magnitude over the same distance. Integration of the measured flux over the first two cm of the scrape-off region gave a total erosion rate of 0.5-1.5 x 10^{19} atoms s^{-1} for stainless steel. This rate is sufficient to account for the globally-averaged Fe influx rate estimated at 0.5-1.5 x 10^{19} s^{-1} from spectroscopic data[4], assuming a $\tau_p \simeq 10$ ms. These measurements indicate the importance of hydrogenic ion sputtering for impurity production in tokamaks but do not prove that such sputtering is the dominant mechanism. Estimates of the impurity introduction rate under similar conditions due to impurity ion sputtering[5] or unipolar arcing of the limiter[5,6] give impurity introduction rates of the same order of magnitude.

A number of studies in other tokamaks have concluded that impurity ion sputtering of the limiter is an important mechanism for metal contamination of plasmas.[7,8] Measurements of impurity fluxes in the edge plasma[9,7] generally indicate fluxes 10^2-10^3 times smaller than the hydrogenic flux; however, the net contribution to sputtering is enhanced for impurity ions by their larger mass and multiple charge which results in a higher impacting energy after acceleration through the sheath potential.

Spectroscopic studies of impurities introduced from biased probes in the DIVA[8] and Macrotor[10] tokamaks show that ion sputtering is an important process when sheath potentials are greater than ~50 eV. However, studies of the correlation of limiter potential with impurity generation in a tokamak have not been performed.

Macroscopic erosion processes which occur on limiter and divertor plates, such as arcing, melting, and evaporation, often dominate the surface morphology, thus preventing the observation of surface changes induced by sputtering. No topographical effects characteristic of sputter damage have been observed on limiters or sample probes introduced into PLT[5], DITE[11], or TFR.[12] However, characteristic sputter cones have been observed on the gold limiter of DIVA.[13]

II. CHARGE EXCHANGE SPUTTERING OF THE WALL

There are numerous calculations and computer codes which include charge exchange sputtering of the wall as the primary source of metallic impurities.[14] Again, the experimental evidence is lacking in present generation tokamaks to designate this process as the dominant metal impurity generation mechanism. One problem is absence of any measurements of the low energy charge exchange flux. Two types of particle energy analyzers are presently being prepared for tokamak measurements[15], and it is likely that surface probes will also be useful for these measurements.[16] Estimates of the charge exchange outflux (~3 x 10^{15} cm^{-2} at $n_e(0) = 1 \times 10^{13}$ cm^{-3}) and characteristic energy (~100 eV) in PLT have been obtained from the previously mentioned surface probe study.[13] Integrating this flux over the torus area and multipling by a typical stainless steel sputtering yield (~.01) results in an Fe influx rate (~10^{19} s^{-1}) of the same order as that produced by ion sputtering of the limiter. However, measurements of the high energy charge

exchange flux[17] and Hα emission[18] have shown that there are substantial toroidal and poloidal asymmetries in the charge exchange flux, thus an average value based on a single position measurement is a dangerous extrapolation.

A few time-resolved studies of impurity behavior during neutral beam heating have been performed.[19-22] However, the data are insufficient to assess the role of increased charge exchange wall sputtering on the observed increases in impurity radiation.

It is important to emphasize that microscopic examination of samples exposed at the wall of PLT[5], TFR[23] and DITE[4] have always shown deposition rather than erosion, and no surface changes characteristic of sputtering have been observed (i.e., smoothing of edges, or preferential sputtering). As higher central ion temperatures are reached with auxiliary heating, and as the pulse length is extended, charge exchange sputtering of the wall should have more of an effect on plasma parameters. However, charge exchange erosion of the wall will always compete with deposition from localized sources (i.e., limiters, beam dumps, etc.).

III. NEUTRAL BEAM EFFECTS

Apart from increased charge exchange wall sputtering during neutral beam heating, there are additional sputtering effects related to neutral beam injection:

(1) Some fraction of the injected neutral beam, depending on the beam energy, plasma density and path length, will penetrate the full plasma path length and sputter the opposing vacuum vessel wall (or neutral beam protective plates). The energy distribution of this "shine-through" fraction is the same as the incident energy distribution. For present generation neutral beam sources (40-50 keV), the effect can result in substantial sputtering and blistering of the affected surface.

(2) Some fraction of the injected neutral beam will not be confined after ionization and will leave the plasma volume on "bad orbits." The fraction of injection particles on bad orbits is typically 10-20% and depends on the plasma current, density and injection geometry. Most bad orbit particles will probably be intercepted by the limiter resulting in increased sputtering of the limiter by higher energy particles.

(3) Impurities intrinsic to the neutral beam are most likely introduced by sputtering within the neutral beam ion source and acceleration grids. Recent measurements of the purity of the ORNL/PLT neutral beam sources[24] have detected a number of beam impurities (most notably Cu, Fe, Cr and W) traceable to materials used iwthin the neutral beam optics (see Table 1). The development of low Z, low sputter yield coatings for source components, and specific ion source conditioning techniques, or the additional complication of mass selective hardware in the beam-line may be necessary to minimize ion source impurities.

REFERENCES

1. The Fusion Reactor Material Program Plan, Sec. III Report DOE/ET-0032/3 (1978).

2. G. M. McCracken and P. E. Scott, "Review of Plasma-Wall Interactions in Tokamaks," Culham Rep. No. CLM-573 (1979).

3. G. M. McCracken, S. A. Cohen, H. F. Dylla, C. W. Magee, S. T. Picraux, S. M. Rossnagel, W. R. Wampler, paper presented at the 9th European Conf. on Controlled Fusion, Oxford, U.K. Sept. 17-21, 1979.

4. E. Hinnov, "Radiation in PLT Discharges," in Princeton Plasma Physics Laboratory Rep: Status of Ohmic Heating in PLT, Vol. II, Sept. 1978.

5. S. A. Cohen, H. F. Dylla, S. M. Rossnagel, S. T. Picraux, J. A. Borders, and C. W. Magee, J. Nucl. Mat. 76 & 77, (1978) 459.

6. H. F. Dylla, "Experience with Arcing in PLT and PDX," in report of the DOE/ORNL Workshop on Arcing Phenomena in Fusion Devices, Knoxville, TN, April 1979.

7. G. Staudenmaier, P. Staib, G. Venus, and TFR Group, J. Nucl. Mat. 76 & 77 (1978) 445.

8. K. Ohasa, et al., J. Nucl. Mat. 76 & 77 (1978) 489.

9. S. A. Cohen and H. F. Dylla, J. Nucl. Mat. 76 & 77 (1978) 425.

10. L. Oren, R. J. Taylor and F. Schwirzke, J. Nucl. Mat. 76 & 77 (1978) 412.

11. D. H. J. Goodall and G. M. McCracken, Culham Laboratory Rep. No. CLM-R167 (1977).

12. P. Staib, private communication.

13. K. Ohasa, et al., Tokai Research Establishment Rep. No. JAERI-M 7935 (1978).

14. D. F. Düchs, D. E. Post and P. H. Rutherford, Nucl. Fusion 17 (1977) 565.

15. See contributions by C. Barnett and D. Voss in Proceedings of the DOE Workshop on New Diagnostics for Tokamak Impurity Measurements, Germantown, MD, May 1979.

16. S. A. Cohen and G. M. McCracken, Princeton Plasma Physics Laboratory, Rep. No. PPPL-1529 (1979), J. Nucl. Mat. (to be published).

17. R. J. Goldston, private communication.

18. S. Suckewer, private communication.

19. S. A. Cohen, J. Nucl. Mat. 63 (1976) 65.

20. J. F. Lyon, et al., Proc. 8th European Conf. on Controlled Fusion and Plasme Physics, Prague 1977 Vol. 1, p. 23.

21. Equipe TFR, Nucl. Fusion (suppl. 1977) Vol. 1, p. 69.

22. E. Hinnov, et al., in Status of Neutral Beam Heating in PLT, Princeton Plasma Physics Laboratory Rep. Vol. 1 May 1978.

23. R. Behrisch, et al., J. Nucl. Mat. 76 & 77 (1978) 457.

24. H. F. Dylla, et al., Bull. Am. Phys. Soc. 23 (1978) 913. Also see L. R. Grisham, et al., Princeton Plasma Physics Laboratory Rep. No. 1484 (1978).

TABLE I

PRELIMINARY RESULTS: NEUTRAL BEAM IMPURITIES

	1 Shot on N.B. Test Stand (40A, 30 keV H^o for 100 ms)				50 Shots on N.B. Test Stand (40A, 30 keV H^o for 100 ms)				52 Shots in PLT (~1 MW D^o Injection for 200 ms)			
	Fe	Cu	W (Ta)	Al	Fe	Cu	W (Ta)	Al	Fe	Cu	W (Ta)	Ti
Impurity Concentration[a] (10^{14} cm^{-2})	2.9	3.2	.13	15.	0.9	0.2	≤.05	5.	<1	4.0	<0.05	1.0
Impurity Fraction in Beam[b] (%)	1.2	1.3	0.05	-	--				--			
Total Impurity in Beam[b] (10^{17})	2.1	2.3	0.09	-	--				<1.2	4.8	<.06	-
Impurity Fraction in PLT[b] at $\bar{n} = 2\times10^{13}$/cc (%)	0.26	0.29	0.01	-	--				<.15	0.6	<.008	-

(a) 2.0 MeV ^{4}He ion backscattering measurements on Be and Si target samples.

(b) The simplifying assumptions used in these calculations are discussed in Ref. 24.

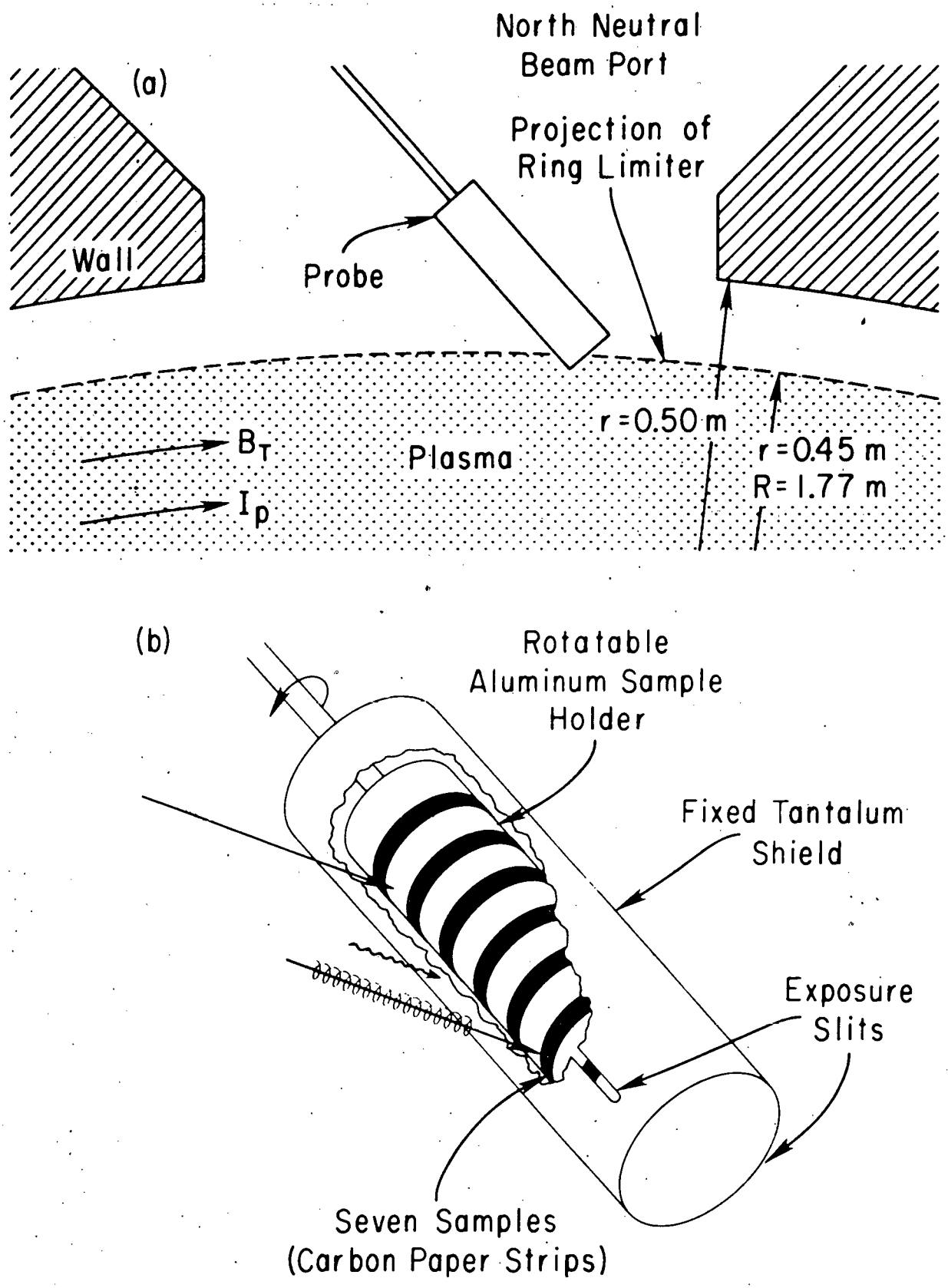

Fig. 1. Schematic of probe: (a) in the plasma boundary, plan view and (b) details of probe.

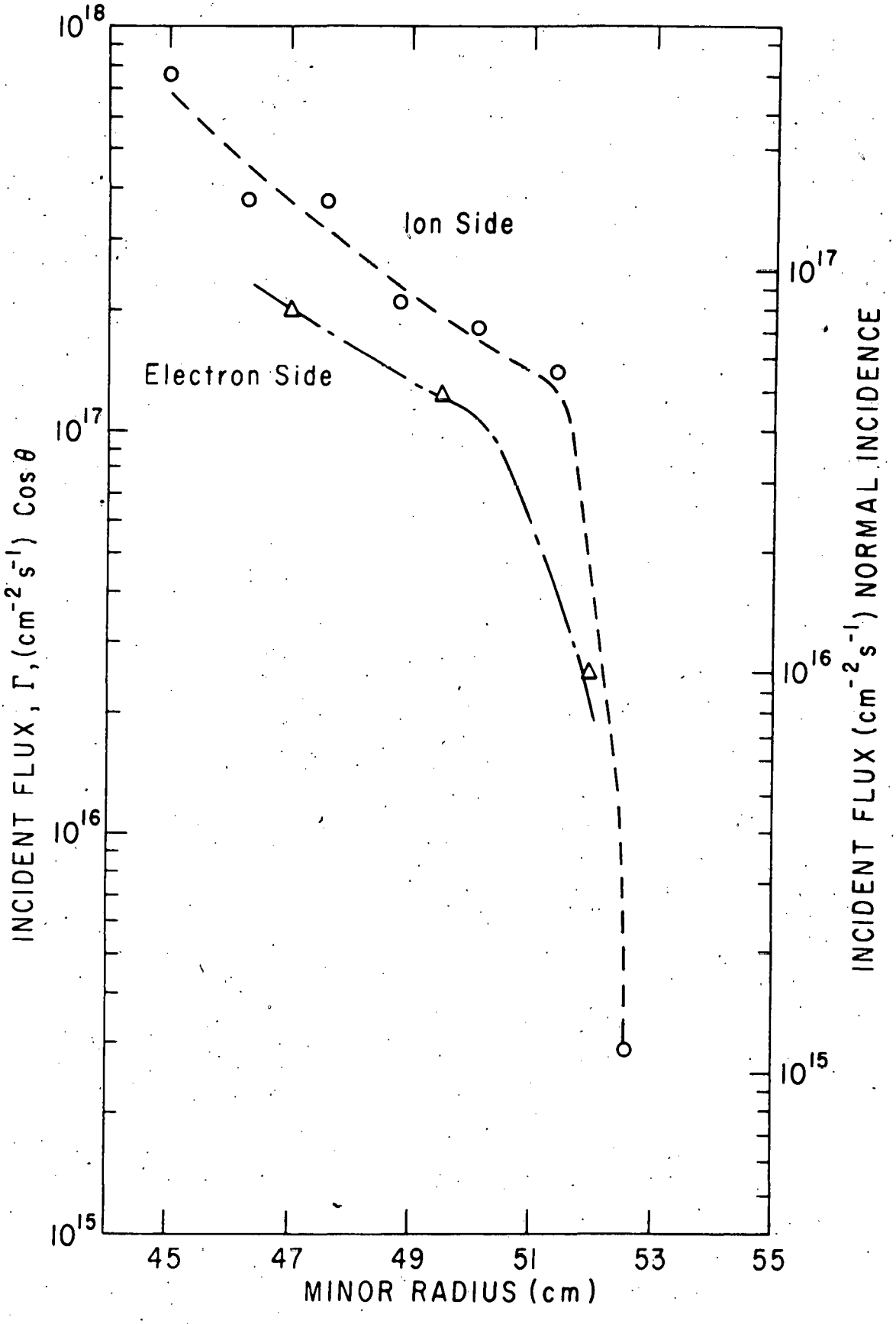

Fig. 2. Incident deuterium flux to the probe calculated from the trapped flux assuming (a) cos θ incident distribution (b) normally incident flux.

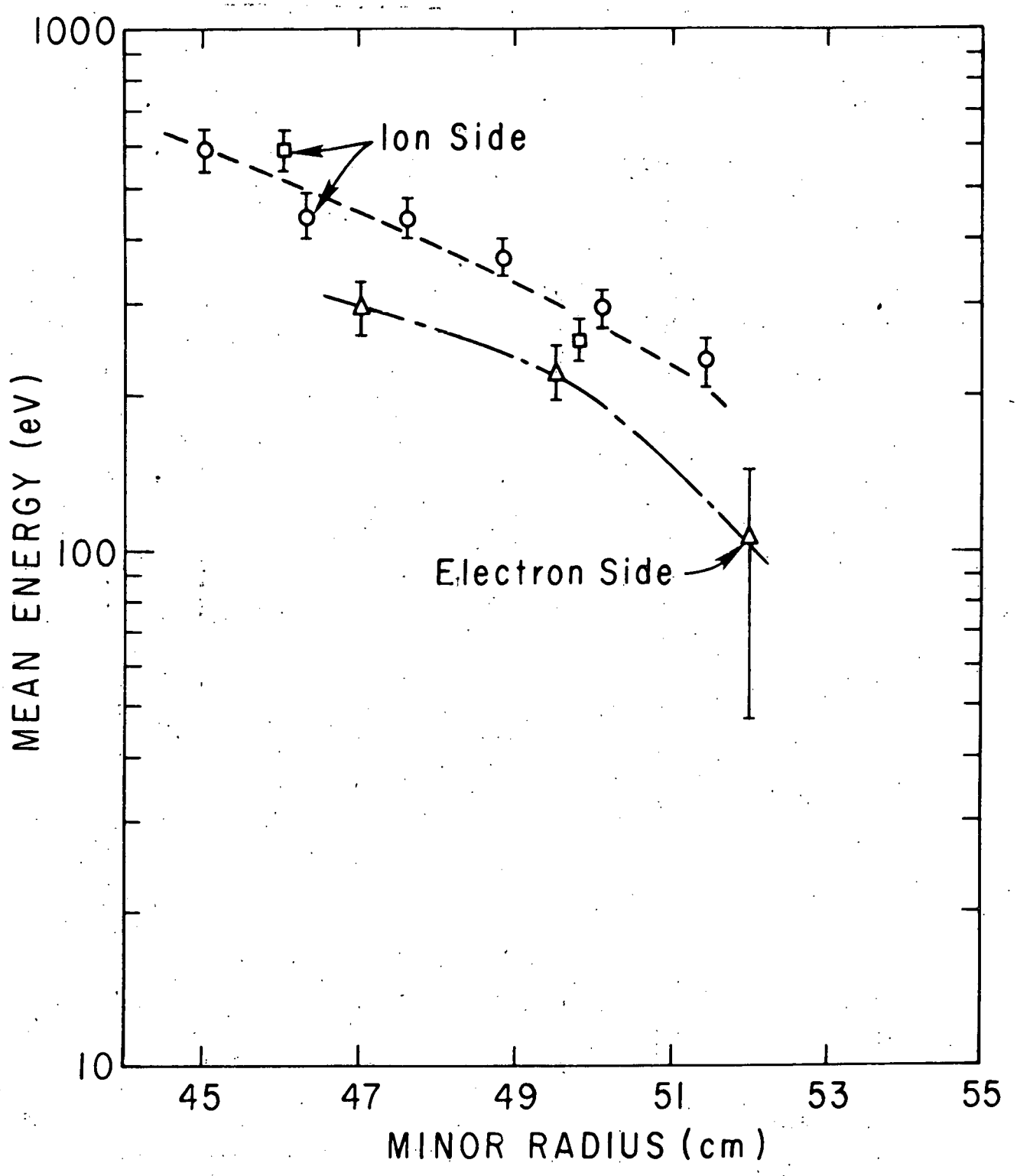

Fig. 3. Mean energy, $\bar{E}$, of incident deuterium obtained from saturation behavior (Δ, 0) and from depth profiles (□). For a Maxwellian distribution $\bar{E} = \frac{3}{2}$ kT.

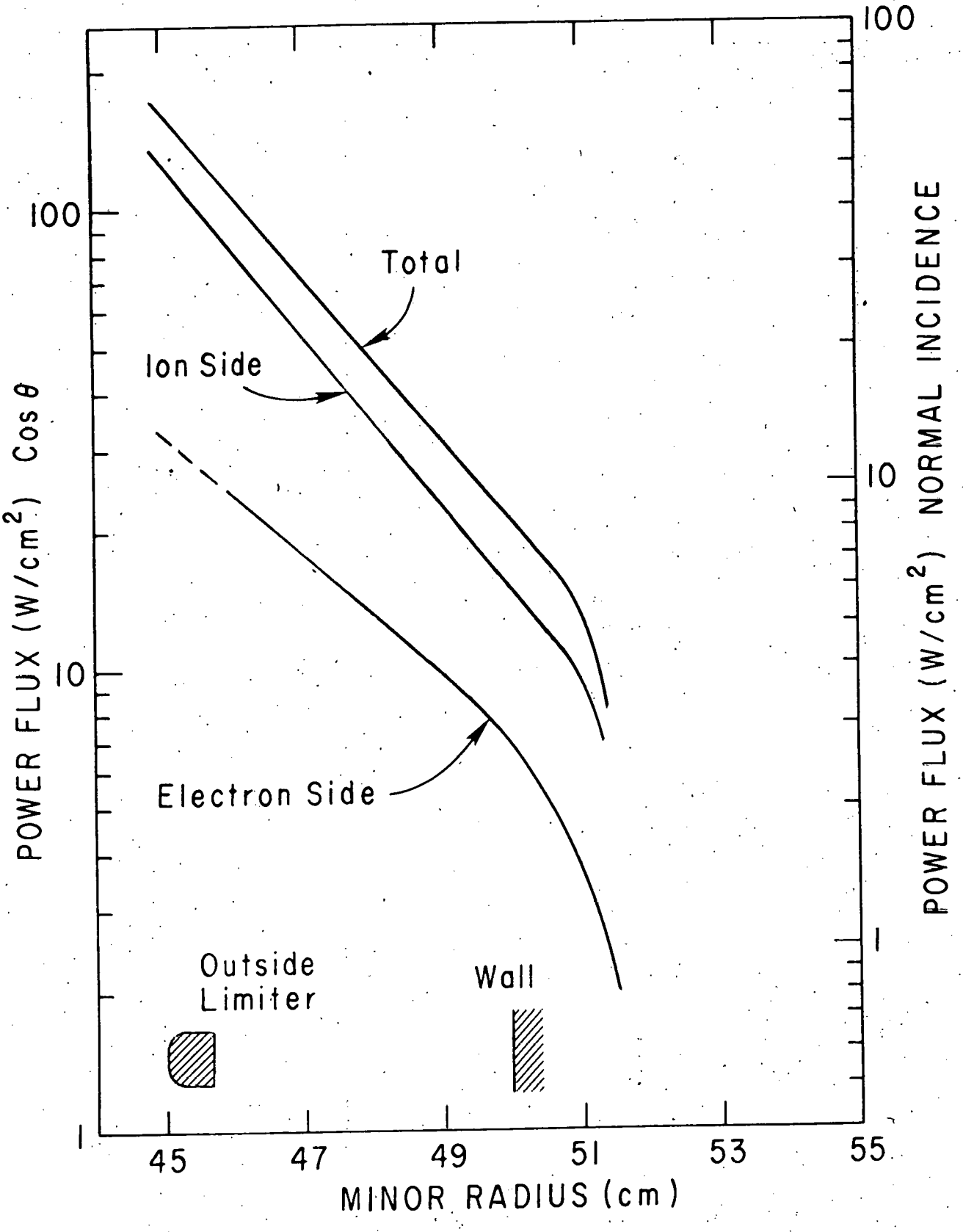

Fig. 4. Power flux to probe due to deuterium bombardment, calculated from the smoothed curves in Figs. 2 and 3. Correction has been made for the angle of probe with respect to B_T.

SURFACE EROSION DUE TO SPUTTERING

Joseph L. Cecchi
Princeton Plasma Physics Laboratory

SUMMARY

Table I summarizes the estimated rates of erosion due to sputtering in various classes of tokamak fusion devices. The only situation in which macroscopic erosion will occur is in reactor-like devices where ion sputtering of the limiter/divertor will result in a erosion rate of > 1 cm/yr and charge exchange neutral sputtering of the first wall could cause erosion at a rate as high as 5 mm/yr. In reactor devices smaller rates of erosion, which could be important for coated components, will occur due to neutral beam bombardment of protective plates (~ .2 mm/yr.). In near term devices, such as TFTR, ion sputtering of the limiter/divertor will cause ~ 20 μm/yr of erosion, while neutral beam sputtering of the protective plates will result in a ~ 2 μm/yr. rate. For present devices erosion due to sputtering is negligible.

TABLE I

ESTIMATED EROSION RATES

DEVICE \ COMPONENT	FIRST WALL	LIMITER/ DIVERTOR†	PROTECTIVE PLATE††
PRESENT	NEGLIGIBLE	NEGLIGIBLE	NEGLIGIBLE
NEAR TERM	NEGLIGIBLE	20 μm/yr.	2 μm/yr.
REACTOR	$\leq$ 5 mm/yr.	> 1 cm/yr.	.2 mm/yr.

†1-10% of first wall area

††~10% of first wall area

I. Introduction

In addition to sputtering being an important mechanism for introducing impurities into fusion plasma devices, it will also effect changes in the surface of materials. Such surface erosion has a number of potential consequences. The surface recession due to sputtering can be important in its own right in a high duty factor reactor environment or, under less severe conditions, where a surface is covered by a thin (~10-50μm) coating as is anticipated in some present and near term devices. Selective erosion of one of the constituents of an alloy can change the surface composition in some materials, possible affecting plasma contamination. Changes in surface morphology due to sputter-induced erosion, such as a roughening of the surface could, lead to changes in the recycling characteristics of the plasma working gas. Surface modifications can also change the emissivity of a material and thus affect its thermal evolution. Finally, local sputtering will result in the eroded material redepositing on other surfaces in the plasma vacuum vessel. In addition to the changes in these surfaces, the freshly deposited material will trap H-isotopes, possibly causing increased tritium retention.

The need for data and calculations to determine the importance of sputter-induced erosion usually coincides with the needs for estimating plasma contamination due to sputtering. One exception is the case of a neutral beam striking an armor plate, where localized sputtering may be unimportant from a contamination point of view, but significant in terms of local erosion and redeposition of eroded material.

In this report the erosion problem is examined for various components in a typical tokamak fusion device including: (1) the first wall, (the vacuum vessel wall or liner) where charge exchange neutrals are predominantly responsible for sputtering; (2) the limiter or divertor neutralizer plate, where ion sputtering due to H isotopes and impurities is important; and (3) the protective plates (armor) where sputtering due to the unabsorbed fraction of the neutral injection beams is important. The emphasis in this report is on the surface recession due to erosion, since the incidence of the more subtle consequences discussed above is difficult to anticipate. Where experimental evidence exists on the occurrence of some of these other processes (e.g. redeposition) it is included.

II. First Wall Erosion

Sputtering of the first wall in a fusion device can occur as a result of bombardment by neutrons, energetic He, H-isotope ions, impurity ions, and charge exchange neutrals. Each of these will be considered.

A. Neutron Sputtering

Because the neutron sputter yield is only ~10^{-4} [BEH 77] the erosion rate from neutron bombardment of the first wall is insignificant. For UWMAK III, for instance, it would be less than 2000 Å/yr.

B. He Sputtering

The surface recession due to energetic He sputtering is inconsequential. Bauer et al. [BAU 79] have shown, however, that He blistering can be a problem in materials where surface removal rate due to sputtering is sufficiently low.

C. H-isotope Ions

Cohen et al. [COH 79A] have estimated that the energy of D^+ ions striking the wall in PLT is ~100 eV. The flux is more difficult to measure, but has been estimated [DOE] to be ~$10^{14} cm^{-2} sec^{-1}$. If we assume a large duty factor characteristic of a reactor, the H-isotope sputtering of Fe (using a sputtering yield of ~10^{-3} [NIS 79] would result in an erosion rate of only ~0.4 μm/yr. It is unlikely that this would be an important erosion mechanism even under reactor-like conditions.

D. Impurity Ions

The sputtering yield for heavy impurity ions can be greater than that for H-isotopes by a factor of ~100 [NIS 79]. The flux, however, should be smaller by at least that factor so it is likely that the effect of impurity ion sputtering will be comparable to that for H-isotope ion sputtering as far as the first wall in concerned.

E. Charge-Exchange Neutral Sputtering

The total charge exchange flux for NUMAK [UW] is $1.7 \times 10^{17} cm^{-2} sec^{-1}$ with an effective temperature of ~200 eV. Taking the sputtering yield to be 10^{-2} (typical for 200 eV D^+ bombarding 304SS [NIS]), the erosion rate would be ~5 mm/yr. The large charge exchange flux in NUMAK is peculiar to that device, however, and almost certainly represents an upper limit. In UWMAK II, for example, the charge exchange flux is ~$7 \times 10^{14} cm^{-2} sec^{-1}$ with an effective temperature of ~8 keV. Taking the sputtering yield to be ~2×10^{-2} we get an erosion rate of only 40 μm/yr.

Near term devices such as TFTR will have a charge exchange flux of ~$3 \times 10^{15} cm^{-2} sec^{-1}$, a most probable energy of ~300 eV [COH 76], and a low duty factor. For a typical Fe sputtering yield of 0.02, the erosion rate would be an inconsequential 0.3 μm/yr.

III. Erosion of the Limiter or Divertor Plate

The limiter or divertor plate in present, near term, and reactor tokamak devices will be subjected to H isotope ion fluxes of ~10^{19}cm^{-2} sec^{-1} [DOE] and impurity fluxes in proportion to the level of plasma contamination. The energy of these ions is affected by their charge and the edge electron temperature which determines the potential of the sheath (~ $3T_e$) through which the ions fall as they strike the limiter/divertor plate. In PLT the energy of D^+ ions striking the limiter has been measured [COH 79] to be ~ 400 eV. This result is inferred from the implantation profile of D in a graphite collector which is scanned through the plasma scrape-off.

In TFR 400, Staudenmaier et al. [STA 78] observed both erosion and deposition of Mo occuring on a carbon probe in the scrape-off region. The rates for each of these processes fell off strongly with increasing distance beyond the limiter, with the erosion rate falling off faster. They inferred that the erosion was caused by sputtering of the Mo limiter due to oxygen ions (possibly multiply charged) accelerated by the plasma sheath potential. Investigations of impurities redeposited on the walls of TFR 400 [SCH 78] show a correlation between local concentrations of redeposited limiter material and trapped deuterium, showing the important connection between limiter erosion and enhanced tritium retention.

In PLT, Cohen et al. [COH 78] concluded that oxygen ion sputtering of the W limiters was an important mechanism responsible for the observed redeposition of W on a surface probe near the wall.

Results from DIVA [OHA 78] show cone formation due to ion sputtering on a gold guard limiter exposed to 10^4 discharges. Ion sputtering is identified as the dominant erosion mechanism of the limiter during the quiet phase of the discharge. Other devices in which ion sputtering of the limiter is a significant erosion mechanism are JFT-2 [GOM 79] and Macrotor [ORE 78].

Because of the considerable ion fluxes, especially the multiply charged impurities, the limiter erosion rate in near term devices such as TFTR could be ~20 um/yr or more. This would be a problem, if low Z and medium Z coatings (10-50 μm) are used to improve the surface characteristic of the limiters. Candidate materials for limiters in TFTR are listed in Table II.

For a reactor, ion sputtering of the limiter/divertor will present the most severe problem since the erosion rates will be very large (> 1 cm/yr.). The need for sputtering data in this case coincides with the need for such rates to determine plasma contamination. Possible materials for reactors are reviewed by Conn [CON 78].

IV. Erosion of Protective Plates

In tokamaks employing neutral beam heating, the vacuum vessel wall must be protected from the unabsorbed fraction of the neutral beam during normal operation, as well as the full neutral beam flux under various fault conditions or when the plates are used in a calorimetric mode. The heat loads on the plates are particularly severe in the latter cases (3-14MW/cm^2) and erosion due to melting or sublimation may be important.

The candidate materials for TFTR protective plates are listed in Table II. Assuming that 10% of the high energy component of the neutral beam is not absorbed by the plasma, Das et al. [DAS 79] estimate from sputtering measurements that ATJ graphite protective plates in TFTR would erode at the rate of ~2 μm/10^4 discharges (an estimated one year running time). Since ATJ graphite probably represents a worst case from an erosion point of view this would not seem to be a problem for near-term devices.

For a reactor which may have 10^2 greater duty factor than TFTR, the erosion rate would be ~.2 mm/yr., assuming the same beam energies and fluxes. This clearly represents an important erosion mechanism and sputtering yields for the candidate materials should be determined for the relevant neutral beam energies.

TABLE II

CANDIDATE MATERIALS FOR TFTR

Vacuum Vessel	Limiters/Protective Plates		
Wall	Bulk	Coatings ~30μm	Claddings ~0.5mm
SS(304LN)	Graphite (ATJS)	TiB_2	V
Inconel 625	Nb	TiC	Ti
	Mo	B_4C	Ni

REFERENCES

[BAU 79] W. Bauer, K.L. Wilson, C.L. Bisson, L.G. Haggmark, and R.J. Goldston, Nucl. Fusion 19 (1979) 93.

[BEH 77] R. Behrisch, O.K. Harling, M.T. Thomas, R.L. Brodzinski, L.H. Jenkins, G.J. Smith, S.F. Wendelken, M.J. Saltmarsh, M. Kaminsky, S.K. Das, C.M. Logan, R. Meisenhevmer, J.E. Robinson, M. Shimotomai, and D.A. Thompson, J. Appl. Phys. 48, 3914 (1977).

[COH 76] S.A. Cohen, J. Vac. Sci. Tech. 13 (1976) 449

[COH 78] S.A. Cohen,H.F. Dylla, S.M. Rossnagel, S.T. Picraux, J.A. Borders, and C.W. Magee, J. Jucl. Mat. 76 & 77 (1978) 459.

[COH 79] S.A. Cohen, private communications. Also see W. Wampler, et al. Princeton Plasma Physics Lab. Report PPPL 1537 (1979) Presented at Miami Conference Jan 1979.

[CON 78] R.W. Conn, J. Nucl. Mat. 76 & 77 (1978) 103.

[DAS 79] S.K. Das, M. Kaminsky, R. Tishler, and J. Cecchi, Fusion Reactor Materials Conf., Miami, Fla. 29-31 Jan 1979.

[DOE] The Fusion Reactor Material Program Plan, Sec. III, Report DOE/ET-0032/3 (1978).

[GOM 79] Y. Gomay, N. Fuyisawa, and M. Maeno, Fusion Reactor Material Conf., Miami, Fla. 29-31 Jan 1979.

[OHA 78] K. Ohasa, S. Sengoku, H. Maeda, H. Ohtsuka, S. Yamamoto, S. Kasai, M. Nagami, K. Odajima, H. Kimura, and Y. Shimomura, Tokai Research Establishment report JAERI-M 7935 (1978).

[ORE 78] L. Oren, R.J. Taylor, and F. Schwirzke, J. Nucl. Mat. 76 & 77 (1978) 412.

[NIS 79] M. Nishi, M. Yamada, S. Suckewer, and E. Rosengaus, PPPL 1521 1979.

[SCH 78] B.M.U. Scherzer, R. Behrisch, R.S. Blewer, H. Schmidl, and TFR group, 10th Symposium on Fusion Technology, Padova, Italy, August 1978.

[STA 78] G. Staudenmaier, P. Staib, G. Venus, and TFR Group, J. Nucl. Mat. 76 & 77 (1978) 445.

LIGHT ION SPUTTERING YIELDS

J. B. Roberto
Solid State Division
Oak Ridge National Laboratory
Oak Ridge, Tennessee 37830

SUMMARY

The present status of light ion sputtering yields is reviewed. The emphasis is on total physical sputtering yields for hydrogen isotopes and helium, and on those parameters which affect total yields such as angle of incidence, dose and temperature. Two energy regions are distinguished; a low-energy near-threshold region characteristic of plasma ion temperatures and a higher energy region characteristic of neutral beams and energetic alphas. In each case, the existing experimental data are reviewed and compared with theoretical predictions for total yields and angular, dose and temperature effects.

For low-energy sputtering, extensive total yield measurements have been reported recently for light ions on a wide variety of metals, metal carbides and oxides, and on iron and nickel alloys. The normal incidence yields can be described by an empirical relationship involving ion and target mass and surface binding energy. Angle of incidence effects in light ion sputtering have been studied less extensively, but can be described adequately by a $(\cos\theta)^{-1}$ dependence except for the lightest ions at higher energies. Temperature effects are not significant in physical sputtering by light ions but can be important when the sputtering is dominated by chemical processes.

For high-energy sputtering, there have been very few experimental measurements for light ions. The existing yield data are described approximately by Boltzmann transport theory although substantial quantitative differences have been observed in some cases. There are no measurements of angle of incidence effects for higher energy light ions although significant deviation from the magnitude of angular effects observed at lower energies is not expected.

In summary, the existing experimental data and empirical relationships for low-energy light ion sputtering are adequate for factor-of-two estimates of total yields in all materials and compounds where the sputtering is determined by collisional effects. For higher energy light ions ($E > 10$ keV), existing theories predict the correct energy dependence of the sputtering but overestimate the yields by factors of as much as ten in some cases. Angle of incidence effects have not been studied extensively but the available data can be modeled adequately using transport theories. Temperature effects are unimportant in collisional sputtering by light ions. Overall, physical sputtering yields by light ions are understood adequately for the present needs of the fusion community with the exception of additional experimental measurements for specific materials at low doses and in the high energy region.

1. Introduction

The physical sputtering of solid surfaces by light ions has been studied for astrophysical considerations and more recently for its possible role in wall erosion and impurity introduction in fusion devices. Much of the early literature has been reviewed in two monographs.[1,2] More recent results can be found in review articles[3] and in an annually updated tabulation.[4] The most extensive data for low-energy light ion sputtering are found in a recently prepared research summary.[5] In the following, the present understanding of light ion sputtering yields is reviewed. The emphasis is on total physical sputtering yields for hydrogen isotopes and helium, and on those parameters which affect total yields such as angle of incidence, dose and temperature.

2. Low-Energy Sputtering

The low-energy or near threshold region includes incident light ion energies from the sputtering threshold (typically 100-200 eV) to the maximum in the sputtering yield (1-3 keV). More generally, this region is characterized by values of the Lindhard dimensionless energy parameter $\varepsilon \lesssim 0.3$ corresponding to the maximum in the nuclear stopping cross section. Low-energy light-ion sputtering is not well understood theoretically,[6] but can be significant in fusion devices since the low-energy region incorporates maxima in both the light-ion flux to the wall and the sputtering yield.

Normal Incidence Yields. Low-energy light-ion sputtering yields have been investigated systematically over the last few years for a wide variety of targets including many metals and proposed coating materials. The ion-target combinations for which fairly complete energy-dependent H, D and He sputtering data are available are listed in Table I. Specific results for B_4C, C, Ti, stainless steel and Mo are shown in Figs. 1a-e. Most of the normal incidence measurements have been performed using gravimetric techniques although other methods such as Rutherford backscattering have led to similar results. Much of the available data are tabulated in references 4 and 5.

The low-energy sputtering yields for a large variety of ion-target combinations show similarities if the energy dependence is characterized by a parameter[7] E/E_{th} where E is the ion energy and E_{th} is the threshold for sputtering as determined from the surface binding energy. This is illustrated in Fig. 2 where normalized sputtering yields for a wide variety of ion-target combinations are shown to fall on a universal curve. Absolute yields for a given ion-target combination can be described by the empirical relationship[5,7]

$$Y = 6.4 \times 10^{-3} M_2 \gamma^{5/3} E'^{1/4} (1 - 1/E')^{7/2} \qquad (1)$$

where M_2 is the target atomic mass number, $\gamma = 4 M_1 M_2/(M_1 + M_2)^2$ is the maximum elastic transferred energy and $E' = E/E_{th}$. The solid curves in Figs. 1a-e are given by Eq. 1 and represent an excellent fit to the experimental data. Eq. 1 is accurate to within a factor of ~2 for normal incidence light ion sputtering yields for most targets for energies up to $20\ E_{th}$.

The results of Figs. 1 and 2 demonstrate the importance of the threshold energy in describing low-energy sputtering yields. For mass ratios $M_1/M_2 \leq 0.4$, the threshold energy for sputtering can be written[5,7]

$$E_{th} = E_B/(\gamma(1-\gamma)) \qquad (2)$$

where E_B is the surface binding energy. Threshold energies for a variety of ion-target combinations are given in Table 2. For E_{th} not listed in the table, an estimate based on Eq. 2 taking E_B as the sublimation energy[8] is usually adequate.

Angle of Incidence. The variation of light-ion sputtering yields with angle of incidence has been studied less extensively, although a somewhat representative group of metal targets has been investigated, as indicated in Table III. Specific results[5] for 1-8 keV H, D and He sputtering of Ni are shown in Fig. 3. Additional data are tabulated in reference 5. For the lightest ions at the higher energies, the yields increase significantly as grazing incidence is approached and can be more than ten times greater than normal incidence yields. The increase is somewhat faster than the $(\cos\theta)^{-1}$ dependence of the energy deposited in the near surface region. This faster than cosine dependence probably reflects anisotropies in the development of the collision cascade.

For heavier ions at lower energies, the angular effects are less pronounced. This is a consequence of increased reflection of the sputtering beam at grazing incidence for heavier and less energetic ions. This result has been observed in computer calculations[9] for the case of 3 keV particles on Cu. Grazing incidence can be approached more closely for lighter ions at the same energy resulting in greater sputtering yields. Angle of incidence effects are probably not significant for ions heavier than He in fusion devices.

The angular effects have been modeled using a sputtering code based on a transport model[10] which removes the approximations of the Sigmund theory which are objectionable for light ions. As shown in Fig. 4, the agreement between theory and experiment for 4 keV H on Ni indicates a reasonable understanding of angle of incidence variations in sputtering. In particular, the angular effects are primarily kinematic and related to calculable quantities such as reflection and cascade geometry which scale with incident energy and ion and target mass.

Flux and Dose Effects. There have been very few measurements of flux and dose effects in light-ion sputtering. The results of a recent measurement[11] for H sputtering of Au are summarized in Fig. 5. These results indicate a constant sputtering yield for 0.5 and 1.0 keV H on Au at doses between 10^{18} and $10^{19}/cm^2$. On the other hand, laser fluorescence measurements[12] for H sputtering of Fe show a significant suppression of the Fe yield for doses below $10^{17}/cm^2$.

Non-linear effects in sputtering due to flux and dose are related primarily to target loading by the incident ions and to surface effects such as oxide layers and surface topography changes. Target loading effects have been studied for a hypothetical Fe-H system by computer simulation.[13] The results suggest that the presence of H can decrease the metal atom physical sputtering yield by as much as a factor of two as compared with the pure metal at high (~ 100 atom per cent) H concentrations.

Oxide layers have also been shown to reduce bulk yields and may account for the low initial Fe yield reported above. The surface condition can influence not only total yields but also the charge state of the sputtered particles which affects their behavior in the tokamak. A proper evaluation of flux and dose effects in tokamaks is closely related to the condition of the surface region and is therefore best studied in situ.

Temperature Effects. For heavy ions, increases in sputtering yields of several orders of magnitude have been observed at high temperatures.[14] These results are explained in terms of a thermal spike model where the spike temperature becomes sufficiently high for evaporation to overtake collisional sputtering. This mechanism is not important in light-ion sputtering since the energy density in the cascade is too diffuse for a significant spike effect.

Nevertheless, temperature variations have been observed in H sputtering of C, stainless steel and SiC. For carbon,[15] increased yields of up to a factor of ~10 have been reported[14] at higher temperatures and are related to the formation of CH_4[16] at the surface of the carbon. In stainless steel, an increase in the sputtering rate of a factor of ~2 is observed at 400 - 500°C. This increase correlates with changes in the surface composition due to diffusion processes in this temperature region. The erosion yield of SiC[17] shows a slight increase (~ 30%) at 600°C as compared with the room temperature value.

Overall, temperature effects are not considered important in physical sputtering by light ions since only a small amount of the particle energy is deposited in nuclear motion. Chemical sputtering effects, however, are very sensitive to temperature and can result in significant yield increases at higher temperatures, particularly in graphite.

3. High-Energy Sputtering

The high-energy region includes light ion energies greater than the maximum in the nuclear stopping, generally above a few keV. Sputtering at neutral beam energies (up to ~100 keV) and by fusion alpha particles (up to 3.5 MeV) fall into this category. High energy sputtering can be described approximately by analytical solutions to transport equations although quantitative differences between experimental and theoretical yield values have been observed.

Normal Incidence Yields. There have been very few measurements of light-ion sputtering yields in the high-energy region. The available experimental data are summarized in Table IV and include no results for stainless steel or for MeV He sputtering. The most extensive results are for Cu[4] where H, D and He normal incidence yields have been measured over a considerable energy range. These results are tabulated in Table V and compared with predictions of the Sigmund[18,19] transport theory. The agreement between theory and experiment is generally within a factor of two and is also observed for high energy light-ion sputtering of B, Ag, and Au.[19,20] On the other hand, hydrogen-isotope sputtering yields for Nb[19] and Mo[21] are ~5 times lower than theoretical values. In general, the Sigmund theory predicts the correct energy dependence of the sputtering and is useful as a first estimate of light-ion physical sputtering yields at high energies. A better estimate of the sputtering yield is often obtained by normalizing to the experimental value at the peak of the sputtering curve and extrapolating to higher energies

assuming a 1/E dependence as predicted by Sigmund. This 1/E dependence for high energy light-ion sputtering is illustrated in Fig. 6 for the case of Cu and Nb targets. Most of the available data in the high-energy region is tabulated in reference 4.

Angle of Incidence. There are no measurements of the variation of light ion sputtering yields with angle of incidence for energies above 10 keV. It is expected, however, that the magnitude of the increases in yield observed at grazing incidence at high energies will not be significantly greater than observed at 10 keV. This is a consequence of the partial offset of increases in angular effects due to the closer approach angles allowed at high energy by the decrease in the nuclear stopping cross section above 10 keV.

Flux, Dose and Temperature Effects. No significant variations are expected for physical sputtering except possibly at low doses (see discussion under low energy sputtering).

4. Preferential and Non-Collisional Sputtering

Preferential sputtering of alloys and compounds generally leads to depletion of the surface layers in the lighter component of the material. For Ta_2O_5, it has been shown[22] that the changes in surface stoichiometry due to sputtering are related to projectile mass and energy. This suggests that the preferential sputtering is a dynamical energy-transfer effect. For carbides,[7] the energy dependence of the yields follows that of the heavy component indicating that the threshold for steady-state sputtering is determined by the heavier atom. The sputtering yields of multi-component systems generally follow the elemental yields when characterized by an appropriate binding energy.

Non-collisional sputtering can include chemical, electronic excitation and thermal evaporation mechanisms. Chemical effects can increase hydrogen-isotope sputtering yields by an order of magnitude or more over collisional sputtering. These effects are described in detail elsewhere in these proceedings. Electronic excitation and thermal evaporation mechanisms are important in alkali halide systems where charge transfer processes and low vapor pressures can lead to increased yields.[23] There is evidence that electronic excitation processes also contribute to the very high sputtering yields of water ice[24] and condensed gases.[25] For insulators and ceramics, the possible role of electronic effects has not been established although results from light-ion sputtering of Al_2O_3, BeO and B suggest that collisional sputtering is the dominant mechanism in these materials .

Acknowledgement

The author thanks M. T. Robinson for helpful discussions during the preparation of this review.

References

1. R. Behrisch, Erg. exakt. Naturwiss. 35, 295 (1964).
2. M. Kaminsky, Atomic and Ionic Impact Phenomena on Metal Surfaces, (Acad. Press, New York 1965).
3. B. M. U. Scherzer, R. Behrisch and J. Roth, p. 353 in Proc. Int. Symp. on Plasma Wall Interaction, Jülich 1976 (Pergammon Press, Oxford 1977).
4. C. F. Barnett et al., Atomic Data for Controlled Fusion Research, Vol. II, ORNL-5207, Oak Ridge 1977.
5. J. Roth, J. Bohdansky, and W. Ottenberger, MPI für Plasmaphysik report IPP 9/26, Garching, May 1979.
6. R. Behrisch et al., Appl. Phys. 18, 391 (1979).
7. J. Roth, J. Bohdansky and A. P. Martinelli, Proc. Int. Conf. on Ion Beam Modification of Materials, Budapest, Sept. 4-8, 1978 (to be published).
8. JANAF Thermo-Chemical Tables, ed. D. R. Stull, H. Prophet, NSRDS-NBS 37.
9. M. Hou and M. T. Robinson, Appl. Phys. 17, 371 (1978).
10. T. J. Hoffman, H. Dodds, M. T. Robinson and D. K. Holmes, Nucl. Sci. Eng. 68, 204 (1978).
11. J. B. Roberto, R. A. Zuhr, J. L. Moore and G. D. Alton, J. Nucl. Mat. (in press).
12. J. Bohdansky, private communication.
13. O. S. Oen and M. T. Robinson, J. Nucl. Mat. 76-77, 370 (1978).
14. M. W. Thompson, Defects and Radiation Damage in Metals, (Cambridge University Press, Cambridge 1969), p. 250.
15. J. N. Smith and C. H. Meyer, J. Nucl. Mat. 76-77, 193 (1978).
16. J. Roth, J. Bohdansky and W. Hofer, p. 309 in Proc. Int. Symp. on Plasma Wall Interaction, Jülich 1976 (Pergammon Press, Oxford 1977).
17. J. Roth, J. Bohdansky, W. Poschenrieder and M. K. Sinha, J. Nucl. Mat. 63, 222 (1976).
18. P. Sigmund, Phys. Rev. 184, 383 (1969).
19. R. Weissman and P. Sigmund, Radiat. Effects 19, 7 (1973).
20. C. Miyagawa, Y. Ato and Y. Moriya, J. Appl. Phys. 49, 6194 (1978).
21. M. Kaminsky, S. K. Das and J. Cecchi, Proc. Tenth S.O.F.T., Padova, Italy, Sept. 4-8, 1978 (to be published).
22. E. Taglauer and W. Heiland, Appl. Phys. Lett. 33, 950 (1978).
23. W. Husinsky et al., J. Appl. Phys. 48, 4734 (1977).
24. W. L. Brown, L. J. Lanzerotti, J. M. Poate and W. M. Augustyniak, Phys. Rev. Lett. 40, 1027 (1978).
25. S. K. Erents and G. M. McCracken, p. 625 in Atomic Collisions in Solids, Vol. II (Plenum, New York 1975).

Tables

Table I. Materials for which energy-dependent normal incidence sputtering yields are available for low-energy H, D and He. Materials in parentheses have less complete yield data. (refs. 4 and 5)

Elements

Be, C, Al, Si, Ti, (V), (Cr), Fe, Co, Ni, Cu, (Zr), Nb, Mo, (Pd), Ag, Ta, W, (Ir), (Pt), Au, (U)

Compounds and Alloys

Al_2O_3, B_4C, BeO, Ni-alloys, SAP, SiC, SiO_2, stainless steels, TaC, Ta_2O_5, TiC, WC, ZrC

Table II. Threshold energies for light-ion sputtering. (ref. 5).

Target	E_{th}(eV)		
	H	D	^{4}He
Al	53	34	20.5
Au	184	94	44
Be	27.5	24	33
C	9.9	11	16
Fe	64	40	35
Mo	164	86	39
Ni	47	32.5	20
Si	24.5	17.5	14
Ta	460	235	100
Ti	43.5		22
V	76		27
W	400	175	100
Zr			60

Table III. Materials for which sputtering yields are available for low-energy light ions as a function of angle of incidence. (refs. 4 and 5)

Materials

Mo, Ni,	(H, D, He)
Nb	(D, He)
Au	(H,D)
TaC, W	(H)

Table IV. Materials for which energy-dependent normal incidence sputtering yields are available for high-energy H, D and He. Materials in parentheses have less complete yield data. (ref. 4)

Elements

(B), (C), (Ti), Cu, Nb, Ag, (Ta), (Au), U

Table V. Comparison of high-energy normal incidence sputtering yields for H, D and He on Cu with theoretical predictions based on Sigmund theory ($\alpha = 1/2$)

Energy (keV)	Yields (Experiment/Theory)		
	H	D	He
10	.016/.017	.062/.035	.23/.26
20	.009/.012	.040/.024	.18/.27
30	.006/.009	.030/.018	.15/.26
50	.004/.006	.019/.013	-
100	.002/.004	.008/.007	-

Figure Captions

Fig. 1. Normal incidence low-energy sputtering yields for H, D, and ^{4}He ions on (a) B_4C, (b) C, (c) Ti, (d) 316 and 304 stainless steel, and (e) Mo. The solid curves are calculated from Eq. 1 using E_{th} from Table II. (ref. 5).

Fig. 2. Universal behavior of the normalized sputtering yield in the threshold region (ref. 7).

Fig. 3. Variation of the sputtering yield with angle of incidence for low-energy light ion sputtering of Ni (ref. 5).

Fig. 4. Sputtering yield dependence on angle of incidence for 4 keV H on Ni (ref. 10).

Fig. 5. Total sputtered material vs ion dose for 0.5 and 1.0 keV H on Au (ref. 11).

Fig. 6. Energy dependence of the normal incidence sputtering yield for light ions on Cu and Nb. The dashed line represents the 1/E dependence expected at high energies from Sigmund theory. (refs. 3 and 4).

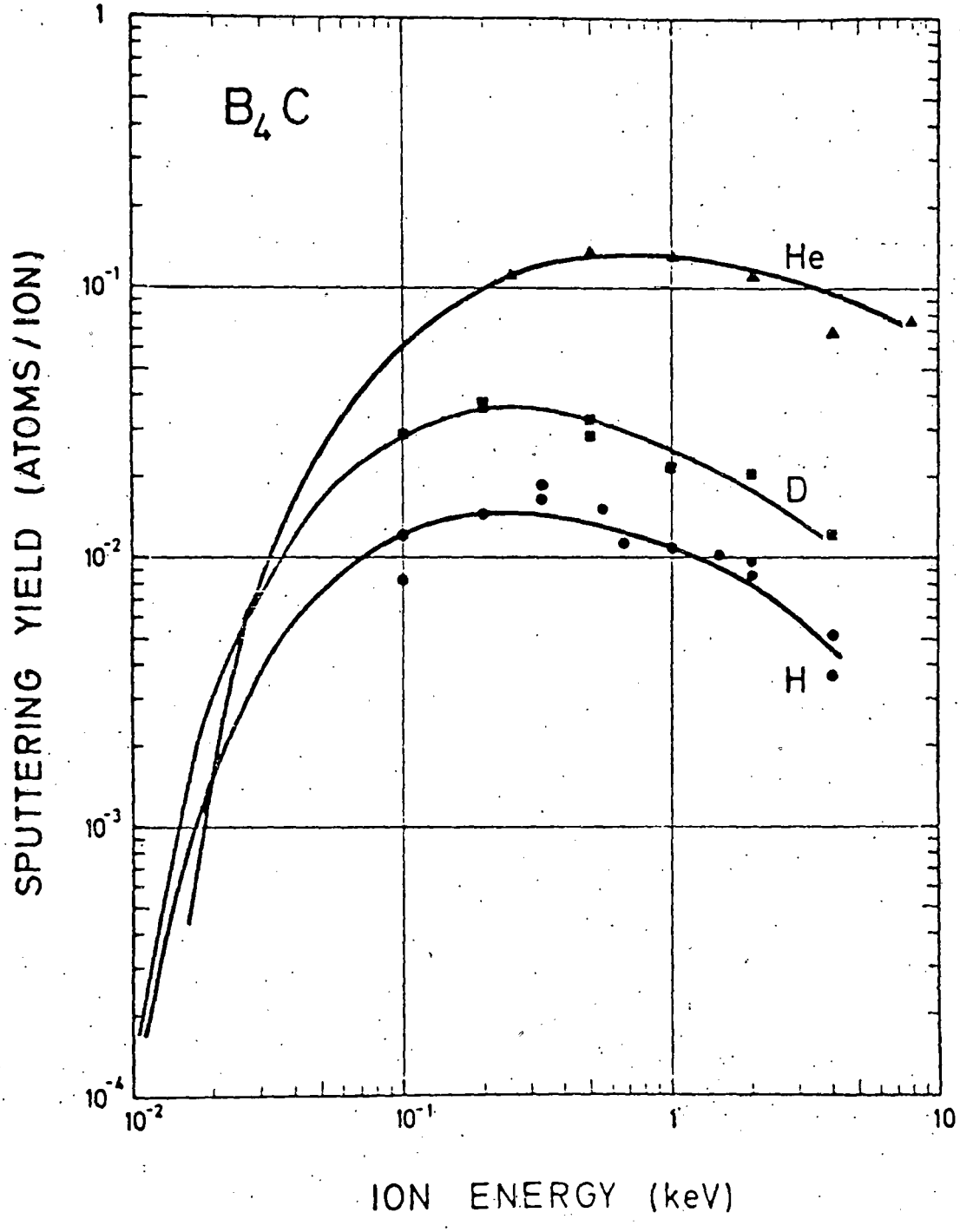
B4C
He
D
H
SPUTTERING YIELD (ATOMS / ION)
ION ENERGY (keV)
1
10-1
10-2
10-3
10-4
10-2
10-1
1
10

Fig. 1-a

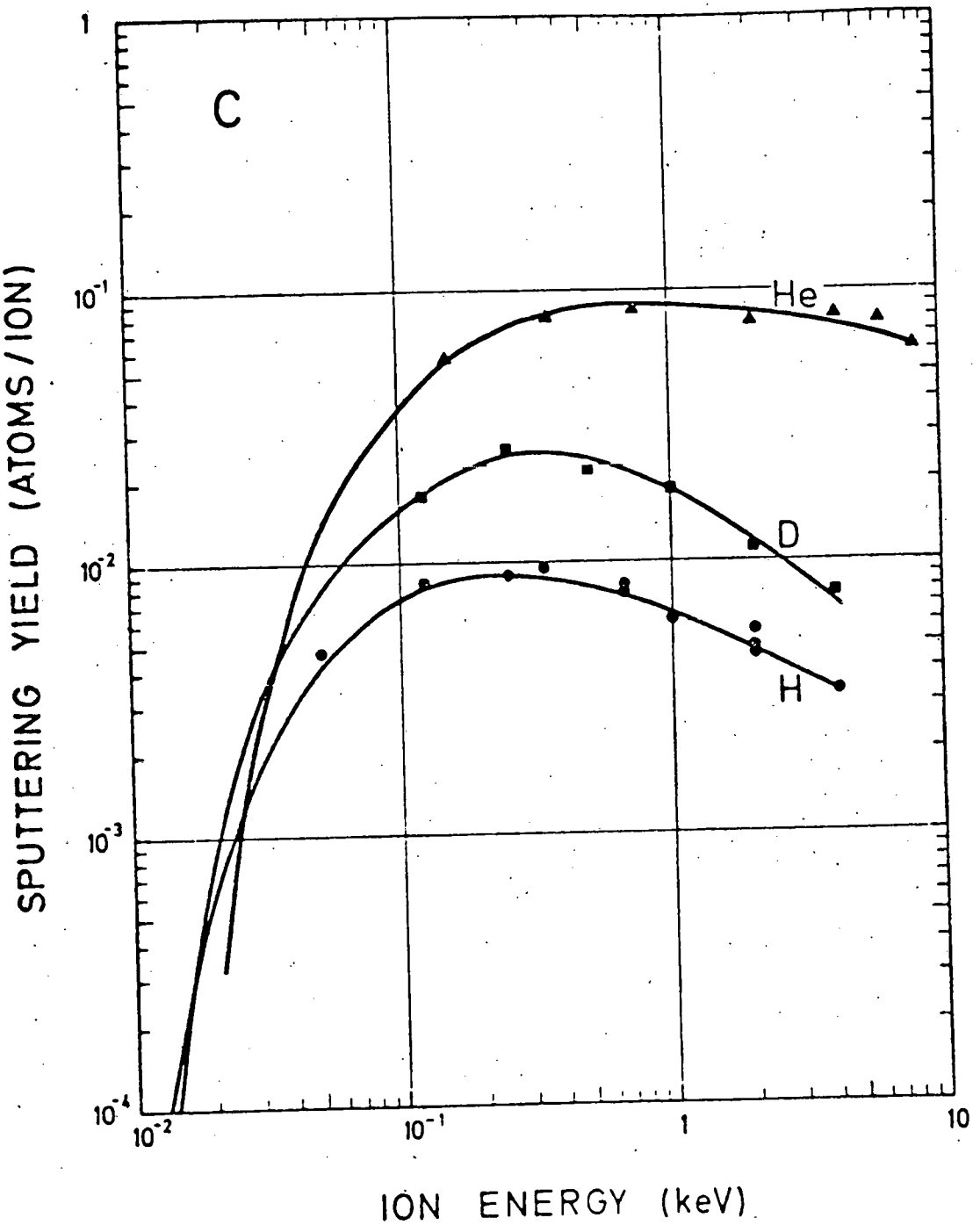
C
He
D
H
SPUTTERING YIELD (ATOMS / ION)
ION ENERGY (keV)
1
10^{-1}
10^{-2}
10^{-3}
10^{-4}
10^{-2}
10^{-1}
1
10

Fig. 1-b

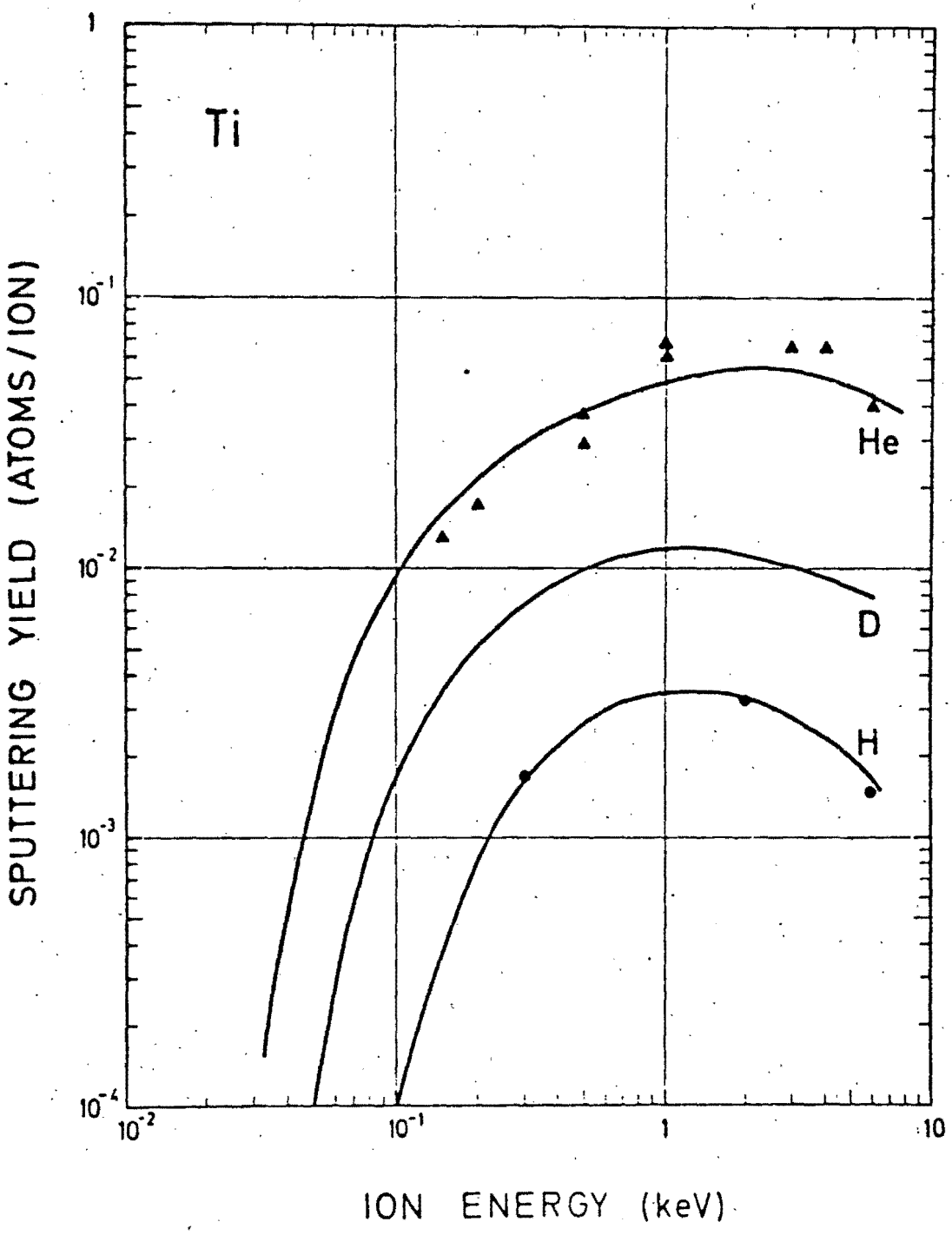
Ti
SPUTTERING YIELD (ATOMS / ION)
ION ENERGY (keV)
He
D
H
1
10^{-1}
10^{-2}
10^{-3}
10^{-4}
10^{-2}
10^{-1}
1
10

Fig. 1-c

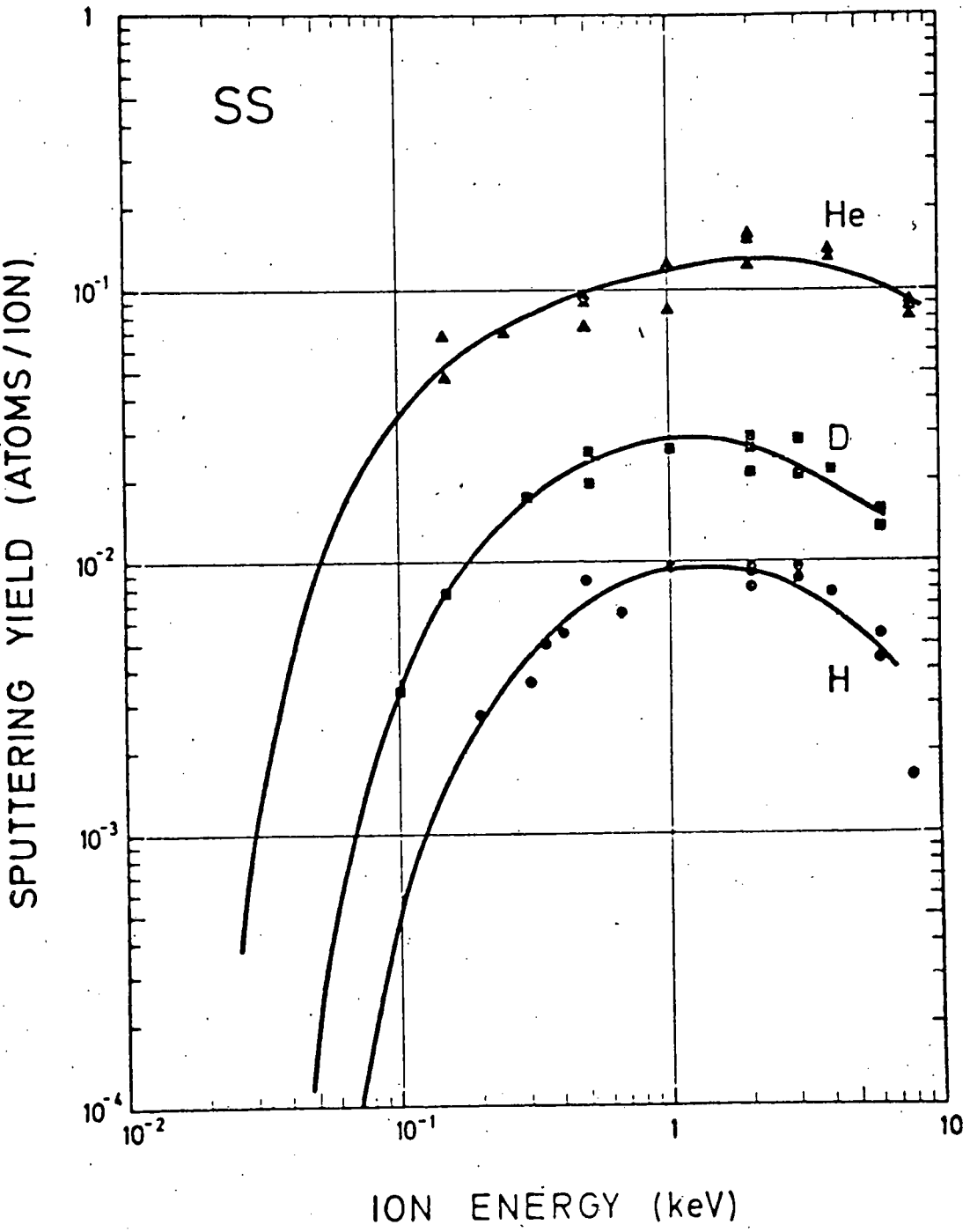
SS
He
D
H
SPUTTERING YIELD (ATOMS / ION)
ION ENERGY (keV)
1
10^{-1}
10^{-2}
10^{-3}
10^{-4}
10^{-2}
10^{-1}
1
10

Fig. 1-d

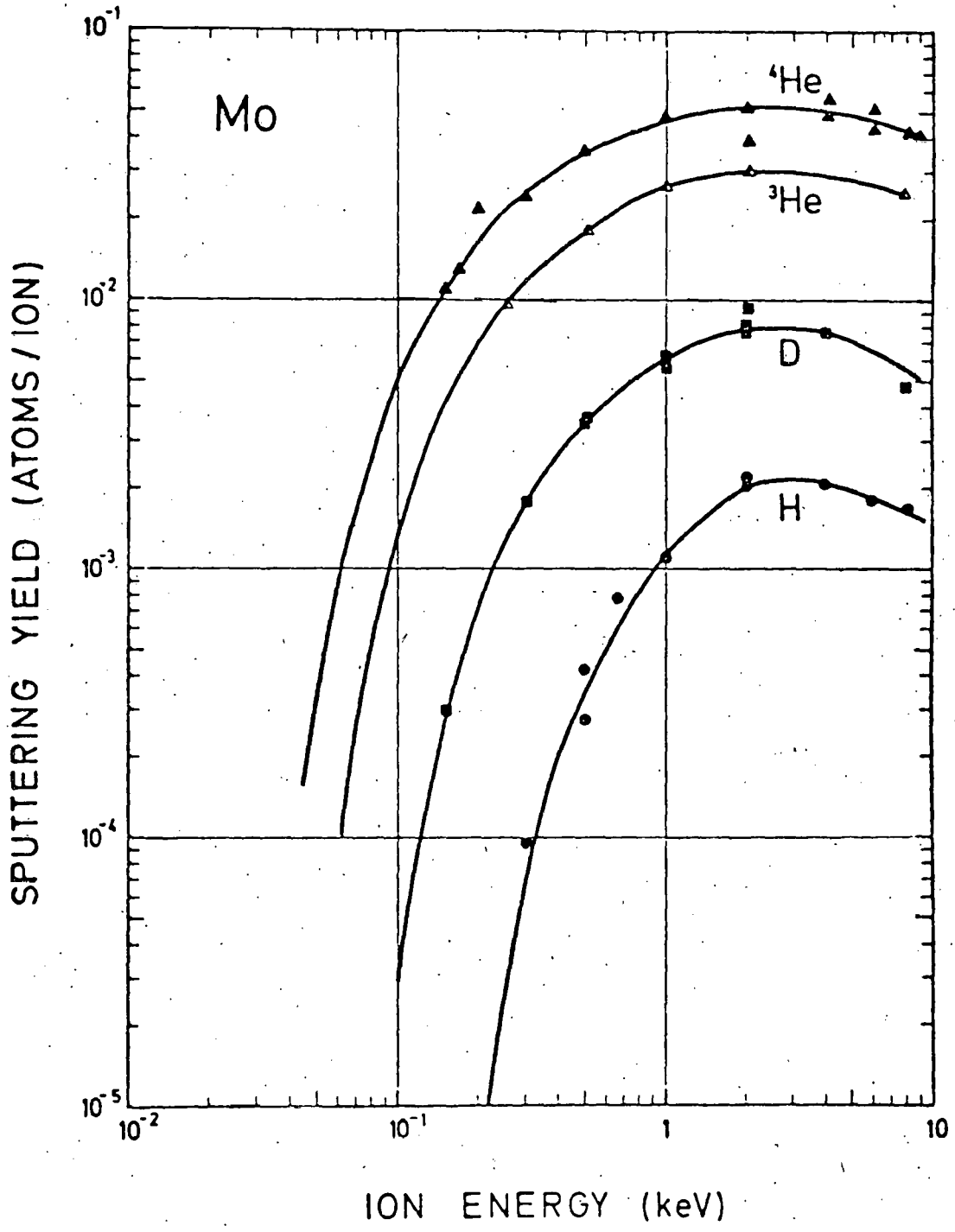
Mo
⁴He
³He
D
H
SPUTTERING YIELD (ATOMS / ION)
ION ENERGY (keV)
10⁻¹
10⁻²
10⁻³
10⁻⁴
10⁻⁵
10⁻²
10⁻¹
1
10

Fig. 1-e

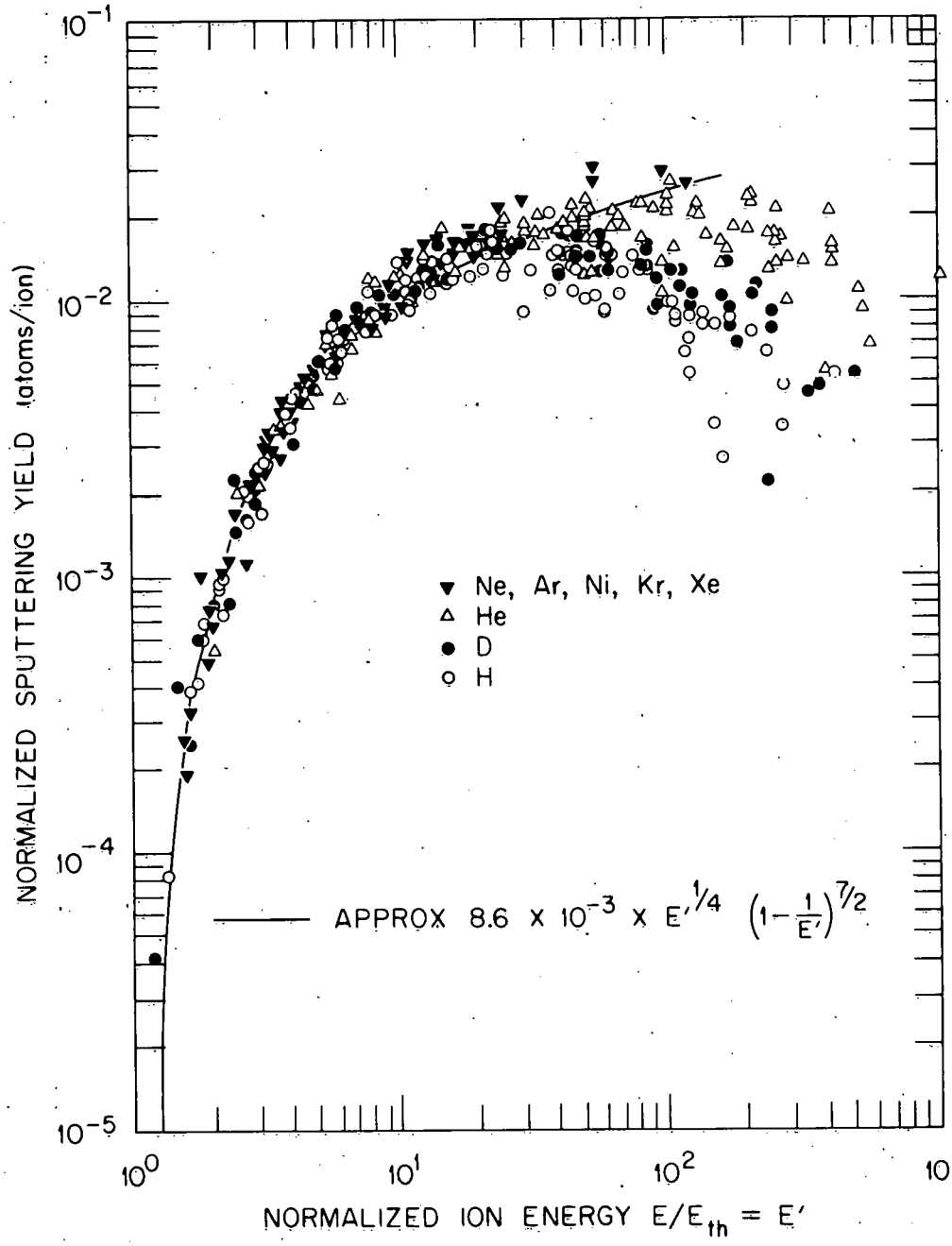
NORMALIZED SPUTTERING YIELD (atoms/ion)
10^{-1}
10^{-2}
10^{-3}
10^{-4}
10^{-5}
10^{0}
10^{1}
10^{2}
10^{3}
NORMALIZED ION ENERGY $E/E_{th} = E'$
▼ Ne, Ar, Ni, Kr, Xe
△ He
● D
○ H
APPROX $8.6 \times 10^{-3} \times E'^{1/4} \left(1-\frac{1}{E'}\right)^{7/2}$

Fig. 2

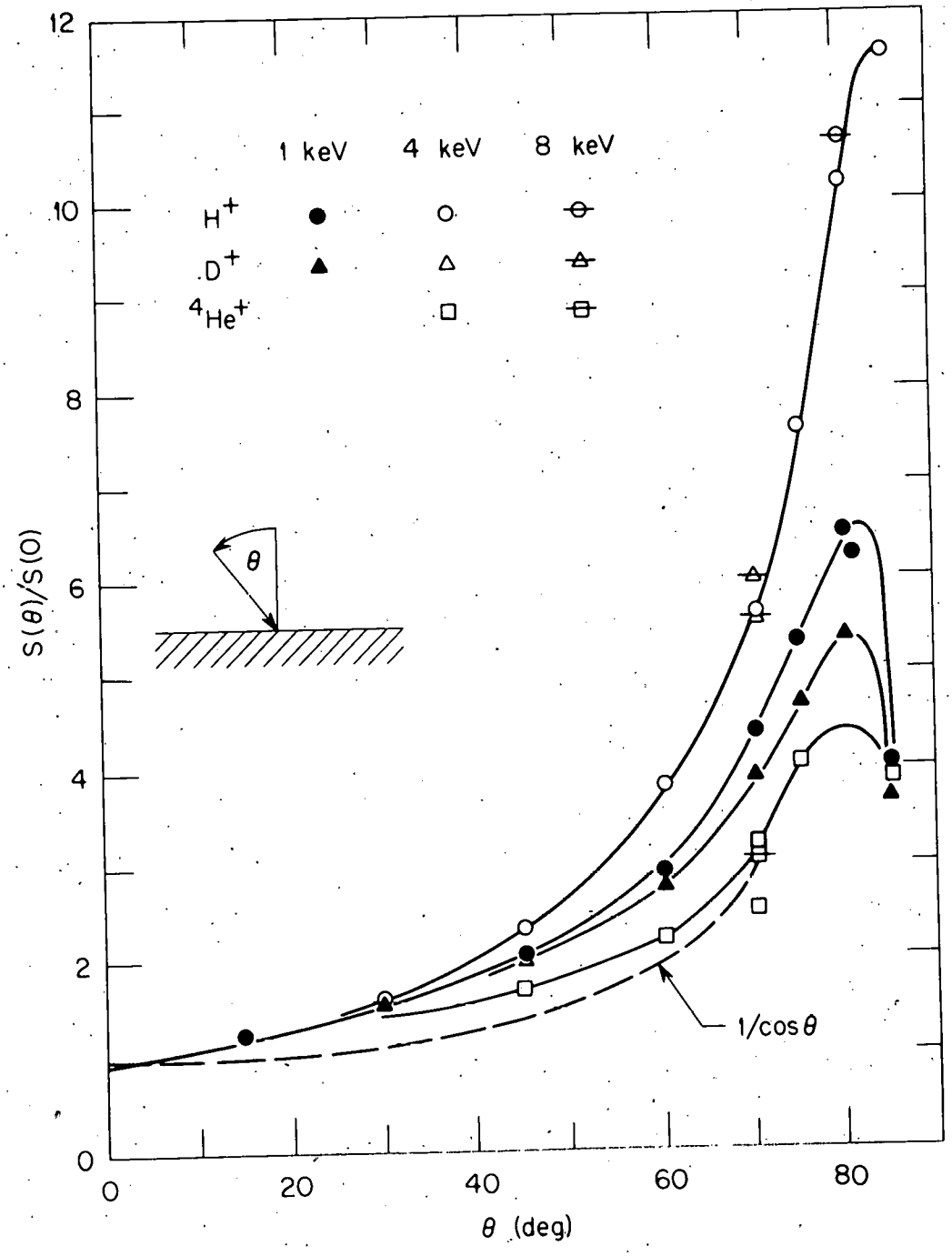

Fig. 3

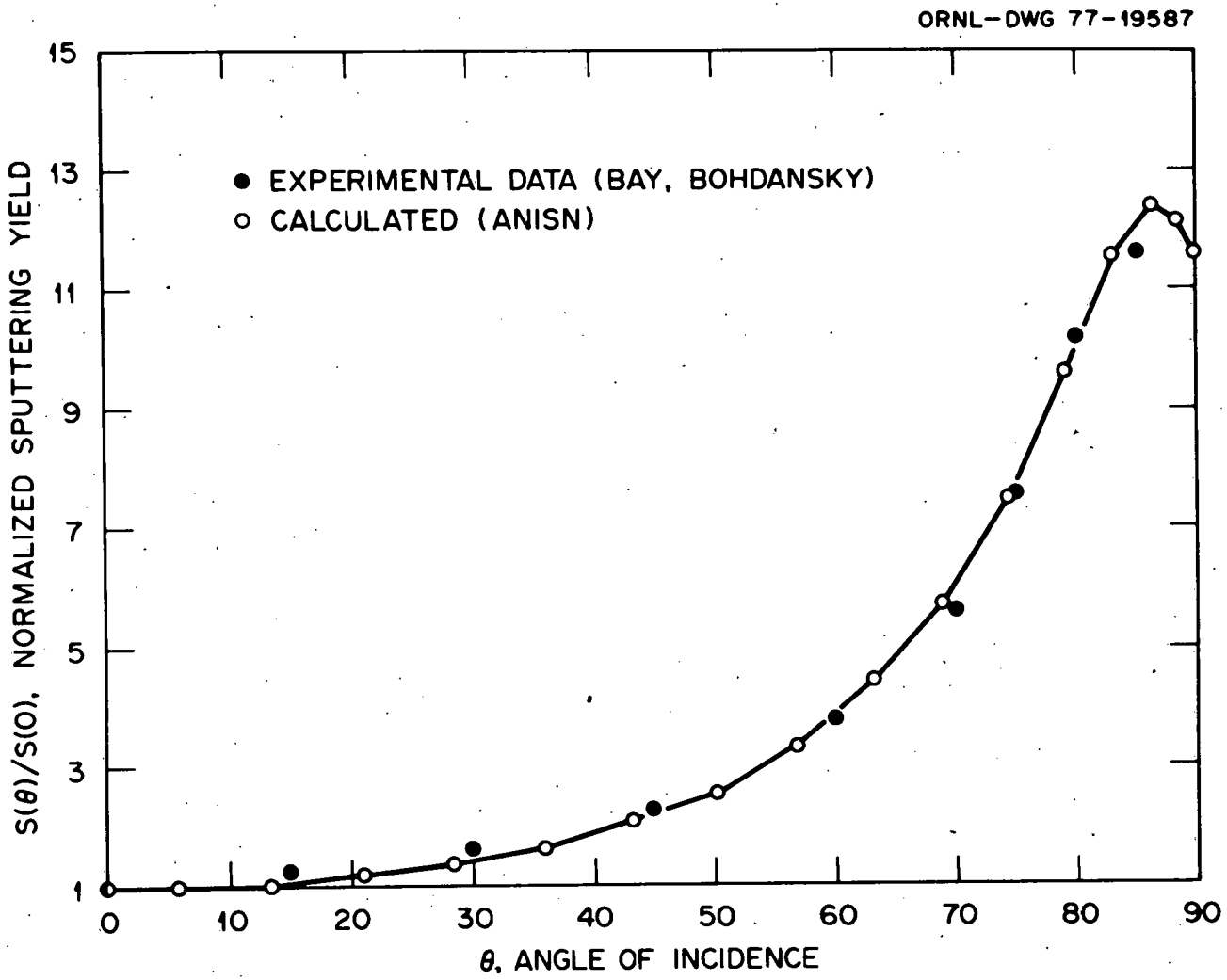

FIGURE 3. SPUTTERING YIELD DEPENDENCE ON ANGLE OF INCIDENCE FOR 4 keV PROTONS INCIDENT ON NICKEL.

Fig. 4

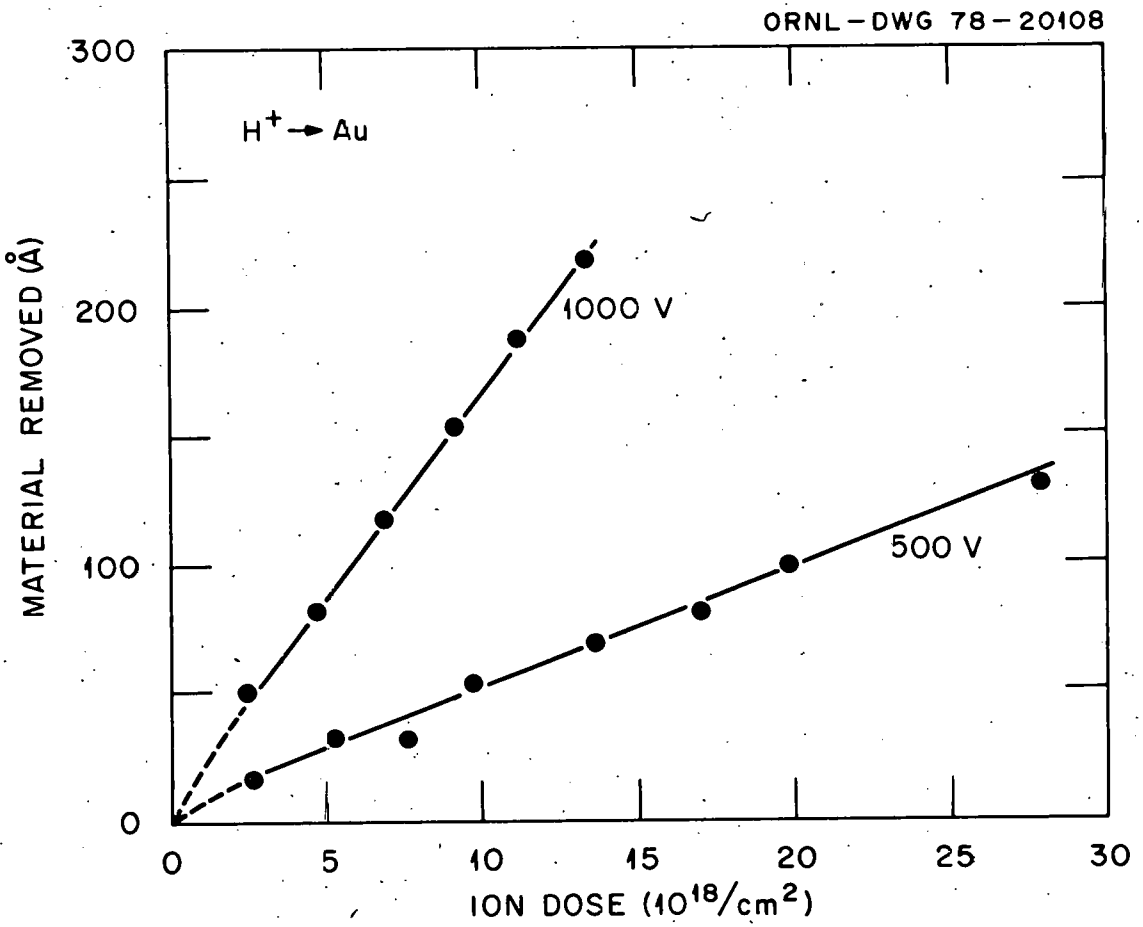
ORNL-DWG 78-20108
300
200
100
0
$H^+ \rightarrow Au$
1000 V
500 V
MATERIAL REMOVED (Å)
0
5
10
15
20
25
30
ION DOSE ($10^{18}/cm^2$)

Fig. 5

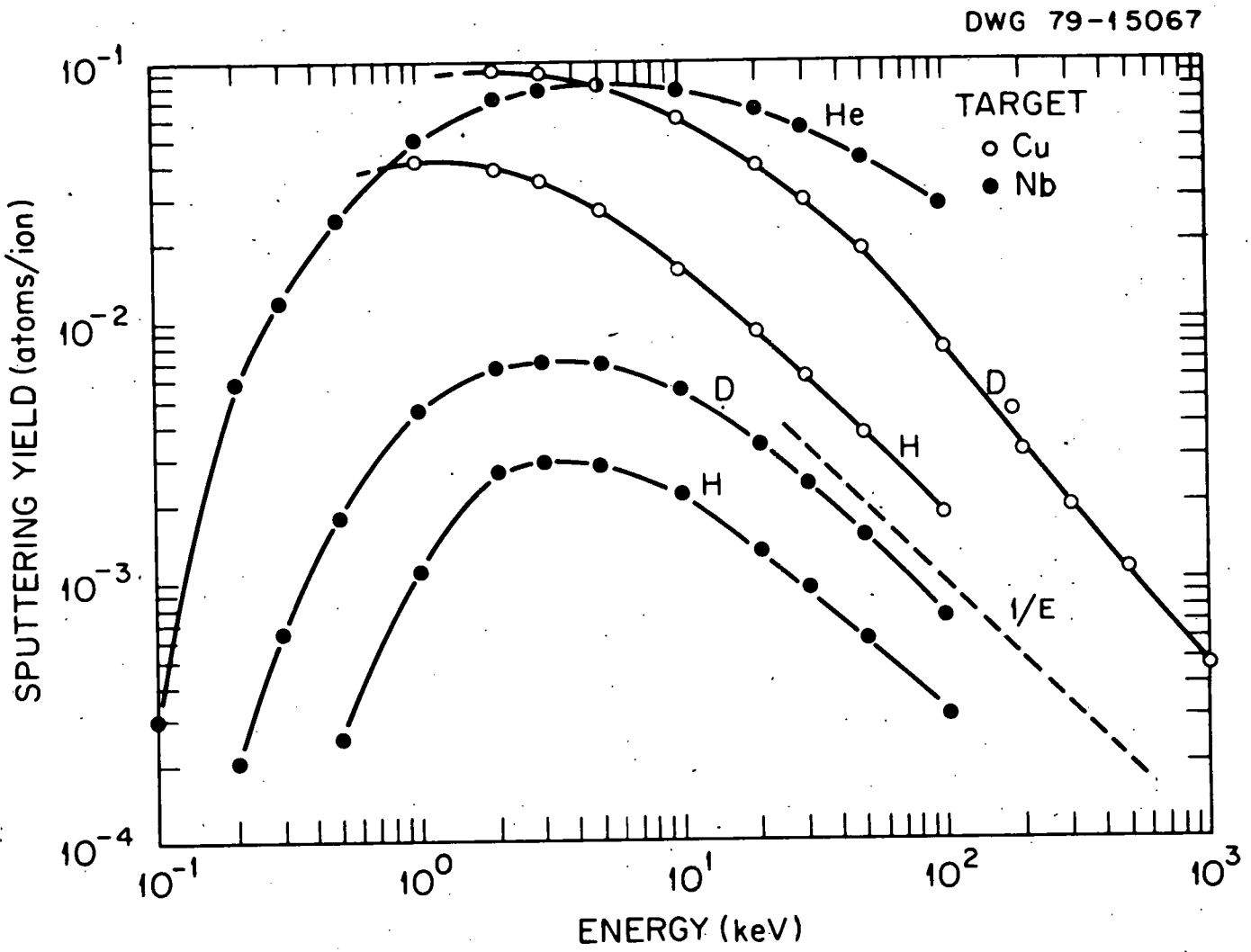
DWG 79-15067
SPUTTERING YIELD (atoms/ion)
ENERGY (keV)
TARGET
Cu
Nb
He
D
H
D
H
1/E
10^{-1}
10^{-2}
10^{-3}
10^{-4}
10^{0}
10^{1}
10^{2}
10^{3}

Fig. 6

SPUTTERING BY PLASMA IMPURITY IONS (Z > 2)

Joe N. Smith, Jr.
General Atomic Company

SUMMARY

Very little information exists on the sputtering of prospective first wall/limiter/divertor materials by heavy impurity ions such as Cr^+, Ni^+, Fe^+, Cu^+, Ti^+, Mo^+, W^+, Ta^+, C^+, O^+, N^+; etc. While estimates to within a factor of 2 to 4 can be made from rare gas data or extant theory in many cases, supporting data for heavy impurity ions is required as a function of:

a. energy from about 1 to 5 keV,

b. dose rate, at least to high enough dose rates to establish the threshold for non-linear effects, if any,

c. target temperature up to temperatures beyond which mechanical properties degrade,

d. incident angle,

e. surface morphology and contamination.

DISCUSSION

Most of the high Z sputtering data currently available is summarized in Figures 1-3. These data are for normal ion incidence on room temperature targets and, for the most part, with no indication of possible dose rate effects. From the limited data already available, it is clear that, since high Z sputter yields can be > 1, impurity sputtering may be significant even at low plasma impurity levels. Limited data for $Cu^+ \rightarrow Cu$ indicates that the incident angle dependence agrees with sec θ, at least out to $\theta = 50°$ with respect to the normal. Figure 4 shows the self ion sputter yield for a number of elements as reported by Almen and Bruce.[1] However, Andersen and Bay[2] have subsequently suggested that much of the indicated variation may result from dose rate effects which were not investigated in the original work.

Although experimental data on sputtering by impurity ions is very limited, a large number of studies have been performed using rare gas ions.[3] To within a factor of 2 to 4, the extant impurity ion data agrees with the rare gas ion data above about 1 keV. Thus, at 10 keV, the yield for Cu^+ (M = 63) $\rightarrow$ Cu is bounded within 25% by the yield for Ar^+ (M = 40) $\rightarrow$ Cu and Kr^+ (M = 84) $\rightarrow$ Cu. Further, theoretical models as discussed by Haggmark elsewhere in this report are much more reliable for heavy ions than for light ($Z \leq 2$) ions. Therefore, first approximations to impurity ion sputtering may be made by inference but must be verified by direct experimental measurement when accuracy is within less than a factor of 2 is desired.

The possibility of significant changes in the sputter yield due to the ion dose rate and the surface temperature are much more likely in the case of impurity ion sputtering than in the case of plasma ion sputtering. Both possibilities result from the larger energy density in a collision cascade for heavy ions, leading to non-linear effects as the dose rate is increased and also possible localized evaporation if the bulk temperature is already elevated for other reasons. Dose rate effects for heavy ions are

clearly indicated in earlier work[2] and must also be investigated for specific impurity ions in sufficient detail to establish a threshold dose rate for non-linear behavior, at least up to rates on the order of 10^{18} ions sec^{-1} cm^2 which may occur on divertor plates. Similarly, temperature effects should be investigated up to anticipated operating temperatures, which, in general, would not exceed about 60% of the melting temperature due to structural considerations.

There are several aspects of tokamak operation which dictate that the energy range for which impurity ion sputtering data is required is different from that for plasma ions ($Z \leq 2$). Due to the presence of multiple charge states for the impurity ions, the energy of such ions dropping through the sheath potential will be several times that of the singly charged plasma ions. Further, the occurrence of charge transfer impurity neutrals originating from the high temperature core of the plasma is highly unlikely. Thus, the energy range of interest for impurity ion sputtering is rather limited, being confined largely to the low keV region.

The impurity ions for which sputter yields are required are those formed from materials and gaseous contaminants frequently found in tokamak plasma chambers. Primary interest is to be attached to those ions arising from the stainless steels (Fe^+, Ni^+, Cr^+), ions formed from adsorbates or gaseous contaminants (e.g., C^+, O^+, N^+) and those arising from limiter/divertor regions (e.g., W^+, Ta^+, Ti^+). Surfaces for which impurity ion yields must be determined include the stainless steels (including, e.g., Inconel and Nicofer), refractories (e.g., W and Ta) and getter materials (e.g, Ti). These requirements can be restated graphically as follows:

Ion		Surface
Fe^+, Ni^+, Cr^+	→	Stainless steel (may be approximated by elemental Fe, Ni or Cr)
C^+	→	W
O^+	→	Ta
N^+	→	Ti
W^+, Ta^+		
Ti^+		

Sputtered particles which enter the edge plasma region may, through collisional processes, become ionized and returned to the wall with insufficient energy to give rise to significant sputtering and may stick to the surface. This fresh metal surface will act as a getter affecting the particle balance in the edge plasma and, in addition, may produce a transient deposit which displays considerably different sputtering behavior than the bulk material. This latter effect would result from surface migration, for times long compared to a surface vibrational period ($\sim 10^{-13}$ sec); the lower attendant surface binding energy could give rise to increased sputtering. Thus, although not directly related to impurity ion sputtering, sticking coefficients of metal atoms on metal surfaces in the range from $\sim$ 2 to $\sim$ 100 eV in the presence of simultaneous ion bombardment are of interest and not readily obtainable from the literature on ion plating or elsewhere.

REFERENCES

1. O. Almen and G. Bruce, Nucl. Instrum. Meth. *11*, 279 (1961).
2. H. Andersen and H. Bay, J. Appl, Phys. *46*, 2416 (1975).
3. M. Kaminsky, Atomic and Ionic Impact Phenomena on Metal Surfaces, Academic Press Inc. (NY) 1965.
4. H. Andersen and H. Bay, Radiat. eff. *19*, 139 (1973); W. Hayward and A. Wolter, J. Appl. Phys. *40*, 2911 (1969).
5. W. Hayward and A. Wolter, J. Appl. Phys. *40*, 2911 (1969); O. Almen and G. Bruce, Nucl. Instrum. Methods *11*, 279 (1961).
6. E. Hechtl, H. Bay and J. Bohdansky, Appl. Phys. (Germany) *16*, 147 (1978).
7. W. Hayward and A. Wolter, J. Appl. Phys. *40*, 2911 (1969).
8. A. Fontell and E. Arminen, Can. J. Phys. *47*, 2405 (1969).
9. A. Summers, N. Freeman and N. Daly, J. Appl. Phys. *42*, 4774 (1971).
10. P. Rol, J. Fluit and J. Kistemaker, Physica *26*, 1000 (1969); O. Almen and G. Bruce, Nucl. Instrum. Methods *11*, 257 (1961).
11. H. Bay, J. Bohdansky and E. Hechtl, Radiat. Eff. (1979) in press.

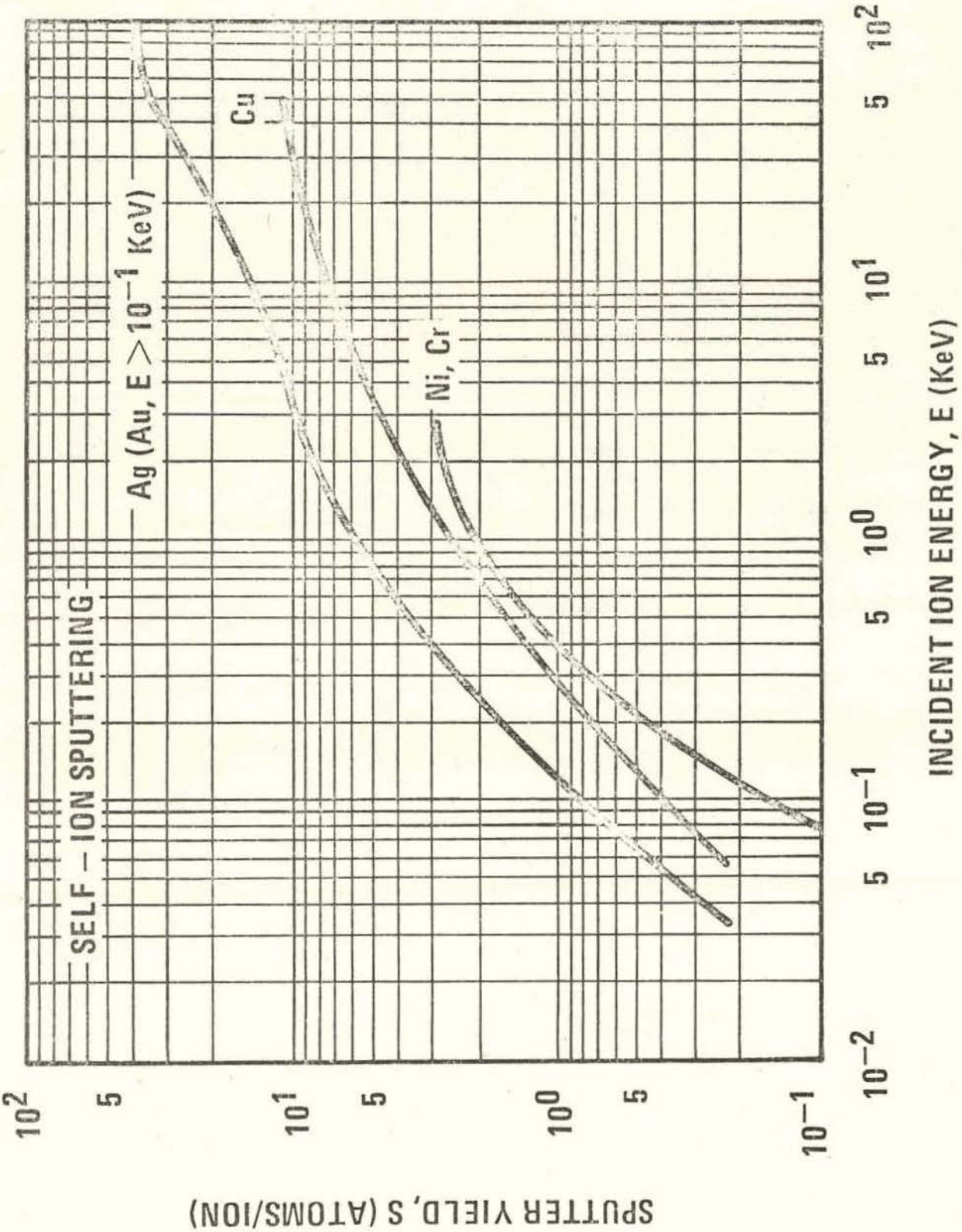

Fig. 1. Normal incidence self-ion sputtering of Ag (Reference 4), Au (Reference 5), Cu (Reference 5), Ni (Reference 6) and Cr (Reference 7). Below $\sim 10^{-1}$ keV the self sputtering of Au falls as much as a factor of two below that shown for Ag.

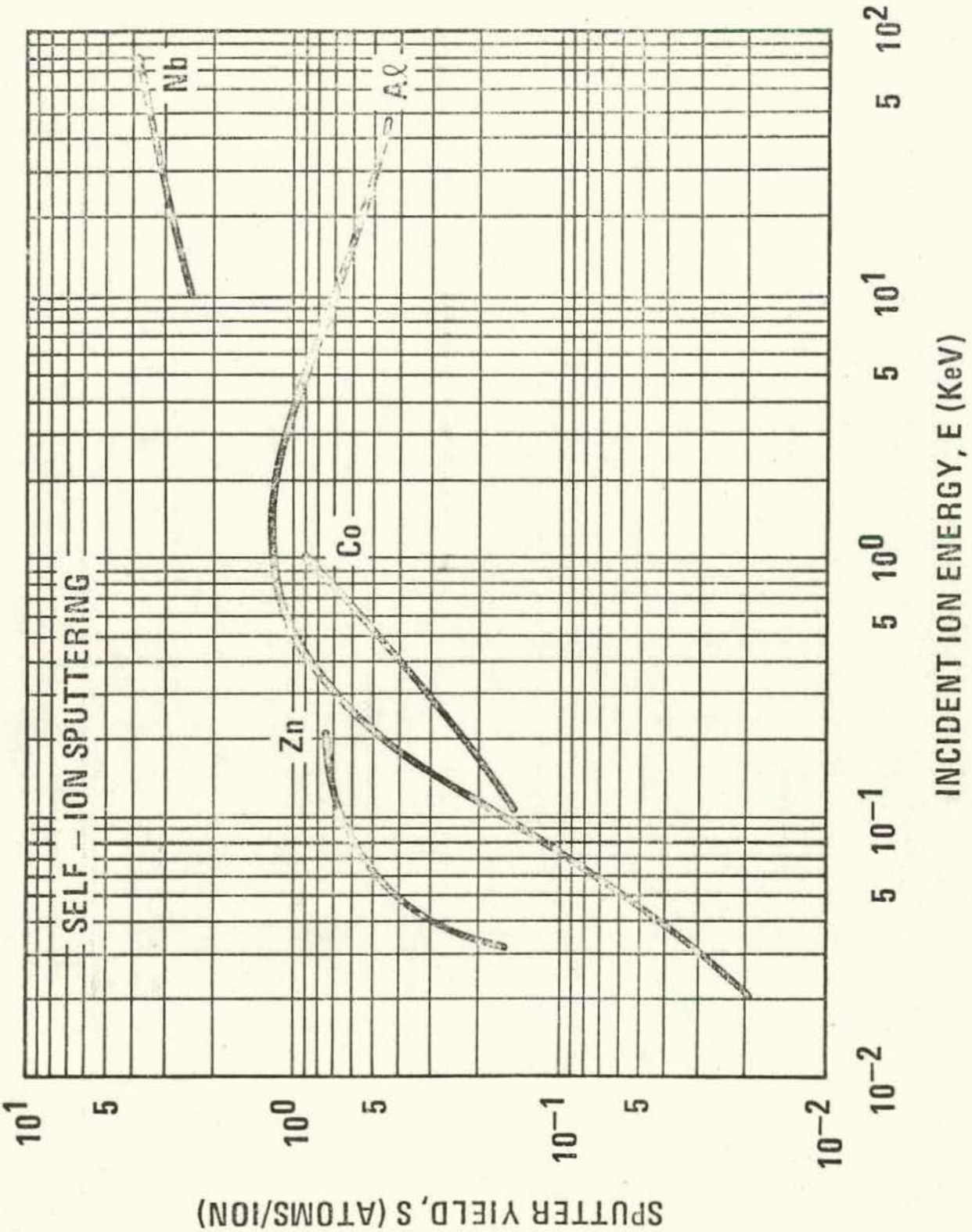

Fig. 2. Normal incidence self-ion sputtering of Zn and Co (Reference 8), Al (Reference 5) and Nb(Refernece 9).

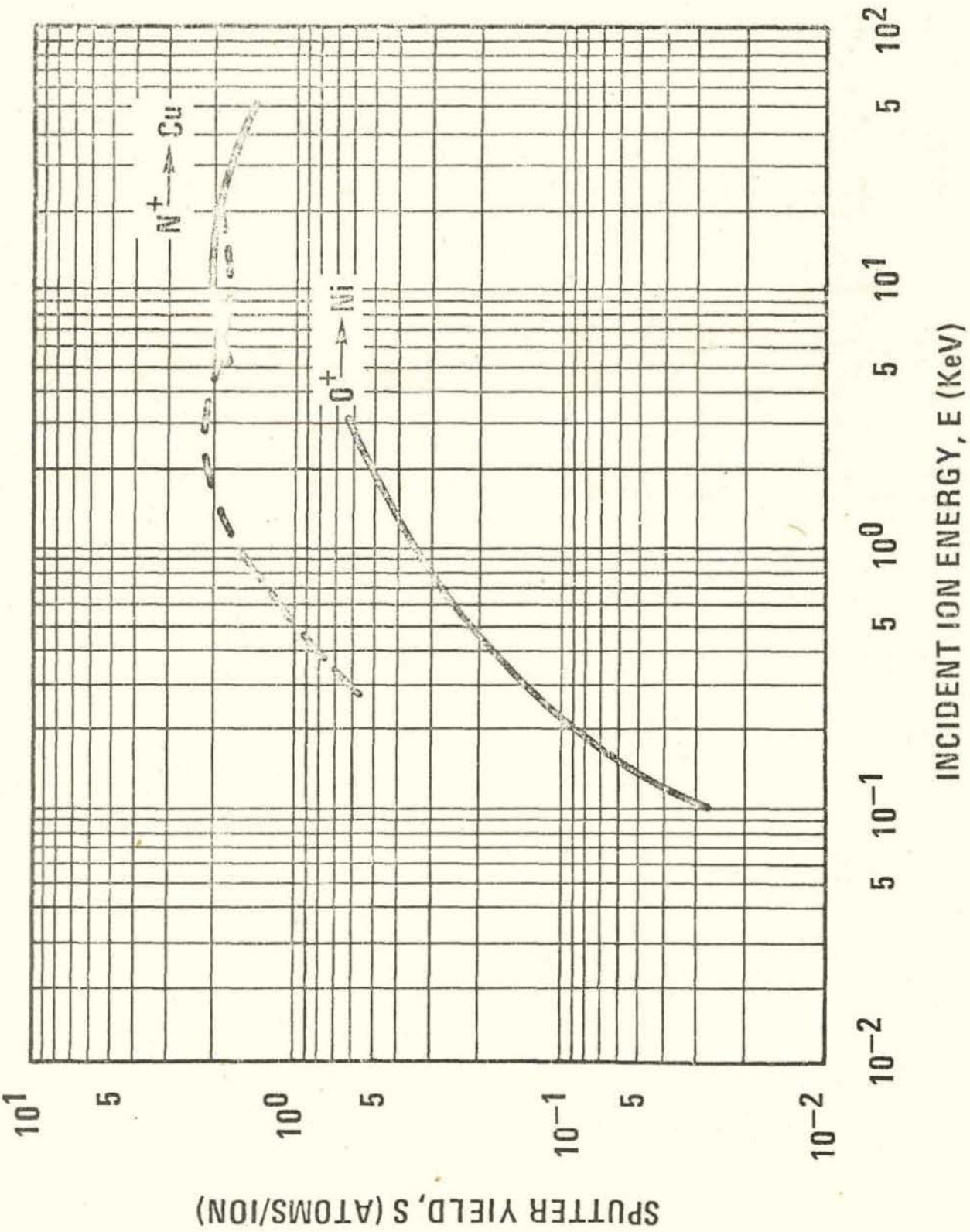

Fig. 3. Sputter of Cu by N^+ (Reference 10) and Ni by O^+ (Reference 11) at normal incidence. Solid curves were obtained with atomic ions. The dashed curve was obtained with diatomic ions and is replotted as the atomic ion yield.

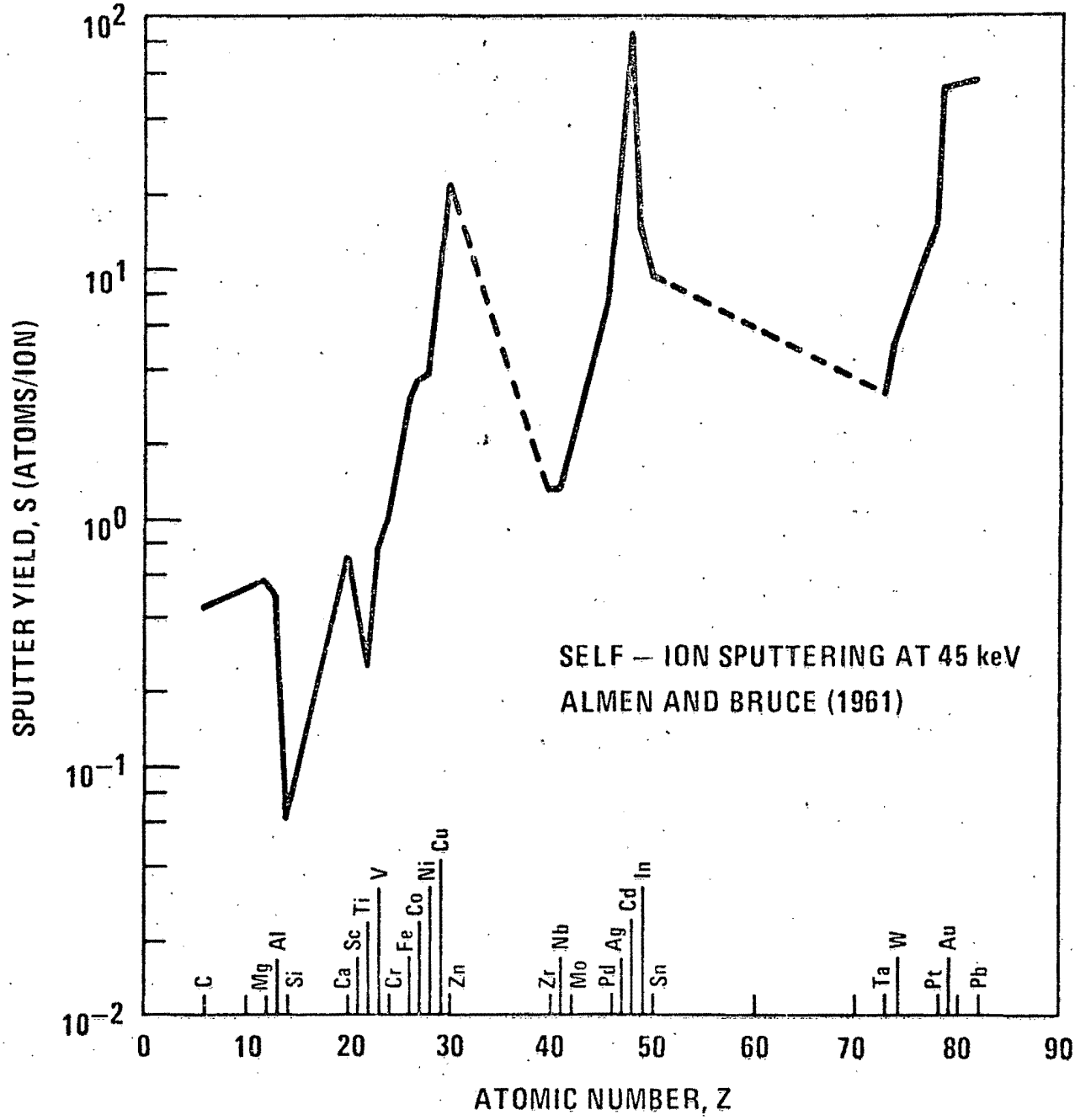

Fig. 4. Self-ion sputtering of several elements at 45 keV from Reference 1. See caveat in text and also Reference 2.

ENERGY AND MASS DISTRIBUTIONS OF SPUTTERED PARTICLES

A.R. KRAUSS and R.B. WRIGHT

Chemistry Division, Argonne National Laboratory, Argonne, IL 60439

INTRODUCTION

This review is primarily concerned with aspects of sputtering as they relate to plasma contamination of a magnetically confined fusion device. experimental methods used to study secondary ions are quite distinct from those used to study sputtered neutrals. The results are dissimilar and the significance for plasma impurity levels is quite different. For this reason, the data has been divided into four categories: 1. energy distributions of neutral sputtered particles, 2. energy distributions of secondary ions, 3. mass spectra of sputtered neutrals and 4. mass spectra of secondary ions. The existing (June 1979) relevant data are summarized in tables 1-4.

Primary interest lies in low energy light ion sputtering although high energy light ion erosion occurs in neutral beam dump areas and is therefore also of some interest. Heavy ion self-sputtering will occur at first wall and limiter surfaces, although presumably to a smaller extent than that associated with light ion sputtering. For experimental and historic reasons, almost all sputtering data have been obtained using Ar^+, Kr^+ or Xe^+ as the bombarding particle. For the most part, the resulting yields and kinetic energy distributions of sputtered atomic species are described by the Sigmund-Thompson random collision cascade (RCC) model (135). To a large extent self-sputtering can therefore be simulated by extrapolation from bombardment with the appropriate inert gas ions. The data listed in the tables represent only a small sampling of the literature on bombardment by Ar^+, Kr^+ and Xe^+. Complete references, however, are to be found at the end of this article and the unabridged tables will be published separately (11).

For low energy light ion sputtering, the mechanism is completely different from that of the RCC model (1). The small amount of experimental data available show that both the kinetic energy distribution of sputtered atoms and relative abundances of the sputtered molecular species depend on the projectile mass and that this dependence is especially pronounced for low mass projectiles. In the many instances for which the appropriate light ion data does not exist, it is necessary to extrapolate from data obtained with heavier inert gas ion bombardment. That data should be used only with extreme caution, although some qualitative conclusions concerning overall trends are possible.

Three types of experiments are listed in tables 1-4. Beam refers to an experiment in which the sputtering is produced by a well-defined ion beam of specified composition, kinetic energy and angle of incidence. Plasma refers to an experiment in which the target is one electrode of a plasma discharge. This arrangement has drawbacks in that the kinetic energy of the bombarding particle is not well-defined, the angle of incidence cannot be readily controlled, and impurities evolved from the chamber walls are deposited on the sample. The major advantage of this scheme is that sputtered neutrals will be excited or ionized by the discharge and their detection simplified. The term SIM refers to an "experiment" in which the sputtering events are simulated by a computer code.

Except for the plasma experiments, most experimental methods do not reject the sputtered ions and represent the total yield rather than that of the neutrals alone. For most clean metal surfaces, the ion yield is a small fraction

of the total, and the total and neutral yields are usually taken as synonymous. It should be noted however, that the error inherent in this assumption is negligible only if the energy and mass distributions do not differ drastically for ion and neutral emission.

For compounds, oxidized surfaces and alkali metals, the ion fraction can lie in the range 50-100% (6,220,402). For near-term plasma devices, such high ion yield materials will be limited to insulators. Hence the secondary ion data will be most relevant if it provides information which may be extrapolated to the neutral sputtered particles. If the energy and mass spectra are sufficiently different to prevent this extrapolation, the ion component may then be responsible for some of the structure appearing in the low intensity portion of the spectra of those experiments which measure the total yield.

Another way of studying sputtered particles is to observe the optical radiation from excited metastable neutral sputtered atoms. The transport properties of such particles in a plasma do not differ drastically from those of the ground state neutral, unlike the secondary ion case. However, absolute photon yield measurements by Tsong and Yusuf (3) indicate that the excited fraction of the sputtered atoms does not exceed 1%. The data does not readily provide information about the molecular structure of the sputtered particles. Average velocities of the metastable atoms have been obtained but until recently no velocity distributions have been measured by this method. Preliminary velocity distribution results (4) indicate a low energy cut-off far above the average ion or neutral velocities. Consequently it must be considered that the details of the excitation process are such that the kinetic energies of the metastable atoms are totally unrepresentative of either the ground state neutral or ionized components of the sputtering yield. This class of experiments has therefore been omitted from the tables.

Insofar as is possible, the references cited are all available in the open literature. The references are cited alphabetically by first author for each of the four data categories. For those cases in which a paper deals with two or more categories it has received a separate listing in each. One reference (5) is not readily available but should not be overlooked. The most exhaustive catalog of secondary ion energy distributions available has been compiled by Rudat and Morrison using 5.5 keV O_2^+ beams in an ion microprobe. The materials studied are too numerous to list here, but the catalog is available from Cornell University as the Materials Science Research Center Report #3056.

1. NEUTRAL ENERGY DISTRIBUTIONS

For 1 keV Ar^+ and Xe^+ bombardment of copper, computer simulation (112) indicates that the shape of the total energy distribution is independent of the mass, energy, and angle of incidence of the bombarding ion, in accord with the random collision cascade (RCC) model of Thompson et al. (135,136). The experimental results are in approximate agreement with this model, usually displaying a peak at $\sim\frac{1}{2}$ the surface binding energy, and a high energy tail which falls off as E^{-2}. However, the predicted dependence on the above three bombardment parameters has been tested only on a rather limited range of materials and even fewer systematic studies have been performed for low energy light ion bombardment where the RCC model is expected to be invalid.

The neutral energy distributions of most elements have been measured by Wehner et al. (130-132) and by Oechsner et al. (102,126,127) using plasma post-ionization or excitation of the sputtered atoms. Most of these measurements

have been done for a very limited combination of beam energies and projectile masses. For bombardment of copper, Stuart and Wehner (131) found the kinetic energies of the sputtered neutrals to be roughly independent of the primary energy but highly dependent on the projectile mass (Fig. 1). However, this work was discontinued in 1970 and has not been resumed (7). Consequently there is not enough data to indicate whether the behavior of Fig. 1 is a general phenomenon. Almost all of the data of Oechsner et. al. and Wehner et. al. was obtained with bombardment by Ar^+ and Xe^+ at $\sim$1 keV and may not be applicable to light ion sputtering.

Experiments under much better defined bombardment conditions have been performed, but only for a much more limited range of materials. Extensive work has been performed on metal halides (117,118,133), but these materials display sputtering mechanisms which are not typical of metals (133). Time of flight measurements of sputtered Au and Cu under argon ion bombardment have been made by Thompson et al. (104,129,134-136). The technique employed is limited to those metals which can be readily neutron activated and in fact has only been applied to gold and copper.

The general features of the energy distributions obtained by this technique are in accord with the RCC model for room temperature targets. However, at elevated temperatures thermal emission gives rise to a very pronounced increase in the yield at very low ion energies for gold (104). There have been no other papers to date on the effect of temperature on the kinetic energy distribution of sputtered neutral atoms.

The English group (129) has also performed one of the few studies on the effect of the angle of incidence (θ_i) and angle of emission (θ_e) on the kinetic energy distribution of the sputtered neutral atoms. They found that for $\theta = \theta_i + \theta_e$ significantly different from 90° there was a pronounced increase in the yield at very high energies, corresponding to recoil emission of surface atoms (Fig. 2). This finding may be especially significant for low energy, light ion sputtering where the sputtering mechanism is more closely related to recoil emission than it is to collision cascade ejection (1). Experimentally, however, the effect was found to depend on the surface structure and consequently on the sputtering history. In general, the recoil emission only became significant after prolonged bombardment had resulted in faceting of the polycrystalline surface.

The maximum kinetic energy resulting from low energy light ion bombardment would be much lower than that shown in Fig. 2, but in a neutral beam injected device there could be a significant number of particles sputtered with kinetic energies far in excess of those expected for cascade sputtering. There has been no comprehensive study of light ion recoil sputtering.

Recently, Doppler-shifted laser fluorescence spectroscopy (DSLS) has been applied as a means of measuring the kinetic energies of sputtered atoms (105,106,116,117). Although the technique appears to have a great deal of promise as a general tool, only a few projectile-target combinations have been examined so far.

Surface adsorption changes the surface binding energy and in the collision cascade model, would therefore be expected to alter the energy distribution. There have been no studies of this effect on sputtered neutrals to data although a related effect for secondary ions is well known. Most of the available data were taken under poor vacuum conditions and with uncharacterized surfaces. Mass spectra of the sputtering products (section 3) often indicates a high degree of contamination.

There is no data on the kinetic energies of neutral particles sputtered from alloys.

The kinetic energy of neutral particles sputtered from compounds has been studied only in the context of metal halide targets (116-118,133) where it was found that the atomic energy distributions were independent of the compound (118). A systematic comparison with the corresponding alkali metal was not performed, but the energy distribution obtained e.g. for potassium atoms sputtered from KI (118) looks quite different from that obtained by other workers (115) for polycrystalline potassium. The metal gives rise to a well-defined peak at $\sim$ 1 eV whereas the data for KI indicates a yield increasing continuously as the kinetic energy approaches zero. Thermal spike emission in the halide has been ruled out as the reason for this difference (118).

Primary current density has been found to have a large effect on the secondary ion energy distribution (242), but similar experiments have not been performed for the sputtered neutrals.

2. SECONDARY ION ENERGY DISTRIBUTIONS

Partly because of the relative ease of detection, secondary ion emission has been studied for a much greater range of parameters than has the neutral emission. These parameters include sample temperature (201,223), primary energy (201,209,212,219), angular dependence (202,211,212,217,219,228,232,234), molecular vs atomic nature of the ejected particle (203,205,207,209,210, 212-215,218,219,223,227,230-233,239-241), surface contamination and oxidation (203,204,207,209,210,212,218-222,227,230,233-238), alloys (205,206,233), compounds (203,205,213,229,231), current density (242) and recoil emission (219,240). However, very few of these experiments have been performed with hydrogen or helium beams (221,232-234) or on surfaces with well-characterized chemical composition (218-223,233,234). For ion-target combinations which have been studied in several laboratories, the results have often been in conflict.

Assuming that secondary ions are ejected by the same mechanism as sputtered neutrals, their energy distribution may be written

$$N^{\pm}(E) = R^{\pm}(E)\, N(E) \qquad 1.$$

where $N(E)$ is the energy distribution of all the sputtered particles and $R^{\pm}(E)$ is the probability that a sputtered particle will escape as an ion. If $R^{\pm}(E)$ is a slowly varying function of energy, the ion energy distribution will look much like that of the neutrals and the secondary ion data can be

used to obtain information about sputtered neutrals. This has been reported by several authors to be the case (209,211,229). Other authors have observed moderate differences between ion and neutral behavior (206,207,218,219,220, 221,223,225,226,233,239) and still others have noted extreme differences (203,204,214,215,218,219,227,228,235-238). Theory is no help in weeding out erroneous data since there is no model of generally accepted validity to describe $R^{\pm}(E)$. The range of proposed behavior for this quantity is sufficiently broad to permit a wide variety of secondary ion behavior.

A rather striking comparison of the Cu^+ energy distribution obtained by sputtering with $\sim$ 40 keV Ar^+ under nominally similar conditions at three different laboratories is shown in Fig. 3. This figure is representative of the discrepancies observed for a wide range of materials. It is believed that the difference is largely the result of differences in surface cleanliness which has a pronounced effect on the ionization probability. To date however, very few of these experiments have provided independent means of analyzing the sputtered surface (218-223,233,234). Additional difficulties may arise from uncorrected ion-optical effects and variations in instrument response with ion energy.

As regards the plasma impurity question, the situation may not be as serious as Fig. 3 would seem to indicate. It is the consensus of this workshop that unless a sputtered positive ion has exceptionally high energy, it would not penetrate the plasma sheath potential and therefore would not provide a source of impurities. High energy ions resulting from recoil ejection have been observed (219,220) and might constitute a problem, but there has been no systematic study of the phenomenon.

Negative ions are produced in large amounts by compounds and contaminated metal surfaces. There is essentially no data on the negative secondary ion energy distributions for such surfaces.

3. NEUTRAL MASS SPECTRA

In part, the topic of this section overlaps with another area of this workshop, reactive sputtering. The distinction between the two areas is somewhat vague and, in order to ensure that significant amounts of data aren't lost "in the crack" some of the results presented in tables 3 and 4 may represent an overlap. The data presented here is consequently not intended to be as exhaustive as that of the previous two sections.

Ion bombardment of clean elemental metal targets will result in the ejection of metal clusters of various sizes in addition to the more abundant atomic ejection. Cluster emission is of interest for fusion applications because the clusters may account for an appreciable fraction of the erosion, because their kinetic energies are different from that of the monomer, and because they may have different ionization cross sections. This latter point will not be dealt with here.

All the atoms within the cluster are ejected as the result of the impact of a single ion, although there is still controversy as to whether the cluster is actually formed before or after emission (312-318,321,328,330,331,401,402, 403,414-416,424,429,433,435,438). Although there are unresolved quantitative discrepancies, it is to be qualitatively expected in either case that for both ions and neutrals, the clusters will have progressively narrower energy distributions and that the peak intensity will shift to lower energies as the cluster size increases. With only a few exceptions (328,424) the experimental results are in accord with this prediction.

As in the previous sections, the data base is rather incomplete, making generalizations somewhat risky. However, Gerhard (315) has predicted, and the experimental results of Gerhard and Oechsner (316) show that for one keV Ar^+ bombardment of a number of metals, the cluster intensity decreases rapidly with increasing cluster size, the dimer yield not exceeding ~10% that of the monomer, while the trimer/monomer ratio is typically a few tenths of a percent. These ratios increase with increasing argon ion energy. It should be noted, however, that these results were obtained by assuming that the collisions with the plasma which produce post-ionization of the sputtered particles do not also produce significant molecular fragmentation. If this assumption is incorrect, molecular emission will be more important than the results indicate.

There are no data on sputtered neutrals which would make it possible to determine the kinetic energies or assess the significance of neutral dimer and trimer yields for light ion bombardment. The yield of ionic clusters shows some differences with neutral cluster emission, but also some similarities which may provide guidance to the expected behavior of light ion-induced neutral cluster emission. The indication is that large clusters are relatively less important for light ion sputtering. This point will be discussed more thoroughly in section 4.

There are virtually no data concerning the ejection of neutral clusters from alloys (306).

Both homonuclear and heteronuclear clusters are ejected by sputtered compounds, or from surfaces with an adsorbed overlayer. The mechanism is believed to be essentially the same as for the sputtering of clean elemental metals, although differences in surface and molecular binding energies quantitatively affect the results. Cluster formation associated, for example, with the sputtering of an oxide, a metal in the presence of oxygen gas, and by sputtering with an oxygen beam are clearly related processes although the results are not identical.

There appears to be only one paper dealing systematically (307) with neutral molecular emission from bulk oxides. For the thirteen oxides studied, MO was the dominant molecule. The molecular fraction, defined as:

$$\eta = \frac{[MO]}{[M]+[MO]} \qquad 2.$$

was found to be related to the M-O bond energy, reaching ~50% for several refractory metals. The experiment was performed in an argon ion discharge, producing bombarding particles of unspecified energy. The target temperature was also unspecified. The metal-oxygen-hydrogen system is an extremely fertile one for the introduction of chemical effects, so extreme caution should be used when extrapolating these results to proton or deuteron bombardment.

There are several papers on the neutral molecular emission from surfaces exposed to an oxygen environment during sputtering (311,312-314), and many more papers in which molecular emission occurs as a result of surface contamination. These surfaces have not been characterized, and the results are not quantitatively reproducible.

There is a substantial amount of data available on the sputtering of metal halides by inert gas beams (321,328,329). Although these materials are not of immediate interest to the fusion community, the experiments appear to be among the most reliable and the results illustrate some of the possible phenomena.

4. SECONDARY ION MASS SPECTRA

The detection of secondary ions provides the basis of the surface-analytical technique known as secondary ion mass spectrosocpy (SIMS). Consequently, the available data far exceeds the amount which can be reasonably catalogued here, and the data in table 4 is far from complete, merely representing a sampling of the data which may be relevant to the plasma-wall problem. As in the previous sections, there is very little light ion data. Quantitatively, the interpretation of the data is plagued with all the difficulties discussed in section 2, and there is a further element of arbitrariness introduced by the energy band pass characteristics of the analyzer.

In order to increase the sensitivity and obtain more reproducible SIMS data, it is common practice to either use an oxygen beam or to flood the sample surface with a jet of oxygen gas. This practice has led to a number of experiments investigating the effect of surface oxide formation on the atomic and molecular secondary ion yields (401-404,407,410-413,423,424, 427-430,434,437). A few experiments have been performed indicating the desirability of similar studies in a hydrogen environment (8,9), but there is little data currently available.

Qualitatively, the intensity of the ion clusters does not drop as rapidly with cluster size as that of the neutral clusters investigated: Homonuclear aluminum ion clusters have been observed containing up to 18 atoms (415) and carbon clusters have been reported containing up to 17 atoms (408). Note however, that all of the post-ionization methods used experimentally result in fragmentation of the neutral clusters and distort the measured multimer distribution. Stability of the resulting electronic configuration also seems to be a much more important criterion for ion cluster intensity than is the case for neutral clusters (426). Consequently, oscillations and even inversions in the size-intensity relation are fairly common. The dimer or trimer ion yield of a clean surface has been found to exceed the monomer yield for Cu (405), AlCu alloy (408), C (408,419) and SiC (418). Experiments have shown that the beam energy and particle mass influence the relative yield of molecular ions (435,438), but no systematic studies have been undertaken. For oxidized metal surfaces, the MO^+/M^+ ratio has been reported to be > 1 for Ti, W, V, Mo, Nb (402).

Ta (437) and U (430), although this conclusion has been disputed for W (423) and Ti (219).

With a few exceptions (328,424) the clusters have lower kinetic energies than the sputtered atoms. If low energy positive ions are effectively returned to the surface by the magnetic field and sheath potential, the ejection of at least the positive ion clusters is probably not a factor in plasma contamination. For negative ions, the MO_n^- yield frequently exceeds the M^- yield, often peaking at n = 2 or 3. It should be noted however, that only non-metal or contaminated metal surfaces exhibit significant negative ion yields. It has been observed that as the mass of the bombarding ion is decreased, the intensity of the C_n^- cluster ejected from SiC decreases rather markedly at high n (418). However the C_2^- yield for 600 eV He^+ bombardment still exceeds the C^- yield by two orders of magnitude. Consequently it appears likely that dimer or trimer ejection may be an important mechanism for negative ion sputtering of a number of materials subject to low energy light ion bombardment.

SUMMARY

To date, the kinetic energies of neutral atoms sputtered by well-defined beams of light ions ($Z \leq 2$) have been studied for only two materials, Au and Fe (113,114,106) with primary energies in the range 10-30 keV. For lower primary energies where the sputtering mechanism is different (1) and the conditions of the Sigmund-Thompson RCC model (135) are no longer met, there is no data at all on the kinetic energies of the sputtered particles. For low energy light ions, a well-developed random collision cascade (RCC) does not form. Instead, sputtering is closely associated with backscattering of the projectile. Consequently it is to be expected that the energies of the sputtered particles will be much more sensitive to the primary energy, angle of incidence, angle of emission, composition and morphology of the near-surface regions. The small amount of data obtained by plasma discharge experiments (131) indicates that the kinetic energies differ very substantially from those corresponding to heavy ion bombardment (Fig. 1).

The same experiment indicates that for primary energies < 1 keV, substantial departure from RCC behavior is observed even for Ne^+ bombardment. Consequently it can not be taken for granted that the kinetic energies of particles sputtered by C^+, N^+, O^+ bombardment in a fusion device will be described by the Sigmund-Thompson model. It should be noted that prediction of the kinetic energies is a much more stringent test of the model than prediction of the sputtering yield. For higher primary energies and for heavier projectiles associated with self-sputtering in a fusion device, both theory and experiment indicate that the Sigmund-Thompson model should adequately describe the kinetic energy distribution of the sputtered particles.

Athough the pertinent energy and mass ranges have not been studied, it appears possible that the neutral cluster emission by low energy light ion sputtering will not contribute substantially to the impurity influx. It should be remembered however that this conclusion is based on the assumption that the experimental technique of plasma post-ionization does not result in significant fragmentation. This question is not entirely settled and there is perhaps some theoretical reason (10) for believing that fragmentation may in fact be significant.

For the emission of secondary ions, the effects of the pertinent parameters have been studied more thoroughly although by no means completely. There are substantial discrepancies in the key results which make it impossible to determine what relevance the data has to the sputtering of neutrals. It has not yet been fully established whether the data pertaining to secondary ion emission are revelant, but there is reason to believe that with the possible exception of high energy recoil emission associated with neutral beam injection, the positive secondary ions do not have a role in plasma contamination.

For non-metallic samples, oxides, or metals contaminated by oxygen or hydrocarbon adsorption, there is significant negative ion emission although quantitative yields are not available. In many cases, molecular ejection is the dominant negative ion sputtering mechanism. Negative secondary ion energy distributions are almost totally unexplored. Instead of being blocked by the sheath potential, negative ions will be pulled inward toward the plasma. They will be subject to the difficulties of cross field transport however, and consequently may not contribute significantly to plasma contamination.

Acknowledgment

The authors would like to thank Dr. Michael Pellin for assistance in the compilation of Tables I-IV.

Table 1. Neutral (total) Energy Distributions

TARGET	SPECIES	METHOD	BEAM	keV	E_{max}(eV)	uA/cm^2	P (torr)	θ_e	θ_i	REFERENCE	COMMENTS
Ag	Ag°, Ag_2°	plasma	Ar^+	1	25	3000	-	-	-	102	
AgBr	Ag°	beam	Xe^+	6	100	500	10^{-7}	0	60	133	
Au	Au°	beam	Ar^+,Xe^+	25,50	4000m/s	200	10^{-5}	35	65	103	Beam mass & energy dep
Au	Au°	beam	Ar^+,Xe^+	10-41	$5x10^3$			45	45	104	Temp. variation, thermal spike
Au(111)	Au°	sim	Ne^+	1.5	508			vary	45	111	
Au	Au°	beam	H^+,He^+,Ar^+	30	100	1500	10^{-6}	0	70	113	
Au	Au°	beam	H^+,He^+,Ar^+	15,30	100	1500	10^{-6}	0	70	114	
Au	Au°	beam	Ne^+,Ar^+,Kr^+ Xe^+	20-60		100			0	119	Average energy only
Au	Au°	beam	Ar^+	20	10^4			vary	45	129	Recoil emission
Be	Be°	plasma	Kr^+	1.2	40	$2x10^4$	-	0	0	132	
Be	Be°	beam	Ar^+	3	150	0.2	10^{-10}	45	45	121	
Bi	Bi°	beam	Kr^+,Xe^+	35		100			0	119	Average energy only
Cr	Cr°	plasma	Kr^+	1.2	80	$2x10^4$	-	0	0	132	
Cu(100)	Cu°-Cu_5°	sim	Ar^+	0.6	12				0	108	
Cu(100)+O_2	CuO°,O°	sim	Ar^+	0.6	6				0	108	
Cu	Cu°	beam	Ar^+	30	15	1500	10^{-6}	0	70	113,114	
Cu	Cu°	sim	Ar^+,Xe^+	1	9				vary	112	Indep of $\theta i, Z_1, E_p$
Cu	Cu°	beam	Ar^+	1-3	20	50	10^{-9}	45	45	124	
Cu	Cu°	beam	Ar^+	2.5	20	50	10^{-9}	45	45	125	
Cu(110)	Cu°	plasma	He^+,Ne^+,Ar^+ Kr^+,Xe^+,Hg^+	0.6	40	$2x10^4$	-	0	0	131	
Fe	Fe°	beam	Ar^+	2	10^4cm/s	540	10^{-8}	0	0	105	DSLS
Fe	Fe°	beam	D^+,He^+,Ar^+	10	10^4cm/s	540	10^{-8}	0	0	106	DSLS
K	K°,K_2°	beam	Ar^+	11	3		10^{-7}			101	Thermal spike
KBr	K°	beam	Ar^+	6	100	500	10^{-7}	0		118	
Mn	Mn°	plasma	Kr^+	1.2	60	$2x10^4$	-	0	0	132	
Mo	Mo°	beam	Kr^+,Xe^+	35		100			0	119	Average energy only
Mo	Mo°	plasma	Kr^+	1.2	90	$2x10^4$	-	0	0	132	
Na	Na°	beam	Ar^+	11	3		10^{-7}			101	Thermal spike
NaCl	Na°	beam	He^+,Ne^+,Ar^+ Kr^+,Xe^+	20	10	50	10^{-7}	0	0	117	DSLS, thermal spike
NaI	Na°	beam	He^+,Ne^+,Ar^+ Kr^+,Xe^+	10-30	10	50	10^{-7}	0	0	116	DSLS, thermal spike
Nb	Nb°	beam	Kr^+,Xe^+	35		100			0	119	Average energy only
Ni	Ni°	beam	Ar^+	2.5	20	50	10^{-9}	45	45	125	
Ni(100)+O_2	Ni°	sim	Ar^+	0.6	7				0	138	
Pb	Pb°	beam	Kr^+,Xe^+	35	-	100			0	119	Average energy only
Pd	Pd°	plasma	Kr^+	1.2	90	-	-	0	0	132	
Re	Re°	plasma	Kr^+	1.2	200	-	-	0	0	132	
Ta	Ta°	plasma	Kr^+	1.2	200	-	-	0	0	132	
Ti	Ti°	beam	Ar^+	2.5	20	50	10^{-9}	45	45	123	
Ti	Ti°	plasma	Ar^+	1	15	3000	-	-	-	127	
U	U°	beam	Ar^+	9	500	~100				139	
V	V°	plasma	Kr^+	1.2	80	-	-	0	0	132	
W	W°	plasma	Kr^+	1.2	90	-	-	0	0	132	
Zn	Zn°	beam	Kr^+,Xe^+	35		100			0	119	Average energy only
Zr	Zr°	plasma	Kr^+	1.2	90	-	-	0	0	132	

Table 2. Ion Energy Distribution

TARGET	SPECIES	METHOD	BEAM	keV	E_{max} (eV)	uA/cm²	P (torr)	θ_e	θ_i	REFERENCE	COMMENTS
Ag	Ag^+	beam	Ar^+	3	275	0.2	10^{-10}	45	45	220	
Ag	Ag^+	beam	O_2^+	5.5	100	100	10^{-8}	int	73	231	
Al	many	beam	Ar^+	6				vary	vary	212	Large shift vs Ei & θ_e
Al	Al^{1-3+}, Al_2^+	beam	Ar^+	40	2000	60	10^{-6}	45	45	214	
Al	Al^+	beam	Ar^+	6.1	100			vary	vary	217	Large shift w/θ_e
Al	Al^+	beam	Ar^+	1.0	150	0.2	10^{-10}	45	45	219	Distribution shifts w/Ei
Al	Al^+	beam	Ar^+	0.5	150	0.2	10^{-10}	vary		219	Large Dist. shifts w/θ_e
Al	Al^{+}_{1-5}	beam	Ar^+	6	100	600	10^{-6}	int		223	Vary temp., channeling
Al(110)	Al^+, Al^{2+}	beam	Ar^+	50	400	75	10^{-6}	45,95	vary	228	channeling
Al	Al^+	beam	O_2^+	5.5	100	100	10^{-8}	int	73	231	
Al	Al^+	beam	Ar^+	43	200	60	10^{-7}	60	35	237	Clean surface not RCC
Al	Al^+, Al_2^+, Al_6^+	beam	Ar^+	10	20	10^{-4}	10^{-8}		0	240	
Al_2O_3	Al^+	beam	Ar^+	43	600	60	10^{-7}	0	30	204	
$Al+O_2$	Al^+, Al_2^+	beam	Ar^+	0.1-0.7	15	10^{-5}	10^{-10}	0	71	209	Looks like neutral dist.
Au	Au^+	beam	Ar^+	43	200	60	10^{-7}	60	35	237	Clean surface not RCC
Au	Au^+	beam	Ar^+	10	50	$6x10^5$	10^{-8}	~40	0	242	Current density
B	B^+	beam	O_2^+	5.5	100	100	10^{-8}	int	73	231	
Be	Be^+	beam	Ar^+	3	275	0.2	10^{-10}	45	45	220	
$Be+O_2$	Many	beam	D_2^+, Ar^+	3	150	0.2	10^{-10}	45	45	221	
C	C^+	beam	Ar^+	40	1000	100	10^{-6}	45	45	215	
C	C^+	beam	O_2^+	5.5	100	100	10^{-8}	int	73	231	
Cr	Cr^+	beam	Ar^+	6.2	20	1000		0	60	206	
Cr	Cr^+	beam	O_2^+	5.5	100	100	10^{-8}	int	73	231	
SS304	Cr^+, $CrOH^+$	beam	H^+, H_2^+, H_3^+	5	12	200	10^{-10}	6	45	233	
SS304	Cr^+	beam	H_3^+	10	20	200	10^{-9}	vary	vary	234	Dist. shifts w/θ_e
Cr	Cr^+	beam	Ne^+, Ar^+, Kr^+	43	200	60	10^{-7}	60	35	236	
Cr	Cr^+	beam	Ne^+, Ar^+, Kr^+	43	200	60	10^{-7}	60	35	237	Clean surface not RCC
Cu	Cu^{1-3+}	beam	Ar^+	10	160		10^{-7}	45	45	211	Looks like neutral dist.
Cu	Cu^+	beam	Ar^+	8				vary	vary	212	E varies w/θ_e & Ei
Cu	Cu^+	beam	Ar^+	2.5	60	15	10^{-9}	45	45	226	
Cu	Cu^+	beam	O_2^+	5.5	100	100	10^{-8}	int	73	231	
Cu	Cu^+	beam	Ne^+, Ar^+, Kr^+	43	200	60	10^{-7}	60	35	236	
Cu	Cu^+	beam	Ar^+	38-47	200	60	10^{-7}	60	35	238	Clean surface not RCC
Cu	Cu^+	beam	Ne^+	5	80	5000	10^{-6}	45	0	243	
Fe	Fe^+	beam	Ar	8				vary	vary	212	E varies w/θ_e & Ei
Fe	Fe^+, Fe_2^+, FeO^+	beam	O_2^+	5.5	100	100	10^{-8}	int	73	231	
SS304	Fe^+, $FeOH^+$	beam	H^+, H^+_2, H^+_3	5	12	200	10^{-10}	6	45	233	
Mg	Mg^+	beam	Ar^+	8				vary	vary	212	
Mg	Mg^+	beam	O_2^+	5.5	100	100	10^{-8}	int	73	231	
Mo	Mo^+	beam	Cs^+, K^+	0.3-2.8						201	Vary temperature
Mo	Mo^+, MoO^+, MoO_3^+	beam	O_2^+, Ar^+	2	250	0.2	10^{-10}	55	65	218	
Mo	Mo^+, Mo_2^+	beam	He^+, Ar^+	1-5				vary	vary	232	Large shift in dist w/θ_e
NaCl	Na^+	beam	He^+	20						229	
Nb	Nb^+	beam	O_2^+	5.5	100	100	10^{-8}	int	73	231	
Nb	Nb^+, Nb_2^+	beam	Ar^+	10	45	10	10^{-9}	~40	0	241	
Nb	Nb^+	beam	Ar^+	10	50	$6x10^5$	10^{-8}	~40	0	242	Current density
Ni	Ni^{1-3+}	beam	Ar^+	6.2	20	1000		0	60	206	
Ni	Ni^+	beam	Ar^+	8				vary	vary	212	E varies w/θ_e & Ei
Ni	Ni^+	beam	Ar^+	2.5	60	15	10^{-9}	45	45	226	
Ta	Ta^+	beam	Ar^+	8				vary	vary	212	E varies w/θ_e & Ei
Ti	Ti^+	beam	Ar^+	3	150	0.2	10^{-10}	55	65	220	
Ti	Ti^+	beam	Ar^+	2.5	60	15	10^{-9}	45	45	224	
Ti	Ti^+, TiO^+_{1-2}	beam	O_2^+	5.5	100	100	10^{-8}	int	73	231	
U	U^+	beam	O_2^+	5.5	100	100	10^{-8}	int	73	231	
V	V^+	beam	O_2^+	5.5	100	100	10^{-8}	int	73	231	
V	V^+	beam	Ne^+, Ar^+, Kr^+	43	200	60	10^{-7}	60	35	237	Clean surf. not RCC
W	W^+, W_2^+	beam	Ar^+	40	1000	100	10^{-6}	45	45	215	
W	W^+	beam	Ar^+	3	260	0.2	10^{-10}	55	65	220	
W	W^+, WO^+	beam	O_2^+	5.5	100	100	10^{-8}	int	73	231	
W	W^{1-4+}	beam	Ar^+	150	1000	200	10^{-6}	40	20	239	
Zr	Zr^+	beam	Ar^+	43	600	60	10^{-7}	0	30	204	
Zr	Zr^+	beam	O_2^+	5.5	100	100	10^{-8}	int	73	231	

int = high voltage extraction to provide angle integrated collection.

Table 3. Neutral (total) Mass Distribution

TARGET	PRINCIPAL SPECIES	METHOD	BEAM	keV	uA/cm^2	P(torr)	θ_e	θ_i	REFERENCE	COMMENTS
Ag	Ag_{1-2}	plasma	Ar^+	1	3000	-	-	-	315	
Ag	Ag_{1-3}	plasma	Ar^+	0.1-1	3000	-	-	-	316	∿12% Ag_2
Ag(100)	Ag, Ag_2, AgO	beam	H^+, D^+, He^+	1-4MeV	100-800	10^{-8}	vary	45	320	∿13% Ag_2
Ag(110)	Ag, Ag_2, AgO	beam	H^+, D^+, He^+	1-4 MeV	100-800	10^{-8}	vary	45	320	
Al_2O_3	Al, AlO, Al_2O	beam	H^+, Ar^+	15		10^{-5}		0	310	
Al_2O_3	Al_2O_2, AlO_{2-3}	beam	Ar^+	50		10^{-5}		0	310	
Al_2O_3	Al, AlO, Al_2O	beam	Ar^+	15&50		10^{-5}		0	317	
Al_2O_3	Al, AlO, Al_2O	beam	H^+	15		10^{-5}		0	317	
Al_2O_3	Many	plasma	H^+, D^+	-		-	-	-	322	
Au	Au_{1-3}	plasma	Ar^+	0.1-1	3000	-	-	-	316	12% Au_2
B_4C	CD_4	beam	D^+	20	10^3	10^{-9}		0	303	Temp. dependence
C	CH_4		H_2^+	6					302	
C	CH_4		H_3^+	2,3,6					302	
C	CH_4	beam	H^+, D^+	20	10^3	10^{-9}		0	309	Temp. dependence
C	Many	plasma	H^+, D^+	-	-	-	-	-	322	
C/Pt	CH_4	beam	H_2^+	5	130	10^{-8}			327	
Cu	$Cu, Cu_2, CuCO$	plasma	Ar^+	0.6	-	-	-	-	306	
Cu	Cu, Cu_2	sim	Ar^+	0.6				0	311	
Cu	Cu_{1-5}	sim	Ar^+	0.6				0	312	
Cu	Cu_{1-3}	plasma	Ar^+	0.1-1	3000	-	-	-	316	9.5% Cu_2
Cu(100,110)	Cu, Cu_2, CuO	beam	H^+, D^+, He^+	1-4 MeV	100-800	10^{-8}	vary	45	320	∿13% Cu_2
Cu+O	Many	sim	Ar^+	0.6				0	314	
Fe_2O_3	Fe, FeO	plasma	Ar^+	-	-	-	-	-	307	
K	K, K_2	beam	Ar^+	11	500	10^{-7}			301	
Mo	Mo_{1-3}	plasma	Ar^+	0.1-1	3000	-	-	-	316	∿3% Mo_2
Nb	Many	plasma	Ar^+	-		-	-	-	306	
Nb_2O_5	Nb, NbO	plasma	Ar^+	-	-	-	-	-	307	∿40% NbO
Ni	Ni, Ni_2	plasma	Ar^+	0.1-1	3000	-	-	-	316	∿4% Ni_2
Ni	Ni, Ni_2	plasma	Ar^+	1	$\sim 10^3$				324	
NiCu	Many	plasma	Ar^+	-	-	-	-	-	306	
Pd	Pd_{1-3}	plasma	Ar^+	0.1-1	3000	-	-	-	316	2.5% Pd_2
Pr_6O_{11}	Pr, PrO	plasma	Ar^+	-	-	-	-	-	307	∿50% PrO
Pt	Pt_{1-3}	plasma	Ar^+	0.1-1	3000	-	-	-	316	3.7% Pt_2
SiC	CD_4	beam	D^+	20	103	10^{-9}		0	303	Temp. dependence
SiC	Many	beam	He^+, Ne^+, Ar^+ Kr^+, Xe^+	0.6	50		∿45	∿45	319	
SiO_2	Si, SiO, O	plasma	Ne^+, Ar^+	-	-	-	-	-	304	
SnO	Sn, SnO	plasma	Ar^+	-	-	-	-	-	307	
Ta	Ta_{1-3}	plasma	Ar^+	0.1-1	3000	-	-	-	316	1.9% Ta_2
Ta_2O_5	Ta, TaO	plasma	Ar^+	-	-	-	-	-	307	>40% TaO
TiO_2	Ti, TiO	plasma	Ar^+	-	-	-	-	-	307	∿40% TiO
W	W_{1-3}	plasma	Ar^+	0.1-1	3000	-	-	-	316	3% WO
Zr	Zr_{1-2}	plasma	Ar^+	0.1-1	3000	-	-	-	316	1.5% ZrO

Table 4. Ion Mass Distribution

TARGET	PRINCIPAL SPECIES	METHOD	BEAM	keV	uA/cm^2	P(torr)	θ_e	θ_i	REFERENCE	COMMENTS
Ag	Ag_{1-3}^+	beam	Ar^+	6.2	1000		0	60	406	
Ag(100)	Ag_{1-2}^+, Ag^{++}	beam	D^+	1 MeV	100-800	10^{-8}	vary	vary	422	
Ag	Many	beam	Ne^+	0.3-0.4	50		45	45	417	
Al	Al^+, AlO_{1-2}^+	beam	Ar^+	3	$\sim 10^{-3}$	10^{-10}	0	70	402	"absolute" yields
$Al+O_2$	Al^+, AlO^+	beam	Ar^+	6	100		int		407	
$Al+O_2$	Al^+, Al_2^+, O^-	beam	Ar^+	0.3-0.7	10^{-3}	10^{-10}	0	71	411	
Al	Al_{1-3}^+, Al_{1-16}^-	beam	Ar^+, Ar^+, Xe^+	4-12	10^3		int	45	415	
Al	Al_{1-5}^+, Al^{++}	beam	Ar^+	6	600	10^{-6}	int		425	
Al	Al_{1-2}^+	beam	Xe^+, Ar^+	2.25-11.6	10	10^{-9}	~40	0	435	Energy dependence
AlCu	Al_{1-11}^+	beam	Ar^+	6	10	10^{-9}	~40	0	408	
AlMg	Many	beam	Ar^+	12	10^3		int	45	415	
Au	Au_{1-3}^+	beam	Ar^+	6.2	1000		0	60	406	
Au	Au^+, Au^-	beam	Ar^+	40	60	10^{-6}	45	45	421	
Au	Au_{1-2}^+	beam	Ar^+	2.25-11.6	10	10^{-9}	~40	0	435	Energy dependence
Au	Au_{1-2}^+	beam	Ar^+	10-12	vary	10^{-8}	~40	0	436	dimer/monomer vs j_p
$Be+O_2$	Many	beam	Ar^+	3	0.2	10^{-10}	45	45	424	
$Be+H_2$	Many	beam	Ar^+	3	0.2	10^{-10}	45	45	424	
Be	Be^+, BeD^+	beam	D_2^+, Ar^+	3	0.2	10^{-10}	45	45	424	
Be	Be_{1-7}^+	beam	Ar^+	10					426	
C	C^-_{1-17}	beam	Ar^+	6.5					408	peak intensity at C_5^-
C	C_{1-10}^-	beam	Ar^+	0.5	50		45	45	419	C_2^- largest peak
C	C_{1-12}^-	beam	He^+, Ne^+ Kr^+, Xe^+	0.6	50		45	45	419	$C_{3,4,5,6}^- \rightarrow C^-$ Intensity
$Cr+O_2$	Many	beam	Ar^+	3	$\sim 10^{-3}$	10^{-10}	0	70	401	"absolute" yields
Cr	Cr_{1-3}^+	beam	Ar^+	6.2	1000		0	60	406	
Cu	Cu^+_{1-7}	beam	Ar^+	-	5000		int	55	405	$Cu_3^+ > Cu^+$
Cu	Cu_{1-15}^+	beam	Ar^+	11					408	Large clusters
Cu(100)	Cu_{1-2}^+, Cu^{++}	beam	D^+	1 MeV	100-800	10^{-8}	var	45	422	
CuCr		beam	Ar^+	6.2	1000		0	60	406	
CuMn		beam	Ar^+	6.2	1000		0	60	406	
$Fe+O_2$	Fe^+, FeO^+	beam	Ar^+	3	$\sim 10^{-3}$	10^{-10}	0	70	401	"absolute"yields
Fe	Many	beam	Ar^+	3	$\sim 10^{-3}$	10^{-10}	0	70	402	"absolute" yields
Fe	Fe_{1-3}^+	beam	Ar^+	6.2	1000		0	60	406	
$Fe+O_2$	Fe_{1-3}^+, FeO_{1-2}^+	beam	O_2^+	6		10^{-7}			429	
FeNi	Fe^+, Ni^+	beam	Kr^+	4	1-20	10^{-6}		45	431	vary composition
FeCr	Fe^+, Cr^+	beam	Kr^+	4	1-20	10^{-6}		45	431	vary composition
Li	Li_{1-9}^+	beam	Ar^+	10			-	-	426	
$Mg+O_2$	Mg^+, MgO^+	beam	Ar^+	3	$\sim 10^{-3}$	10^{-10}	0	70	402	"absolute" yields
Mn	Mn_{1-3}^+	beam	Ar^+	6.2	1000		0	60	406	
$Mo+O_2$	Mo^+, MoO_{1-2}^+	beam	Ar^+	3	$\sim 10^{-3}$	10^{-11}			404	
Mo	Mo_{1-3}^+	beam	Ar^+	6.2	1000		0	60	406	
Mo	Mo^+, Mo_2^+	beam	Ne^+, Ar^+	5			vary	vary	432	Angular dependence
Mo	Mo_{1-2}^+	beam	Ar^+	2.25-11.6	10	10^{-9}	~40	0	435	Energy dependence
NaBr	Na_nBr_{n-1} (n=2-4)	beam	Ar^+	3	10^{-2}	10^{-10}	int		416	
NaCl	Na_nCl_{n-1} (n=2-12)	beam	Ar^+	3	10^{-2}	10^{-10}	int		416	
Nb	Nb_{1-3}^+	beam	Ar^+	6.2	1000		0	60	406	
Nb	Nb_{1-2}^+	beam	Ar^+	2.25-11.6	10	10^{-9}	~40	0	435	Energy dependence
Nb	Nb_{1-2}^+	beam	Ar^+	10-12	vary	10^{-8}	~40	0	436	Dimer/monomer vs j_p
$Ni+O_2$	Ni_{1-3}^+, Ni_2O^+	beam	Ar^+	0.15-1.5	$\sim 10^{-3}$	10^{-10}	0	71	413	
Ni	Ni_{1-2}^+, O^-	beam	Ar^+	40	60	10^{-6}	45	45	421	
Si	Si_{1-7}^+	beam	Ne^+, Ar^+, Kr^+, Xe^+		1-10	10^{-9}		0,45	438	Vary primary energy
SiC	Many	beam	Xe^+	0.6	50		45	45	418	
Ta	Ta_{1-2}^+	beam	Ar^+	2.25-11.6	10	10^{-9}	~40	0	435	Energy dependence
Ti	Ti^+, TiO_{1-2}^+	beam	Ar^+	3	$\sim 10^{-3}$	10^{-10}	0	70	402	"absolute" yields
Ti	Ti_{1-3}^+	beam	Ar^+	6.2	1000		0	60	406	
$Ti+D_2$	Many	beam	Ar^+	40					424	
$U+O_2$	U^+, UO^+, UO_2^+	beam	O_2^+	6	1000	10^{-7}		45	430	
V	V_{1-3}^+	beam	Ar^+	6.2	1000		0	60	406	
$W+O_2$	W^+, WO_{1-2}^+	beam	Ar^+	3	$\sim 10^{-3}$	10^{-10}	0	70	402	"absolute" yields
W	W_{1-2}^+	beam	Ar^+	2.25-11.6	10	10^{-9}	~40	0	435	Energy dependence
W	W_{1-2}^+	beam	Ar^+	10-12	vary	10^{-8}	~40	0	436	Dimer/monomer vs j_p
W	W^{++}, W_{1-12}^+	beam	Ar^+	150	200		45	20	433	

References

Introduction

(1) R. Behrisch, G. Maderlechner, B.M.U. Scherzer and M. T. Robinson, Appl. Phys. 18 (1979) 391.

(2) H. Overeijnder, A. Haring and A. E. deVries, Rad. Eff. 37 (1978) 205.

(3) I.S.T. Tsong and N. A. Yusuf, Appl. Phys. Lett. 33 (1978) 999.

(4) S. Dzioba, O. Auciello and R. Kelly, submitted to Rad. Eff.

(5) M. A. Rudat and G. H. Morrison, Cornell University Materials Science Center Report #3056.

(6) K. Wittmaack, Secondary Ion Production in *Inelastic Ion-Surface Collisions*, Tolk, Tully, Heiland and White eds., Academic Press (1977).

(7) G. K. Wehner, private communication.

(8) A. R. Krauss and D. M. Gruen, J. Nucl. Mat. 63 (1976) 380.

(9) W. O. Hofer, H. L. Bay and P. J. Martin, J. Nucl. Mat. 76 & 77 (1978) 156.

(10) P. Joyes, private communication.

(11) A. R. Krauss and R. B. Wright, to be published.

(101) A. P. M. Baede, W. F. Jungmann and J. Los, Physica 54 (1971) 459.

(102) F. Bernhardt, H. Oechsner and E. Stumpe, Nucl. Inst. Meth. 132 (1976) 329.

(103) H. Beuscher and K. Kopitski, Z. für Physik 184 (1965) 382.

(104) G. E. Chapman, B. W. Farmery, M. W. Thompson and I. H. Wilson, Rad. Eff. 13 (1972) 121.

(105) A. Elbern, Thesis, KFA Julich (1977) unpublished.

(106) A. Elbern, E. Hintz and B. Schweer, J. Nucl. Mat. 76 & 77 (1978) 143.

(107) B. J. Garrison, N. Winograd and D. E. Harrison, Jr., J. Chem. Phys. 69 (1978) 1440.

(108) B. J. Garrison, N. Winograd and D. E. Harrison, Jr., submitted to Surf. Sci.

(109) D. E. Harrison, Jr., W. L. Moore, Jr. and H. T. Holcombe, Rad. Eff. 17 (1973) 167.

(110) D. E. Harrison, Jr., P. W. Kelly, B. J. Garrison and N. Winograd, Surf. Sci. 76 (1978) 311.

(111) H. F. Helbig, J. Vac. Sci. Tech. 13 (1976) 368.

(112) M. Hou and M. T. Robinson, Appl. Phys. 18 (1979) 381.

(113) P. G. Hucks, thesis, Univ. Köln (1978).

(114) P. Hucks, G. Stocklin, E. Vietzke and K. Vogelbruch, J. Nucl. Mat. 76 & 77 (1978) 136.

(115) E. Hulpke and Ch. Schlier, Z. Physik 207 (1967) 294.

(116) W. Husinsky, R. Bruckmuller, P. Blum, F. Viehlbock, D. Hammer and E. Benes, J. Appl. Phys. 48 (1977) 4734.

(117) W. Husinsky and R. Bruckmuller, Surf. Sci. 80 (1979) 637.

(118) G. P. Können, J. Grosser, A. Haring, A. E. deVries, and J. Kistemaker, Rad. Eff. 21 (1974) 171.

(119) K. Kopitzki and H. E. Stier, Z. Naturforsch 17 (1962) 346.

(120) K. Kopitzki and H. E. Stier, Phys. Lett. 4 (1963) 232.

(121) A. R. Krauss and D. M. Gruen, submitted Surf. Sci.

(122) J. J. Low and A. F. Wagner, submitted Surf. Sci.

(123) T. R. Lundquist, thesis, University of Maryland, 1979.

(124) T. R. Lundquist, J. Vac. Sci. Tech. 15 (1978) 684.

(125) T. R. Lundquist, to be published.

(126) H. Oechsner and L. Reichert, Phys. Lett. 23 (1966) 90.

(127) H. Oechsner, Z. Phys. 238 (1970) 433.

(128) J. Politiek and J. Kistemaker, Rad. Eff. 2 (1969) 129.

(129) I. Reid, B. W. Farmery and M. W. Thompson, Nucl. Inst. Meth. 132 (1976) 317.

(130) R. Stuart, K. Brower and W. Mayer, Rev. Sci. Inst. 34 (1963) 425.

(131) R. Stuart and G. K. Wehner, J. Appl. Phys. 35 (1964) 1819.

(132) R. V. Stuart, G. K. Wehner and G. S. Anderson, J. Appl. Phys. 40 (1969) 803.

(133) M. Szymonski, H. Overeijnder and A. E. deVries, Rad. Eff. 36 (1978) 189.

(134) M. W. Thompson and R. S. Nelson, Phil Mag. 7 (1962) 2015.

(135) M. W. Thompson, Phil. Mag. 18 (1968) 377.

(136) B. W. Farmery and M. W. Thompson, Phil. Mag. 18 (1968) 415.

(137) R. A. Weller and T. A. Tombrello, Rad. Eff. 37 (1978) 83.

(138) N. Winograd, B. J. Garrison, T. Fleisch, W. N. Delgass and D. E. Harrison, Jr., J. Vac. Sci. Tech. (in press).

(139) C. E. Young, P. M. Dehmer, R. B. Cohen, L. G. Pobo and S. Wexler, J. Chem. Phys. 64 (1976) 306.

(201) A. A. Adylov, V. I. Veksler and A. M. Reznik, Sov. Phys. Sol. St. 11 (1970) 1441.

(202) A. A. Adylov, V. I. Veksler and A. M. Reznik, Sov. Phys. Sol. St. 14 (1973) 2696.

(203) A. R. Bayley, P. J. Martin and R. J. MacDonald, Nucl. Inst. Meth. 132 (1976) 459.

(204) A. R. Bayley and R. J. MacDonald, Rad. Eff. 34 (1977) 169.

(205) A. Benninghoven, Ann. Phys. 15 (1965) 113.

(206) G. Blaise and G. Slodzian, Rev. Phys. Appl. 8 (1973) 105.

(207) G. Blaise, Fundamental Aspects of Ion Microanalysis in *Material Characterization Using Ion Beams*, J. P. Thomas and A. Cachard, Eds, Plenum Press (1978).

(208) R. Castaing and J. F. Hennequin, C. R., Acad. Sci. (Paris) 262 (1966) 1008B.

(209) P. H. Dawson, Surf. Sci. 57 (1976) 229.

(210) P. H. Dawson, J. Vac. Sci. Tech. 14 (1977) 786.

(211) E. Dennis and R. J. MacDonald, Rad. Eff. 13 (1972) 243.

(212) J. F. Hennequin, J. de Phys. (Paris) 29 (1968) 655.

(213) F. Honda, G. M. Lancaster, Y. Fukuda and J. W. Rabalais, J. Chem. Phys. 69 (1978) 4931.

(214) Z. Jurela and B. Perovic, Can. J. Phys. 46 (1968) 773.

(215) Z. Jurela, Rad. Eff. 19 (1973) 175.

(216) H. Kerkow and M. Trapp, Int. J. Mass Spec. Ion Phys. 13 (1974) 113.

(217) K. Komori and J. Okano, Int. J. Mass Spec. Ion Phys. 27 (1978) 379.

(218) A. R. Krauss and D. M. Gruen, Appl. Phys. 14 (1977) 89.

(219) A. R. Krauss and D. M. Gruen, Nucl. Inst. Meth. 149 (1978) 547.

(220) A. R. Krauss and D. M. Gruen, J. Nucl. Mat. (in press).

(221) A. R. Krauss and D. M. Gruen, Surf. Sci. (in press).

(222) A. R. Krauss and D. M. Gruen, (submitted to Surf. Sci.).

(223) R. Laurent and G. Slodzian, Rad. Eff. 19 (1973) 181.

(224) T. R. Lundquist, thesis (Univ. of Maryland, 1979).

(225) T. R. Lundquist, J. Vac. Sci. Tech. 15 (1978) 654.

(226) T. R. Lundquist, to be published.

(227) R. J. MacDonald and P. J. Martin, Surf. Sci. 67 (1977) 237.

(228) P. J. Martin and R. J. MacDonald, Rad. Eff. 32 (1977) 177.

(229) S. Miyagawa, J. Appl. Phys. 12 (1973) 5617.

(230) A. E. Morgan and H. W. Werner, Surf. Sci. 65 (1977) 687.

(231) M. A. Rudat and G. H. Morrison, Surf. Sci. 82 (1979) 549.

(232) G. A. Schootbrugge, A.G.J. deWitt and J. M. Fluit, Nucl. Inst. Meth. 132 (1976) 321.

(233) J. N. Smith, Jr., J. Nucl. Mat. 78 (1979) 117.

(234) J. N. Smith, Jr., IEEE Trans. Nucl. Sci. NS-26 (1979) 1292.

(235) K. J. Snowdon, Proc. 3rd Int. Conf. Sol. Surf. (Vienna) 1977.

(236) K. J. Snowdon, Rad. Eff. 38 (1978) 141.

(237) K. J. Snowdon and R. J. MacDonald, Int. J. Mass Spec. Ion Phys. 28 (1978) 233.

(238) K. J. Snowdon and R. J. MacDonald, Int. J. Mass Spec. Ion Phys. 29 (1979) 101.

(239) G. Staudenmaier, Rad. Eff. 13 (1972) 87.

(240) K. Wittmaack, Surf. Sci. 53 (1975) 626.

(241) K. Wittmaack and G. Staudenmaier, Appl. Phys. Lett. 27 (1975) 318.

(242) K. Wittmaack, Nucl. Inst. Meth. 132 (1976) 381.

(243) V. E. Yurasova, et al., Rad. Eff. 20 (1973) 89.

3. Neutral (total) Mass Distribution

(301) A.P.M. Baede, W. F. Jungmann, and J. Los, Physica 54 (1971) 459.

(302) R. Behrisch, Fusion-First Wall Problems in *Critical Materials Problems in Energy Production*, C. Stein, ed., Academic Press (1976) 128.

(303) C. Braganza, G. M. McCracken and S. K. Erents, Proc. Int. Symp. Plasma Wall Interactions, Julich, October 1976, Pergamon.

(304) J. W. Coburn and E. Kay, Appl. Phys. Lett. 18 (1971) 435.

(305) J. W. Coburn and E. Kay, Appl. Phys. Lett. 19 (1971) 350.

(306) J. W. Coburn, E. Taglauer and E. Kay, J. Vac. Sci. Tech. 12 (1975) 151.

(307) J. W. Coburn, E. Taglauer and E. Kay, Jap. J. Appl. Phys. Suppl. 2 Pt. 1 (1974) 501.

(308) J. Comas and C. B. Cooper, J. Appl. Phys. 38 (1967) 2956.

(309) S. K. Erents, C. M. Braganza and G. M. McCracken, J. Nucl. Mat. 63 (1976) 399.

(310) P. A. Finn, D. M. Gruen and D. L. Paige, Adv. Chem. series, M. Kaminsky, ed., Radiation Effects on Solid Surface.

(311) B. J. Garrison, N. Winograd and D. E. Harrison, Jr., submitted to Surf. Sci.

(312) B. J. Garrison, N. Winograd and D. E. Harrison, Jr., J. Chem. Phys. 69 (1978) 1440.

(313) B. J. Garrison, N. Winograd and D. E. Harrison, Jr., Phys. Rev. B 18 (1978) 6000.

(314) B. J. Garrison and N. Winograd, to be published.

(315) W. Gerhard, Z. Phys. B 22 (1975) 31.

(316) W. Gerhard and H. Oechsner, Z. Phys. B 22 (1975) 41.

(317) D. M. Gruen, P. A. Finn, and D. L. Page, Nucl. Tech. 29 (1976) 309.

(318) D. E. Harrison, Jr. and C. B. Delaplain, J. Appl. Phys. 47 (1976) 2252.

(319) R. E. Honig, 5th Int. Conf. Ion. Phenomena in Gases, H. Maecker, ed. North-Holland (1976).

(320) M. Kaminsky, Adv. Mass. Spec. 3 (1966) 69.

(321) G. P. Können, J. Grosser, A. Haring, A. E. deVries and J. Kistemaker, Rad. Eff. 21 (1974) 171.

(322) G. M. McCracken and J. W. Partridge, J. Nucl. Mat. 63 (1976) 373.

(323) H. Oechsner and W. Gerhard, Phys. Lett. 40A (1972) 211.

(324) H. Oechsner and W. Gerhard, Surf. Sci. 44 (1974) 480.

(325) H. Oechsner, Z. Phys. 261 (1973) 37.

(326) A. J. Smith, L. A. Cambey and D. J. Marshall, J. Appl. Phys. 34 (1963) 2489.

(327) J. N. Smith, Jr. and C. H. Meyer, Jr., J. Nucl. Mat. 76 & 77 (1978) 193.

(328) M. Szymonski, H. Overeijnder and A. E. deVries, Rad. Eff. 36 (1978) 189.

(329) H. M. Windawi and C. B. Cooper, Phys. Lett. 43A (1973) 491.

(330) N. Winograd, B. J. Garrison, T. Fleisch, W. N. Delgass and D. E. Harrison, Jr., J. Vac. Sci. Tech. 16 (1979) 629.

(331) N. Winograd, D. E. Harrison, Jr. and B. J. Garrison, Surf. Sci. 78 (1978) 467.

(332) J. R. Woodyard and C. B. Cooper, J. Appl. Phys. 35 (1974) 1107.

(401) A. Bennighoven, Surf. Sci. 35 (1973) 427.

(402) A. Benninghoven, Surf. Sci. 53 (1975) 596.

(403) A. Benninghoven, H. Bispinck, O. Ganschow and L. Wiedmann, Appl. Phys. Lett. 31 (1977) 341.

(404) A. Benninghoven, O. Ganschow and L. Wiedmann, J. Vac. Sci. Tech. 15 (1978) 506.

(405) M. Bernheim, G. Blaise and G. Slodzian, Int. J. Mass. Spec. Ion Phys. 10 (1972) 293.

(406) G. Blaise and G. Slodzian, Rev. de Phys. Appl. 8 (1973) 105.

(407) G. Blaise and M. Bernheim, Surf. Sci. 47 (1975) 324.

(408) G. Blaise, Fundamental Aspects of Ion Microanalysis in *Material Characterization Using Ion Beams*, J. P. Thomas and A. Cachard, eds. Plenum (1978).

(409) A. B. Campbell III and C. B. Cooper, J. Appl. Phys. 43 (1972) 863.

(410) R. Castaing and J. F. Hennequin, Adv. Mass. Spec. 5 (1971) 419.

(411) P. H. Dawson, Surf. Sci. 57 (1976) 229.

(412) P. H. Dawson, Phys. Rev. 15 (1977) 5522.

(413) P. H. Dawson and W. C. Tam, Surf. Sci. 81 (1979) 164.

(414) T. Fleisch, G. L. Ott, W. N. Delgass and N. Winograd, Surf. Sci. 81 (1979) 1.

(415) R. F. K. Herzog, W. P. Poschenrieder and F. G. Satkiewicz, Rad. Eff. 18 (1973) 199.

(416) F. Honda, G. M. Lancaster, Y. Fukuda and J. W. Rabalais, J. Chem. Phys. 69 (1978) 4931.

(417) R. E. Honig, J. Appl. Phys. 29 (1958) 549.

(418) R. E. Honig, 5th Int. Conf. Ion. Phenomena in Gases, H. Maecker, ed., North-Holland (1962).

(419) R. E. Honig, Adv. Mass. Spec. 2 (1963) 25.

(420) Z. Jurela and B. Perovic, Can. J. Phys. 46 (1968) 773.

(421) Z. Jurela, Rad. Eff. 19 (1973) 175.

(422) M. Kaminsky, Adv. Mass. Spec. 3 (1966) 69.

(423) A. R. Krauss and D. M. Gruen, Appl. Phys. 14 (1977) 89.

(424) A. R. Krauss and D. M. Gruen, Surf. Sci. (in press).

(425) R. Laurent and G. Slodzian, Rad. Eff. 19 (1973) 181.

(426) M. Leleyter and P. Joyes, Rad. Eff. 18 (1973) 105.

(427) R. J. MacDonald and P. J. Martin, Surf. Sci. 67 (1977) 237.

(428) J. Maul and K. Wittmaack, Surf. Sci. 47 (1975) 358.

(429) A. E. Morgan and H. W. Werner, Appl. Phys. 11 (1976) 193.

(430) A. E. Morgan and H. W. Werner, Surf. Sci. 65 (1977) 687.

(431) M. Riedel, T. Nenadovic and B. Perovic, Acta Chim. Acad. Sci. Hung. 97 (1978) 177.

(432) G. A. v.d. Schootbrugge, A. G. J. deWit and J. M. Fluit, Nucl. Inst. Meth. 132 (1976) 321.

(433) G. Staudenmaier, Rad. Eff. 13 (1972) 87.

(434) H. W. Werner, Surf. Sci. 47 (1975) 301.

(435) K. Wittmaack and G. Staudenmaier, Appl. Phys. Lett. 27 (1975) 318.

(436) K. Wittmaack, Nucl. Inst. Meth. 132 (1976) 381.

(437) K. Wittmaack, Surf. Sci. 68 (1977) 118.

(438) K. Wittmaack, Phys. Lett. 69A (1979) 322.

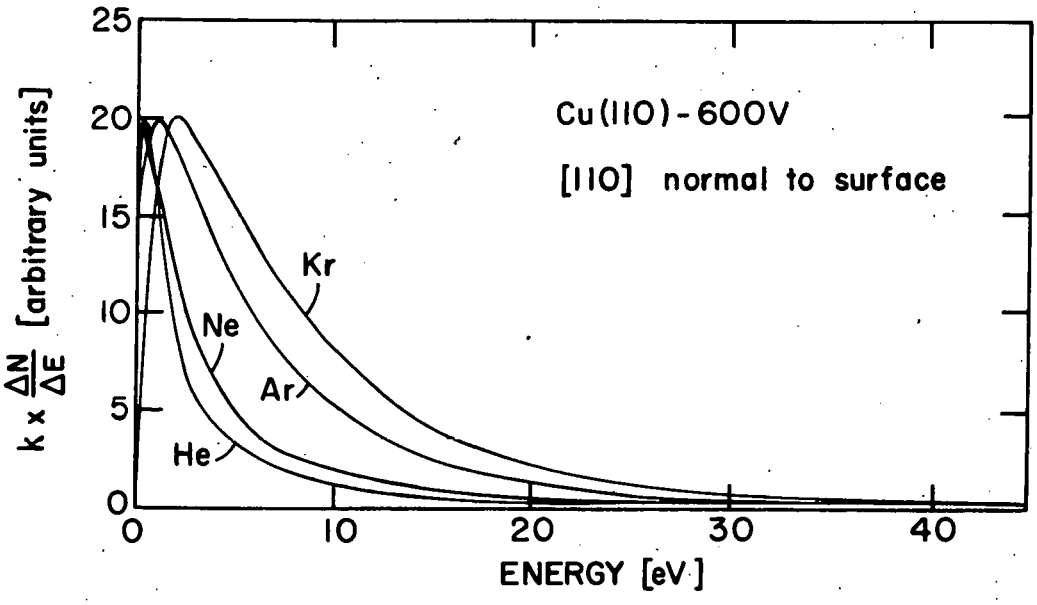

FIG. 1. Kinetic energy distributions for neutral Cu atoms sputtered from a Cu (110) crystal in the normal direction by four different 600 eV inert gas ion beams. [After Stuart and Wehner (131)].

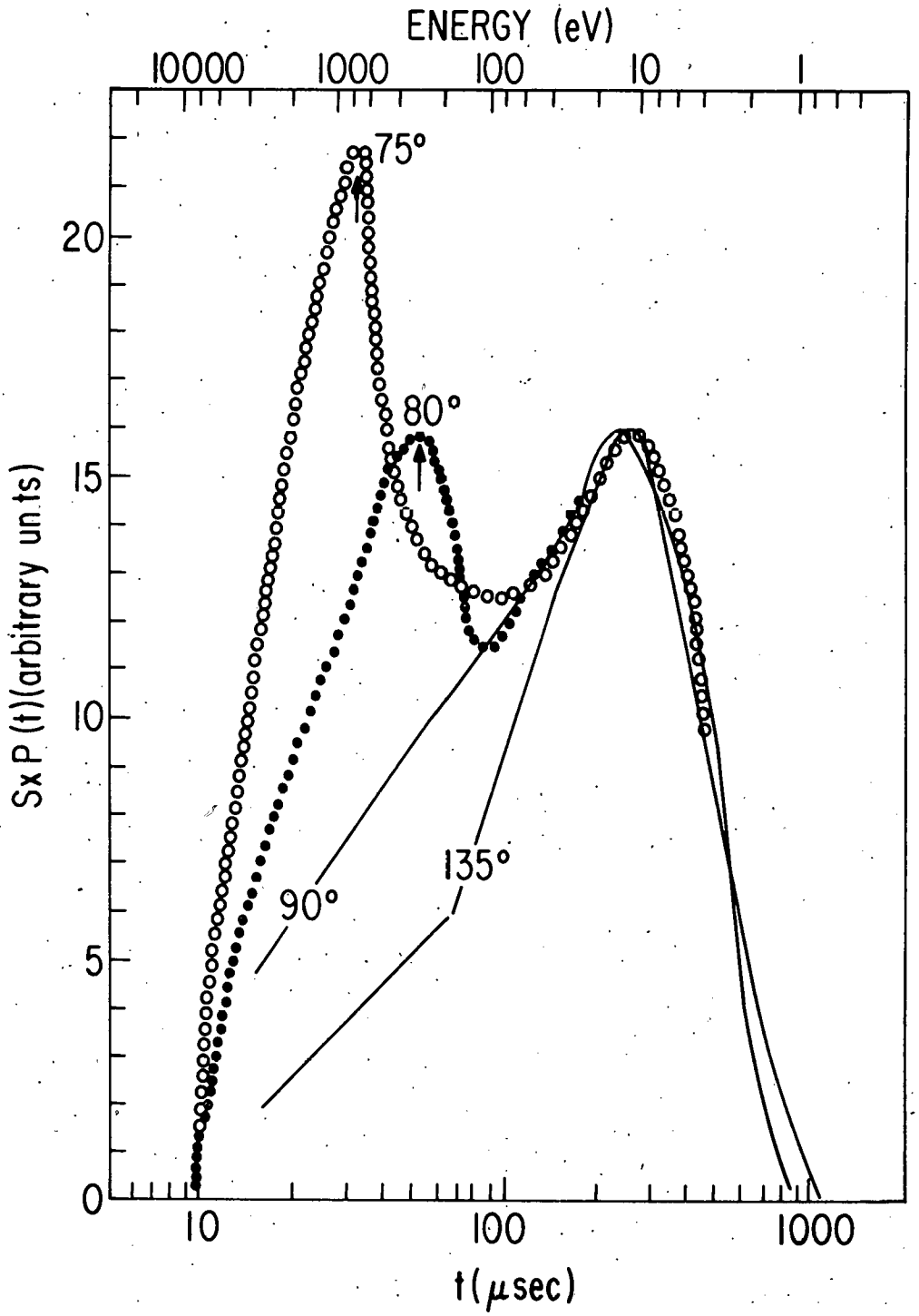

FIG. 2. Variations in the shape of the time-of-flight spectrum with recoil angle $\theta' = \theta - 180°$ shown on each curve. The samples are polycrystalline Au bombarded with 20 keV Ar^+ at 45° to the surface normal. [After Reid, Farmery and Thompson (129)].

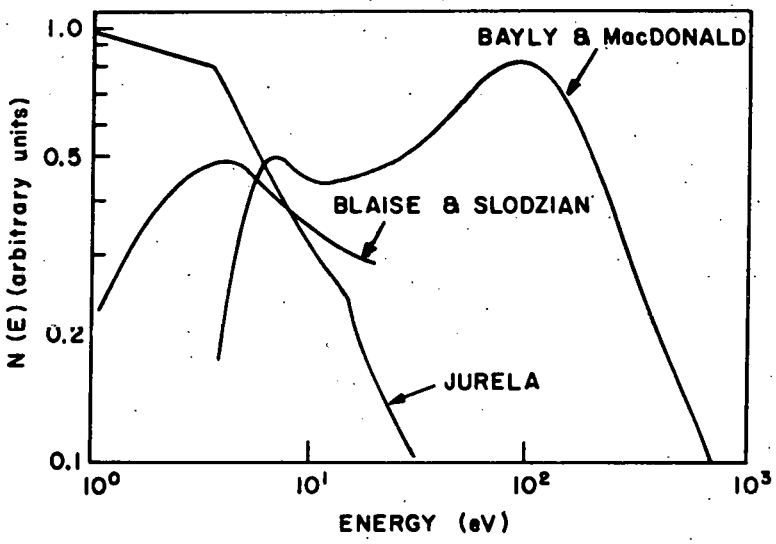

FIG. 3. A comparison of the secondary ion energy spectra obtained by various authors for polycrystalline copper. Jurela: 40 keV Ar^+, 60 uA cm^{-2}, 2 x 10^{-6} torr. Blaise and MacDonald: 43 keV Ar^+, 1000 uA cm^{-2}, 1 x 10^{-7} torr. Bayly and MacDonald: 43 keV Ar^+, 60 uA cm^{-2}, 1 x 10^{-7} torr. [After Snowdon and MacDonald (237)].

ANGULAR DISTRIBUTION OF SPUTTERED PARTICLES

M. Kaminsky
Argonne National Laboratory, Argonne, Illinois

SUMMARY

... Information about the angular distribution of particles sputtered from materials of interest for the fusion program under light ion bombardment ($Z_1 \lesssim 2$) for the energy range from ~ 100 eV $\lesssim E \lesssim 1$ MeV is scarce.

... The corresponding information for medium-Z ion bombardment (e.g. plasma impurity ions, such as C^+, N^+, O^+, CO^+) for the energy range from ~ 100 eV $\leq E \leq 120$ eV is also scarce.

... There exists more information on the ejection of sputtered particles from monocrystalline targets [emission along preferred directions — ("spot patterns")] than from polycrystalline targets (for reviews see references 1-5).

... The few data available on the angular distribution of particles sputtered from polycrystalline or amorphous materials indicate the following trends:

... The energy of the incident ion influences the angular distribution of sputtered particles. For example, for Hg^+ ions impinging on Ni, Fe, Pt and Mo surfaces at normal incidence, the angular distribution is considered to be "under-cosine" (i.e. more particles are scattered in directions parallel to the surface and fewer in the direction of the surface normal) for ion energies of $\sim$ 100 eV, and approach a "near-cosine" distribution at 1 keV [Ref. 6] (see Fig. 1). Cooper and Comas [7] reported "under-cosine" distributions for 160-200 eV A^+ ions bombarding silver surfaces, Patterson and Tomlin [8] for 10 keV A^+ on gold surfaces, and Chiplonkar et al. [9] for 3-7 keV A^+ on silver surfaces. A change from an "under-cosine" distribution to a cosine distribution with increasing ion energy was reported by Chiplonkar et al. [10].

A cosine distribution has been reported by Gronlund and Moore [11] for 4 keV Ne^+ on Ag, and by Kaminsky et al. [12] and Das et al. [13] for 40-, 60-, and 120-keV D^+ bombardment of Mo. (See Fig. 2). An "over-cosine" distribution has been reported by several authors (e.g. Ref. 8, 14) for keV noble gas ions bombarding noble metals (e.g., Ag, Au).

... The angle of incidence has been observed to influence the angular distribution of sputtered particles significantly [e.g. Refs. 8, 11, 15, 16, 17, 18, 19]. In most of these experiments Hg^+ ions [6], D^+ ions [11], and noble gas ions were used with energies ranging from $\sim$ 100 eV to several ten keV on targets such as noble metals, Cu, Ta, and W. For example, some results obtained by Gurwin et al. [16] are shown in Fig. 3.

In general, it has been observed that as the angle of incidence increases (towards more oblique angles), that the maximum in the angular distribution shifts towards directions which come close to those the incident ion beam would be directed to if it were specularly reflected from the surface. Furthermore, Oechsner, et al. [19] observed for 1 keV A^+ bombardment of Cu and Ta at an angle of incidence of 50°, that the maximum in the angular distribution has shifted farther from the surface normal for the Ta target than for the Cu target (see Fig. 4). (The latter has higher sputter yield and lower surface binding energy than Ta).

... The surface topography (e.g. surface faceting, cone formation) has also been observed to influence the angular distribution of sputtered particles significantly, particularly at oblique angles of incidence [see Refs. 16, 20, 21].

REFERENCES ON SPUTTERING

REVIEWS

[1] H. Oechsner, Applied Physics 8, 185 (1975).

[2] R. S. Nelson, "The Observations of Atomic Collisions in Crystalline Solids," North Holland Pub. 1968.

[3] G. Carter and J.S. Colligon, "Ion Bombardment of Solids," American Elesvier Pub. 1968.

[4] M. Kaminsky, "Atomic and Ionic Impact Phenomena on Metal Surfaces," Springer Verlag, 1965).

[5] R. Behrisch, Ergebn. Exakt. Naturwiss. 35, 295, 1964.

ANGULAR DISTRIBUTION AS FUNCTION OF ION ENERGY

[6] G. K. Wehner and D. Rosenberg, J. Appl. Phys. 31, 177, (1960).

[7] C. B. Cooper and J. Comas, J. Appl. Phys. 36, 2891 (1965).

[8] H. Patterson and D. H. Tomlin, Proc. Roy. Soc. A265, 474 (1962).

[9] S.R. Rane and V. T. Chiplonkar, Indian Pure and Appl. Phys. 3 131 (1965).

[10] V. T. Chiplonkar and S. R. Rane, Proc. Indian Acad. Sci. A61, 100 (1965).

[11] F. Gronlund and W. J. Moore, J. Chem. Phys. 32, 1540 (1960).

[12] M. Kaminsky, S.K. Das and J. Cecchi, Proc. 10th S.O.F.T. Conference, Padova, Italy, Sept. 4-8, 1978.

[13] S.K. Das, M. Kaminsky, R. Tishler and J. Cecchi, J. Nucl. Mat. (in print).

[14] S.B. Karmohapatro and A.V. Narasinham, Proc. Symp. on Collision Processes Dehradun, Proc. Natl. Acad. Sci., India, Sec. A33, 629 (1963).

ANGULAR DISTRIBUTION AS A FUNCTION OF ANGLE OF INCIDENCE

[15] E. Formann, F.P. Viehböck, H. Wotke, Phys. Lett. 23, 558 (1966).

[16] B.M. Gurmin, Yu. A. Ryzhov, I.I. Skharban, Bull. Acad. Sci. USSR Phys. Ser. (USA) 33, 752, (1969).

[17] G. Betz, R. Dobrozemsky, F.P. Viehbock, Niederl. Tidjschr. Vacuumtechn. 8, 203 (1970).

[18] K. Rödelsperger, W. Krüger and A. Scharmann, Z. Physik, 83 (1974).

[19] J. Birk and H. Oechsner, Dechma-Dagv Tagung, Frankfurt (1974).

ANGULAR DISTRIBUTION AS A FUNCTION OF SURFACE TOPOGRAPHY

[20] V. Littmark and W. O. Hofer, J. Materials Sciences, 13 2577 (1978).

[21] K. Rödelsperger and A. Scharmann, Nucl. Instr. Meth. 132 355 (1976).

ADDITIONAL RECENT REFERENCES ON THE ANGULAR DISTRIBUTION OF SPUTTERED PARTICLES (Information provided through courtesy of Prof. H. Oechsner).

"The angular distribution of sputtered particles measured by RBS analysis of the collected particles," B. Emmoth and M. Braun, Proc. 7th Inter. Vac. Congr. and 3rd Inter. Conf. Solid Surfaces (Vienna, 1977) Vol. II, S. 1465.

"Measurement of the angular distribution of sputtering efficiency with a thermal particle detector," D. Hildebrandt and R. Manns, Rad. Effects 31, 153 (1977).

"Angular distribution of sputtered Mo and Ag during He^+ and Ar^+ ion bombardment," B. Emmoth, Th. Fried and M. Braun, J. Nucl. Mat. 76 & 77, 129 (1978).

"Energy and angular distribution of gold and copper atoms sputtered with either 15 or 30 keV H^+, He^+ and Ar^+ ions," P. Hucks, G. Stocklin, E. Vietzke and K. Vogelbruch, J. Nucl. Mat. 76 & 77, 136 (1978)

"A new technique for the measurement of sputtering yields," Z. E. Switkowski, F. M. Mann, D. W. Kneff, R. W. Ollerhead and T. A. Tombrello, Rad. Effects 29, 65 (1976).

"Composition variations as a function of ejection angle in sputtering of alloys," R. R. Olson and G. K. Wehner, J. Vac. Sci. Technol. 14, 319 (1977).

"Angular distribution in sputtering of metals by 10 keV inert-gas ions," D. Hildebrandt and R. Manns, phys. stat. sol. (a) 51, (1979), K151

"Composition and isotope variations in sputtering as a function of the ejected angle," G. K. Wehner, R. R. Olson and M. E. King, Proc. 7th Intern. Vac. Congr. and 3rd Intern. Conf. Solid Surfaces, (Vienna 1977), Vol. II, S. 1461.

"Data on Low Energy Ion Sputtering," J. Roth, J. Bohdansky, W. Ottenberger, Garching Report IPP 9/26, May 1979.

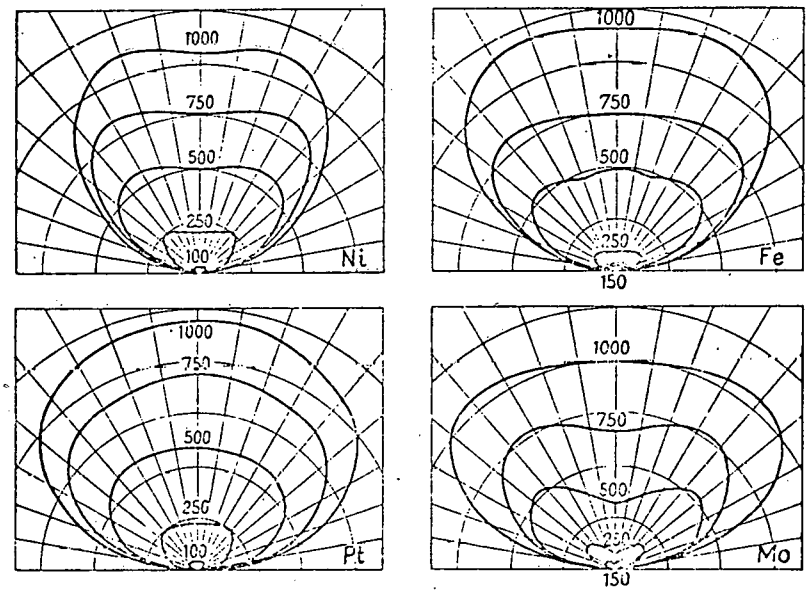

FIG. 1 Polar diagram of the angular distribution of material sputtered from Ni, Pt, Fe, and Mo targets by Hg^+ ions at normal incidence with energies of 150 eV (or 100 eV), 250 eV, 500 eV, 750 eV, and 1000 eV (Wehner et al [6]).

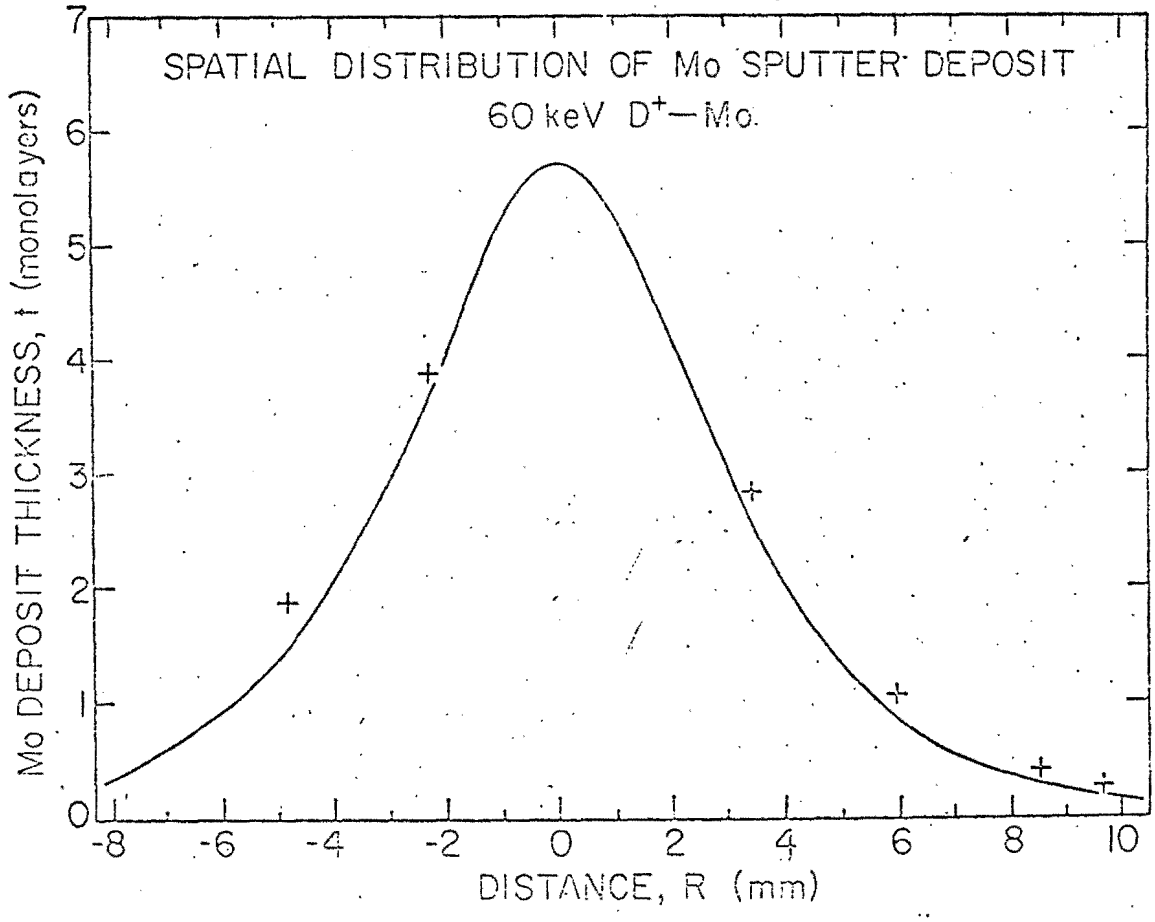

FIG. 2. Variation of the Mo deposit thickness t as a function of distance R on the substrate as measured from the center of the deposit spot (R=0) along radial directions. The solid curve is based on calculated values using equation (1). The experimentally determined values are indicated by +. For a target spot of radius r, a distance R is measured from the center of the deposit along a radial direction of the deposit spot, the deposited material density ρ, and the deposit thickness t, the emitted mass M is given by

$$M = 2\pi\rho r^2 \left(1 - \frac{t}{\sqrt{\left[1 - \left(\frac{R}{\ell}\right)^2 + \left(\frac{r}{\ell}\right)^2 \right]^2 + 4\left(\frac{R}{\ell}\right)^2}} \right) \qquad (1)$$

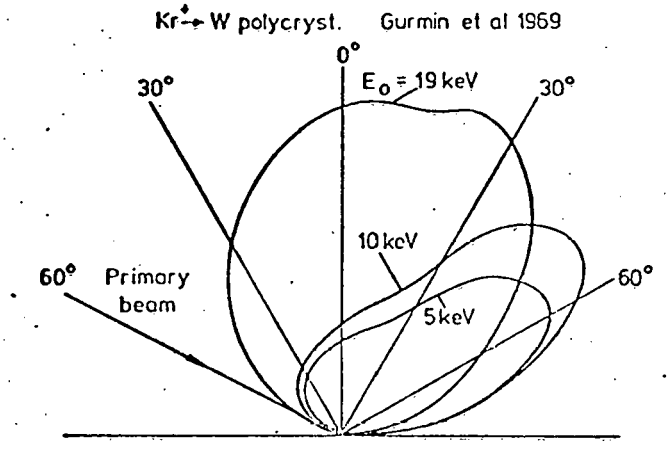

FIG. 3. Angular distributions of sputtered material for polycrystalline W bombarded with oblique incident Kr^+ -ions of different energies [16].

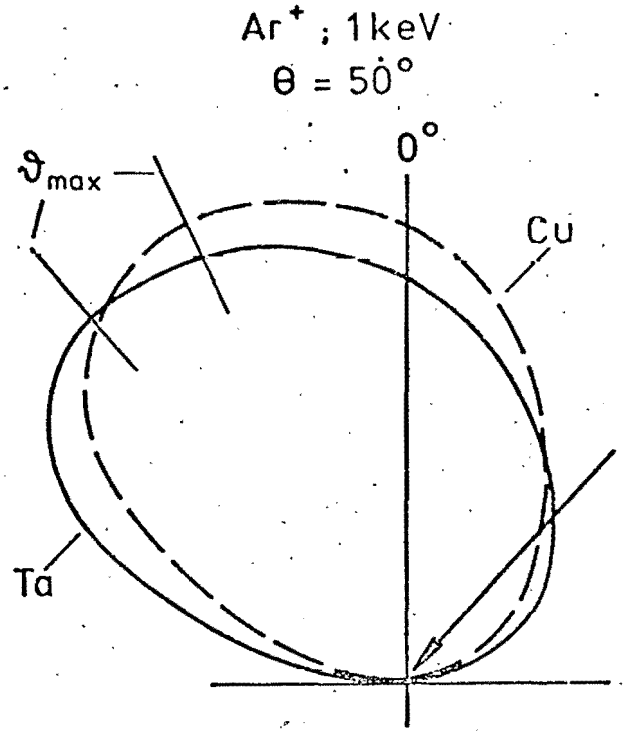

FIG. 4. Angular distributions of sputtered particles for polycrystalline Cu and Ta bombarded with 1 keV Ar^+ under $\theta = 50°$ against the target normal [19].

REACTIVE SPUTTERING AND CHEMICAL EROSION*

R. R. Rye
Sandia Laboratories,† Albuquerque, N. M. 87185

Introduction

In the following, concentration has been on those chemical processes that lead to removal of wall material and not on how these processes affect other problem areas such as permeation, conductivity, etc. For chemical effects the main consideration has to be given to the active forms of hydrogen, both from the standpoint of incident particle flux and inherent chemical reactivity. This restricts the range of materials one needs to consider, however, to materials containing atoms from the right hand side of the periodic table, since few metal hydrides are volatile. Trace impurities, where known, have to be considered from the standpoint of their potential ability to modify the surface and thus change the physical sputtering yield. The chemical effects that have been summarized here clearly show that one cannot simply ask what is the sputtering yield of pure material x with particle y. The results are too critically dependent on the surface composition.

Summary

Of the materials of interest to the fusion program only the chemistry of carbon is relatively well defined, and even in this case the complexity of the chemistry is such that erosion yields ranging over five orders of magnitude are reported. For other materials, such as the carbides, only the general outline of the surface chemistry relevant to the fusion program is becoming known; while in other areas, such as reactive sputtering and radiation assisted surface chemistry, the effects are well known in other technological areas but relatively little is known about these effects under the unique environment produced in a fusion device.

Information is sparce on oxides and carbides. From information that is presently available, however, it is obvious that this information must be obtained in conjunction with surface analytical techniques. The surface chemistry of these more complex materials is too sensitive to surface composition to depend on single measurements of "pure" materials.

*This article sponsored by the U.S. Department of Energy under Contract DE-AC04-76-DP00789.
†A U.S. Department of Energy Facility.

This is true for both physical sputtering and chemical erosion. The same extreme surface sensitivity makes it imperative that we have information concerning in-situ material compositions and the flux of particles, including impurities, to the wall and limiter surfaces. The impurity flux will define, to a certain extent, the wall composition especially in present day machines where the time between discharges is long.

In light of the large effects seen for radiation (e, α, etc.) enhanced chemical erosion in integrated circuit manufacture and the lack of similar information for fusion type environments, it is clear that this is an area in which it is imperative to identify the magnitude of the problem.

LITERATURE SUMMARY

A. Chemical Erosion

Figure 1 contains a summary prepared by Behrisch[1,2] of the erosion yields reported by various authors for the chemical reaction of graphite with thermal atoms and energetic ions of hydrogen and oxygen. The apparent diversity in this data reflects the complex chemistry of graphite. In general, however, the data show a temperature maximum, T_m, at $\sim$ 500 C which results from a competition between the desorption of hydrogen and reaction with carbon. Such strong temperature dependence is characteristic of chemical reactions and can be used to distinguish between physical sputtering and chemical erosion. A similar T_m has been observed by Braganza et al. for D^+ at energies up to 30 keV.[3] At these energies the range of the particle is such that the reaction is between surface carbon and implanted D which diffuses to the surface with thermal energies. Consistent with this, the release of both D_2 and CD_4 follow the same form over the whole period of bombardment.[3] These results would indicate that the erosion of graphite by hydrogen bombardment is dominated by chemical reaction at all energies.

The large spread in reported values for the erosion yield reflected two related factors: the variability of graphite samples and the effect of damage. It is well known that the reactivity of graphite is strongly dependent on the type of carbon used,[4] and that erosion is differential with respect to orientation.[4,5] Preferential attack occurs at the prism plane[5]. Surface damage, which in the case of graphite means breaking C-C bonds, creates a chemically active surface and enhances erosion. The erosion yield curves in Fig. 1 above $\sim 10^{-2}$ were all obtained with energetic hydrogen ions and probably reflect the enhancement due to surface damage. Veprek et al.[6] have shown experimentally that this is a major effect. Fig. 2 from their paper shows the effect of irradiation with 2 MeV He^+ on the subsequent reactivity in a low energy H_2 discharge. They conclude from this study that a reaction probability up to 10^{-2} can be expected at 500 C regardless of the original quality of the graphite.[6]

The reaction of graphite with O is similar to that with H, but with quantitative differences in the reaction products and T_m. T_m for O is $\sim$ 1500 C vs. $\sim$ 500 C for H. One should note that the reaction yields are comparable; the vertical scales in Fig. 1 differ by a factor of 10^2. Methane is the major product with H but, consistent with the diversity of stable hydrocarbons, a large array of minor products are also produced.[7] In contrast the carbon-oxygen system has a much less extensive chemistry yielding only CO and CO_2.[1,2]

The carbides are much less well understood. The more complex surface chemistry has led to results which differ on fundamental points. Braganza et al. report that the reaction of 20 keV D^+ with B_4C and SiC is specific to the carbon atom yielding CD_4 with a T_m of $\sim$ 800 K.[8] Roth et al. also show a specific reaction with C of SiC but one which did not show any pronounced temperature dependence[9]. In contrast to these, Veprek and Haque suggest that a protective layer of SiO_2 makes SiC inert to chemical attack[4]. The results of Yamashina et al.[10] given in Fig. 3 show that the presence of surface oxygen has a profound effect on the chemical erosion of SiC and is probably the source of the basic differences that have been reported. For clean SiC, Fig. 3a, 700 eV D^+ reacts preferentially with the Si atoms producing a surface rich in carbon. As suggested by Veprek and Haque, surface oxygen forms SiO_2 but this is protective only of the Si. On this partially passivated surface, Fig. 3b, the reaction of 700 eV D^+ is now selective to the carbon atoms producing a surface rich in Si. That the reaction of SiC with hydrogen is controlled by chemical effects is clearly shown in Fig. 4 from Mohri et al.[11] In contrast to H^+, "sputtering" pure physical sputtering with Ar^+ removes both Si and C at equal rates, and at 600 C the preferential reaction of H^+ with Si is greatly reduced.

In general, one can expect quite complex behavior with non-elemental materials. During Ar^+ sputtering of TiC in the presence of oxygen, Sproul and Richman[12] report a preferential removal of carbon, reaction with O_2 and the formation of titanium oxycarbide of the form TiC_xO_y.

B. Reactive Sputtering and Radiation Enhanced Chemical Erosion

Reactive sputtering is physical sputtering in the presence of a reactive gas. This effect has been extensively studied by the electronics industry for integrated circuit manufacture, and the data primarily involves Ar^+ sputtering in the presence of O_2 and N_2. The general results are illustrated in Fig. 5 from Cantagrel and Marchal[13] where the Ar^+ milling rate is plotted vs. the oxygen pressure for Al, Cr, Mn, V, Si and SiO_2. One observes the sputtering rate of the pure material at low oxygen pressures and the sputtering of the corresponding oxide at high oxygen pressures[13] suggesting a competition between oxidation and physical sputtering. This competition is clearly seen in Fig. 6 where the data is replotted vs. the poisoning ratio or ratio of the rate of arrival of O_2 to the sputter rate. The break between the two extremes occurs at poisoning ratios between 0.1 and 10. If no stable oxide exists (i.e. Ag[14]) the effect is

small, and for those cases where the effect is large the sputtered species is the oxide or the nitride[15,16,17].

Abe and Yamashina have derived a semi-empirical equation[14] which, on the basis of three experimentally determined parameters, is capable of giving a complete description of the pressure dependence. This model with slight modifications has been applied to a number of systems, including Mo[14,18], Ti[14,18], Fe[16], Co[16], Zr[17], Ta[18], and W[18].

A related area which has received considerable interest in the electronics industry is radiation-assisted chemical erosion. Unfortunately, the reaction systems that have been investigated are of specific interest to that particular industry. With the exception of the work of Veprek et al. on carbon[6], essentially no work has been done on systems of interest to the fusion program. The effects, however, can be illustrated with the well-characterized work of Coburn and Winters[19] on etching with XeF_2. Fig. 7 shows the effect of 450 eV Ar^+ on the XeF_2 etching of Si, and Fig. 8 the effect of 1500 eV electrons on the same reactionwith SiO_2. The effect of electrons is especially dramatic. SiO_2 is unreactive towards either XeF_2 or electrons while the combination of XeF_2 and electrons etches SiO_2 at the rate of $\sim$ 200 A/min.

REFERENCES

1. R. Behrisch, Proc. of Fusion Reactor Conf., Miami Beach, FL, to be published in J. Nucl. Mater.
2. B. M. U. Scherzer, R. Behrisch and J. Roth, Proc. Int. Symp. Plasma Wall Interaction, Julich, Oct. 1976, p. 353.
3. C. M. Braganza, S. K. Erents and G. M. McCracken, J. Nucl. Mater., 75, 220 (1978).
4. S. Veprek and M. R. Haque, Appl. Phys. 8, 303 (1975).
5. M. Balouch and D. R. Olander, J. Chem. Phys. 63, 4772 (1975).
6. S. Veprek, A. P. Webb, H. R. Oswald and H. Stuessi, J. Nucl. Mater. 68, 32 (1977).
7. R. R. Rye, Surface Science 69, 653 (1977).
8. C. Braganza, G. M. McCracken and S. K. Erents, Proc. Int. Symp. Plasma Wall Interactions, Julich, Oct. 1976, p. 257.
9. J. Roth, J. Bohdansky, W. Poschenrieder and M. R. Sinha, J. Nucl. Mater. 63, 222 (1976).
10. T. Yamashina, M. Mohri, K. Watanabe, H. Doi and K. Hayakawa, J. Nucl. Mater. 76, 202 (1978).
11. M. Morhi, K. Watanabe and T. Yamashina, J. Nucl. Mater. 75, 7 (1978).
12. W. D. Sproul and M. H. Richman, Thin Solid Films 28, L39 (1975).
13. M. Cantagrel and M. Marchal, J. Mater. Sci. 8, 1711 (1973).
14. T. Abe and T. Yamashina, Thin Solid Films 30, 19 (1975).
15. E. Hollands and D. S. Campbell, J. Mater. Sci. 3, 544 (1968).
16. J. Heller, Thin Solid Films 17, 163 (1973).
17. F. Shinoki and A. Itok, J. Appl. Phys. 46, 338 (1975).
18. J. Hrbek, Thin Solid Films 42, 185 (1977).
19. J. W. Coburn and H. F. Winters, Surface Sci., in press.

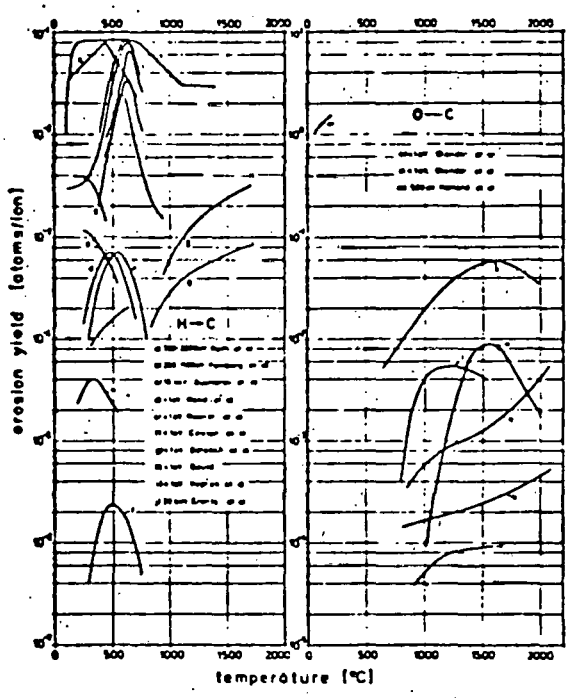

Erosion yields of graphite due to the interaction with thermal and with energetic hydrogen and oxygen. The erosion has been measured by weight loss or by CH_4 and/or CH_2 production [42].

FIG. 1 From Behrisch (Ref. 1)

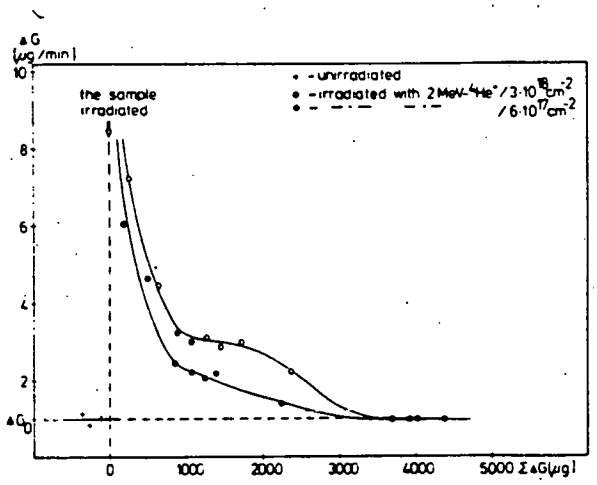

Effect of radiation damage on the reactivity of graphite. ΔG = differential weight losses of the sample during plasma erosion; ΣG = total weight loss; and ΔG_0 = differential weight losses of unirradiated sample.

FIG. 2 From Veprek et al. (Ref. 6)

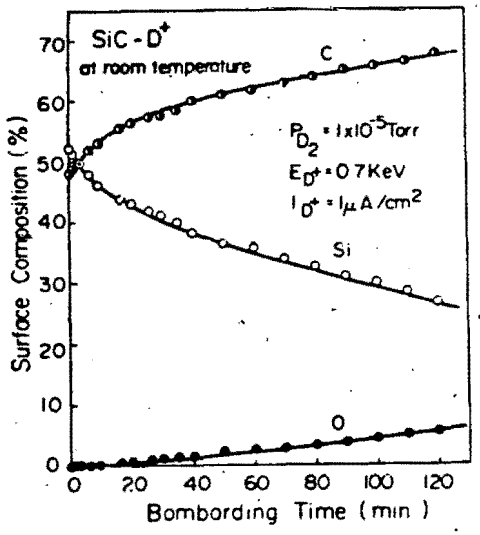

a. The variation of surface composition of clean SiC during deuteron sputtering at room temperature.

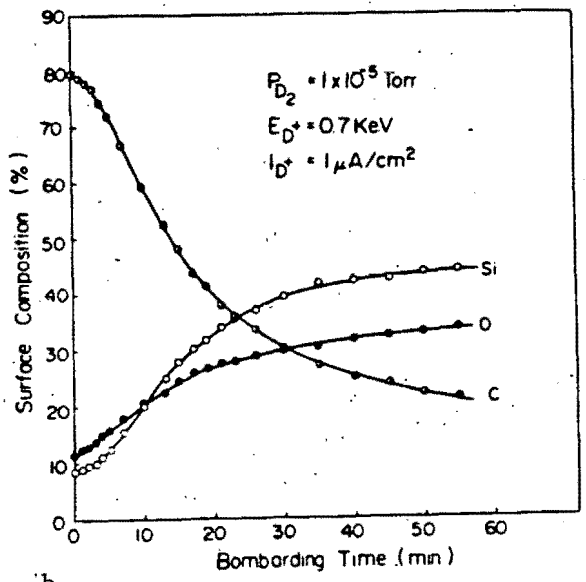

b. The variation of surface composition of SiC during deuteron sputtering when the oxide exists on the surface.

FIG. 3 From Yamashina et al. (Ref. 10)

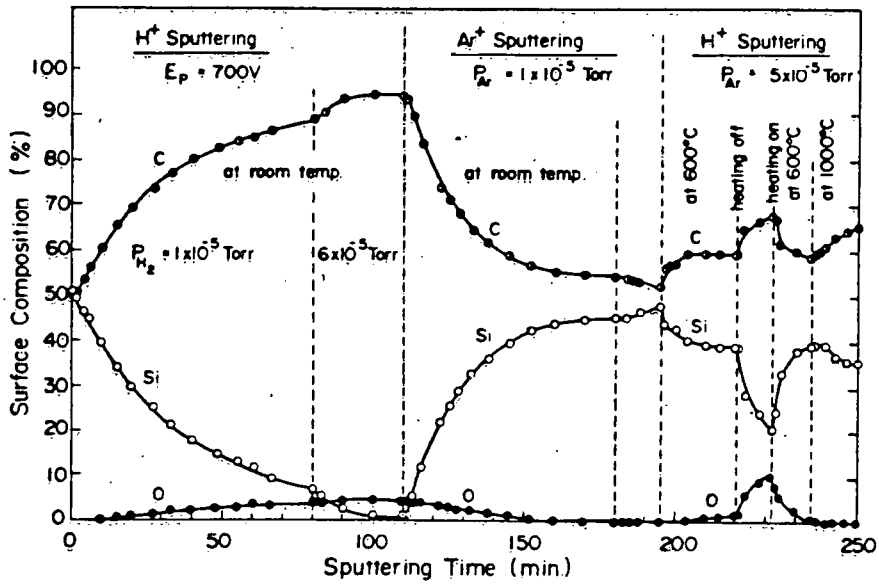

Variation of surface composition during borbardment with H^+ and Ar^+ ions at various temperature.

FIG. 4 From Mohri et al. (Ref. 11)

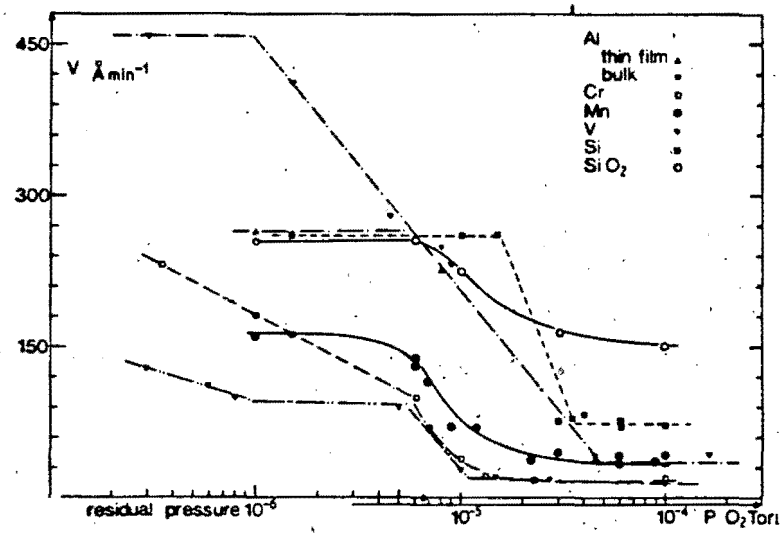

Al, Cr, Mn, V, Si, SiO_2 milling rate as a function of oxygen pressure.

FIG. 5 From Cantagrel and Marchal (Ref. 13)

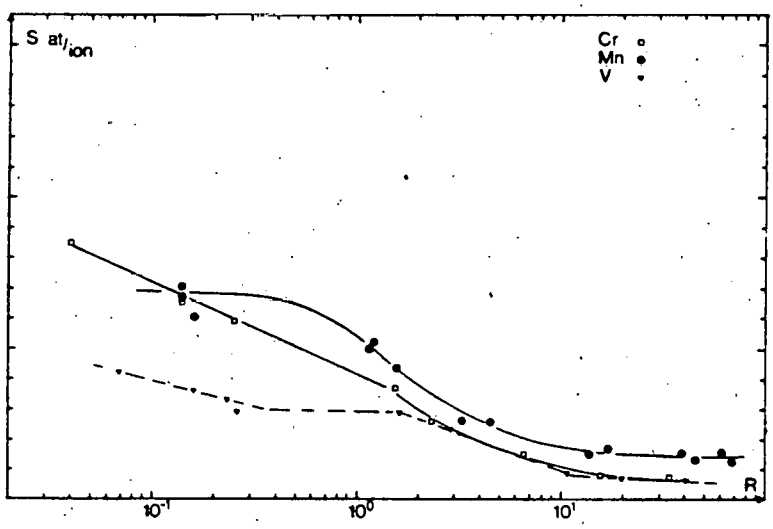

Cr, Mn, V, sputtering yield as a function of the poisoning ratio.

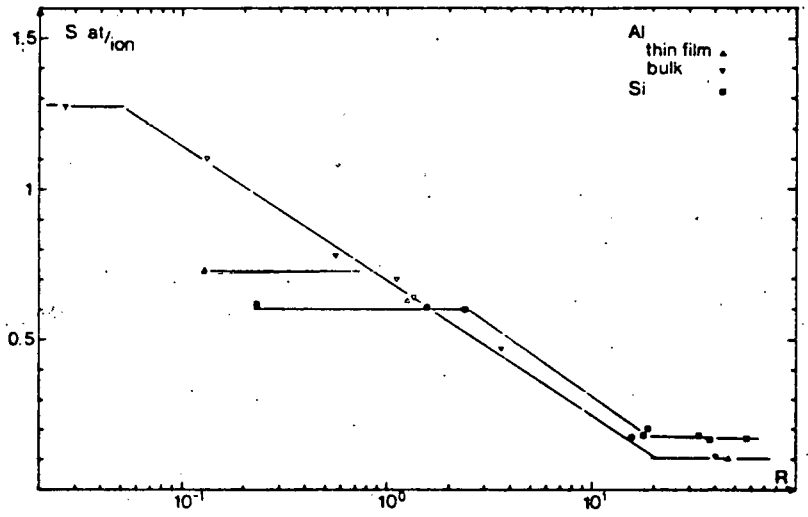

Al, Si, sputtering yield as a function of the poisoning ratio.

FIG. 6 From Cantagrel and Marchal (Ref. 13).

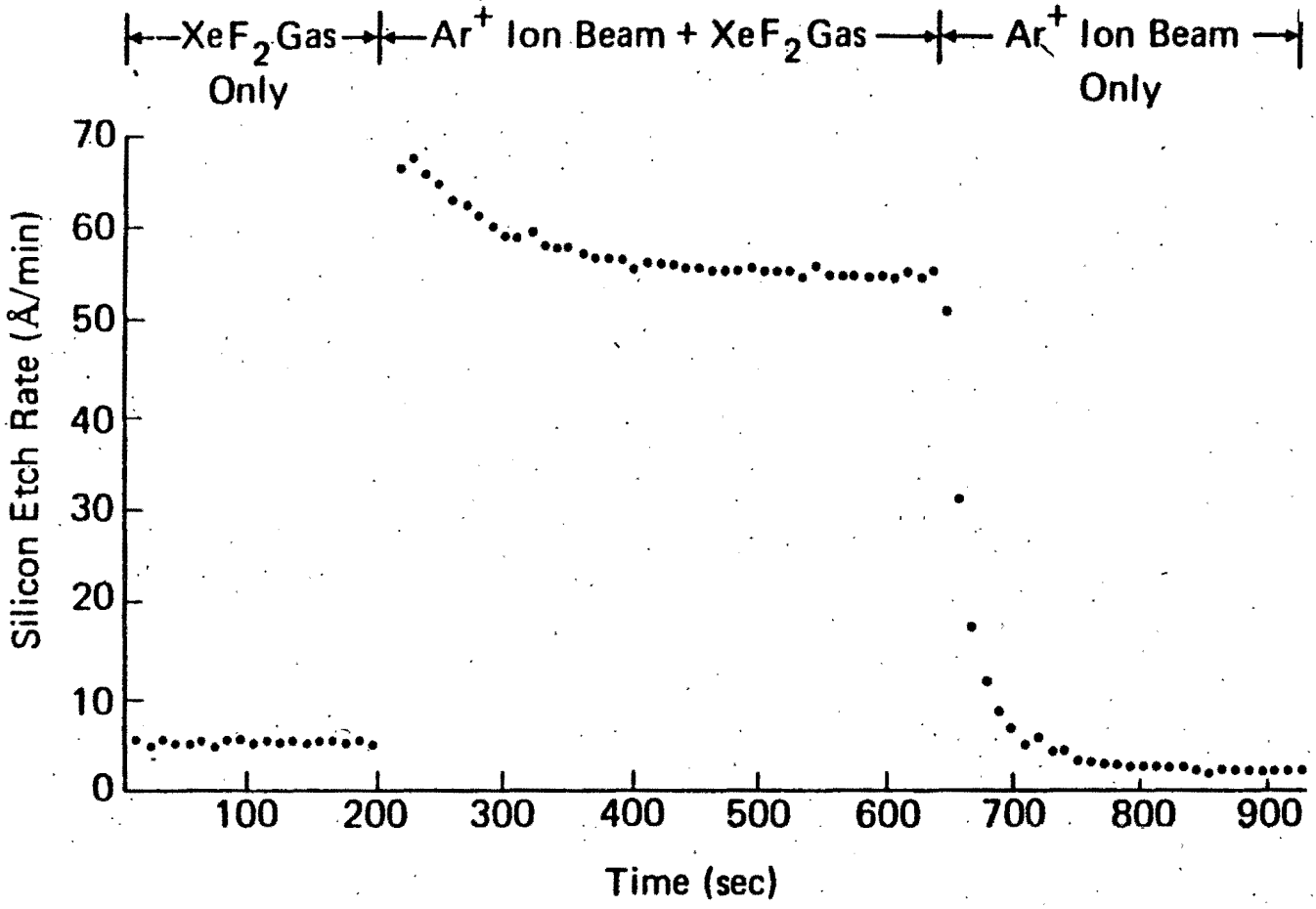

Ion-Assisted Gas-Surface Chemistry using Ar^+ and XeF_2 on Silicon. (Volatile reaction product.)

Ar^+ energy = 450eV
Ar^+ current = 0 (t<200 sec)
= 2.5μa (t>200 sec)
XeF_2 flow = 2×10^{15} mol/sec (t<660 sec)
= 0 (t>660 sec)

(The Ar^+ current density and the XeF_2 flux are not uniform over the Si surface. The effective area for the Ar^+ current and the XeF_2 flux are estimated at 0.1 cm^2 and 0.3 cm^2 respectively.)

FIG. 7 From Coburn and Winters (Ref. 19)

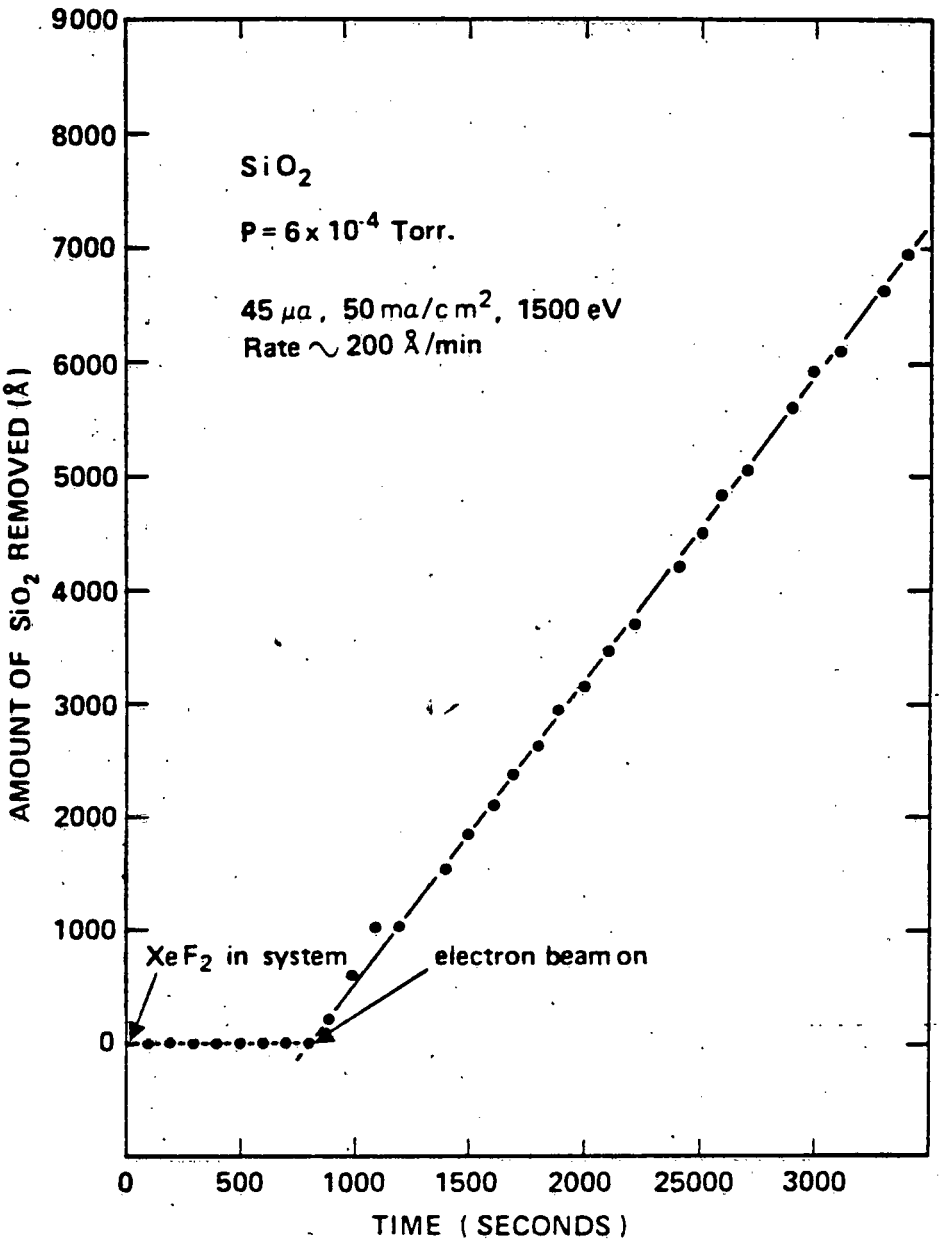

Electron-Assisted Gas-Surface Chemistry using 1500eV electrons and XeF_2 on SiO_2. P(total)=6×10^{-4} Torr with most of the ambient gas being xenon. Neither exposure to XeF_2 nor an electron beam produces etching by itself. Simultaneous exposure produces an etch rate of ~200Å/min.

FIG. 8 From Coburn and Winters (Ref. 19)

SYNERGISMS IN SPUTTERING AND BLISTERING OF SURFACES *

K. L. Wilson
and
W. Bauer

Sandia Laboratories, Livermore

Abstract

In the evaluation of impurity introduction, a consideration is the effect of surface alteration on the physical sputtering yield. Synergistic effects of this type considered in this review include surface roughness and gas (H and He) loaded surfaces. In addition, the effects of sputtering on He induced surface blistering are also assessed.

*This work was supported by U.S. Department of Energy.

I. Contribution of Blistering to Impurity Introduction

Blistering is the general term for surface deformation resulting from the agglomeration of implanted gas atoms such as H and He. This deformation may take the form of micron diameter circular blisters or repetitive exfoliation of surface layers. Generally the blister thickness is of the order of the mean ion range. Recent reviews of blistering can be found in reference 1. Hydrogen blistering of first wall materials such as stainless steel is considered unlikely [2]. On the other hand, helium blistering is potentially a serious source of impurity introduction.

A number of factors influence the importance of He blistering, such as the He energy spectrum emanating from the plasma, angular and spatial distribution, flux and total sputtering yield. Blistering due to low energy polyenergetic He^+ spectra [3, 4] is unlikely. However, the high energy component (3.5 MeV) of the unconfined α flux may give rise to surface exfoliation or blistering [5 - 8]. Detailed calculations [5 - 8] indicated that blistering from these 3.5 MeV alpha particles is possible primarily in early D-T devices with small minor radii and moderate confinement conditions. The possibility of surface erosion by α's is reduced due to the simultaneous surface recession from low energy D,T sputtering. For wall materials with relatively high sputtering yield such as Be, blistering may not occur. However, first walls constructed from low sputtering materials such as Mo are quite likely to undergo helium induced exfoliation in certain regions [7]. This competition between sputtering of the surface and blister exfoliation from high

energy He implantation has recently been experimentally demonstrated [9]. Sufficient data and calculations exist in the area of blistering and its impact on impurity introduction that some prediction of tokamak operation can be confidently made.

II. Synergism of Sputtering and Surface Alteration (Roughness and Gas Loading)

The synergistic effects of surface topography changes and near surface gas loading on wall erosion mechanisms such as sputtering are not well understood. Little data are available for H isotopes and He in the flux and energy range relevant to fusion energy. In this section of the paper, existing data on the effects of surface roughness and gas loading on physical sputtering are summarized and areas where additional research is needed are proposed.

At first glance, data on the effects of surface roughness (either naturally occurring or deliberately produced) on physical sputtering appear contradictory. Both increased and decreased physical sputtering yields (S) have been reported for gas atom bombardment of rough surfaces compared to smooth surfaces. However, a more detailed study of the data base shows that increased sputtering yields (over smooth surface yields) are associated with "faceted" or "furrowed" surfaces, while decreased sputtering yields are observed with "conical" surfaces. Faceted surfaces are those with surface features inclined at small angles to the surface, as shown in the figure section. Experimental evidence for increased S can be found in references 10-16. Of particular interest is the 3 KeV D_2^+

implantation of 304 stainless steel by Von Seefeld [13]. He observed a change in S from 2.1 x 10^{-2} for fluences <10^{19} atom/cm^2 to 3.5 x 10^{-2} for fluences up to 4 x 10^{19} atom/cm^2 as the surface roughened. Roth [14] observed a 30 - 70% increase in the sputtering yield of stainless steel implanted with protons at room temperature to 600°C and tentatively attributed it to surface topography changes. Behrisch [15] found no dose dependence on the sputtering yield for fluences of hydrogen from 3 x 10^{19} to 2.4 x 10^{20} atoms/cm^2 on stainless steel. This indicates that the increased yield due to natural surface roughening is only a transient phenomenon that disappears by fluences on the order of 10^{19} atoms/cm^2. A similar dose dependence for He^+ sputtering of Inconel for fluences up to 4 x 10^{19} atoms/cm^2 has been reported by Bohdansky [16]. A detailed calculation of the sputtering yield from faceted surfaces can be found in the paper by Littmark and Hofer [17]. Their work indicates that the sputtering yield can increase by factors of 4 or more for certain angular facets. The higher yield on faceted surfaces is attributed to the larger effective incidence angle of the ions.

Decreases in the sputtering yield for surfaces with dense conical protrusions or honeycomb structures have also been reported in the literature [18 - 25]. Relevant measurements to fusion include the W dendrite measurements of Ziegler [24] and the Be sputtering measurements of Mattox [25]. Ziegler reported a factor of 3 decrease in the sputtering yield for 4 KeV He^+ on W dendrites compared to smooth surfaces. (His other measurements using a gas discharge may have been influenced by the different discharge characteristics above a flat and dendritic surface.) Mattox reported a decrease in the H sputtering yield of 30 - 40% due to a needle-like surface topography on Be that developed by fluences of

$\sim 10^{21}$ ions/cm^2. The decrease in sputtering yield for these conical or needle-like surfaces has been attributed to the increased probability of recapture of ejected atoms by neighboring protrusions [17]. The only exception is the increased S for He^+ on the Ti and V surfaces with cone formation produced by oxygen exposure [26]. However, the cones were only observed on certain grains, and it is possible that the effects of oxygen exposure was a larger influence on S than surface topography.

Since virtually all the H, He sputtering measurements (especially the weight loss measurements) have been made at high ion fluences ($> 10^{19}$ atoms/cm^2), these data already include the effects of naturally occurring surface roughening due to the bombardment. More experimental work on deliberate surface modifications such as dendrite growth or honeycomb structures that lower S should be pursued. However, to date the measurements of the increase or decrease of sputtering yield due to surface topography appear to be limited to a factor of 3 or less.

The changes in sputter yield due to gas loading of the near surface are not well documented. As listed by Andersen [27], gas trapping can affect sputtering by:

1) Influencing the collision cascade
2) A change in the surface binding energy of lattice atoms
3) Induced phase change

Blank [28] has reported up to a 60% yield enhancement of Xe^+ sputtering of Si when the surface was pre-saturated with Xe. He found that the trapped Xe influenced the surface binding energy, the nuclear stopping power, and Sigmund's α function. He concluded that

"this effect is very large for light element targets with low sputtering yield bombarded with heavy ions." EerNisse [29] observed a change in the sputtering yield of 45 KeV He^+ on Au from S = 0.046 at a fluence of 5×10^{16} to 0.14 at a fluence of 5×10^{17}. The change was attributed to surface binding energy changes from the stress of implanted helium. Thus, gas loading can be a detectable effect at low fluences.

However, at high fluences, the present H and He sputtering data base has been determined for gas saturated surfaces. Metals such as stainless steel have reached steady state near surface saturation concentrations of hydrogen or helium by fluences of $\lesssim 10^{18}$ atoms/cm^2 [2,4]. Furthermore, H sputtering yields from metals such as Ti [30], which readily form hydride surface layers upon H bombardment at room temperature, also reflect the influence of gas loaded surfaces. Scherzer [31] has characterized the existing weight loss sputtering data as representative of a multicomponent system made up of the target lattice saturated with the implanted ions. No data appear available for H sputtering of He loaded surfaces. However, data for He sputtering of He loaded metals such as Ni can be fit with the same target parameters as H sputtering of Ni [32]. It seems unlikely, therefore, that H physical sputtering of He loaded surfaces will be a major effect.

Thus the present data consist primarily of high fluence measurements relevant to long burn time, high duty cycle fusion devices. However, for devices such as PLT, Doublet and ISX the relevant sputtering yields are in a low dose ($\lesssim 5 \times 10^{16}$ H/cm^2 per discharge) regime where the yield may not achieve the high fluence steady state value. For example, recent measurements by Bohdansky [33] using laser fluorescence spectroscopy indicate that

the H sputter yield of Fe up to a dose of 6×10^{16} H/cm^2 is an order of magnitude lower than that previously reported at higher doses ($> 6 \times 10^{18}$ H/cm^2). This effect may explain the discrepancy between the observed Fe concentration in the PLT plasma compared to the BALDUR [34] transport calculations using high fluence sputter yields.

So far we have discussed synergisms only on physical sputtering. A significant contribution to impurity introduction may be made by chemical sputtering, in particular, if significant use of first wall materials such as carbon is made. It is expected that gas loading and operational temperatures will be important factors in the overall chemical sputtering yield of materials such as carbon [35]. Limited data relevant to fusion needs are available and more effort is required if carbon or other reactive components are expected to be used and exposed to the plasma.

III. Conclusions

The effect of blistering or exfoliation on the overall plasma induced sputtering has been reviewed and found to be potentially serious only for the high energy α component. Sufficient data and calculations are available to predict the importance of the effect for various tokamak configurations.

The synergistic effect of surface roughness on the sputtering yield has been summarized and found to enhance or decrease the yield by less than a factor of 3 depending on the topography. Sputtering measurements on surfaces deliberately designed to decrease the yield such as dendrite growth or honeycomb structures should be continued. Sputter yields from

polished surfaces, while of interest from a fundamental point of view, are not relevant to plasma modelers who require yields from realistic surfaces.

The synergistic effect of gas loaded surfaces on the sputter yield has been reviewed and found to reach steady state at H isotope doses of order 10^{19} H/cm^2. The effect is inevitably incorporated in the measured yield at high doses.

There is a need to study sputter yields at low doses ($\lesssim 10^{16}$ H/cm^2) to determine the effects of adsorbed gas layers, low gas loading, etc. These data are important for plasma modeling of present devices where H isotopes and wall fluences generally do not exceed $\sim 5 \times 10^{16}$/cm^2 per pulse.

If the use of reactive materials such as carbon is contemplated, considerable work on gas synergism, especially at high temperatures, needs to be done.

REFERENCES

1. S. K. Das and M. Kaminsky, Proceedings of the "Symposium on Radiation Effects on Solid Surfaces", Chicago ACS Meeting, August 25, 1975, Advances in Chemistry Series 158, ACS (1976), 112.

2. K. L. Wilson, G. J. Thomas, and W. Bauer, Nuclear Technology 29 (1976), 322.

3. Scherzer, B.M.U., J. Vac. Sci. Technol. 13 (1976), 420.

4. K. L. Wilson, L. G. Haggmark, and R. A. Langley, Proceedings of the International Symposium on Plasma Wall Interaction, Jülich, October 18-22, 1976, Pergamon Press, 401.

5. W. Bauer, K. L. Wilson, C. L. Bisson, L. G. Haggmark, and R. J. Goldston, Trans. Am. Nucl. Soc. 27 (1977), 267.

6. W. Bauer, J. Nucl. Mater. 76 & 77 (1978), 1.

7. W. Bauer, K. L. Wilson, C. L. Bisson, L. G. Haggmark, and R. J. Goldston, Nuclear Fusion 19 (1979) 93.

8. G. Femske, L. Hively, G. Miley, and M. Kaminsky, to be published.

9. W. Bauer, K. L. Wilson, C. L. Bisson, L. G. Haggmark, and R. J. Goldston, J. Nucl. Mater. 76 & 77 (1978) 396.

10. O. Almen and G. Bruce, Nucl. Instr. and Methods 11 (1961) 257.

11. P. D. Davidse and L. I. Maissel, J. Appl. Phys. 37 (1966) 574.

12. J. J. Ph. Elich, H. E. Roosendaal, H. H. Kersten, D. Onderdelinden, J. Kistemaker, and J. D. Elen, Rad. Eff. 8 (1971), 1.

13. H. Von Seefeld, H. Schmidl, R. Behrisch, and B.M.U. Scherzer, J. Nucl. Mater. 63 (1976), 215.

14. J. Roth, J. Bohdansky, W. O. Hofer, J. Kirschner, in ref. 4, 309.

15. R. Behrisch, J. Bohdansky, G. H. Oetjen, J. Roth, G. Schilling, and H. Verbeek, J. Nucl. Mater. 60 (1976), 321.

16. J. Bohdansky, H. L. Bay, and J. Roth, Proc. 7th Inter. Vac. Congr. & 3rd Intern. Conf. Solid Surfaces (Vienna 1977).

17. V. Littmark, W. O. Hofer, J. Mat. Sci. 13 (1978), 2577.

18. N. Laegreid and G. K. Wehner, J. Appl. Phys. 32 (1961), 365.

19. D. Rosenberg and G. K. Wehner, J. Appl. Phys. 33 (1962), 1842.

20. G. K. Wehner and D. J. Hajicck, J. Appl. Phys. 42 (1971), 1145.

21. N. Laegreid and S. D. Dahlgren, J. Appl. Phys. 44 (1973), 2093.

22. S. N. Cramer and E. M. Oblow, Nucl. Fusion 15 (1975), 339.

23. K. P. Brown, Culham Laboratory Report, UKAEA CLM/RR/J2/2, 1977.

24. J. F. Ziegler, J. J. Cuomo, and J. Roth, Appl. Phys. Let. 30 (1977), 268.

25. D. M. Mattox and D. J. Sharp, Sandia Laboratories Report, SAND 78-1030J.

26. W. O. Hofer, H. L. Bay, and P. J. Martin, J. Nucl. Mater. 76 & 77 (1978), 156.

27. H. H. Andersen and H. L. Bay, J. Appl. Phys. 46 (1975), 1919.

28. P. Blank and K. Wittmaack, Rad. Effects 27 (1975), 29.

29. E. P. EerNisse, Appl. Phys. Lett. 29 (1976), 14.

30. J. Bohdansky, J. Roth, M. K. Sinhce, and W. Ottenberger, J. Nucl. Mater. 63 (1976), 115.

31. B.M.U. Scherzer, R. Behrisch, and J. Roth, in ref. 4, p. 353.

32. L. G. Haggmark, W. D. Wilson, J. Nucl. Mater. 76 & 77 (1978), 149.

33. J. Bohdansky, private communication.

34. C. E. Singer, this workshop.

35. S. K. Erents, C. M. Braganzd and G. M. McCracken, J. Nucl. Mater. 63 (1976), 399.

Figure Captions

(1) Scanning electron micrographs of 316 stainless steel implanted with 300 keV He at four different temperatures to a dose of 4 x 10^{18} He atom/cm^2. Note multiple flake exfoliation at 300 and 500°C. [34]

(2) Surface deformation observed after 20 keV bombardment to 1.2x10^{18} He^+ cm^{-2} at 575K, for samples with: (a) no pre-implantation; (b) pre-implantation to 0.1 atom fraction He with 3-15 keV He^+; (c) 0.2 atom fraction; (d) 0.3 atom fraction. Note the disappearance of blisters in (d). [4]

(3) Calculation of the probability of surface exfoliation from 3.5 MeV alpha particle bombardment of stainless steel with the calculated incident angular distribution as a function of wall temperatures (T_m=melting temperature (K)) and surface recessional velocity due to sputtering from the D,T charge exchange neutral flux with the indicated energy (plasma edge temperature). [7]

(4a) Typical facet structures obtained at very different irradiation and target conditions. (a) Scanning electron micrograph of polycrystalline Inconel bombarded with 4 keV helium ions. From H. L. Bay and J. Bohdansky, private communication. (b) Replica micrograph of a (100) copper single crystal bombarded with 20 keV neon ions. From J. J. Ph. Elich. [17]

(4b) Definition of structure parameters, coordinate systems and reference planes. [17]

(4c) Relative total sputtering yields for a faceted surface with facet angles $\alpha = 30^o$, $\beta = 60^o$, $f_i = \cos^{-2} \Theta_i$, $f_o = \cos \Theta_o$. [17]

(5a) Energy dependence of proton sputtering yield of stainless steel 316 at 80°C and 500°C. [14]

(5b) Surface topography of proton irradiatiated stainless steel at different temperatures. [14]

(6a) Typical tungsten surface which has been covered with single-crystal dendrites. Only the largest dendrites can be seen, with the largest dendrites being about 80 μm high. The dendrites are single crystals, with their <111> axes aligned to a common axis within 2°. [24]

(6b) Sputtering yield (atoms out/ions in) of various metal for ^4He ion bombardment. Also shown are the results of sputtered tungsten dendrite surfaces subjected to ion fluxes from an rf plasma discharge, and a mono-energetic accelerator beam. The yields from the discharge are plotted at the bias voltage of the discharge system. The solid and dashed lines are experimental and theoretical sputtering values for other materials. [24]

(7a) Surface morphology of vacuum deposited beryllium as a function of hydrogen ion (1000 eV) dosage. [25]

(7b) Hydrogen ion erosion yield of vacuum-deposited beryllium and of bulk beryllium. [25]

(8a) Model of honeycomb cell. [22]

(8b) Sputtering ratios for varying angular source distributions. [22]

(9) Sputtering yields versus 20 keV xenon fluence. The accuracy in the absolute sputtering yields is indicated by the error bars. The accuracy in the relative yields is much better. [28]

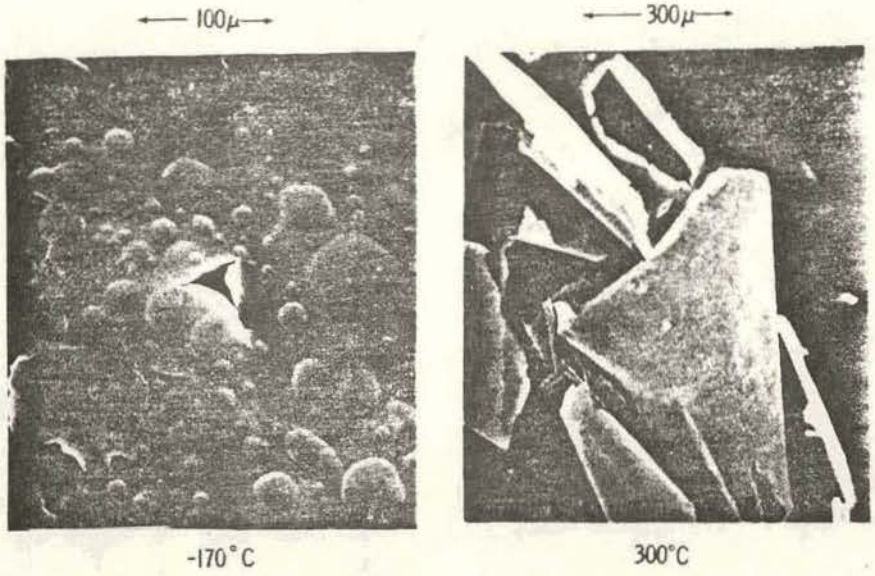

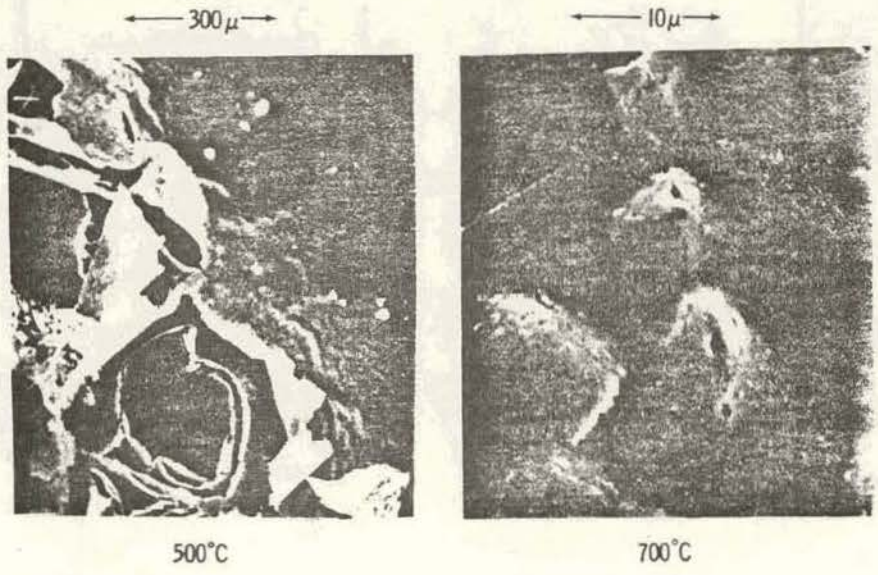

Figure 1

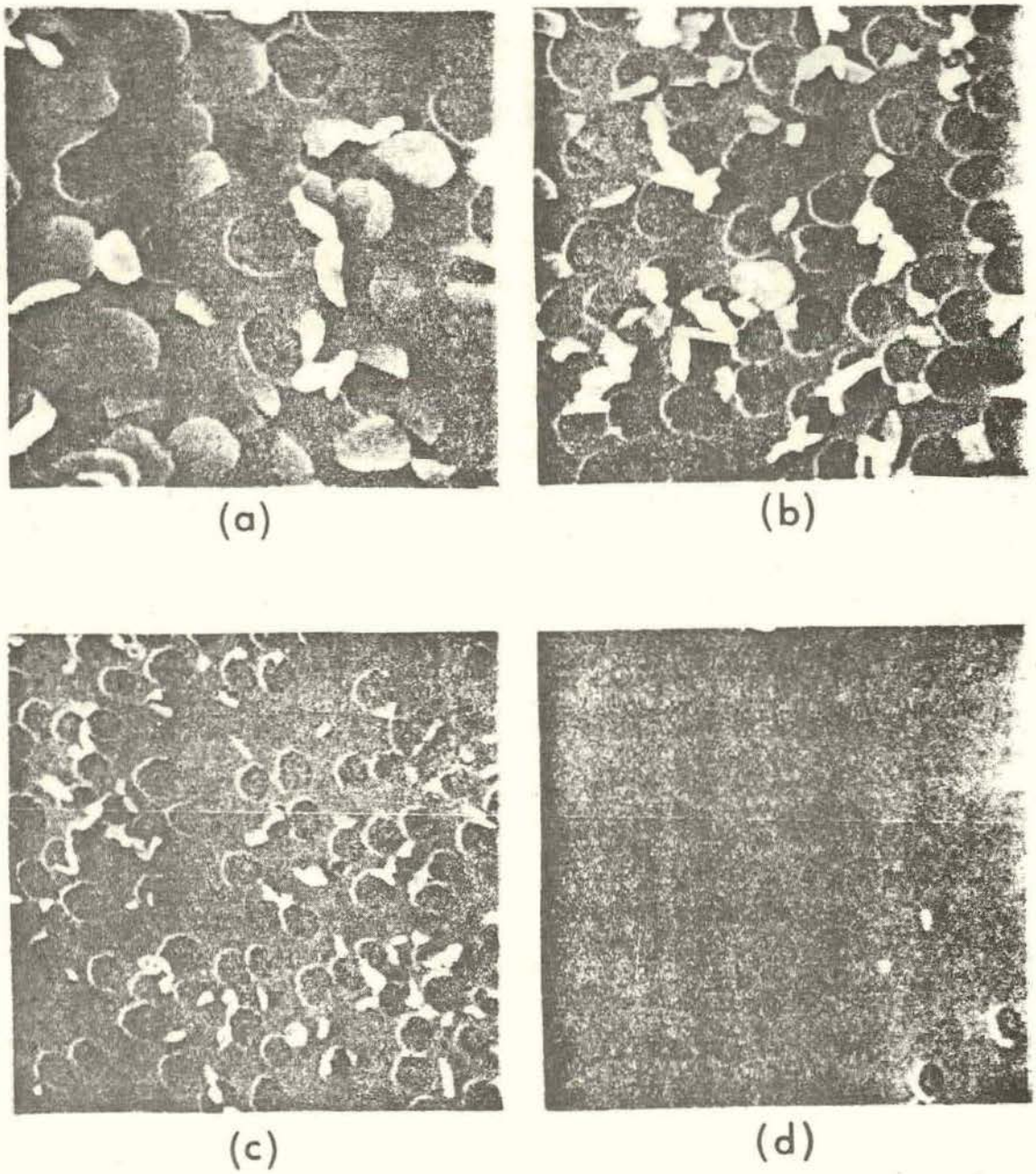

Figure 2

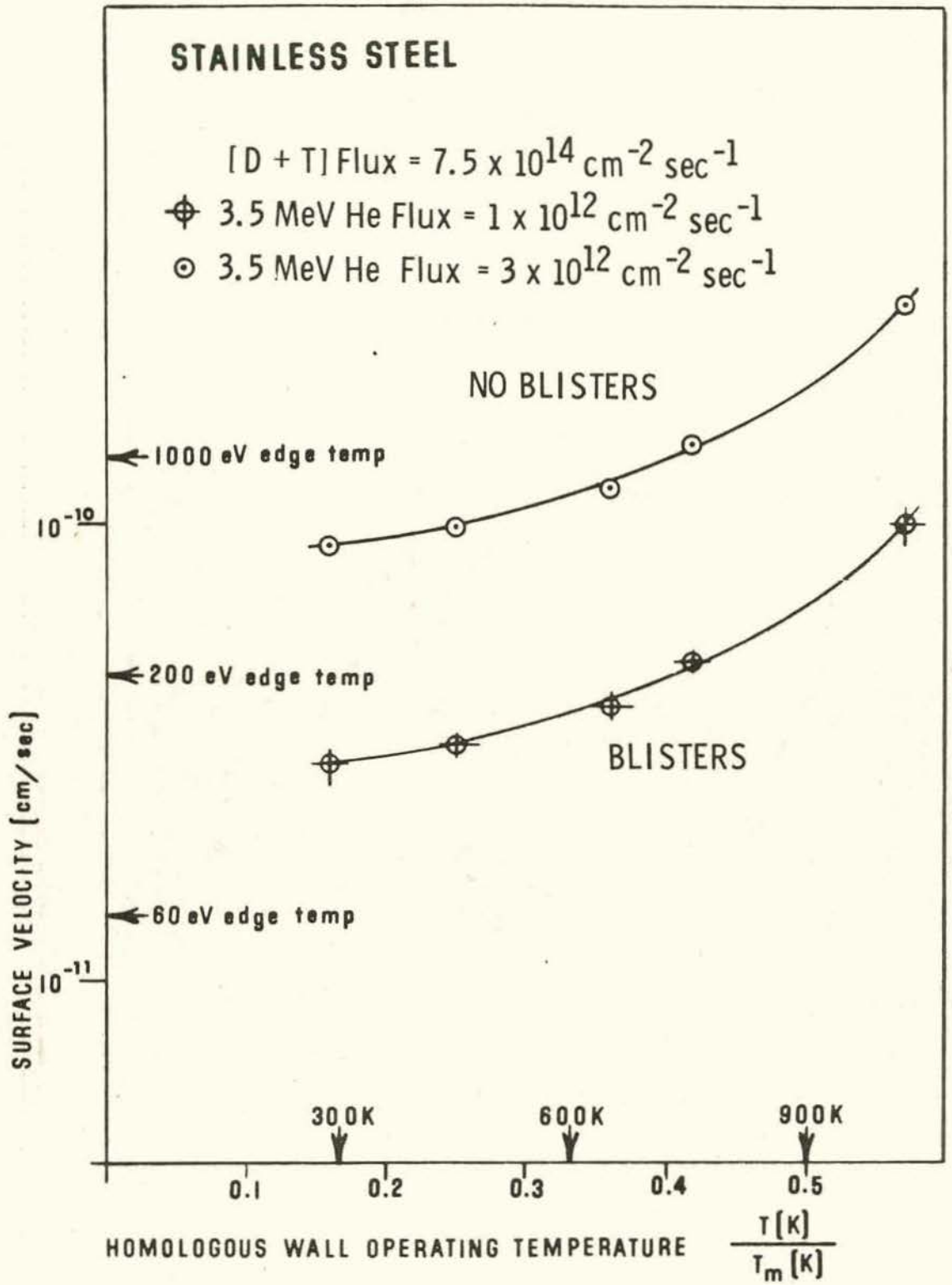
STAINLESS STEEL
[D + T] Flux = 7.5 x 10^14 cm^-2 sec^-1
3.5 MeV He Flux = 1 x 10^12 cm^-2 sec^-1
3.5 MeV He Flux = 3 x 10^12 cm^-2 sec^-1
NO BLISTERS
1000 eV edge temp
200 eV edge temp
60 eV edge temp
BLISTERS
10^-10
10^-11
SURFACE VELOCITY [cm/sec]
300K
600K
900K
0.1
0.2
0.3
0.4
0.5
HOMOLOGOUS WALL OPERATING TEMPERATURE
T[K] / Tm[K]

Figure 3

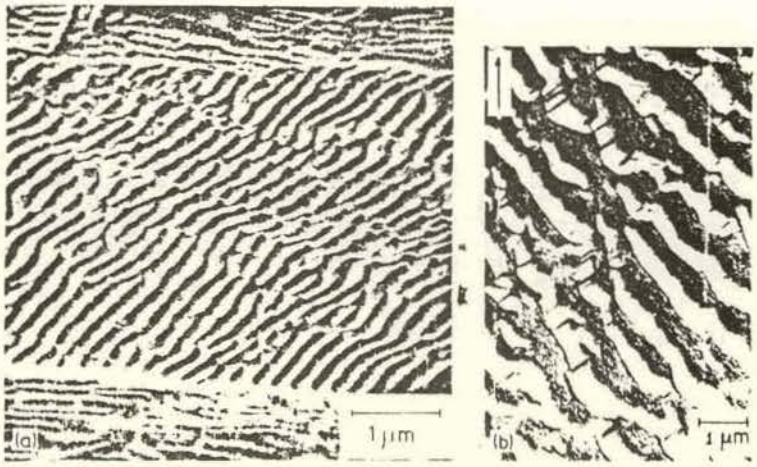

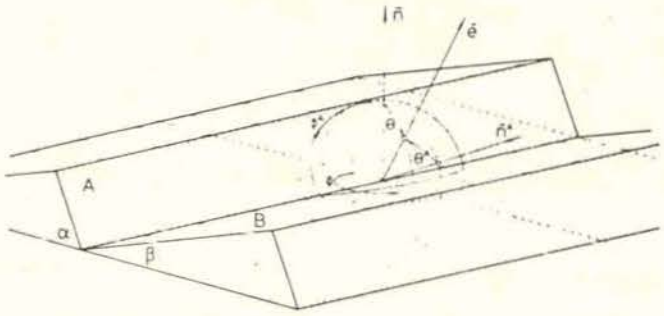

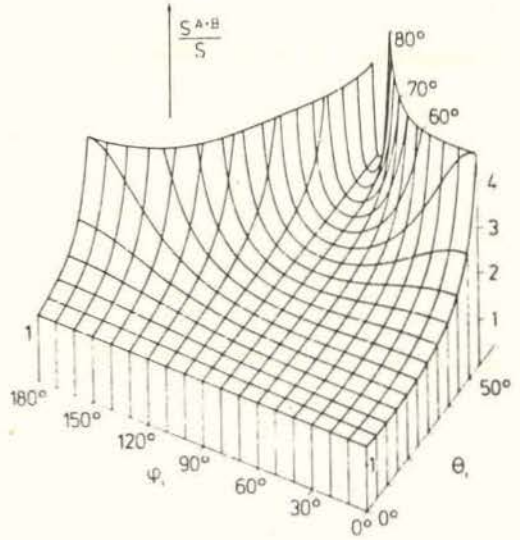

Figure 4

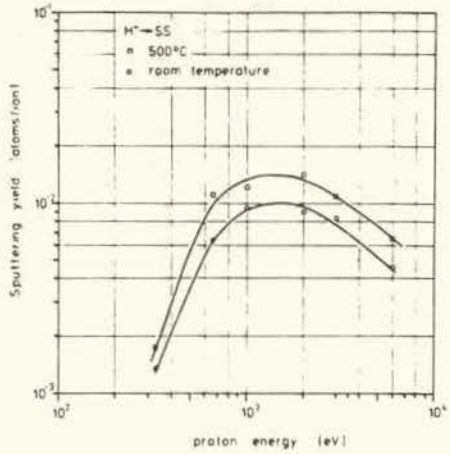
H⁺→SS
500°C
room temperature
Sputtering yield (atoms/ion)
proton energy (eV)

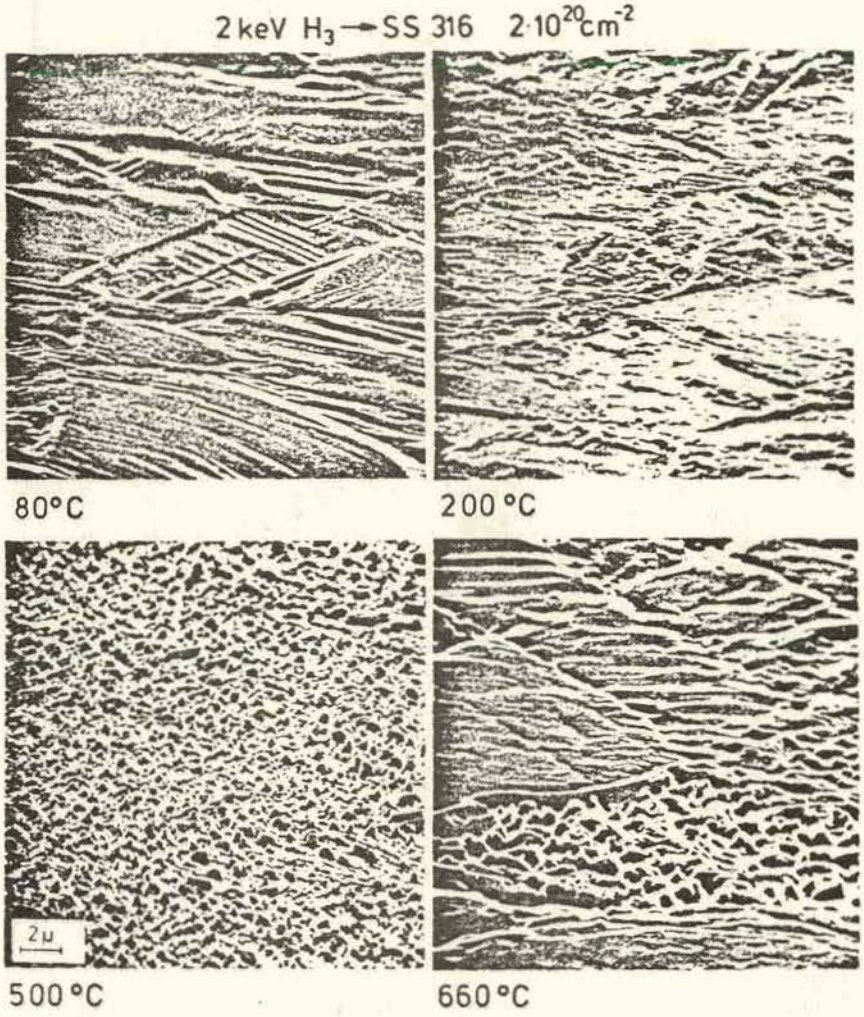
2 keV H3 → SS 316 2·10^20 cm^-2
80°C
200°C
2μ
500°C
660°C

Figure 5

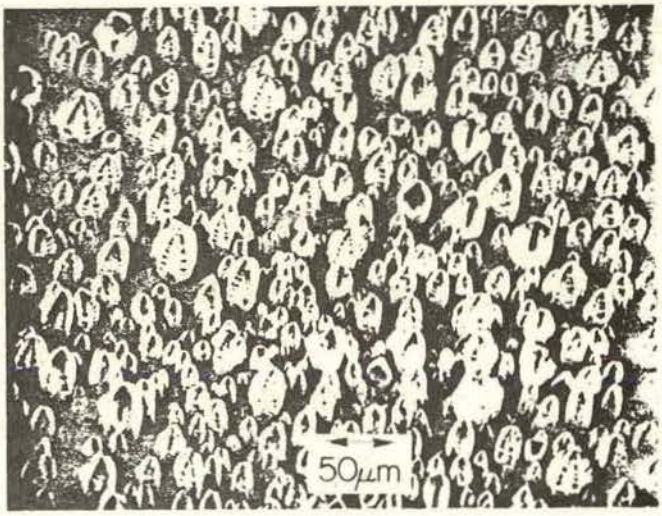
50μm

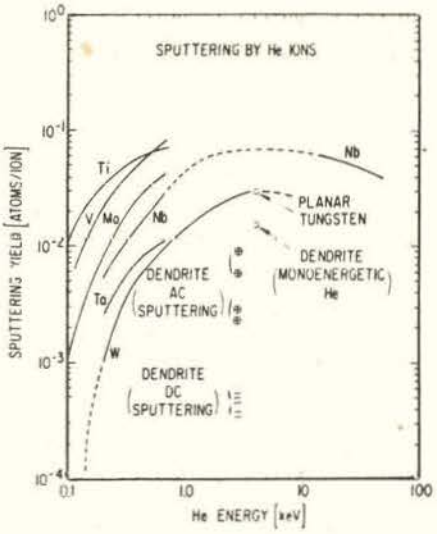
SPUTTERING BY He IONS
SPUTTERING YIELD [ATOMS/ION]
He ENERGY [keV]
Ti
V
Mo
Nb
Ta
W
Nb
PLANAR TUNGSTEN
DENDRITE (MONOENERGETIC He)
DENDRITE AC SPUTTERING
DENDRITE DC SPUTTERING

Figure 6

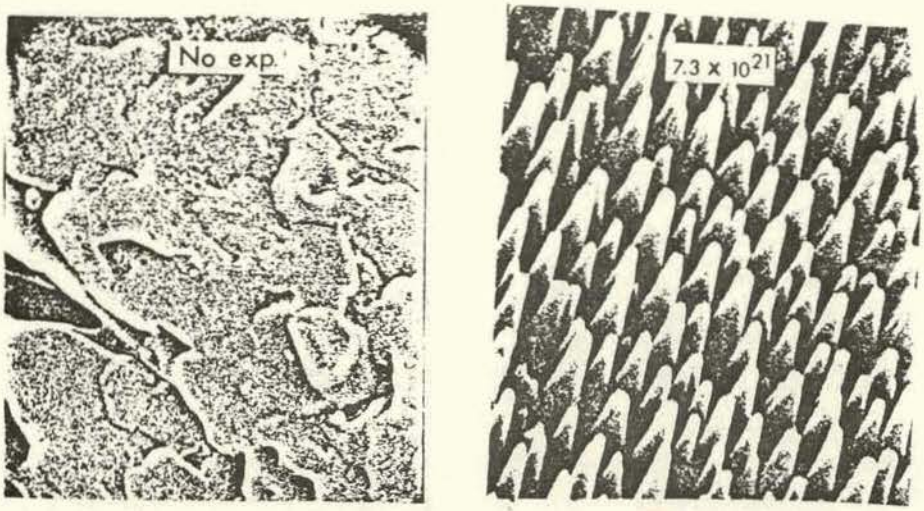
No exp.
7.3 x 10^21
0.5μ

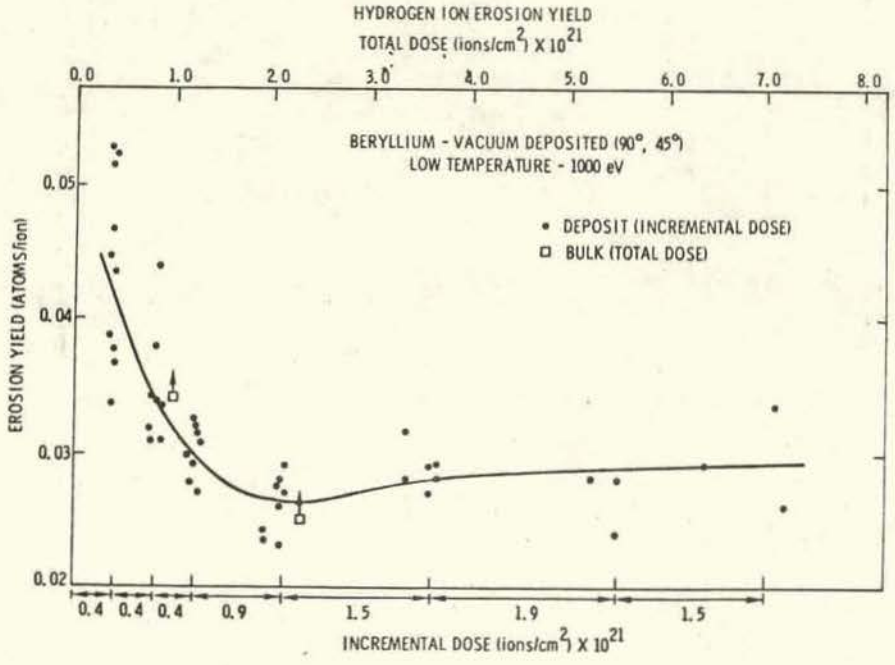
HYDROGEN ION EROSION YIELD
TOTAL DOSE (ions/cm²) X 10²¹
0.0
1.0
2.0
3.0
4.0
5.0
6.0
7.0
8.0
BERYLLIUM - VACUUM DEPOSITED (90°, 45°)
LOW TEMPERATURE - 1000 eV
DEPOSIT (INCREMENTAL DOSE)
BULK (TOTAL DOSE)
EROSION YIELD (ATOMS/ion)
0.05
0.04
0.03
0.02
0.4
0.4
0.4
0.9
1.5
1.9
1.5
INCREMENTAL DOSE (ions/cm²) X 10²¹

Figure 7

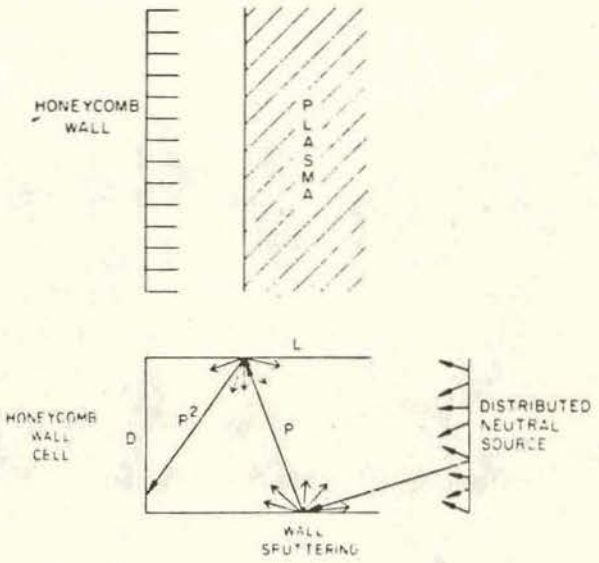
HONEYCOMB WALL
PLASMA
L
HONEYCOMB WALL CELL
D
P²
P
DISTRIBUTED NEUTRAL SOURCE
WALL SPUTTERING

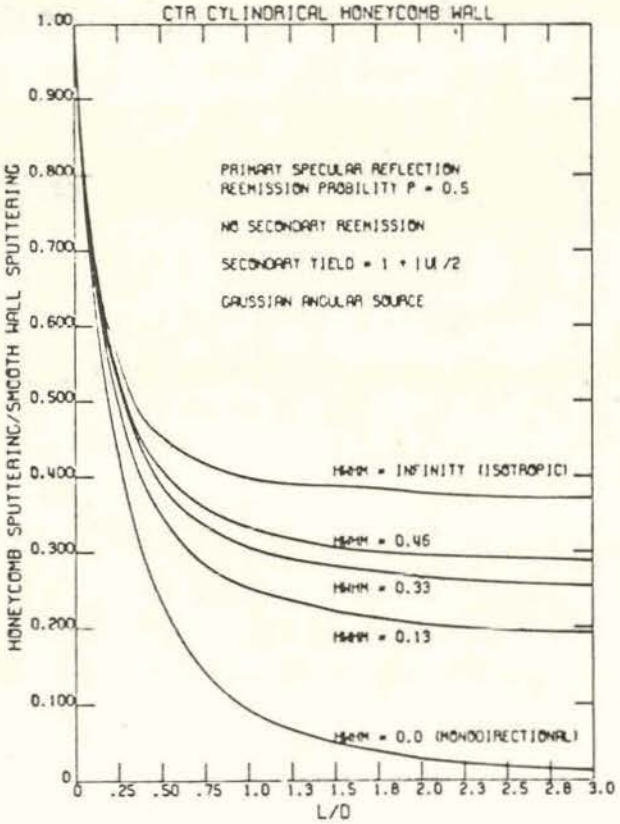
CTR CYLINDRICAL HONEYCOMB WALL
PRIMARY SPECULAR REFLECTION REEMISSION PROBILITY P = 0.5
NO SECONDARY REEMISSION
SECONDARY YIELD = 1 + |U|/2
GAUSSIAN ANGULAR SOURCE
HONEYCOMB SPUTTERING/SMOOTH WALL SPUTTERING
L/D
1.00
0.900
0.800
0.700
0.600
0.500
0.400
0.300
0.200
0.100
0
0 .25 .50 .75 1.0 1.3 1.5 1.8 2.0 2.3 2.5 2.8 3.0
HAPM = INFINITY (ISOTROPIC)
HAPM = 0.46
HAPM = 0.33
HAPM = 0.13
HAPM = 0.0 (UNIDIRECTIONAL)

Figure 8

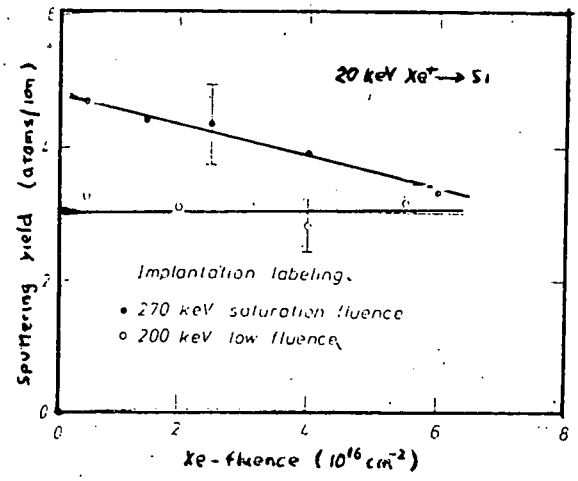
20 keV Xe+ → Si
Implantation labeling.
• 270 keV saturation fluence
o 200 keV low fluence
Sputtering yield (atoms/ion)
Xe-fluence (10^{16} cm^{-2})
0
2
4
6
8

Figure 9

NEUTRON SPUTTERING

M. Kaminsky

Argonne National Laboratory

SUMMARY

.. For the sputtering of metals by energetic neutrons several types of neutron sources have been used which provide neutrons with energy spectra which are typical for the kind of source used. For example, in sputtering experiments neutrons from fission processes, the (d,Be) reaction, and the (d,t) reaction have been used [for a review see Ref. 1]. In addition, ion simulation experiments of neutron sputtering by the use of 16 MeV protons have been performed [see Ref. 2].

.. Fast neutron sputtering yields for different metals irradiated for neutrons from fission processes and the (d,Be) reaction have been reported by various authors to vary from $\sim (5.7 \pm 0.8) \times 10^{-3}$ to $(1.8 \pm 0.56) \times 10^{-6}$ atom/neutron (see enclosed Table 1 and Refs. 3-9). To what extent differences in the target materials used, (e.g. Fe and Au), in the surface microstructures, and in the neutron spectra account for the observed differences in the yield values cannot be clearly delineated.

.. Neutron sputtering yields for different metals (e.g. Nb, Au) for energetic neutrons from the (d,t) reactions have been reported by various authors to vary from $\sim 3 \times 10^{-3}$ to $\sim 1.1 \times 10^{-5}$ atom/neutron (see enclosed Table II and Refs. 10-16). In addition, in a round robin experiment [2] two types of cold-rolled Nb targets with different surface finishes were used in irradiations with neutrons from the (d,t) reaction, the (d,Be) reaction (with 40-MeV d) and with 16 MeV protons. Total sputtering yields in the range 1.4×10^{-5} to $\lesssim 2.6 \times 10^{-3}$ atoms/neutron were reported (see enclosed Table III taken from Ref. 2). The participants in the round robin experiment concluded that the estimated probable shutter yield value is no larger than 10^{-4} atom/neutron.

Two of the three groups using neutrons from the (d,t) reaction observed that the target material was not only emitted atomistically but also in the form of micrometer sized chunks. One of the groups using neutrons from the (d,t) reaction, and the two groups using 16-MeV protons did observe only atomistically released Nb. Furthermore, for the sputtering of cold rolled vanadium with two different surface finishes by (d,t) neutrons, total sputtering yields ranging from $\lesssim 5 \times 10^{-5}$ to 4.5×10^{-4} atoms/neutron have been reported [17]. For one type of target both atomistically sputtered vanadium and the emission of vanadium chunks was observed, while for the other type of target only atomistically sputtered vanadium was observed.

.. Based on the sputtering yields reported for cold rolled Nb and V under (d,t) neutron irradiation it is generally agreed [1, 2, 17] that the surface erosion of fusion reactor components by neutron sputtering will not be significant. However, as pointed out in Ref. 1 and 17, the effect of chunk emission on plasma contamination will need to be assessed. In turn, it has been speculated [1, 17] that the chunk emission is only a transient phenomena during the start-up of a new fusion reactor and may not need to be considered for the long-term operation of such reactors.

.. Fast neutron sputtering yields for some materials which have been calculated by several authors [1,18] using Sigmund's theory are listed in Table IV. The calculated values are generally lower than the experimental values listed in Tables I and II. Sigmund's theory, based on the development of displacement cascades, cannot account for the observed chunk emission. Robinson [18] has shown, that dynamic interferences between cascades can also not account for chunk emission. A model for chunk emission was developed by Guinan [19] who pointed out that the collision cascade resulting from a neutron hit can produce local stresses large enough, according to Griffith's criterion, to nucleate a penny-shaped crack about the size of the cascade. Such a microcrack could then be driven to micrometer size by the stress field of locally stored energy under certain conditions. Two types of dislocation arrays, unstressed single pile-ups and sub-boundary climb pile-ups, were identified as candidates for the needed energy storage configuration. He pointed out that each such configuration would have suffered more than one appropriate neutron hit in the experiments of references 13-15.
Robinson et al. [20] have extended Guinan's model to provide arguments for the dependence of chunk emission on protrusions or steps on the surface. They also suggested oxide intrusions as an alternative source for large internal stresses.

REFERENCES

[1] P. Dusza, S.K. Das and M. Kaminsky. Adv. in Chemistry Ser. 158, 65 (1976).

[2] R. Behrisch, O.K. Harling, M.T. Thomas, R.L. Brodzinski, L.H. Jenkins, G. J. Smith, J.F. Wendelken, M.J. Saltmarsh, M. Kaminsky, S.K. Das, C.M. Logan, R. Meisenheimer, J.E. Robinson, M. Shimotomai, and D. A. Thompson, J. Appl. Phys. 48, 3914 (1977).

[3] D.W. Norcross, B.P. Fairand, and J.N. Anno, J. Appl. Phys. 37, 621 (1966).

[4] K. Verghese, Trans. Am. Nucl.Soc. 12, 544 (1969).

[5] M.A. Kirk, T.H. Blewitt, A.C. Klauk, T.L. Scott and R. Malewicki, J. Nucl. Mat. 53, 179 (1974).

[6] T.S. Baer and J.N. Anno, J. Appl. Phys. 43, 2453 (1972).

[7] T.S. Baer and J.N. Anno, J. Nucl. Mat. 54, 79 (1974).

[8] K. Keller and R.V. Lee, Jr., J. Appl. Phys. 37, 1890 (1966).

[9] L.H. Jenkins, T.S. Noggle, R.E. Reed, M.J. Saltmarsh, and G.J. Smith, Appl. Phys. Lett. 26, 426 (1975).

[10] R.I. Garber, G.P. Dolya, V.M. Kolyada, A.A. Modlin, and A.I. Fedorenko, JFTP Lett. 7, 296 (1968).

[11] K. Keller, Plasma Phys. 10, 195 (1968).

[12] R. Behrisch, R. Gahler and J. Kalus, J. Nucl. Mat. 53, 182 (1974).

[13] O. Harling, M.T. Thomas, R.C. Brodzinski, and L. A. Ranticelli, Phys. Rev. Lett. 34, 1340 (1975).

[14] M. Kaminsky, S.K. Das, J. Nucl. Mat. 60, 111 (1976).

[15] M. Kaminsky, J.H. Peavey and S.K. Das, Phys. Rev. Lett. 32, 599 (1974).

[16] M. Kaminsky and S.K. Das, J. Nucl. Mat. 53, 162 (1974).

[17] M. Kaminsky and S.K. Das, J. Nucl. Mat. 66, 333 (1977).

[18] M. T. Robinson, J. Nucl. Mat. 53, 1974, 201.

[19] M. Guinan, J. Nucl. Mat. 53, 1979, 171.

[20] J.E. Robinson, B.S. Yarlagadda and R. A. Sacks, J. Nucl. Mat. 63, 432, 1976.

Table I Fast Neutron Sputtering Yields for Different Metals Irradiated with Neutrons from Fission Processes and the (*d*,Be) Reaction

Neutron Source		*Target Metal*[a]	*Neutron Energy*[b]	*Neutron Dose (neutrons/cm²)*	*Sputtering Yield S_n (atom/neutron)*	*Reference*
^{235}U Fission	Battelle Research Reactor	Au	spectrum	4×10^{17}	$(1.0 \pm 0.3) \times 10^{-4}$	3
	Bulk Shielding Reactor, ORNL	Au	"	not stated	$(1.83 \pm .56) \times 10^{-6}$	4
	CP-5, ANL	Au (monocrystal)	"	2.1×10^{17}–5.5×10^{17}	1×10^{-3}–6×10^{-3}[c]	5
	Battelle Research Reactor	Fe	"	2×10^{18}	$(5.7 \pm 0.8) \times 10^{-3}$	6
		Fe	"		$4.5 \pm 0.7 \times 10^{-3}$[d]	7
		(at 200°–340°C)	(average ~ 2.0 MeV)	7.8×10^{18}–1.4×10^{19}	3×10^{-3}–8×10^{-3}	7
Pu–Be		Au	mean ~ 4.2	3.6×10^{11}–7.3×10^{11}	0.5[e]	8
D–Be	(40-MeV D⁺, cyclotron)	Au (electropolished)	spectrum [0–35 MeV peak ~ 15 MeV]	4×10^{16}	$< 7 \times 10^{-5}$[f], $< 3 \times 10^{-5}$[g]	9
		Au (cold-rolled)		2.5×10^{13}	$< 7 \times 10^{-5}$[f], $< 1.3 \times 10^{-4}$[g]	
		Nb (monocrystalline)		3.5×10^{18}	$< 3 \times 10^{-5}$[f]	
		Nb (discharge machined)		3.3×10^{16}	$< 3 \times 10^{-5}$[f,g]	

[a] All targets are polycrystalline unless stated otherwise.
[b] Only neutrons with energies larger than 0.1 MeV were considered as contributing to sputtering and accounted for in the total dose value quoted. The maximum neutron energy can go up to 7 MeV, but the fluence at the high energy tail is 2–3 orders of magnitude smaller than at 0.1 MeV.
[c] Revised to 1.8×10^{-5} atom/neutron (*32*).
[d] Revised value of the one in Ref. *30*.
[e] The same authors later suggested (*23*) that there may have been large systematic errors in this value.
[f] Forward sputtering yield.
[g] Backward sputtering yield.

Table II Summary of (d,t) Neutron Sputtering Yields for Different Metals[a]

Target Metal[b]	*Neutron Dose (neutrons/cm²)*	*Sputtering Yield S_n (atom/neutron)*	*Reference*
Au (monocrystalline)	2.3×10^{13}	3×10^{-3}	10
Au	2.4×10^{13}	$< 6 \times 10^{-4}$	11
Au	1.9×10^{14}	3.3×10^{-4}[c], 2.6×10^{-4}[d]	12
Au (annealed)	5×10^{14}–2.6×10^{16}	2.5×10^{-5}–4.5×10^{-4}[c], 1.2×10^{-5}–2.0×10^{-4}[d]	13
Nb (cold-rolled, lightly etched, 5–10 μm microfinish)	5×10^{15}–1.5×10^{16}	$< 2 \times 10^{-4}$–7.6×10^{-4} (2.2×10^{-3})[e] [includes contribution from chunk deposits of 5×10^{-5}–1.6×10^{-4} (1.6×10^{-3})[e]]	14
	5×10^{15}	$< 6 \times 10^{-5}$	13
Nb (cold-rolled, lightly electropolished, ~ 5 μm microfinish)	4.6×10^{15}	$< 2 \times 10^{-4}$–1.7×10^{-3} (3.7×10^{-2})[e] [includes contribution from chunks of 0–1.1×10^{-3} (3.6×10^{-2})[e]]	14, 15, 16
Nb (annealed, electropolished)	4.3–4.6×10^{15}	$< 2 \times 10^{-4}$–5.2×10^{-4} (6–8×10^{-4})[e] [contribution from chunks, 0–2×10^{-5} (1–3×10^{-4})[e]]	13
Nb (monocrystalline)	1.7×10^{15}	$< 2 \times 10^{-4}$	
Nb (cold-rolled, electropolished, 1–5 μm microfinish)	5×10^{14}–2.6×10^{16}	1.1×10^{-5}–5.9×10^{-4}[c], 1.5×10^{-5}–1.3×10^{-3}[d]	13
Nb (cold-rolled, heavily etched, 1–4 μm microfinish)	5×10^{14}–2.6×10^{16}	6.4×10^{-5}– $< 2.3 \times 10^{-4}$[c], $< 4.4 \times 10^{-5}$– $< 1.0 \times 10^{-3}$[d]	13
Nb (cold-rolled, lightly etched, 1–4 μm microfinish)	5×10^{14}–2.6×10^{16}	$< 3.6 \times 10^{-5}$[c], 8.5×10^{-4}[d]	13

[a] The mean energy of neutrons is 14.1 MeV.
[b] All targets are polycrystalline metals unless stated otherwise.
[c] Backward sputtering yield.
[d] Forward sputtering yield.
[e] These are highest values observed in a run.

Table III. Summary of Results

Laboratory	No. and type of targets	No. of collectors	Type and energy of irradiating particle	Sputtering ratio atoms/neutron or proton	Chunks Size (avg) (μm)	Chunks Density (avg) (No./cm²)	Methods of analysis and sensitivity limits	Comments
PNL	2 Nb(A)[a]	2	14.8-Mev neutrons	$\leq 6.6\times10^{-5}$ to $\leq 2.6\times10^{-3}$	...	...	Neutron act. anal. Sensitiv. 2×10^{11} to 2×10^{12} atoms	Yields are independent of fluence. Lowest values of S_n should still be considered as upper bounds on the sputtering ratio. Background from blank runs averages 2×10^{12} atoms per collector.
PNL	2 Nb(B)[b]	3	14.8-Mev neutrons	$\leq 6.0\times10^{-5}$ to $\leq 1.3\times10^{-3}$	...	...		
ANL	6 Nb(A)	6	14.8-MeV neutrons	7×10^{-5} to 7×10^{-4}	0.2—1.7	0—11	RBS (5×10^{-4})[c]	Collectors from blank experiments with type Nb(A) targets which had not been exposed to 14.8-MeV neutron irradiation, but had received identical handling, procedures revealed no chunk deposits.
ANL	2 Nb(B)	4	14.8-MeV neutrons	$<2\times10^{-5}$ to $<3\times10^{-4}$	...	...	IMMA (1×10^{-3})[c] SEM (~0.1-μm-diam chunks) AES (1×10^{-2})[c] IMMA scan of collector area facing Nb(A) was 4.85 cm², and facing Nb(B) was 3.64 cm².	
LLL	1 Nb(A)	1	14.8-MeV neutrons	1.45×10^{-4}	2	39	IMMA and SEM used to examine 1.3 cm²	Collectors from a blank experiment with a target of type Nb(A) and no neutrons had 1.8×10^{11} cm² atoms on the collector and no observable chunks.
LLL	1 Nb(B)	1	14.8-MeV neutrons	1.36×10^{-5}	...	...		
ORNL	3 Nb(A)	6	(d, Be), d = 40 MeV broadly peaked at 15 MeV	...	...		SEM, chunk resolution $\gtrsim$0.5-μm particles	Examined 20, 1-mm² areas on each of 18 collectors.
	3 Nb(B)	6		...	...			
McMaster U.	2 Nb(A)	4	16-MeV protons	$\lesssim 4\times10^{-4}$	...	...	0.2 cm² by SEM[d] 0.5 cm² by AES[d]	Negative results for Nb detection in all cases.
	2 Nb(B)	4	16-MeV protons	$\leq 8\times10^{-4}$	...	...	0.1 cm² by SEM[d]	
LLL	1 Nb(A)	1	16-MeV protons	2.2×10^{-5}	...	...	IMMA 0.5 μm chunk resolution and ~10^{10} atoms/cm² sensitivity	Sputtering ratios believed to be accurate to within a factor of 5.
	1 Nb(B)	1	16-MeV protons	2.2×10^{-5}	...	...		

[a] Nb(A)—targets prepared by ANL (see Sec. IIA).
[b] Nb(B)—targets prepared by Battelle (see Sec. IIA).
[c] Sensitivity values are quoted in monolayers of niobium on Si (111) collectors.
[d] Minimum net area estimated more than 1 cm² actually scanned.

Table IV Fast neutron sputtering yields S_n, for some materials calculated using Sigmund's Theory.

Target Metal	Uo (ev/atom)	$\langle \sigma E_D \rangle$ [††] for 14-MeV neutrons (ev - cm^2 x 10^{20})	Sputtering Yields S_n (atom/neutron)	
			Forward S_n for 14-MeV neutrons*	Random S_n for ^{235}U Fission neutron spectrum [†††]
C	7.4	4.26 (2.8)	2.4×10^{-6} (1.6×10^{-6})	-
Al	3.36	16.4 (17.5)	2.1×10^{-5} (2.2×10^{-5})	2.4×10^{-5}
Ti	4.89	19.8	1.7×10^{-5}	-
V	5.33	23.7	1.9×10^{-5}	-
Cu	3.52	(25.3)	(3.0×10^{-5})	1.9×10^{-5}
Nb	7.59	27.3 (24.5)	1.5×10^{-5} (1.4×10^{-5})	8.9×10^{-6}
Au	3.80	(18.2)	(2.0×10^{-5})	1.1×10^{-5}

[††] The values are taken from Parkin et. al. ; the values in parenthesis are taken from Robinson.

[†††] The S_n values were calculated by Robinson in Ref. 18.

* The S_n values in parenthesis were calculated using the $\langle \sigma E_D \rangle$ values given by Robinson and others were calculated using $\langle \sigma E_D \rangle$ values given by Parkin et. al.

SPUTTERING: THEORY-MODELLING

I. Transport Theory, Computer Simulation, and Monte Carlo*

L. G. Haggmark
Sandia Laboratories, Livermore, California

Many attempts [1-7] have been made to theoretically predict physical sputtering yields of various materials bombarded by energetic ions. These attempts fall into two broad categories: The first involves the use of transport theory [1-4], e.g. solution to the Boltzmann transport equation, and the other involves the use of computer simulations or Monte Carlo techniques [5-17]. The former rely on direct analytic or numerical procedures while the latter, by their nature, attempt to simulate the actual physical processes. These two theoretical approaches will be discussed below, with emphasis on the more comprehensive or recent formulations.

Transport Theory

Until recently, the most detailed theoretical treatment of sputtering of amorphous materials was done by Sigmund [3]. Sigmund used a semi-analytic approach known as the moments method to solve the Boltzmann transport equation. Using several assumptions, he obtained an analytic solution which showed the sputtering yield was proportional to the recoil energy density deposited at the surface and inversely proportional to the surface binding energy (e.g. heat of sublimation). The assumptions or restrictions included in the Sigmund formulation involve the neglect of the surface in determining the deposited recoil energy and the neglect of bulk binding energies. Furthermore, the recoils are assumed to be isotropic in nature. Even with these and other assumptions, comparisons of Sigmund's predicted sputtering yields with experimental data have shown good agreement for heavy ions. However, the agreement is rather poor for low energy, light ion sputtering yields which are of particular interest for fusion applications. Even when some adjustments are made to the theory, the predicted yields are still a factor of 10 or more greater than experimental data. Behrisch, et al. [17], using the MARLOWE program [18], have recently calculated the recoil energy density from light ions moving toward the surface and with the recoils being above a given threshold energy. When this energy density is used in Sigmund's analytical solution, the agreement with experiment is greatly improved.

---

*This work supported by the U.S. Department of Energy.

One of the most recent developments in sputtering theory is the work of Hoffman, et al. [4]. They have used the highly developed discrete ordinates method to obtain sputtering yields. This method is a numerical solution of the Boltzmann equation and can treat finite medium problems. Using LSS theory for nuclear scattering and electronic stopping and a planar potential surface barrier, good agreement is obtained between the predictions and the experimental data for both light and heavy ions. This method shows great promise since it can determine not only sputtering yields but also angular and energy distributions of sputtered particles as a function of the incident energy and angle.

Computer Simulation and Monte Carlo Methods

During the last fifteen years, there have been a number of sputtering studies which have used computer simulation and Monte Carlo techniques (see Table I). In contrast to the continuous slowing down which occurs in transport theory, these techniques allow the discrete nature of the target and the atomic collisions to be taken into account explicitly. The use of computer simulation has ranged from binary collision calculations of the recoil energy deposited at the surface [10,17] to molecular dynamics calculations [7-9,19] in which the simultaneous motion of a large number ($\sim$ 200) of atoms are followed. Simulations in the latter category require a great deal of computer time and, thus, are not well suited for routine sputtering calculations. These type of computer simulations are principally useful for investigations of detailed mechanisms for atomic processes in crystals or perhaps for some very specific input to binary collision calculations.

In the last two years several approaches [1]-17] have addressed the cases of low energy, light ion sputtering using more realistic interactomic potentials. These approaches have used the simulation formalisms that are contained in two computer programs: MARLOWE [18] and TRIM [20]. Both of these programs use the binary collision approximation and generally base their nuclear scattering and electronic stopping on similar formalisms. The major difference between them lies in the target structure. The MARLOWE program follows particle trajectories relative to a crystal lattice; whereas, the TRIM program considers the target atoms at random locations (amorphouse). The TRIM program was recently extended to follow the 3-dimensional trajectory and all directional angles, so that anisotropy effects at non-normal incidence can be studied. [Biersack, private communication].

When these programs were extended to simulate sputtering, further differences were introduced in the formulation of the cascade formation and surface ejection processes. Biersack [12,13] and Haggmark and Wilson [14] include a bulk binding energy E_b which is subtracted from the energies transferred to target atoms. These two extensions of the TRIM program differ still in that Haggmark and Wilson's E_b is larger than that of Biersack's. Hou and Robinson [16], using MARLOWE, have $E_b = 0$. In the case of the surface binding energy, both Biersack and Hou and Robinson

invoke the planar potential barrier model (i.e. surface binding energy $E_s=E_{HS}\sec^2\theta$, where E_{HS} is the heat of sublimation). Haggmark and Wilson use the isotropic potential barrier model, i.e. independent of θ, but with $E_s \simeq 1.3E_{HS}$. Even with some of these basic differences, each of these sputtering formalisms predict sputtering yields as a function of energy whichagree reasonably well with experimental data.

The isotropic model and the planar model of the surface binding are probably oversimplifications of the actual physical process. However, Hou and Robinson's calculations show that the planar model gives a more realistic representation of the sputtered energy spectrum relative to experimental data. Jackson's [19] molecular dynamics calculations indicate that the surface binding energy is dependent on the ejection angle θ, although it is unclear from his limited results if this angular dependence is as strong as the $\sec^2_\theta$ dependence in the planar model. Further molecular dynamics calculations in this regard should aid in resolving this issue and also the issue of the bulk binding energy.

Conclusions

1. Sigmund's theory seems adequate for determining heavy ion sputtering yields and is only suitable for low energy, light ion when special conditions are imposed for calculating the deposited recoil energy density.

2. The discrete ordinates method of Hoffman, et al. provides good results for both light and heavy ions.

3. The present computer simulation and Monte Carlo methods using the binary collision approximation provide sputtering yields usually within a factor of 2, or better, of experimental data.

4. Molecular dynamic calculations can be useful to resolve differences in the simulation models relative to bulk and surface binding energies.

5. The calculated sputtering yields may be sensitive to the choice of stopping powers and interatomic potentials being used, particularly at low energies.

6. To aid the plasma physicists and fusion reactor design engineers, the discrete ordinates method and/or the simulation techniques can be used to provide sputtering yields and sputtered particle energy and angular distributions for realistic incident energy and angular distributions.

References

1. W. J. Brandt and R. Laubert, Nucl. Instr. Meth. 47, 201 (1967).

2. M. W. Thompson, Phil. Mag. 18, 377 (1968).

3. P. Sigmund, Phys. Rev. 184, 383 (1969).

4. T. J. Hoffman, H. L. Dodds, Jr., M. T. Robinson, and D. K. Holmes, Nucl. Sci. Eng. 68, 204 (1978).

5. P. V. Pavlov, D. I. Telel'baum, E. I. Zorin, and V. I. Alekseev, Fiz. Tver. Tela 8, 2679 (1966) [Sov. Phys.-Solid State 8, 2141 (1967)].

6. G. Betz, R. Dobrozemsky, and F. P. Viehböck, Int. J. Mass Spectrom. Ion Phys. 6, 451 (1971).

7. D. E. Harrison, Jr., N. S. Levy, J. P. Johnson, III, and H. M. Effron, J. App. Phys. 39, 3742 (1968).

8. D. E. Harrison, Jr., W. L. Moore, Jr., and H. T. Holcombe, Rad. Effects 17, 167 (1973).

9. D. E. Harrison, Jr., and C. B. Delaplain, J. Appl. Phys. 47, 2252 (1976).

10. J. E. Robinson, Rad. Effects 23, 29 (1974).

11. I. Ishitani and R. Shimizu, Appl. Phys. 6, 241 (1975).

12. K. E. Ecker and J. P. Biersack, VIIth Int. Conf. on Atomic Collisions in Solids, Moscow, 19-23 Sept. 1977.

13. J. P. Biersack, W. Kaczerowski, J. Ney, B. K. H. Rahim, A. Riccato, G. R. Thacker, and H. Vecker, J. Nucl. Mater. 76 & 77, 640 (1978).

14. L. G. Haggmark and W. D. Wilson, J. Nucl. Mater. 76 & 77, 149 (1978).

15. O. S. Oen and M. T. Robinson, J. Nucl. Mater. 76 & 77, 370 (1978).

16. M. Hou and M. T. Robinson, Appl. Phys., 18, 381 (1979).

17. R. Behrisch, G. Maderlechner, B. M. U. Scherzer, and M. T. Robinson, Appl. Phys., 18, 391 (1979).

18. M. T. Robinson and I. M. Torrens, Phys. Rev. B9, 5008 (1974).

19. D. P. Jackson, Can. J. Phys. 53, 1513 (1975).

20. J. P. Biersack and L. G. Haggmark, submitted for publication.

Table I

Various Computer Simulation and Monte Carlo Approaches to Sputtering

	Projectiles	Targets	Displacement Threshold E_d	Bulk Binding E_b	Surface Binding E_s	Comments
Pavlov, et al. (1966)	B,Aℓ	Si	E_b	30 eV	0	
Betz, et al. (1971)	Xe,Ar	C,Si,Cu, Ge,Ag,Cd Au	0	0	$E_{HS}, \frac{E_{HS}}{\cos^2\theta}$	
Harrison, et al. (1968,1972,1976)	Ar	Cu	Molecular Dynamics			
J. E. Robinson (1974)	H,D,He	Nb	No Knock-ons Considered, calculated F_D			
Ishitani and Shimizu (1975)	Ar	Si	15.8 eV	0	$\frac{7.83 \text{ eV}}{\cos\theta}$	
Biersack (1977) TRIM	H,He,Ag, Bi,Kr	Nb,Au	E_b	E_{FP}	$\frac{E_{HS}}{\cos^2\theta}$	
Haggmark and Wilson (1978) TRIM	He,H,D,T	C,Ni,Mo,Au	E_b	$E_{HS}+E_{1V}^f+E_I^*$	$\sim 1.3\ E_{HS}$	
Oen and M. T. Robinson (1979) MARLOWE	H	FeH, FeH_2	5 eV	0	0	Sputtering of H
Hou and M. T. Robinson (1979) MARLOWE	He,Ar,Ne Kr,Xe,Au	Cu	E_{HS}	0	$\frac{E_{HS}}{\cos^2\theta}$	
Behrisch, et al. (1979) MARLOWE	H,D,He	Fe,Mo	E_{HS}	0	$\frac{E_{HS}}{\cos^2\theta}$	
			0-12 eV	0	N.A.	Calculated F_D

E_{HS}: Heat of sublimation

E_{FP}: Frenkel pair formation energy

E_{1V}^f: Vacancy formation energy

E_I^*: "Effective" Interstitial formation energy

F_D: Deposited recoil energy density

N.A.: Not applicable

Examples of Theoretically Predicted Sputtering Yields

Sigmund's Theory Compared to Experimental Data
[Phys. Rev. 184, 383 (1969)]

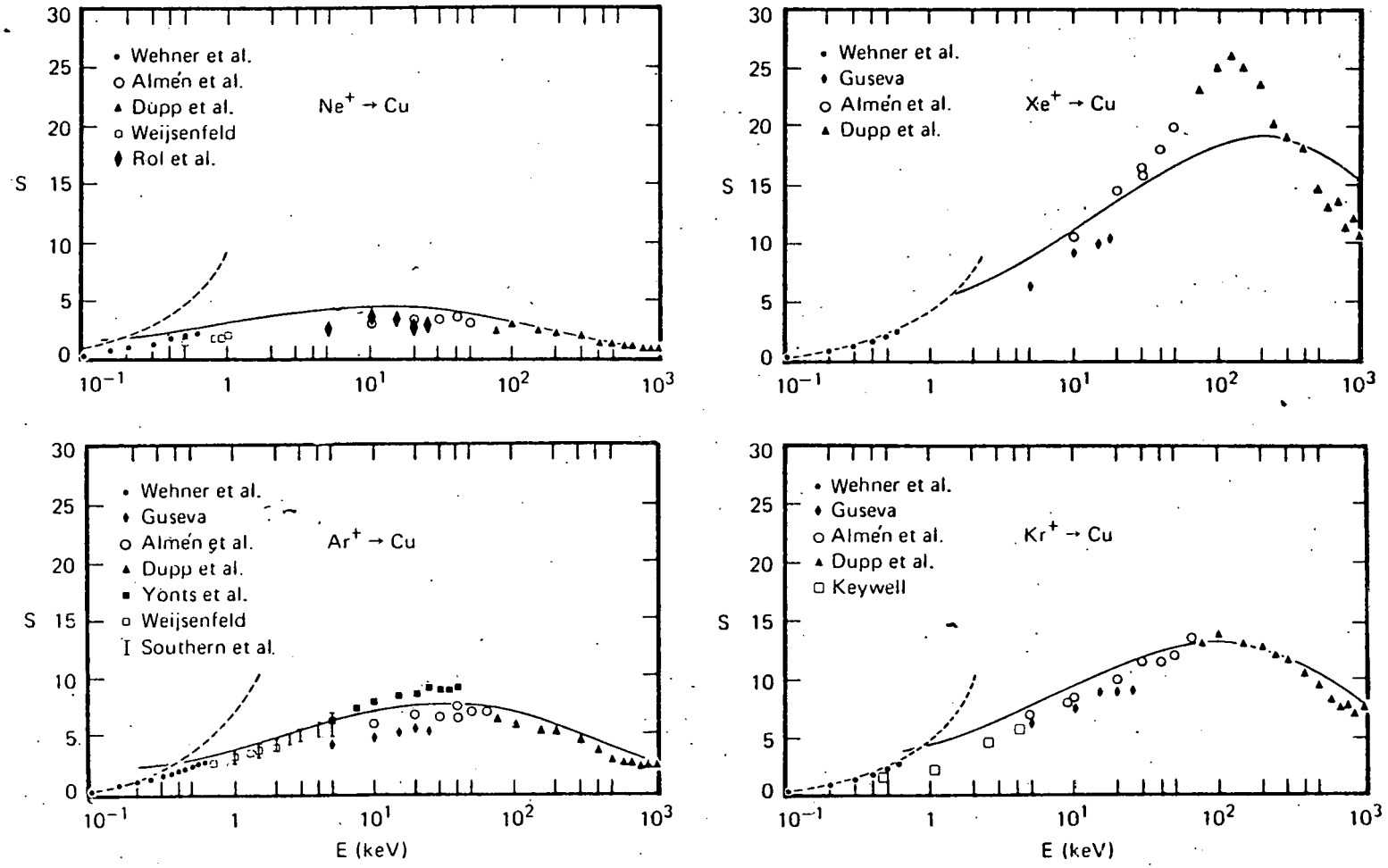

Hou and Robinson (MARLOWE)
[Appl. Phys. 18, 381 (1979)]

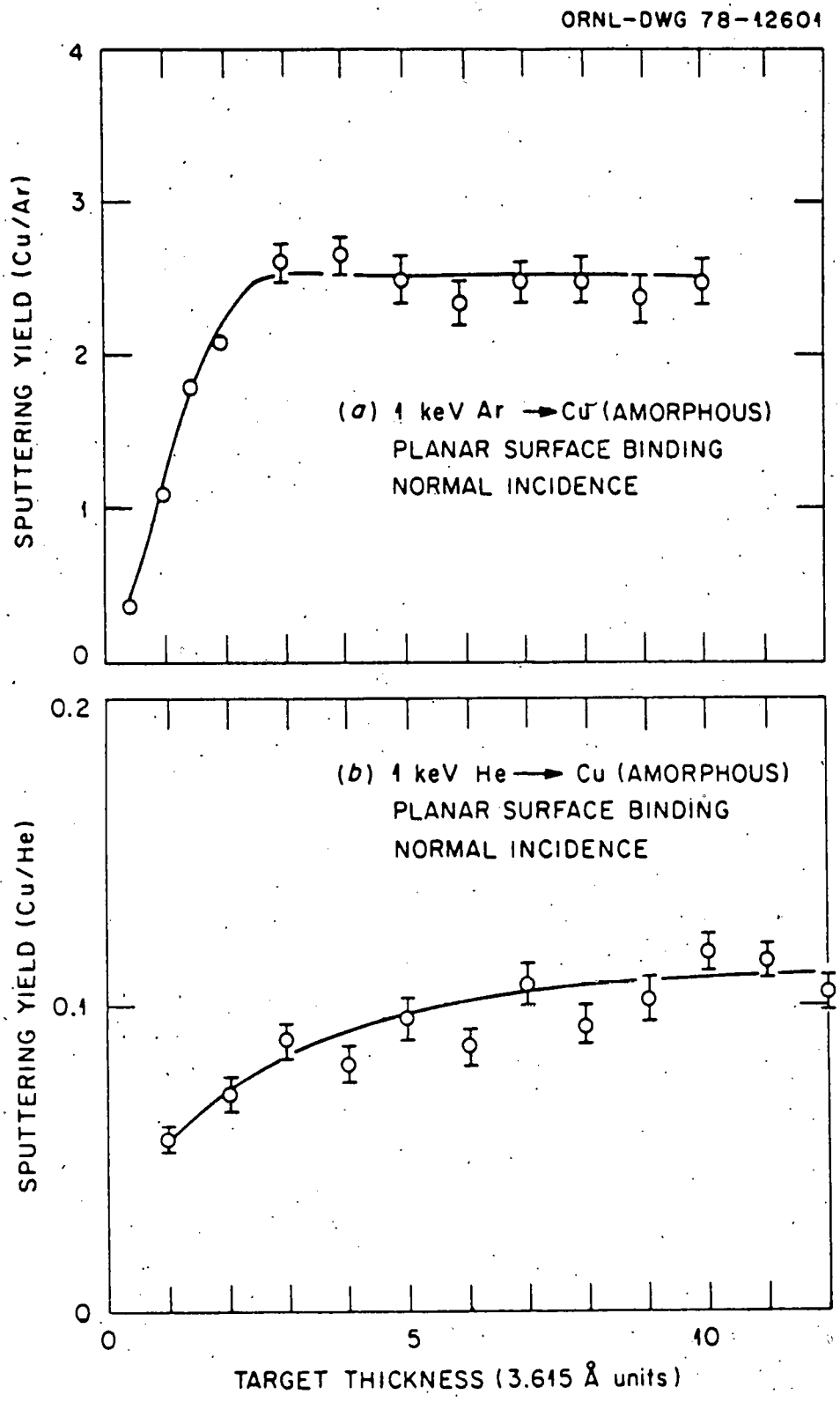

Hou and Robinson
[Appl. Phys. 18, 381 (1979)]

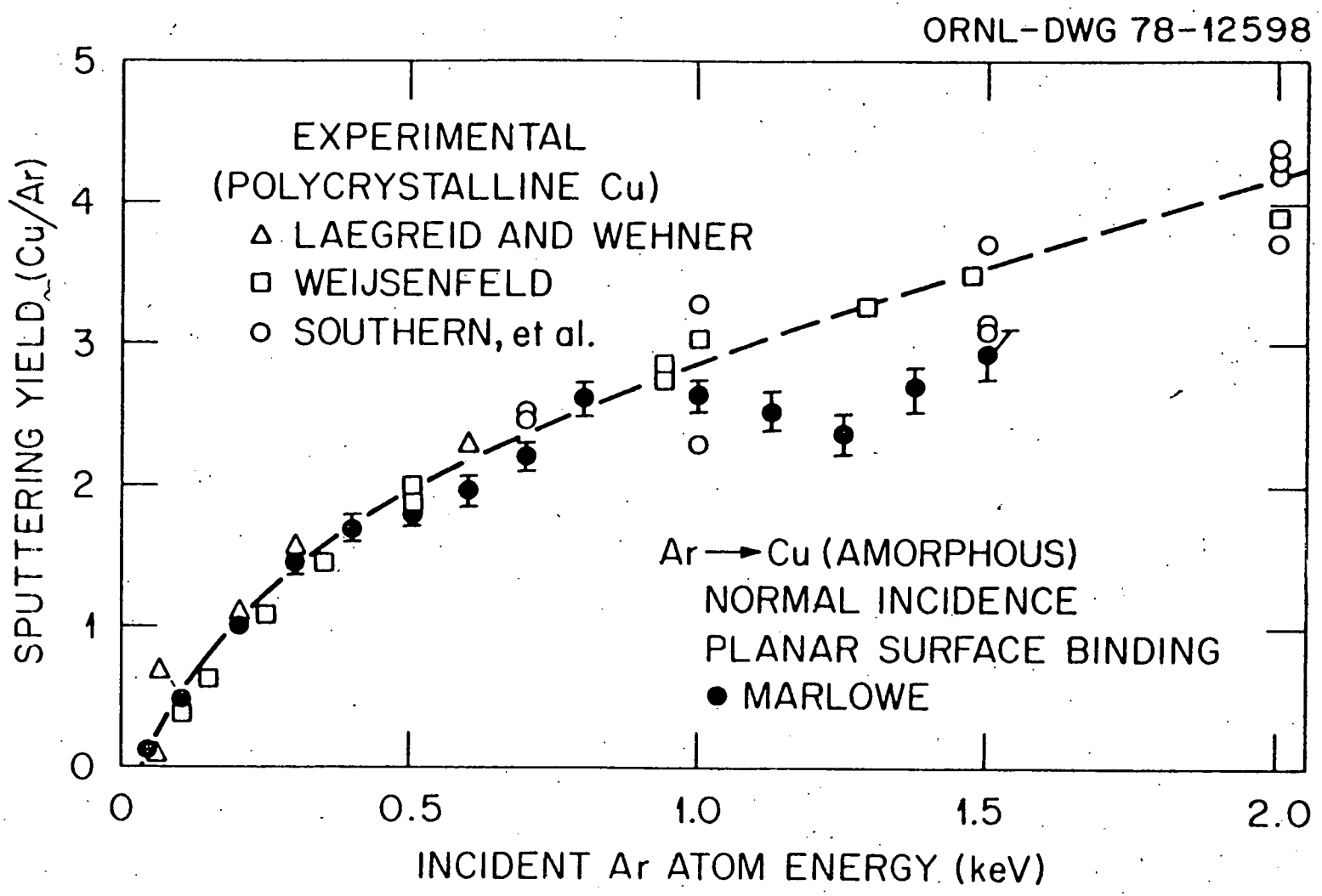

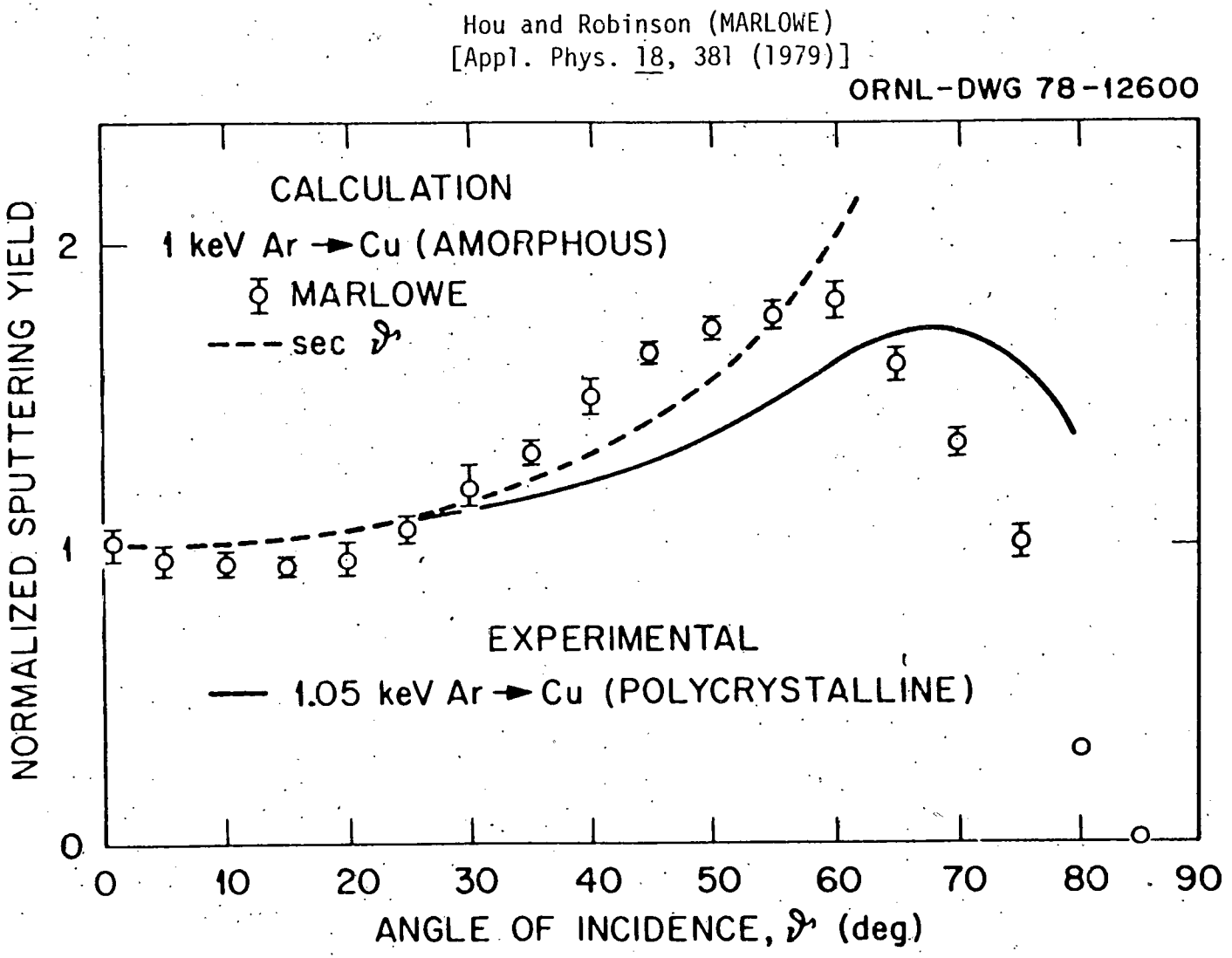
Hou and Robinson (MARLOWE)
[Appl. Phys. 18, 381 (1979)]
ORNL-DWG 78-12600
CALCULATION
1 keV Ar → Cu (AMORPHOUS)
MARLOWE
sec ϑ
EXPERIMENTAL
1.05 keV Ar → Cu (POLYCRYSTALLINE)
NORMALIZED SPUTTERING YIELD
0
1
2
0
10
20
30
40
50
60
70
80
90
ANGLE OF INCIDENCE, ϑ (deg)

Hou and Robinson
[Appl. Phys. 18, 381 (1979)]

ORNL-DWG 78-12599

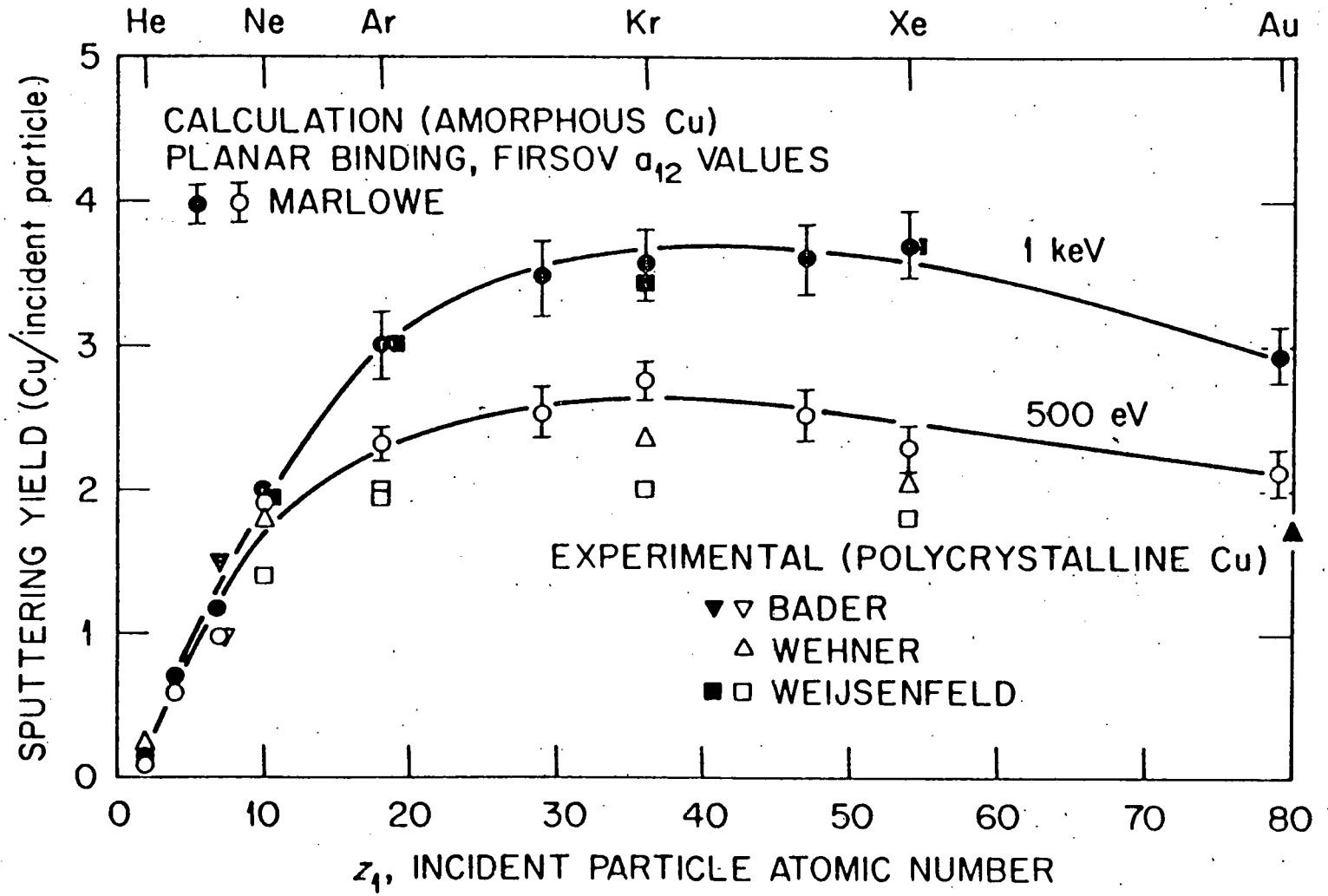

Hou and Robinson (MARLOWE)
[Appl. Phys. 18, 381 (1979)]
ORNL-DWG 78-12597

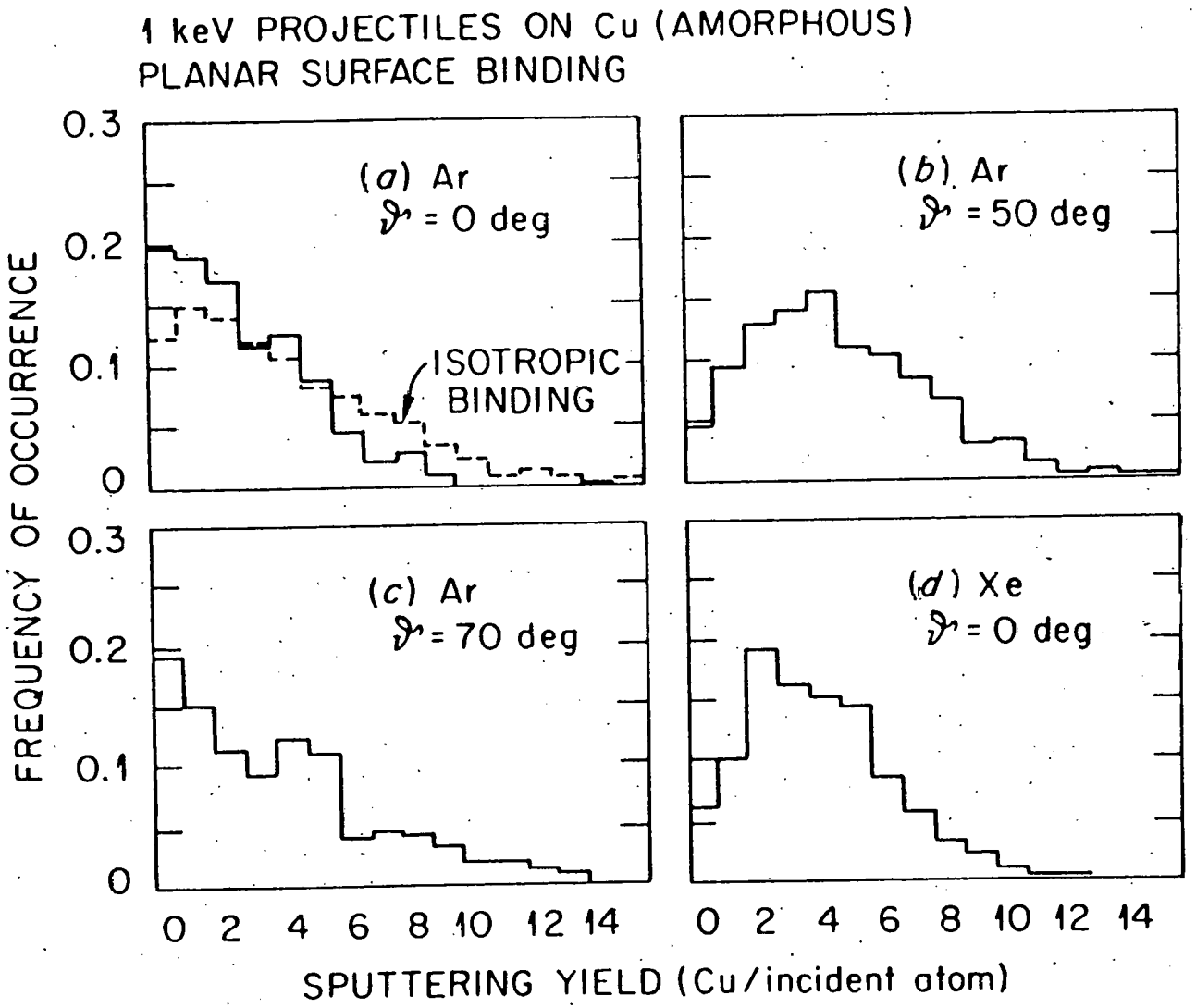

Hou and Robinson (MARLOWE)
[Appl. Phys. 18, 381 (1979)]

ORNL-DWG 78-12596

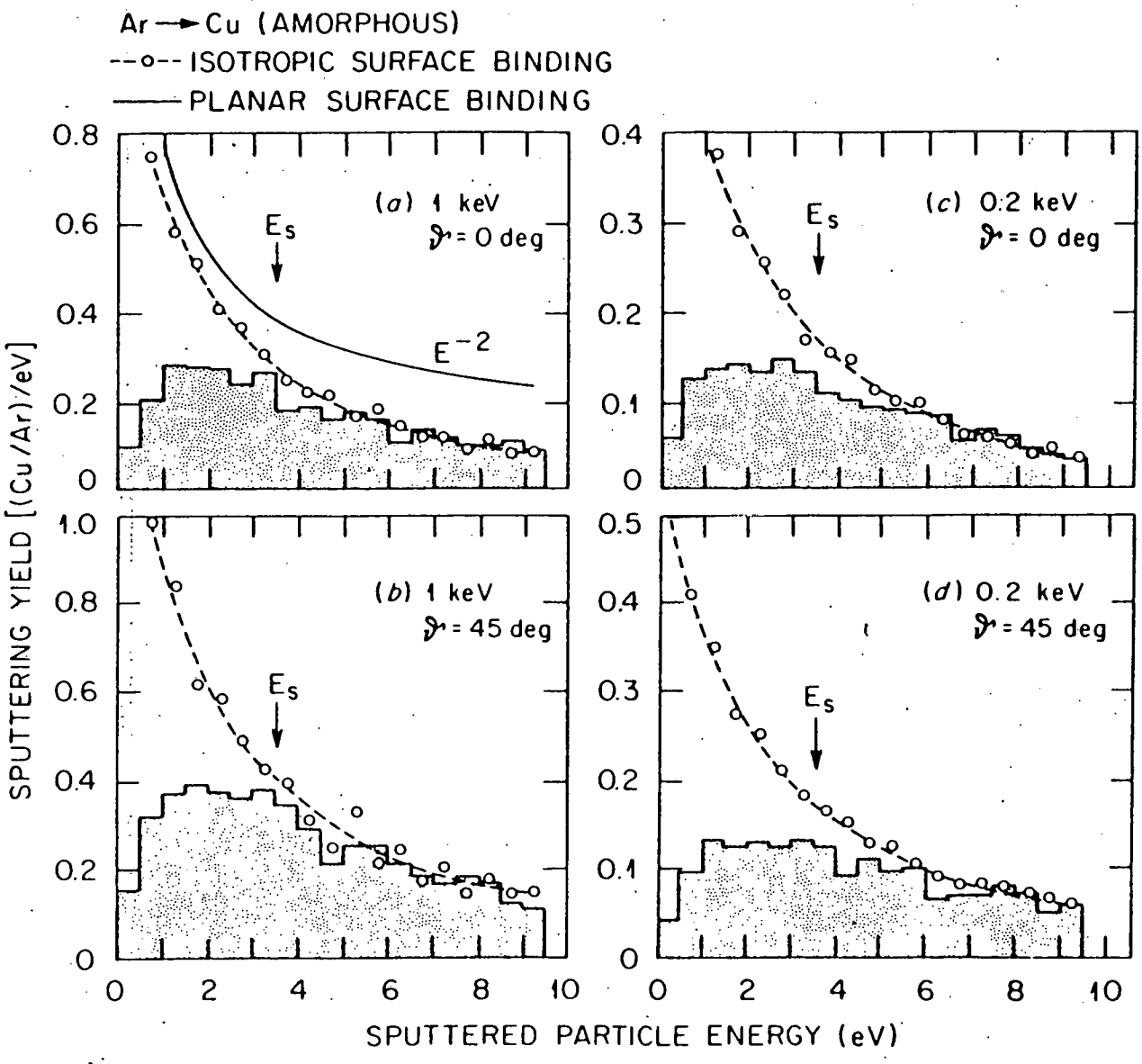

Hou and Robinson (MARLOWE)
[Appl. Phys. 18, 381 (1979)]

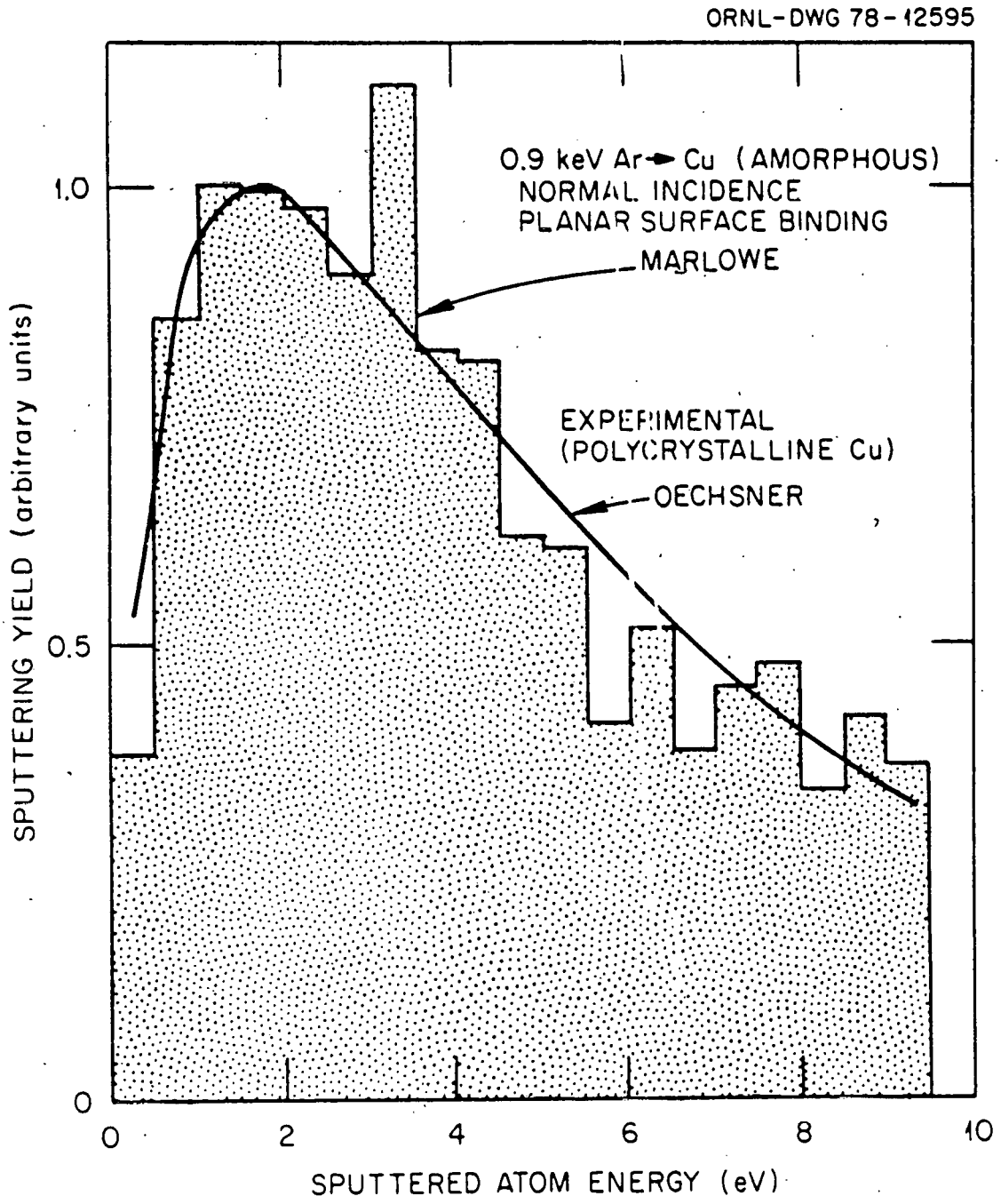

Hou and Robinson (MARLOWE)
[Appl. Phys. 18, 381 (1979)]

ORNL-DWG 78-12594

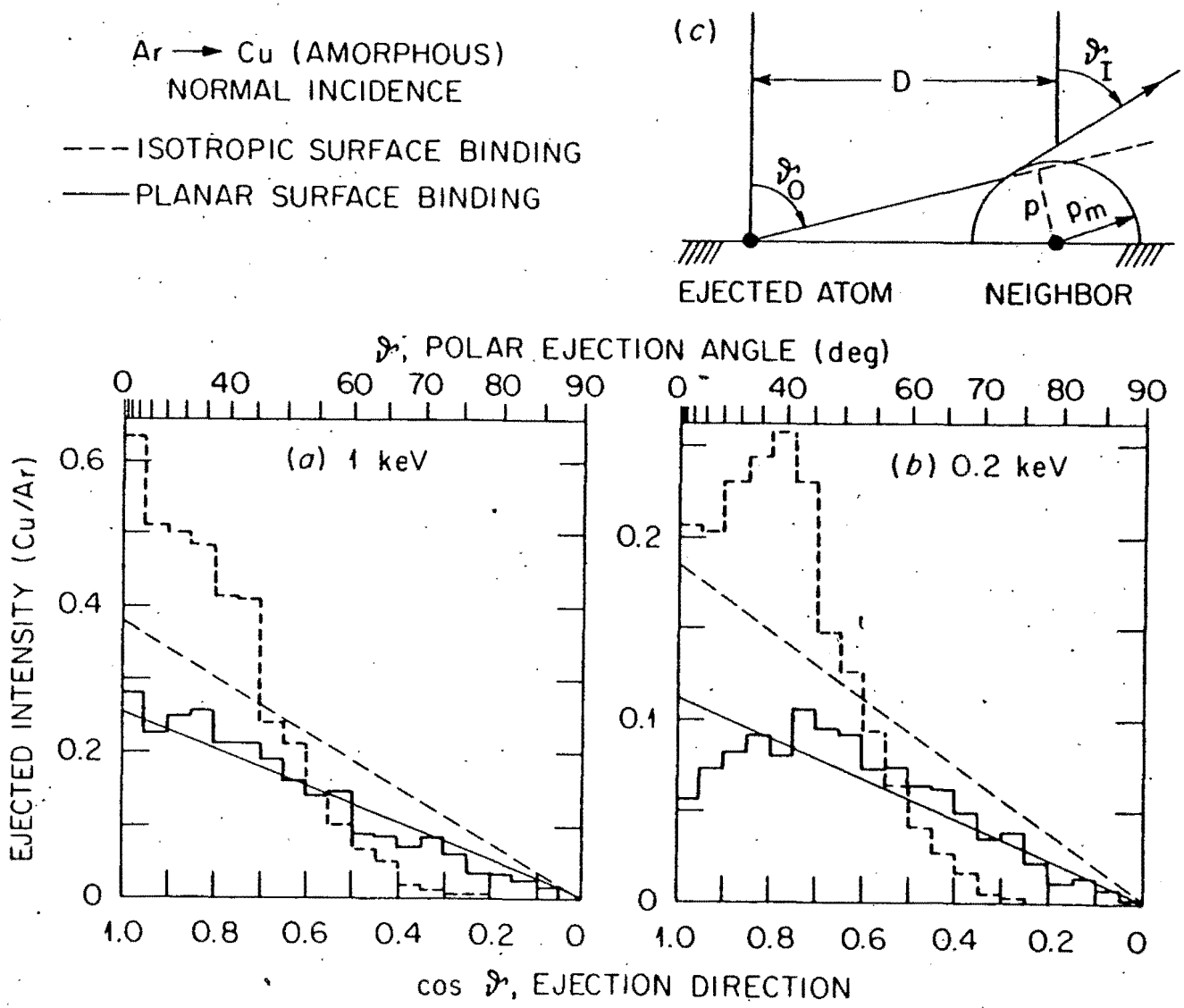

Comparison of Sigmund's Theory with Experimental Data (Behrisch, et al.)

[Appl. Phys. 18, 391 (1979)]

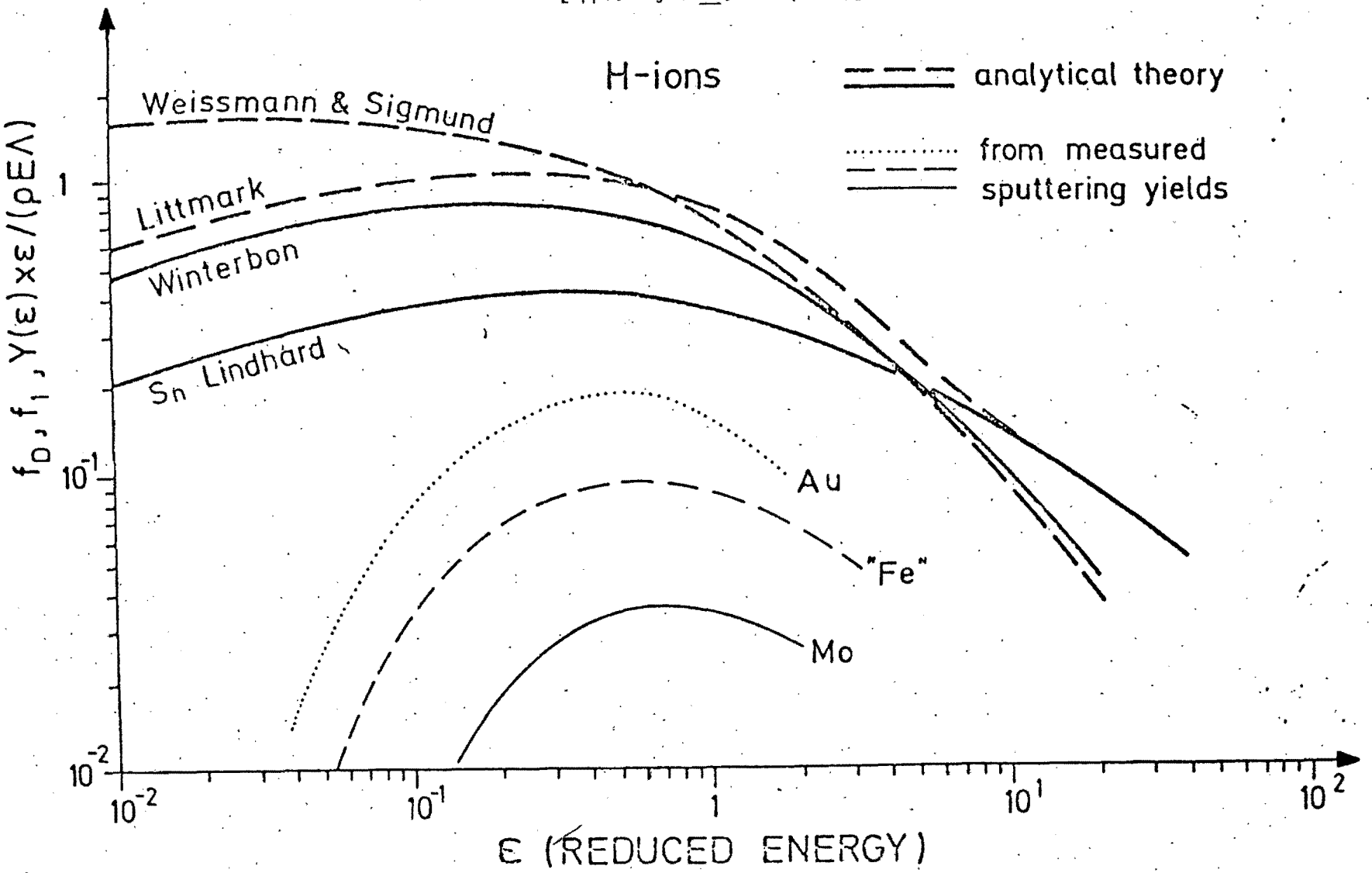

Comparison of Sigmund's Theory with Experimental Data (Behrisch, et al.)

[Appl. Phys. 18, 391 (1979)]

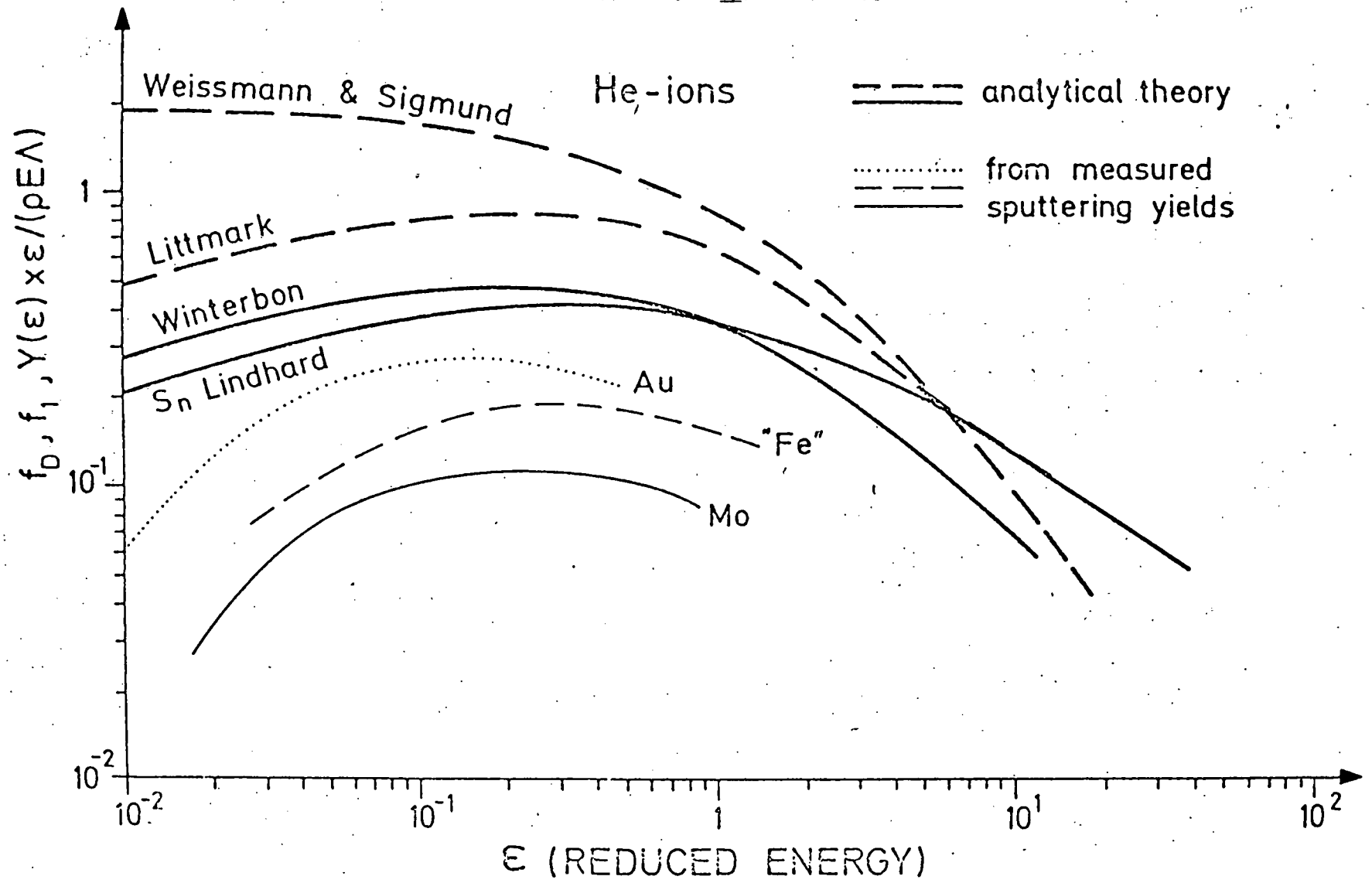

Behrisch, et al.
[Appl. Phys. 18, 391 (1979)]

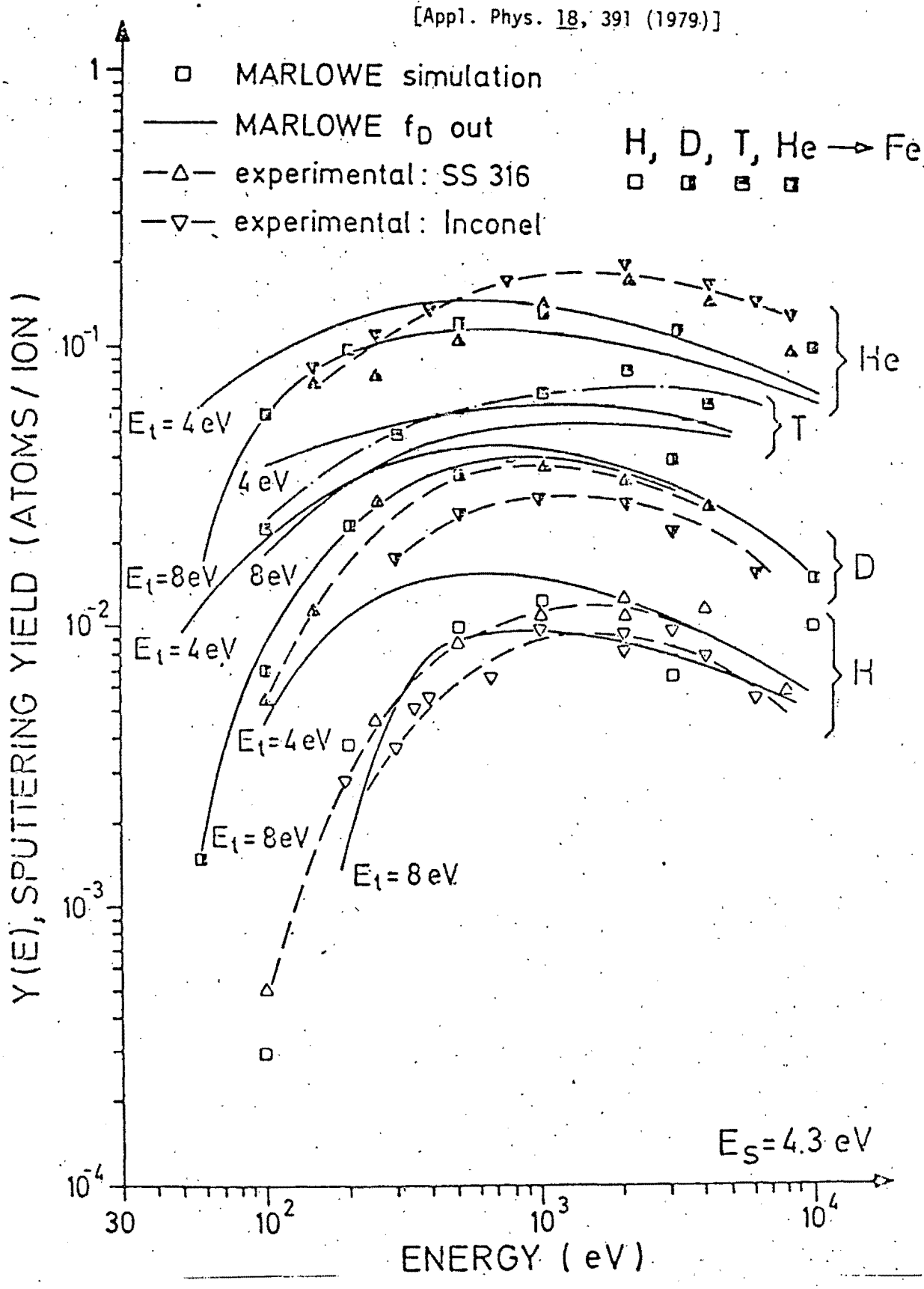

Behrisch, et al.
[Appl. Phys. 18, 391 (1979)]

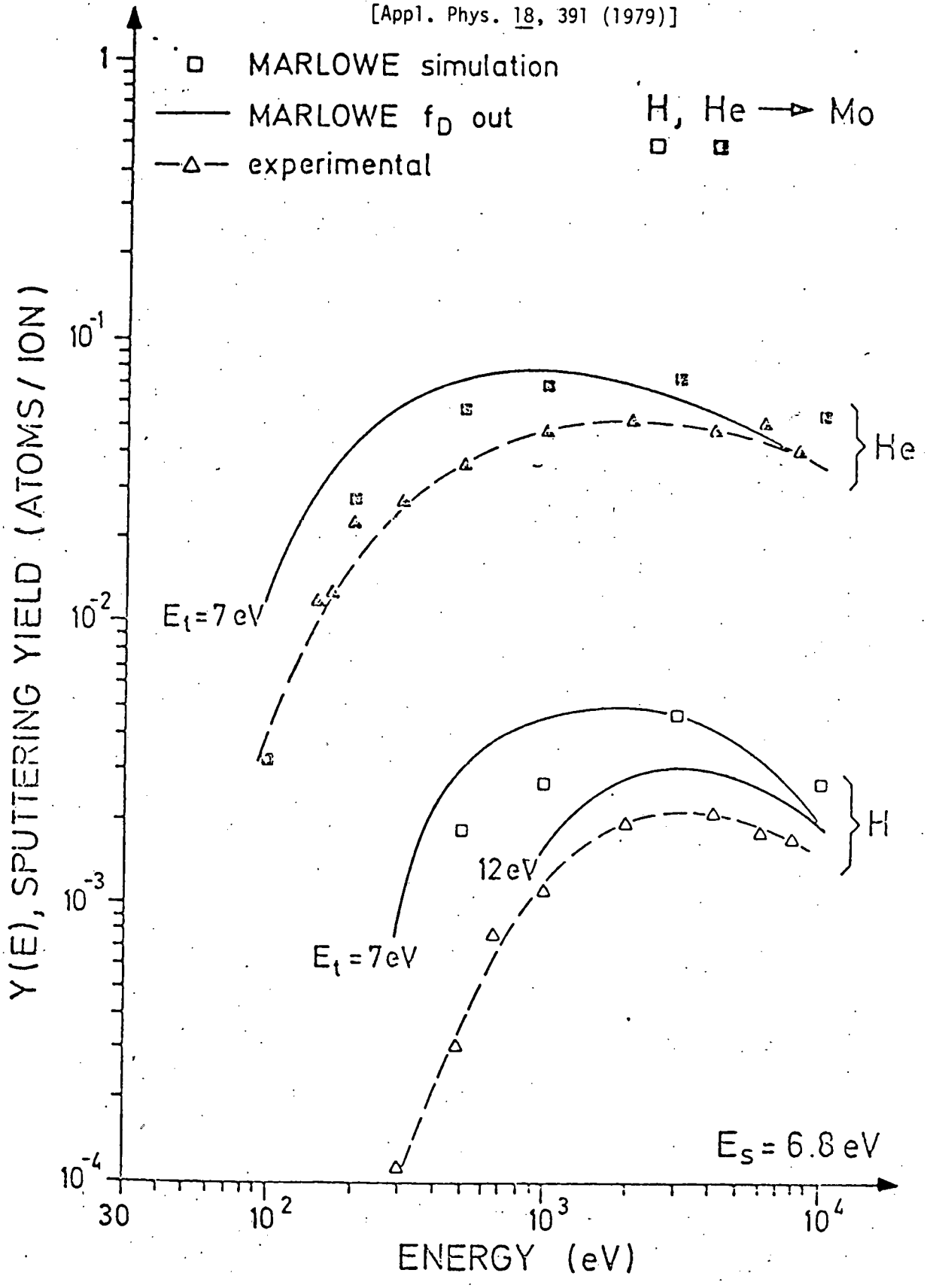

Behrisch, et al. (MARLOWE)
[Appl. Phys. 18, 391 (1979)]

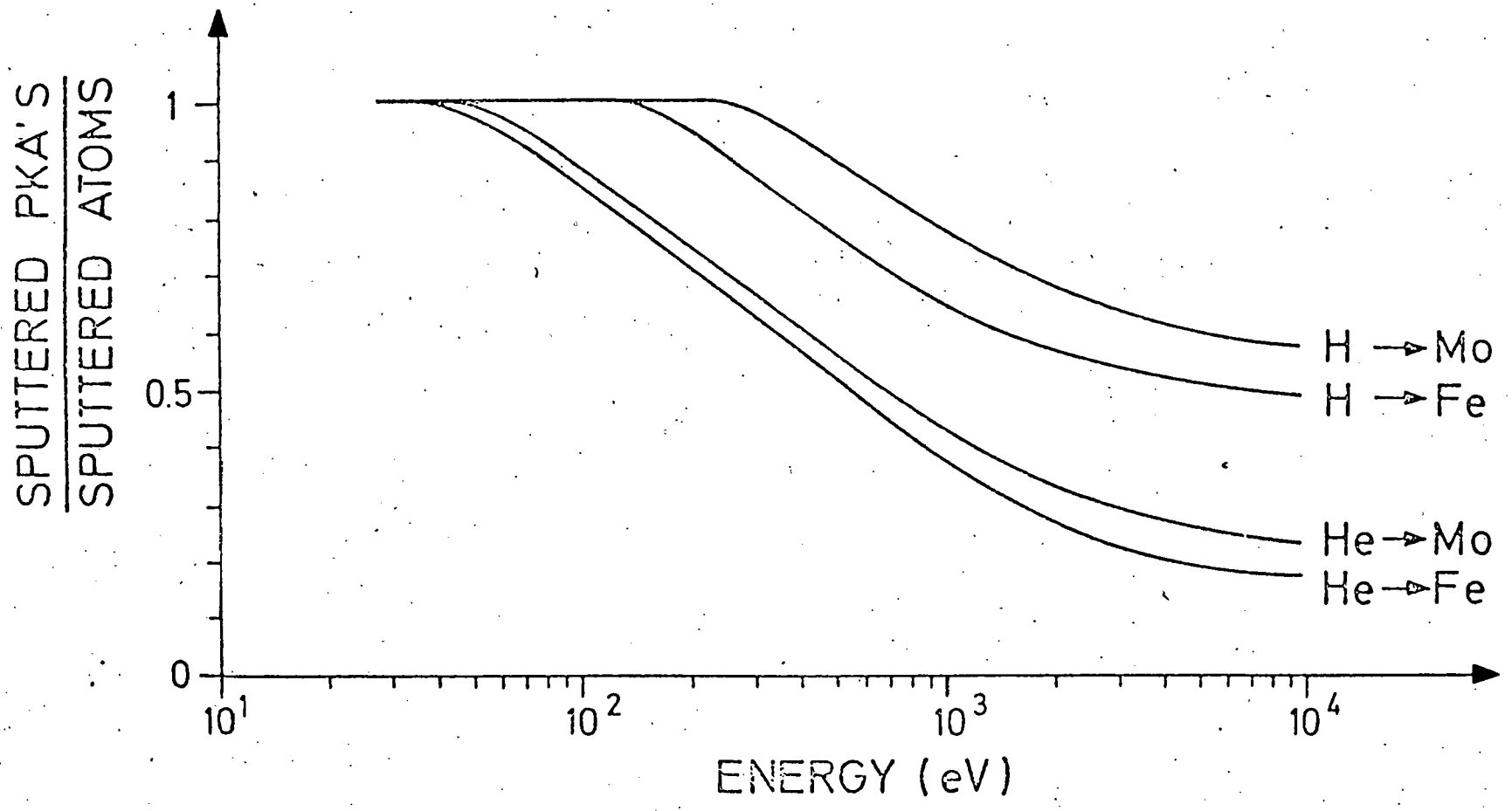

Hou and Robinson (MARLOWE)
[Appl. Phys. 18, 381 (1979)]
ORNL-DWG 78-12602

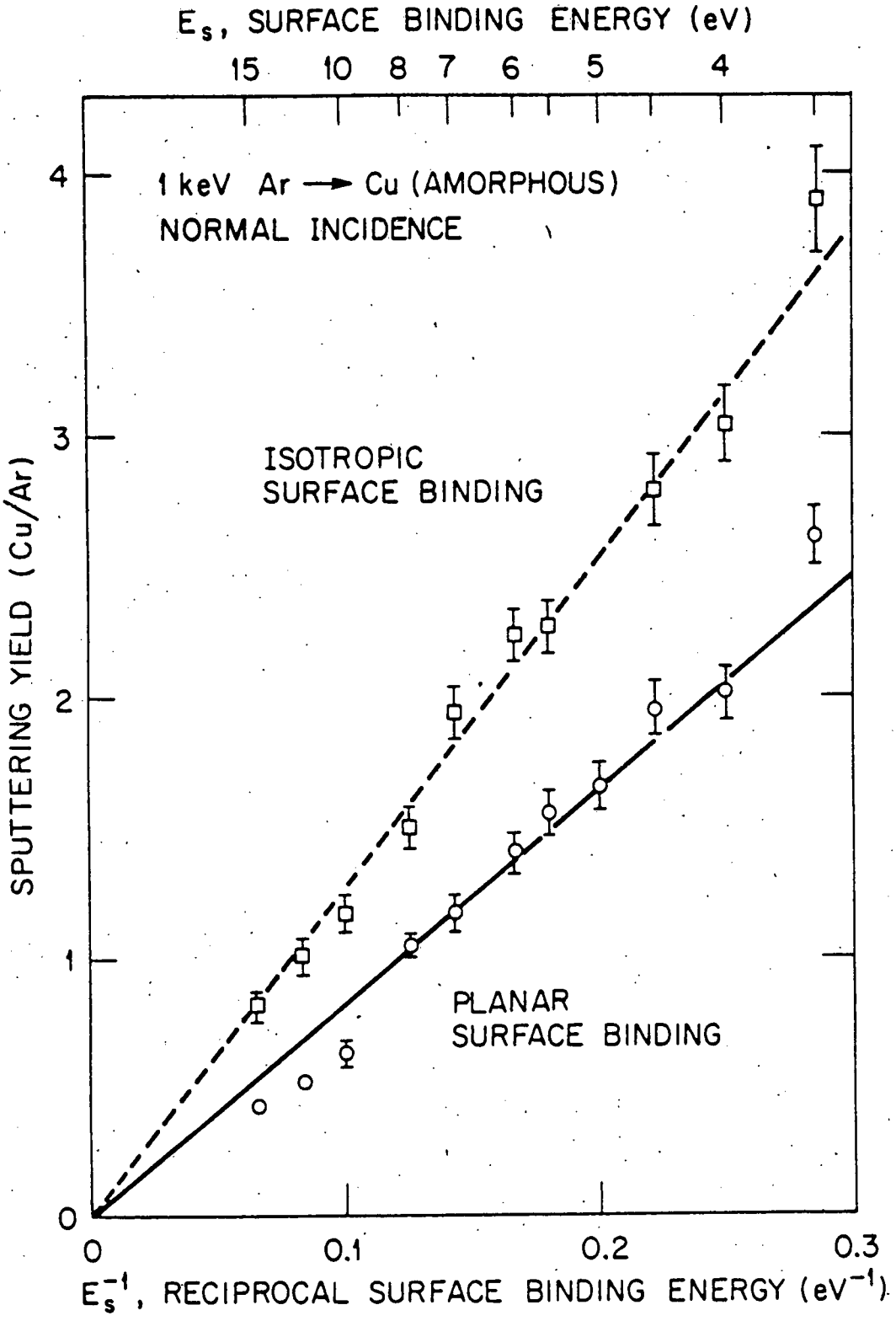

Oen and Robinson (MARLOWE)

[J. Nucl. Mater. 76 & 77, 370 (1978)]

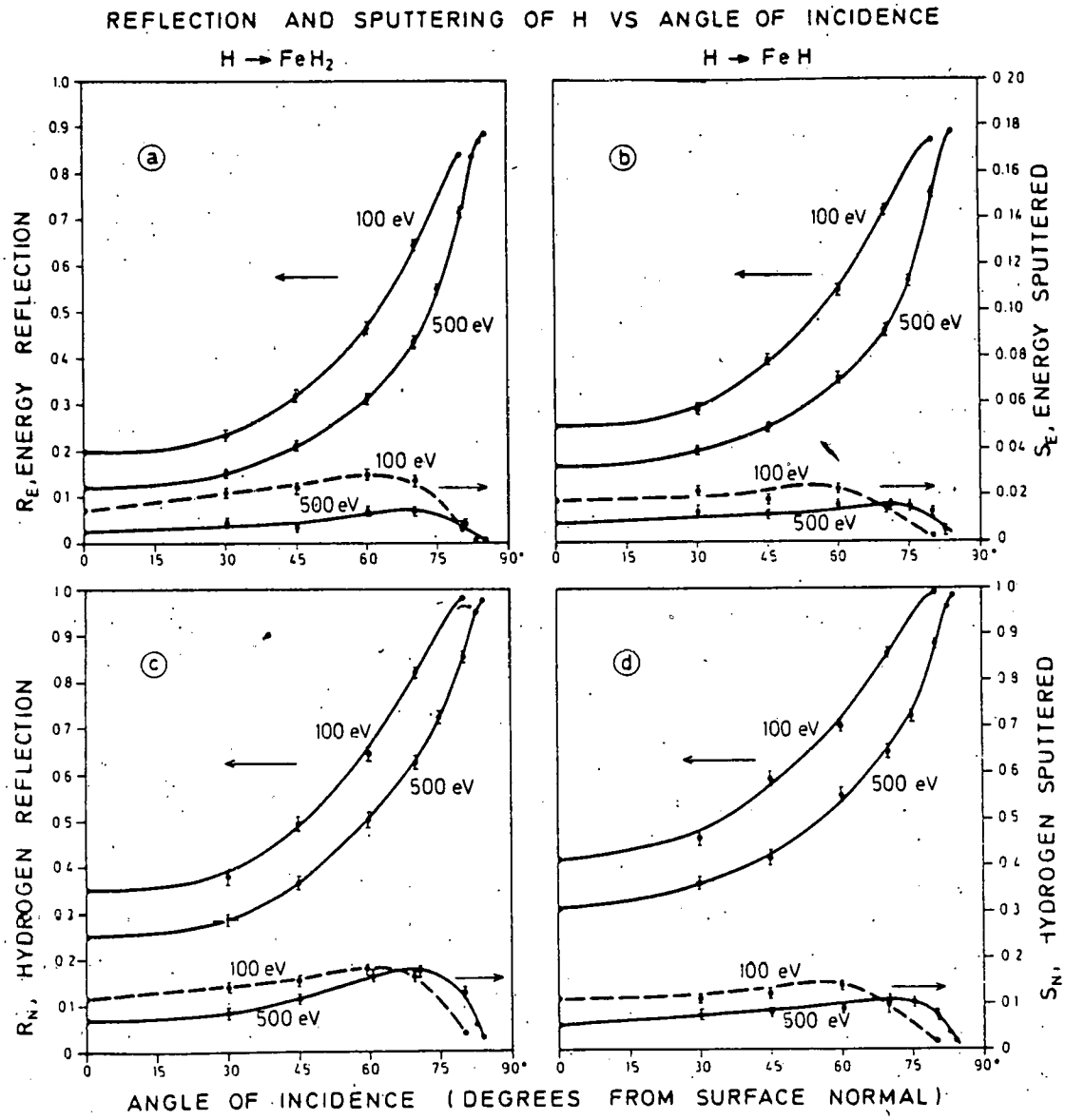

Fig. 3. Particle and energy reflection coefficients and sputtering yield (S_N) and the fraction of incident energy carried by sputtered particles (S_N) as functions of the angle (measured from surface normal) of the incident beam.

Haggmark and Wilson (TRIM)

[J. Nucl. Mater. 76 & 77, 149 (1978)]

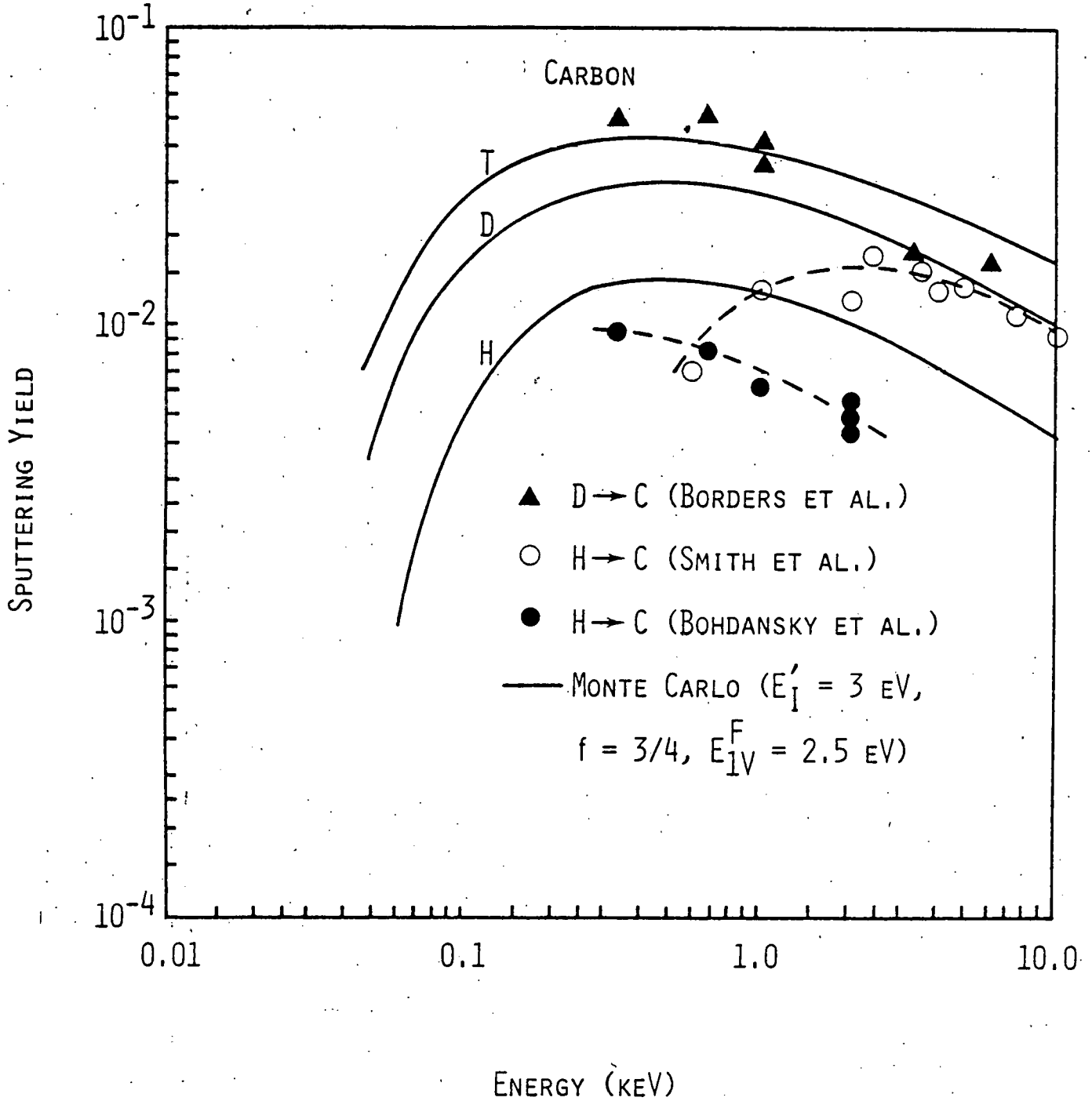

Haggmark and Wilson (TRIM)
[J. Nucl. Mater. 76 & 77, 149 (1978)]

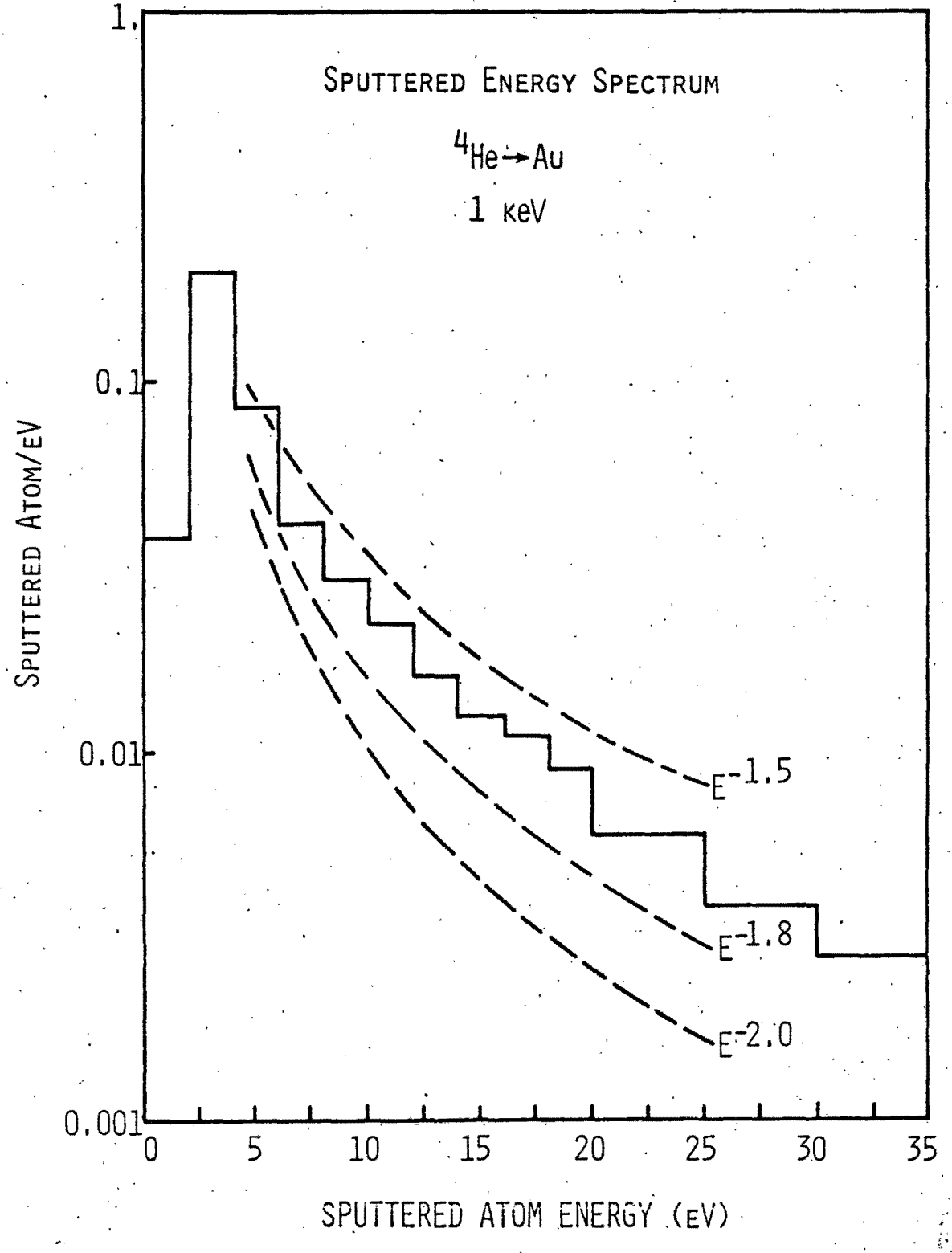

Haggmark and Wilson (TRIM)

[J. Nucl. Mater. 76 & 77, 149 (1978)]

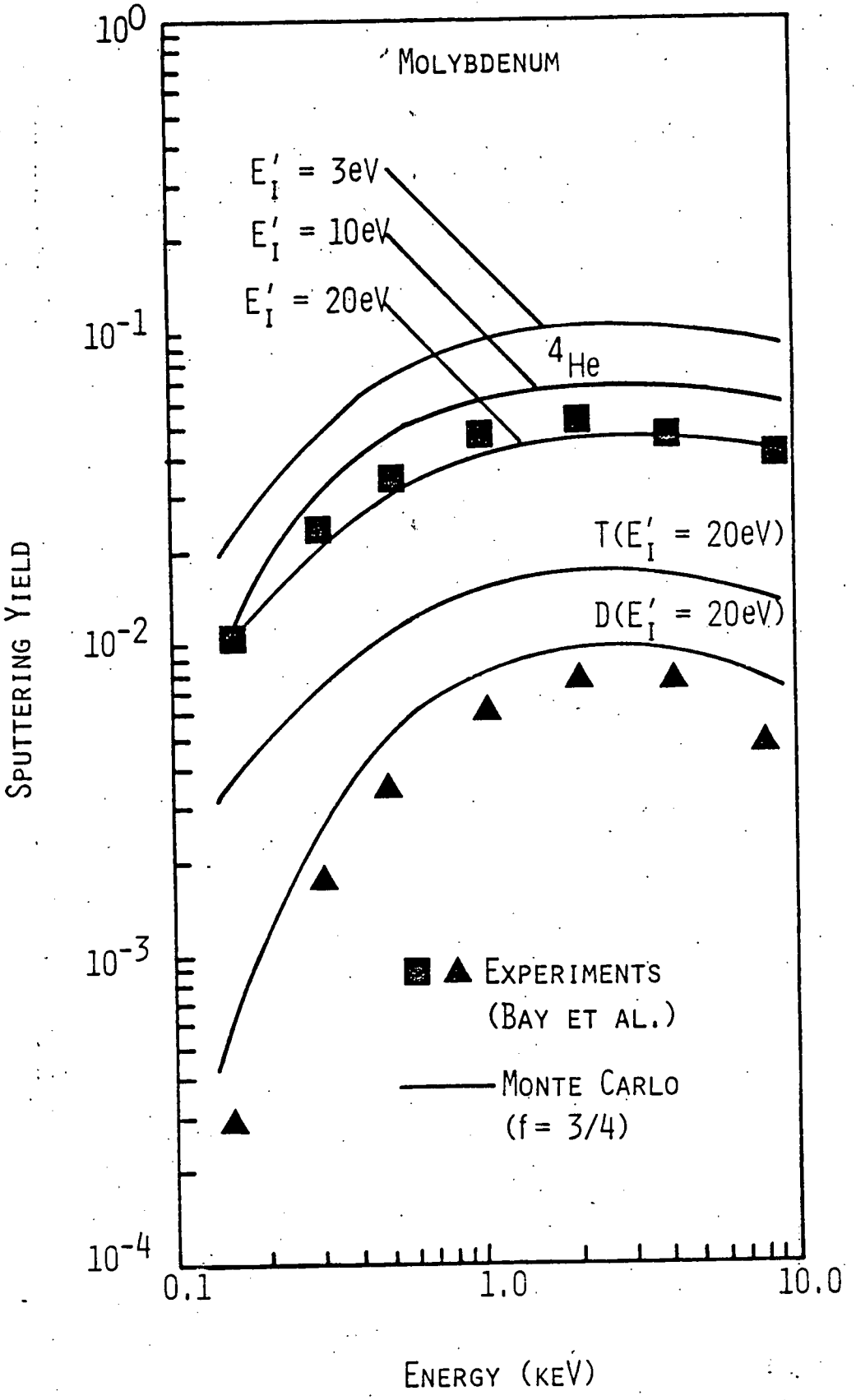

Haggmark and Wilson (TRIM)

[J. Nucl. Mater. 76 & 77, 149 (1978)]

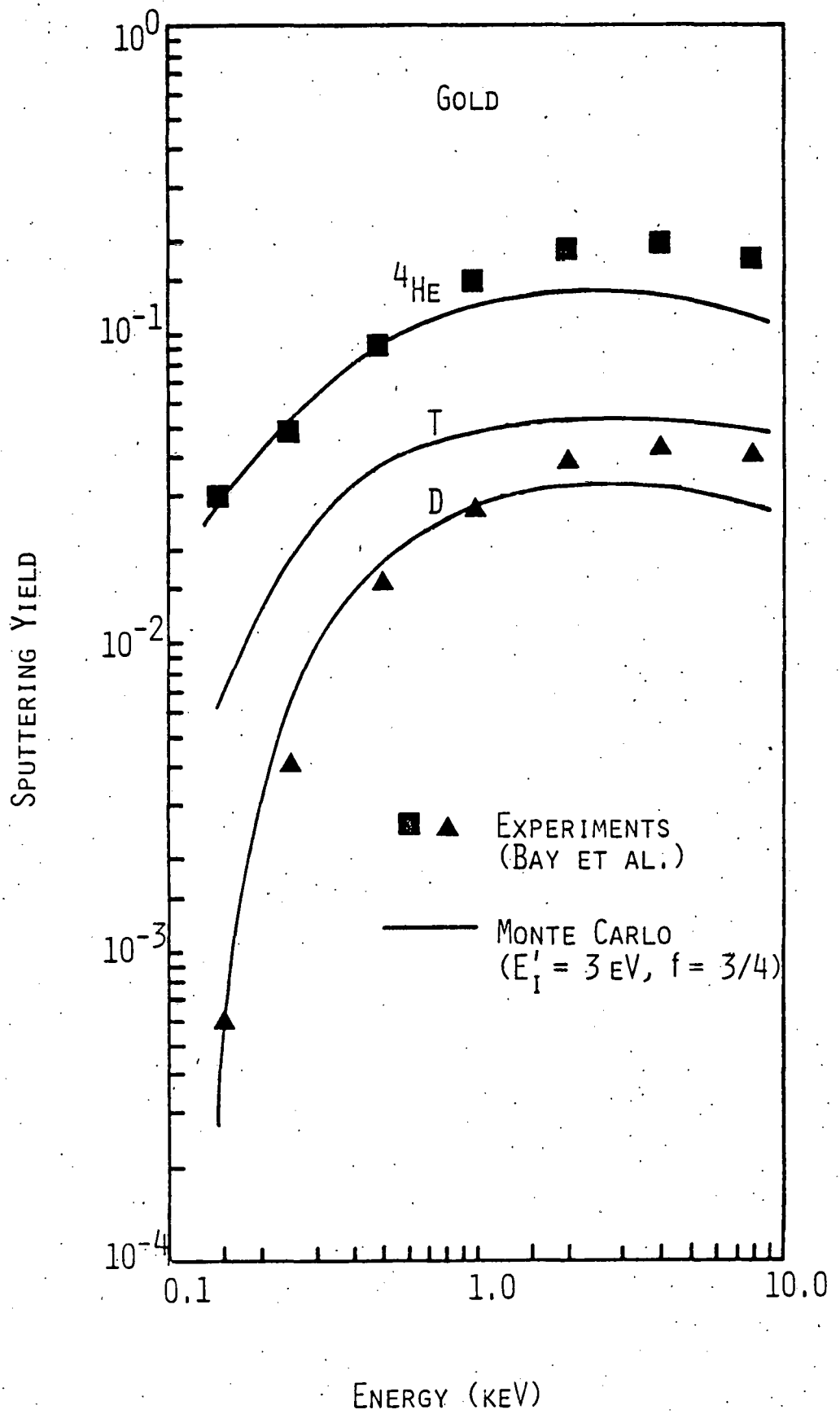

Haggmark and Wilson (TRIM)

[J. Nucl. Mater. 76 & 77, 149 (1978)]

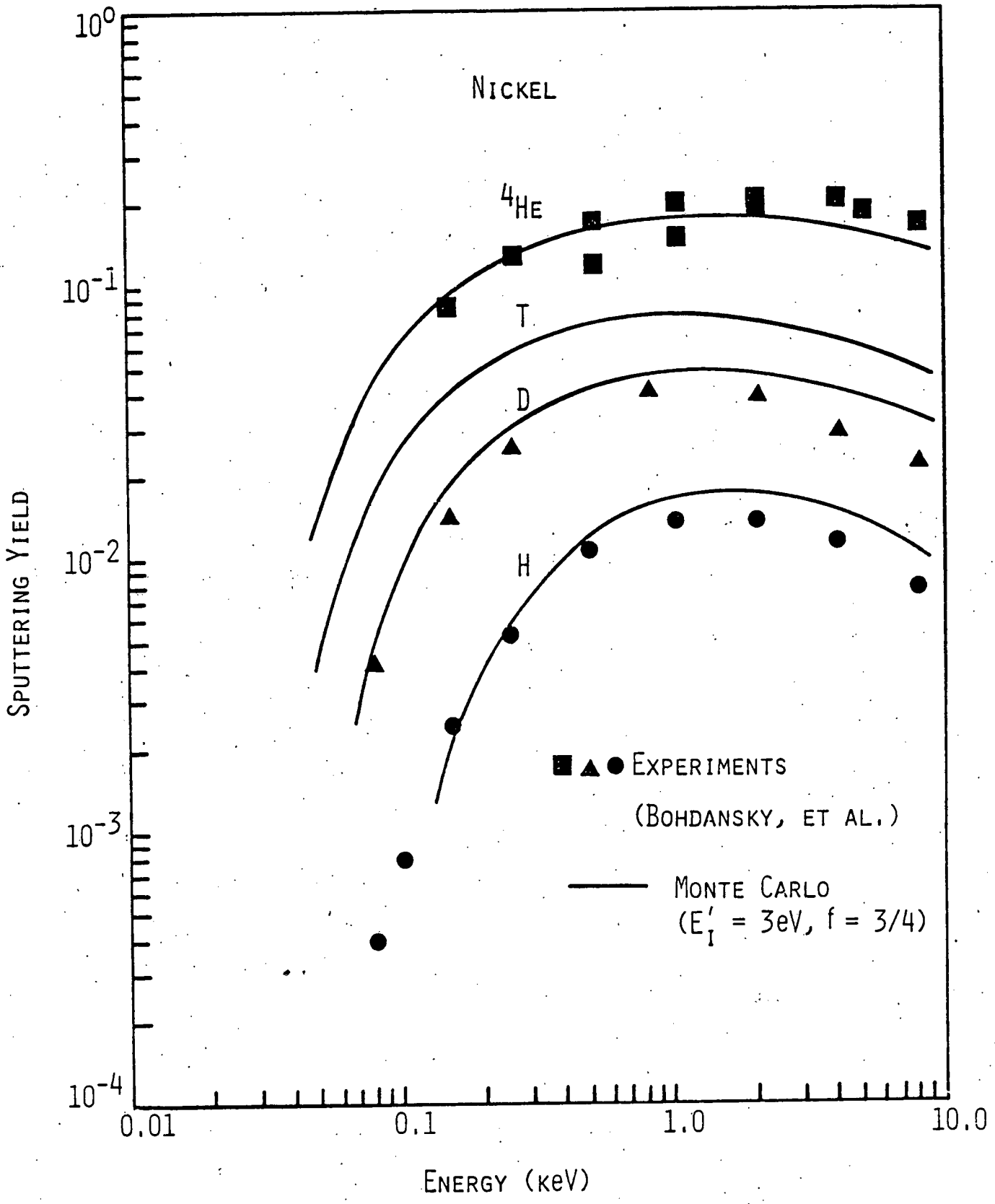

Haggmark and Wilson (TRIM)

[J. Nucl. Mat. 76 & 77, 149 (1978)]

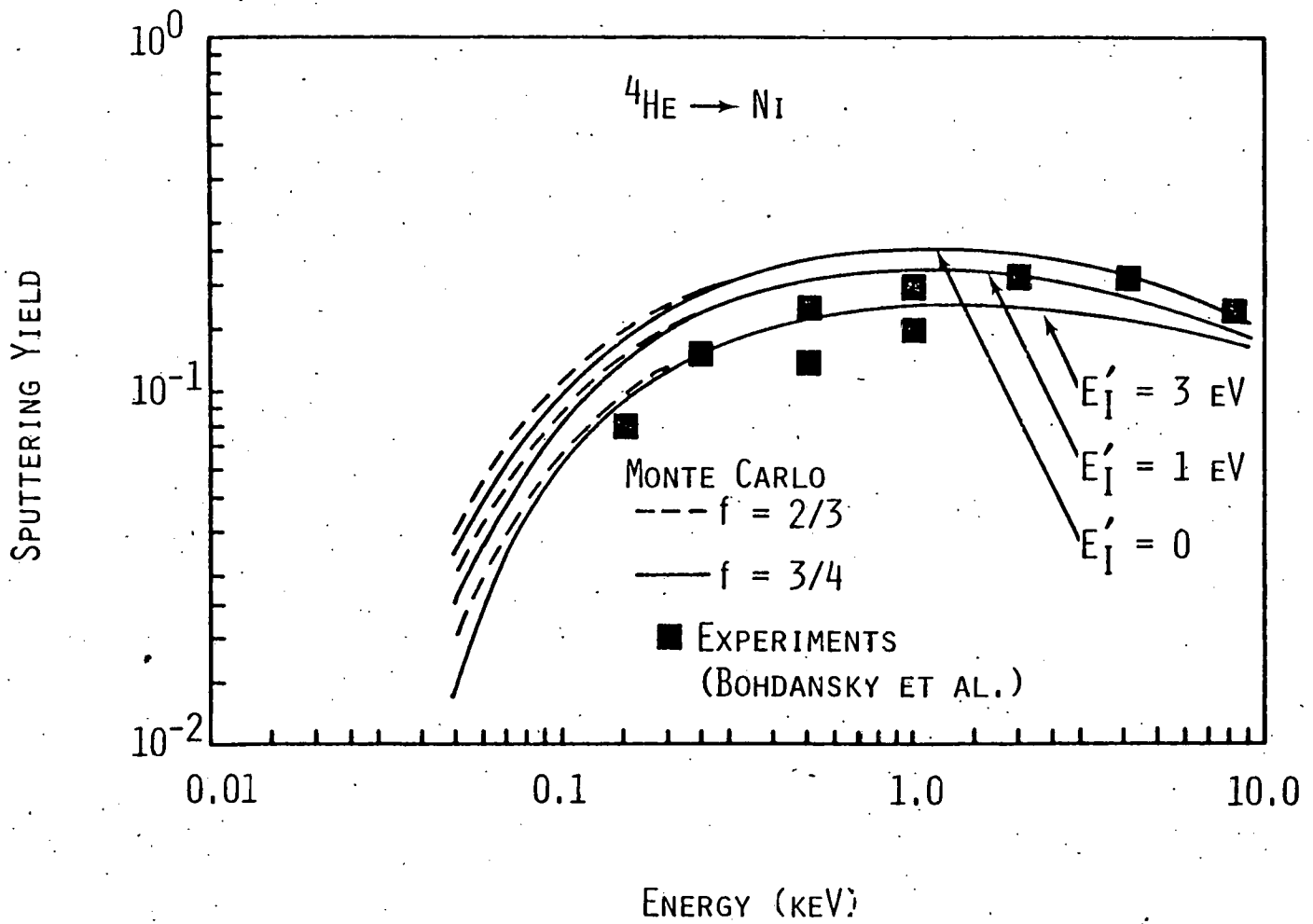

Hoffman, et al. (Discrete Ordinates Method)
[Nucl. Sci. Eng. 68, 204 (1978)]

SPUTTERING CALCULATIONS

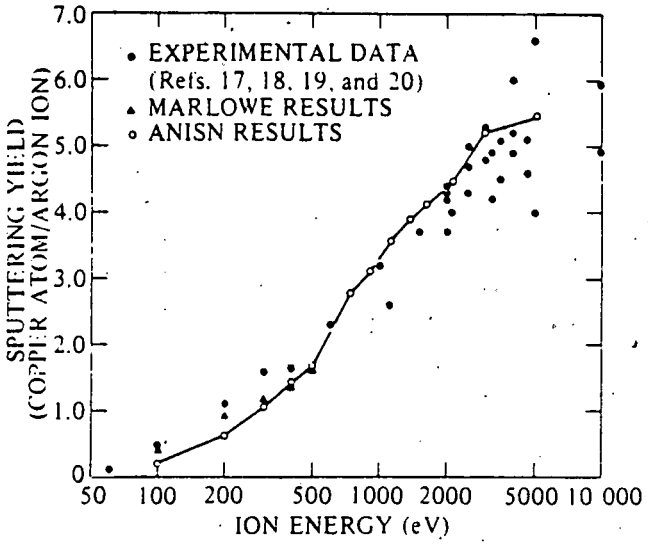

Fig. 3. Sputtering yield for argon incident on copper.

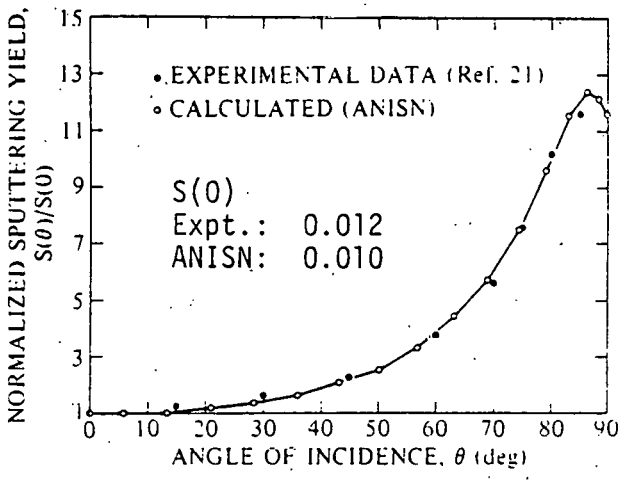

Fig. 5. Sputtering yield dependence on angle of incidence for 4-keV protons incident on nickel.

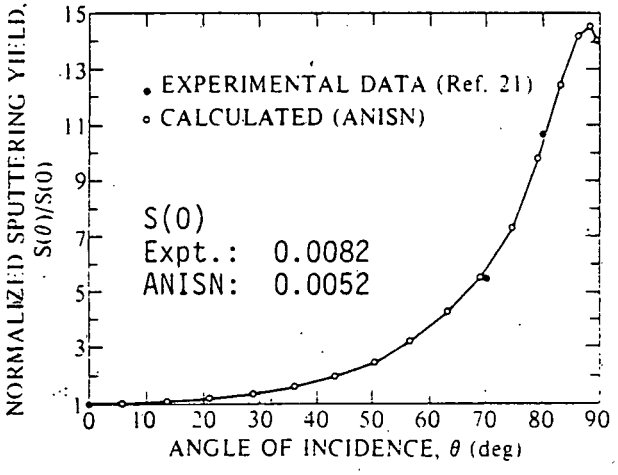

Fig. 4. Sputtering yield dependence on angle of incidence for 8-keV protons incident on nickel.

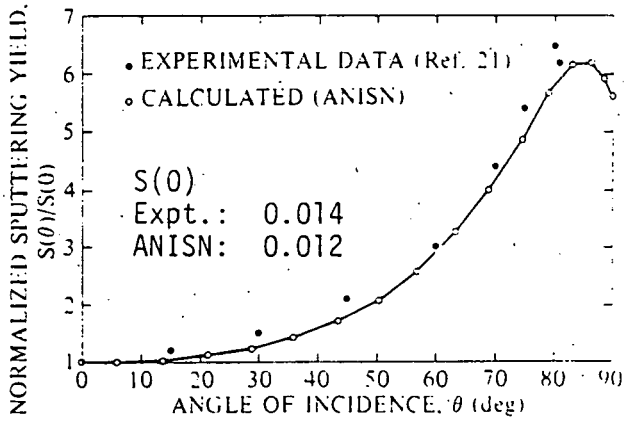

Fig. 6. Sputtering yield dependence of angle of incidence for 1-keV protons incident on nickel.

II. Analytical Expressions: Physical Sputtering

Dale L. Smith
Argonne National Laboratory, Argonne, Illinois

The need for analytical expressions to represent physical sputtering yields of fusion reactor first-wall materials arose primarily from the sensitivity of the plasma performance to minor concentrations of impurities and the lack of experimental data. Of particular significance is the number of parameters that must be considered. Important parameters include:

- incident ion (or neutral)
- ion energy
- angle of incidence
- wall (target) material
- morphology of wall surface

For the fusion reactor applications the conditions of primary interest are the light ions and relatively low energies ($\leq$ 1 keV). Until recently, these were the areas where experimental data were more sparse. Also, theories developed were less applicable for these same conditions.

Early estimates of sputtering yields for light ions were developed by Goldman and Simon[1] and Pease.[2] The analyses were based on high-energy ions where the primary collision between the incident ion and target atom can be treated as a Coulomb collision. For energies $E > E_B$ (where E_B is typically several keV for hydrogen isotopes incident on transition metals), these calculations give the correct order of magnitude for sputtering yields and approach a 1/E energy dependence at high energies.

Figure 1 shows a plot of the predicted sputtering yields for deuterium and helium on niobium compared with experimental data. Nearly all of the more recent analytical expressions for physical sputtering are based on the theory developed by Sigmund.[3,4] Using the Boltzmann transport equation, Sigmund obtained the following solution for the sputtering yield of amorphous solids.

$$S(E,\eta) = \Lambda \cdot F(x=0,E,\eta)$$

where Λ, which is a constant characteristic of the solid, is given approximately by

$$\Lambda = \frac{0.042}{U_o N}$$

where U_o is the surface binding energy and N is the atomic density of the target material. The F term is the deposited energy function that can be further defined by

$$F(x=0,E,\eta) \doteq \alpha \cdot N \cdot S_n(E)$$

where $S_n(E)$ is the nuclear stopping power, and α is a factor that contains the dependence of the sputtering yield on the angle of incidence of the ion, the mass ratio of the ion and target atom, and the interaction potential. The x=0 relates to the depth of energy deposition in the target, E is the ion energy and η is the angle of incidence. Various assumptions and approximations for the factors in F have been used by different investigators to obtain expressions for the sputtering yields.

Several energy dependent sputtering-yield curves for hydrogen ions incident on Fe (stainless steel) are shown in Fig. 2. Weissman and Sigmund[4] based their calculations on Lindhard's[5] model for the nuclear stopping power and calculated values of α. Although the Sigmund theory gives a reasonable approximation of sputtering yields for heavier ions, the predicted sputtering yields for light ions are grossly overestimated when compared with experimental data. Also, the general shape of the energy dependent curve for light-ion sputtering does not agree with experimental observation at low energies.

Sputtering yields predicted by Littmark[6] are based on slightly different deposited energy functions which give reduced sputtering yields at lower energies. The calculated values are still much higher than the experimental results.

Danyluk and Bratt[7] obtained similar results at the higher energies and empirically fit a low-energy curve with a direct energy dependence.

Guseva[8] used the Sigmund formalism to develop expressions for the sputtering yields of light ions. In order to obtain better agreement with experimental data, the α parameter was adjusted by correlation with existing sputtering data. Guseva's results give over a factor of six greater peak sputtering yields for molybdenum than for tungsten when bombarded by hydrogen.

Smith[9,10] has developed a model that gives the energy-dependent physical sputtering yields for various plasma particles incident on candidate first-wall materials. The expression for the physical sputtering yield, which is based on both theoretical and experimental considerations, is given in terms of the atomic and mass numbers of the incident and target atoms, the surface binding energy of the target material and the energy of the incident particle. The general shapes of the sputtering yield curves are based on theoretical models, whereas the magnitudes of the yields are derived primarily from experimental data. Characteristics of the original sputter-yield curves[9] include: (a) a direct energy

dependence at low incident particle energy, (b) a 1/E dependence at high incident particle energies, and (c) a peak at intermediate energies where the yield is relatively insensitive to energy. The recent modification[10] incorporates a threshold energy term into the expression to give an asymptotic approach to zero sputtering at the threshold rather than the abrupt cutoff originally presented. The modified sputtering yield is given by

$$S(E) = \frac{20}{U_o} Z_1^2 Z_2^2 \frac{M_1}{M_2} \frac{(E-E_{th})}{(E-E_{th} + 50\, Z_1 Z_2)^2}$$

where

$$E_{th} = \frac{(M_1 + M_2)^2}{4M_1M_2} U_o \quad \text{for } M_1 \leq M_2$$

$$E_{th} = \frac{M_2}{M_1} U_o \quad \text{for } M_1 > M_2$$

Predicted sputtering yields from this model are shown in Figs. 3-7 with available experimental data. Fairly good agreement with experiments has been obtained for several candidate wall materials.

Although this model was developed for metal wall materials, it has been extended to certain stable compounds. The agreement with recent data for SiC and B_4C given in Figs. 8 and 9 is suprisingly good, particularly with respect to the shape of the curve.

The angular dependence of the sputtering yield has received less attention. Winters[11] has presented a review of physical sputtering that summarizes the work on the effect of the incident angle on the sputtering yield. The cosine dependence gives a fairly good approximation of some of the data for angles up to 70 degrees from the normal. Calculations based on Sigmund's theory give a fairly good approximation to experimental data for argon ions to angles of 70 degrees. Data with which to compare calculated values for light ions are rather sparse. Further work on light ions and low angles of incidence (> 70 degrees from the normal are needed. Although effects of surface condition have received some attention by experimentalists, limited effort has been expended on theoretical considerations.

References

1. D. Goldman and A. Simon, Phys. Rev. 111, 383 (1958).

2. R. S. Pease, Rendiconti S.I.F. Corso 13, 158 (1960).

3. P. Sigmund, Phys. Rev. 184, 383 (1969).

4. R. Weissman and P. Sigmund, Rad. Effects 19, 7 (1973).

5. J. Lindhard, et al., Mat. Fys. Medd. Don. Vid. Selsk. 36, 10 (1968).

6. U. Littmark, et al., Nucl. Instr. Meth . 132, 661 (1976).

7. S. Danyluk and P. Bratt, Argonne National Laboratory, Argonne, Illinois, Report ANL/CTR-TM-60 (1976).

8. M. I. Guseva and Y. V. Martynenko, J. Nucl. Mater. 63, 241 (1976).

9. D. L. Smith, J. Nucl. Mater. 75, 20 (1978).

10. D. L. Smith (to be published).

11. H. F. Winters, in Radiation Effects on Solids, M. Kaminsky, ed., American Chemical Society, Washington, D.C. (1976).

12. J. Bohdansky et al., J. Nucl. Mat. 76 & 77, 163 (1978).

13. M. Kaminsky and S. K. Das, Proc. 10th Symp. on Fusion Technology, Padova, Italy, September 4-8, 1979.

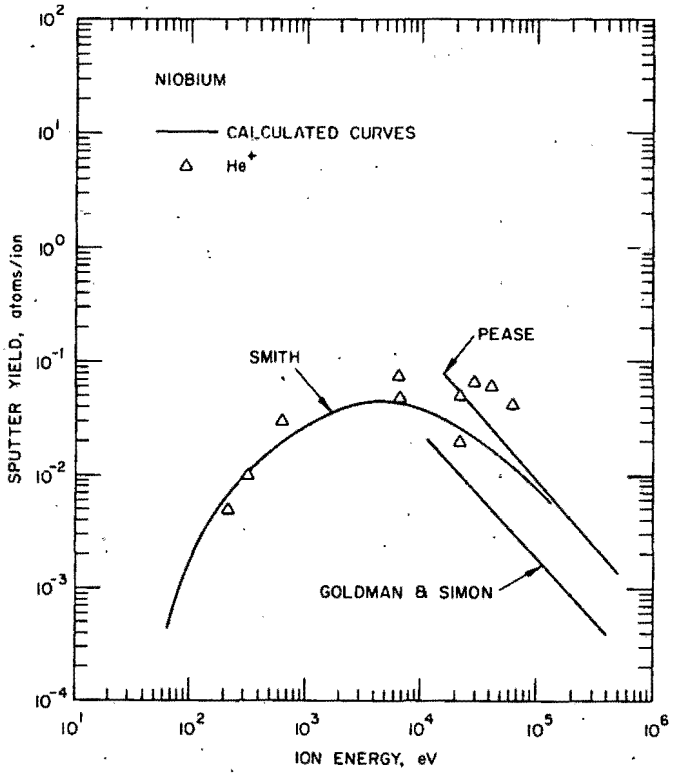

FIG. 1. Plot of calculated energy-dependent physical sputter yield curves for niobium (1,2,9,10) showing comparison with available experimental data. (See Refs. 14, 22-26 in Ref. 9).

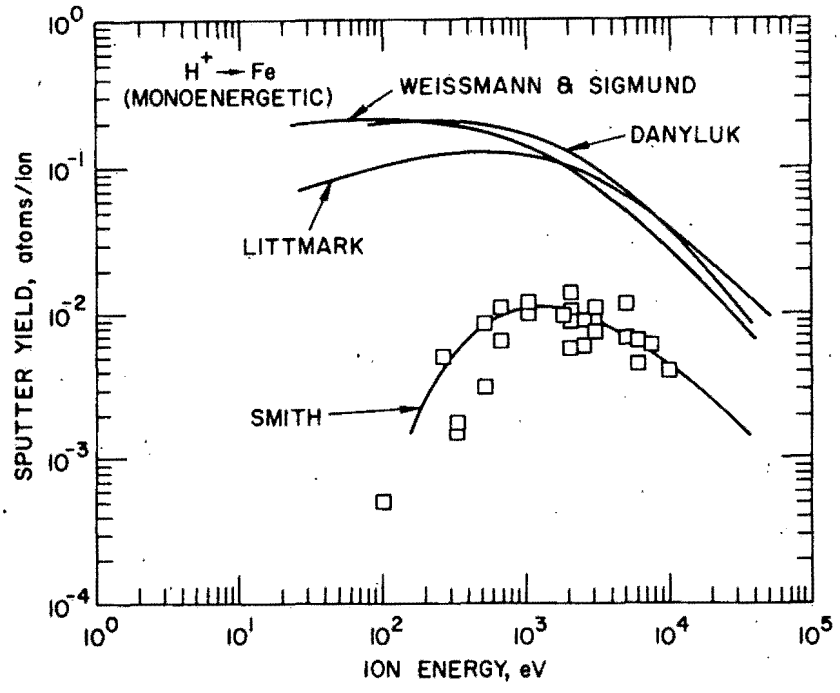

IG. 2. Plot of calculated energy-dependent physical sputter yield curves for iron (4,6,7,9,10) showing comparison with experimental data (see Refs. 14-21 in Ref. 9 and Ref. 12).

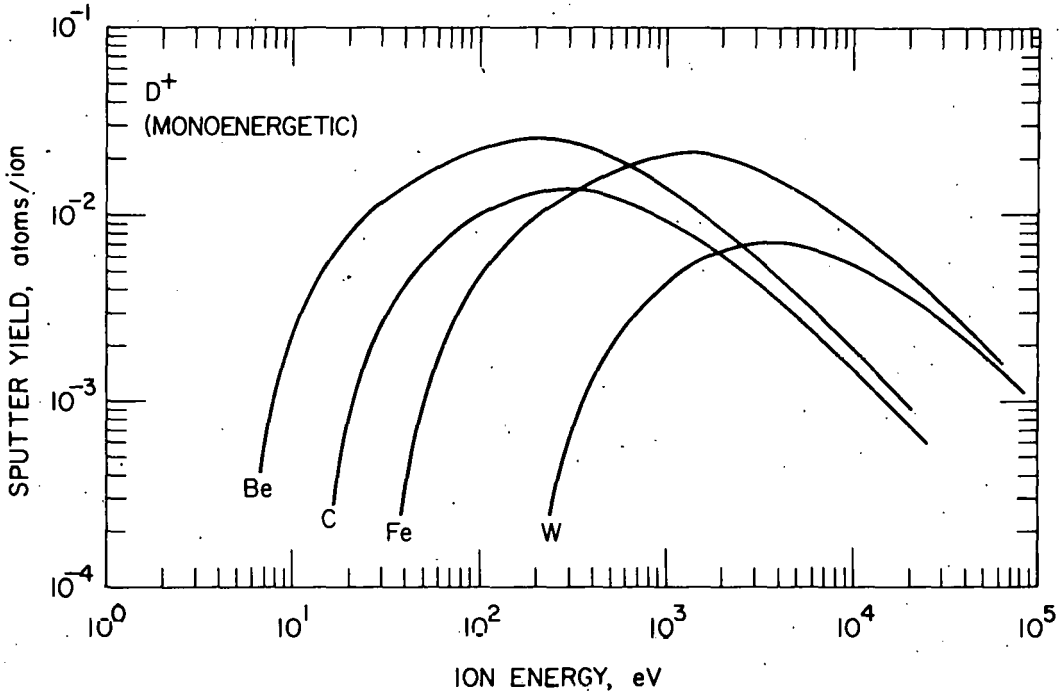

FIG. 3. Calculated energy-dependent physical sputtering yields for deuterium on candidate first-wall materials.

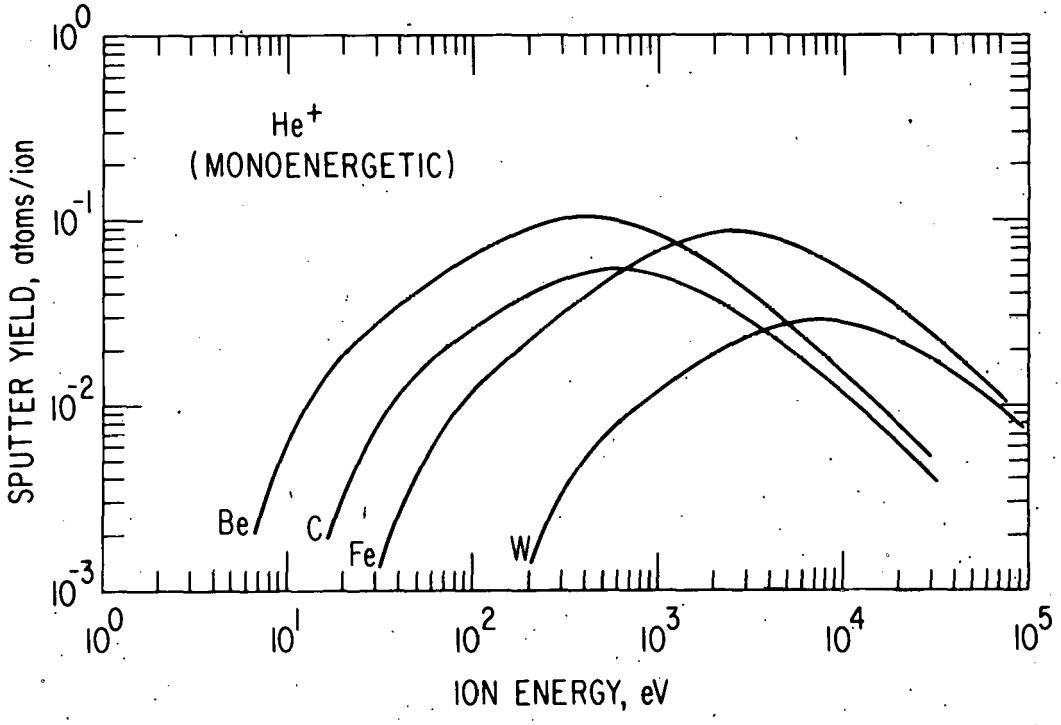

FIG. 4. Calculated energy-dependent physical sputtering yield for helium on candidate first wall materials.

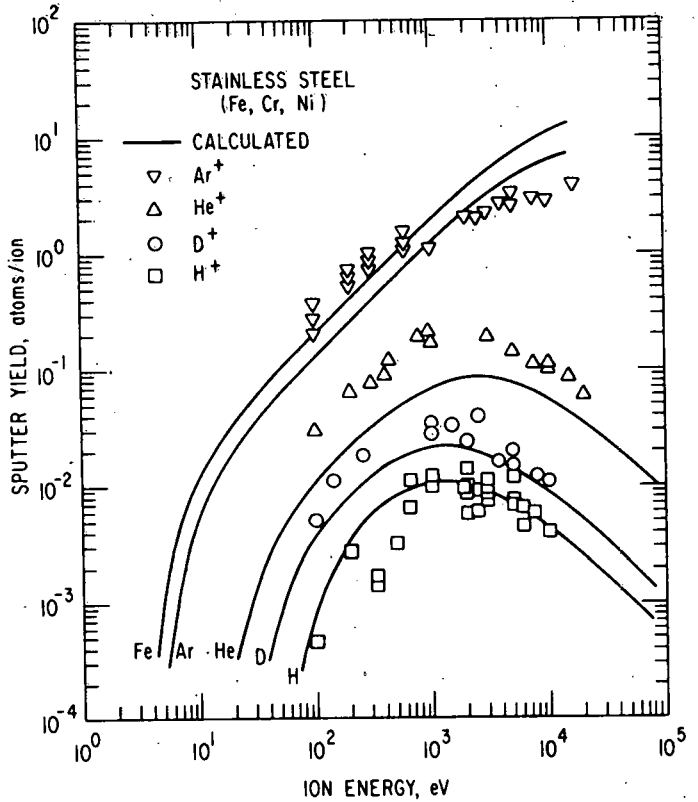

FIG. 5. Plot of calculated energy-dependent sputtering yield curves for iron (stainless steel) showing comparison with experimental data (Refs. 14-21 in Ref.9 plus recent data of Bohdansky, et al. in Ref. 12).

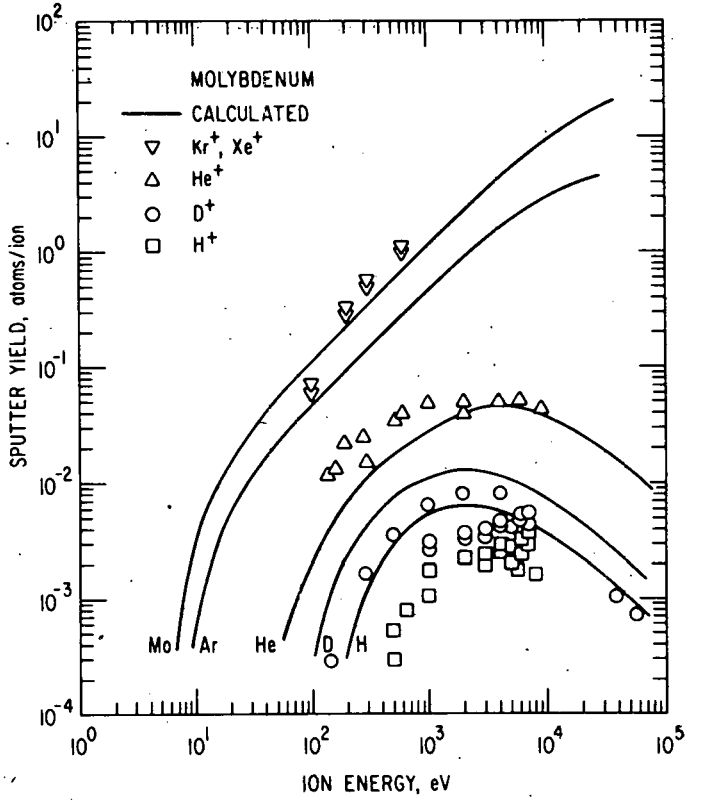

FIG. 6. Plot of calculated energy-dependent physical sputtering yield curves for molybdenum showing comparison with experimental data [Refs. 14, 26-28 in Ref. 9 plus recent data of Bohdansky (Ref. 12) and Kaminsky (Ref. 13)].

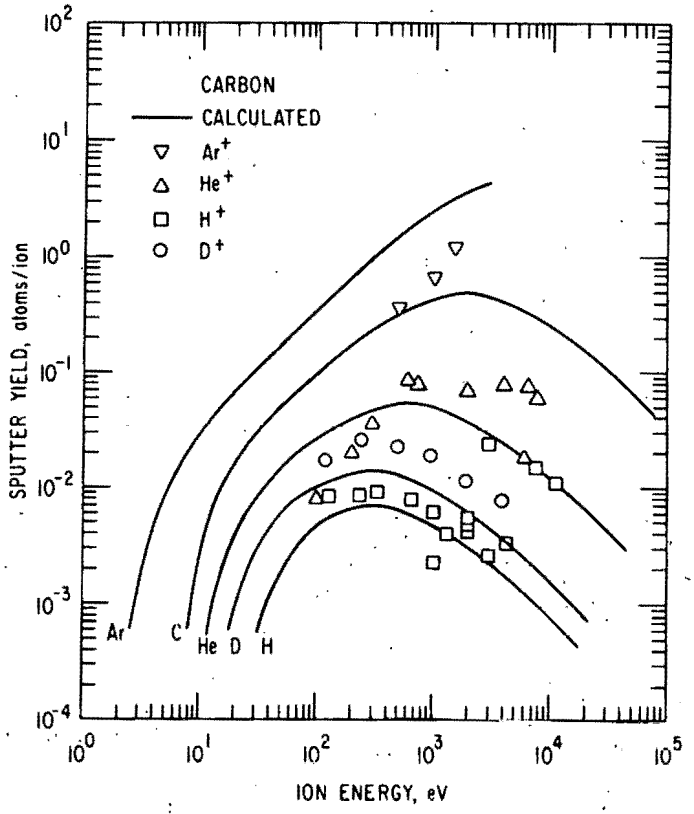

FIG. 7. Plot of calculated energy dependent physical sputtering yield curves for carbon showing comparison with experimental data (Refs. 14,16,21,26 in Ref. 9 plus recent data of Bohdansky, et al. in Ref. 12).

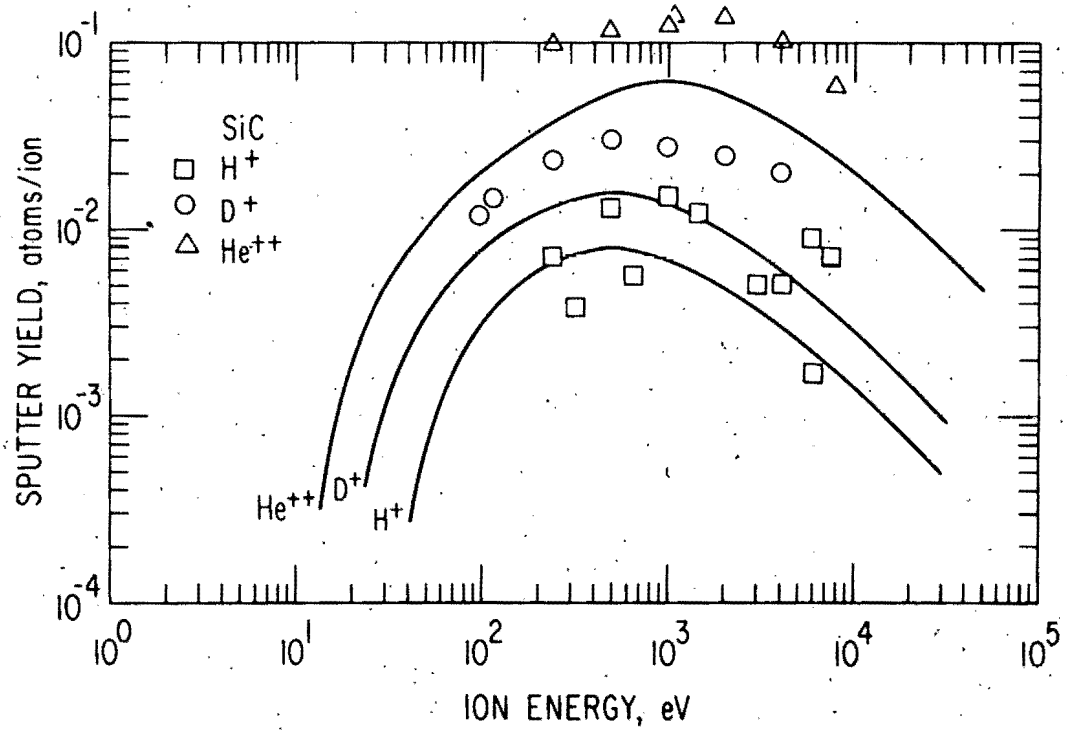

FIG. 8. Plot of calculated energy-dependent physical sputtering yield curves for SiC showing comparison with experimental data of Bohdansky.

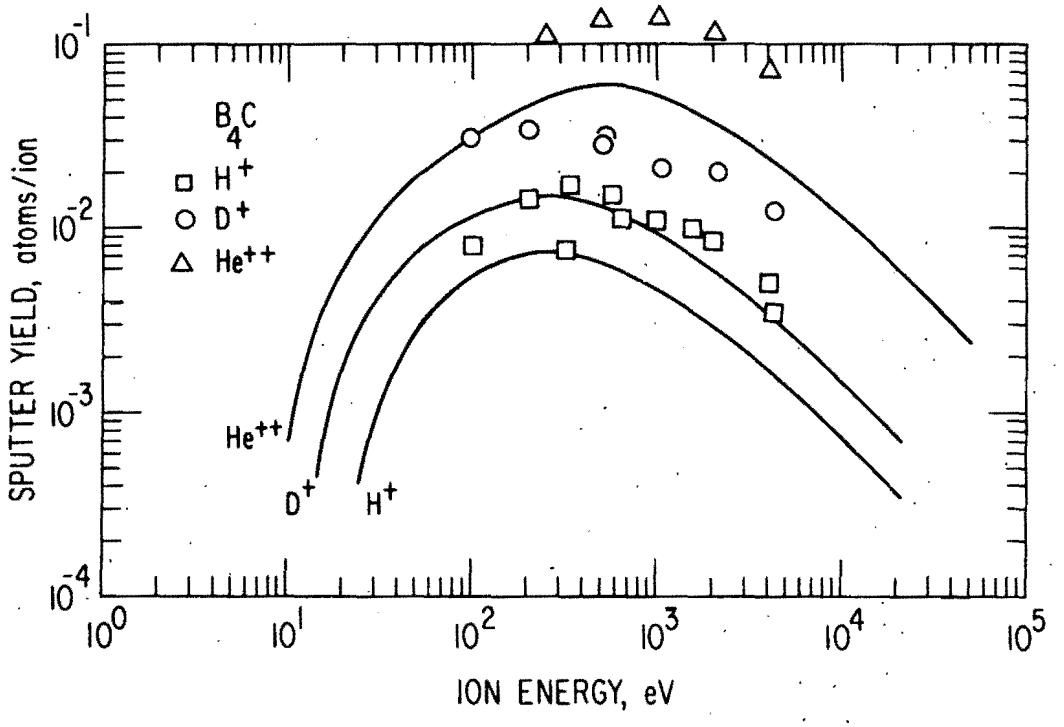

FIG. 9. Plot of calculated energy-dependent physical sputtering yield curves for B_4C showing comparison with experimental data of Bohdansky.

III. TRIM-Neutron-Sputtering Calculations

J.P. Biersack
Hahn-Meitner Institut, 1000 Berlin 39, Fed. Rep. of Germany
and
A. Riccato and W. Kaczerowski
Technische Universitat Berlin, 1000 Berlin 12, Fed. Rep. of Germany

High fluence experiments with 14.1 MeV neutrons are often simulated by 16.4 MeV proton experiments which are more readily accessible and require shorter irradiation times. Based on nearly equal nuclear cross sections, similar radiation effects were expected for protons and neutrons, but were never proved rigorously. A more detailed analysis is now carried out by using the TRIM-Monte Carlo code for following the trajectories and cascades of nuclear reaction products and recoils. Nuclear cross sections of Kammerdiener and Logan are used for the recoil production, and a Moliere potential is applied to the slowing down and cascading recoils. In niobium a "bulk binding energy" of 8 eV (Frenkel energy) and a "surface binding energy" of 2 eV is used in the TRIM program. The results are the following sputter yields: neutrons (forward direction) 14 x 10^{-6} atom/neutron, neutrons (backward direction) 0.2 to 0.3 x 10^{-6} atom/neutron. For protons (forward direction) 24 x 10^{-6} atom/proton, and for protons (backward direction) 10 x 10^{-6} atom/proton. About 10 x 10^{-6} atoms/proton can be attributed to the Coulomb interaction of protons, equally effective in forward and backward direction, since primary recoils receive a momentum nearly normal to the proton direction and, hence, the forward to backward ratio is increased from 2.4 for the proton case to 45 to 60 for the neutron case. The general conclusion is that nuclear reaction products and recoils from nuclear scattering events result in equal escape and sputter yields, but that the additional Coulomb scattering of protons affects the total sputtering yield and the forward to backward ratio considerably.

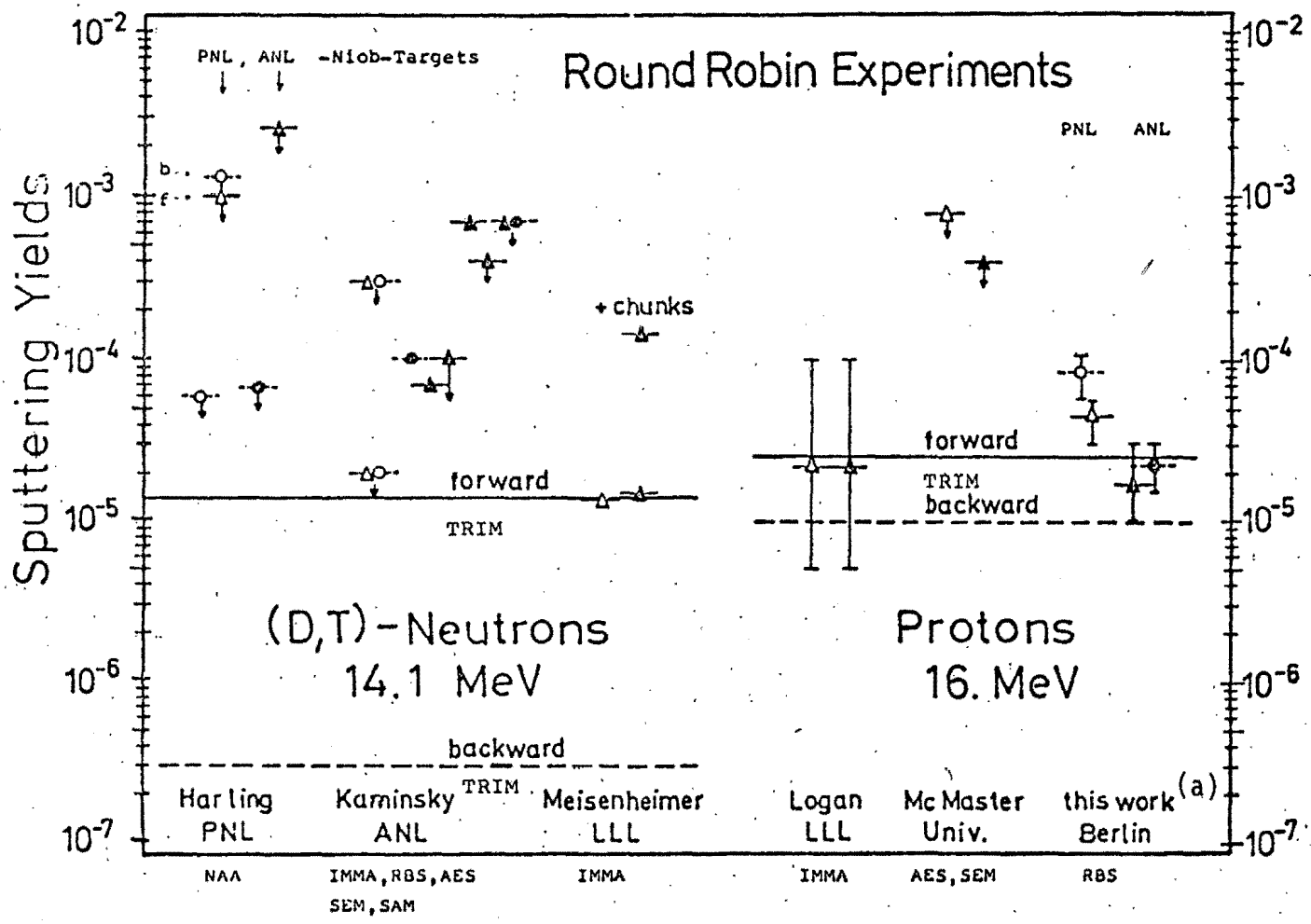

Fig. 1. Summary of measured sputter yields of RR targets [atomic sputtering only].
Full lines: theor. results forward (TRIM).
Dashed lines: theor. results backward (TRIM).
Circles: backward sputter yields measured.
Triangles: forward sputter yields measured.
Arrows pointing down: only upper limits could be determined.

(a) H. Uecker et al., to be published.

Fig. 2.

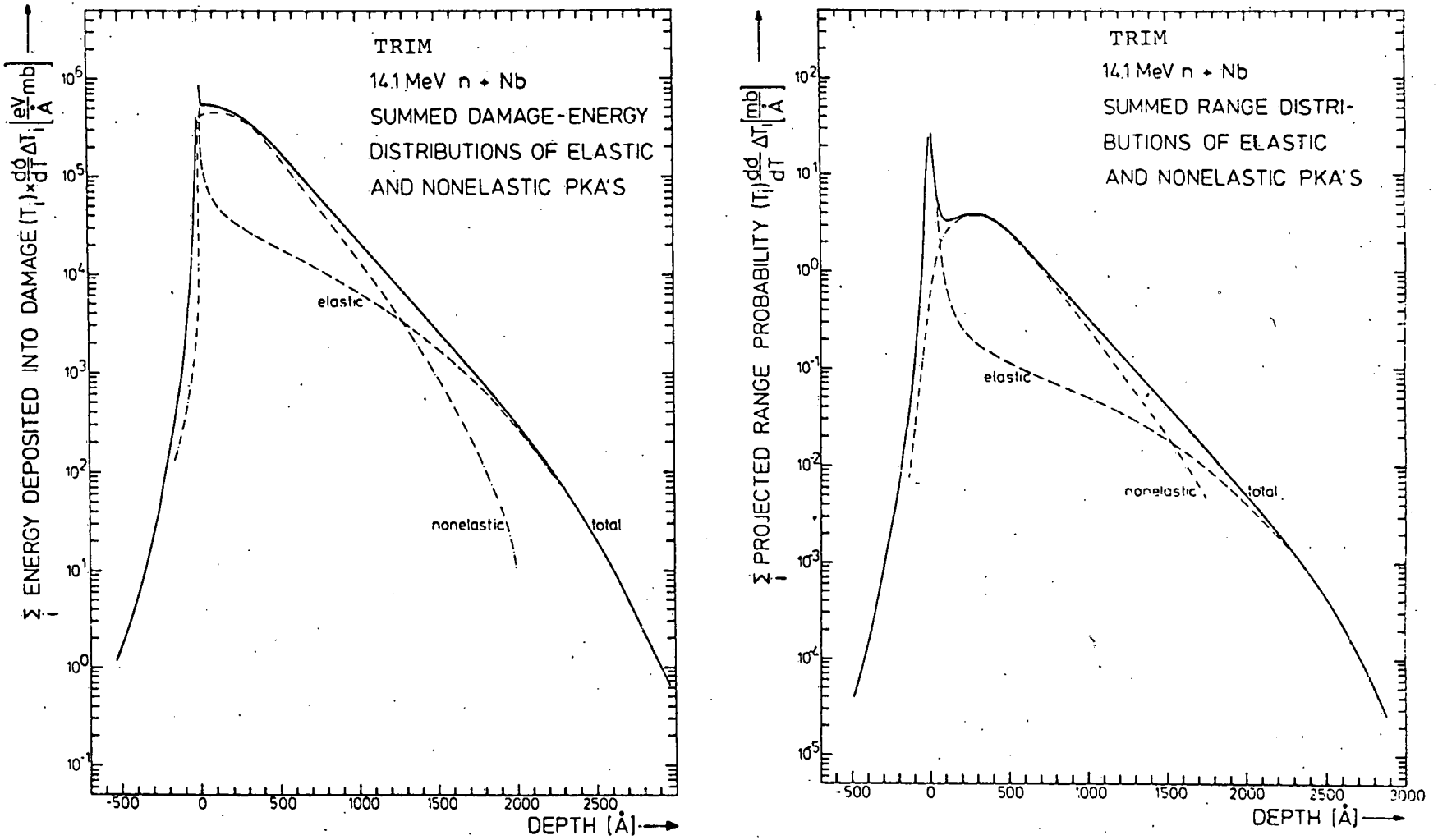

Fig. 2. Range and damage, elastic and non-elastic, 14.1 MeV neutron primary knock-on atoms (PKA's).

Fig. 3(a)

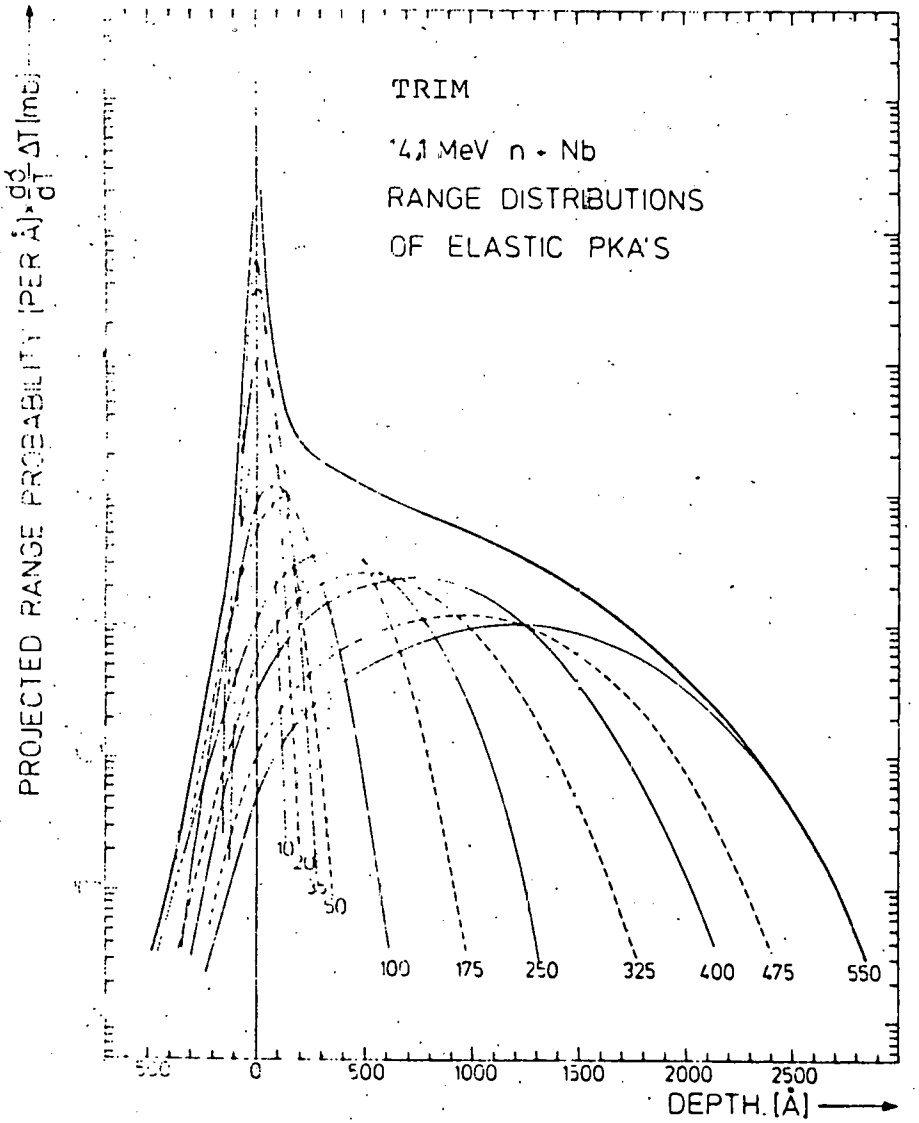

Fig. 3(b)

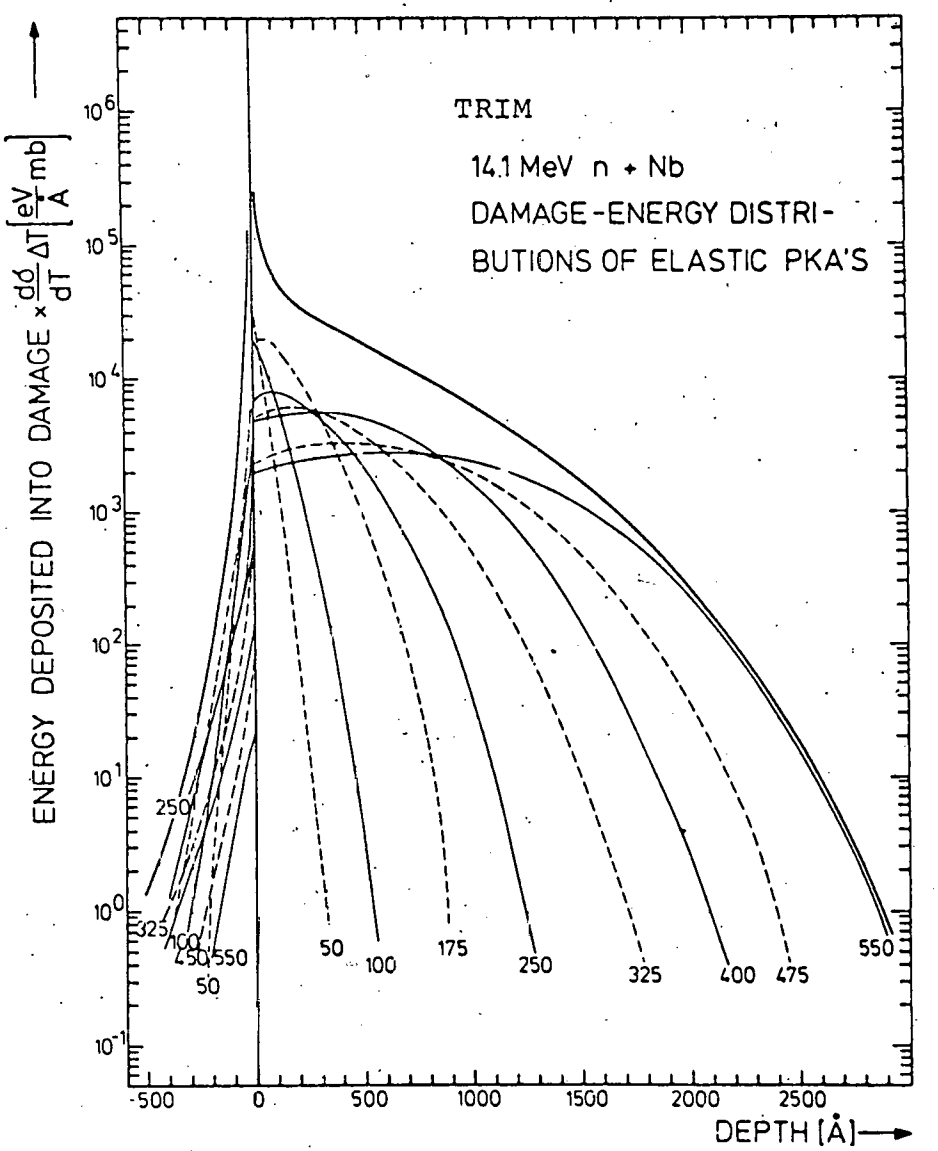

FIGURE 3: The parameter used in Fig. 3(a) and 3(b) indicates the primary recoil energy in units of keV. It should be noted that the starting angle of the primary recoil has been accounted for in the calculation.

Fig. 4.

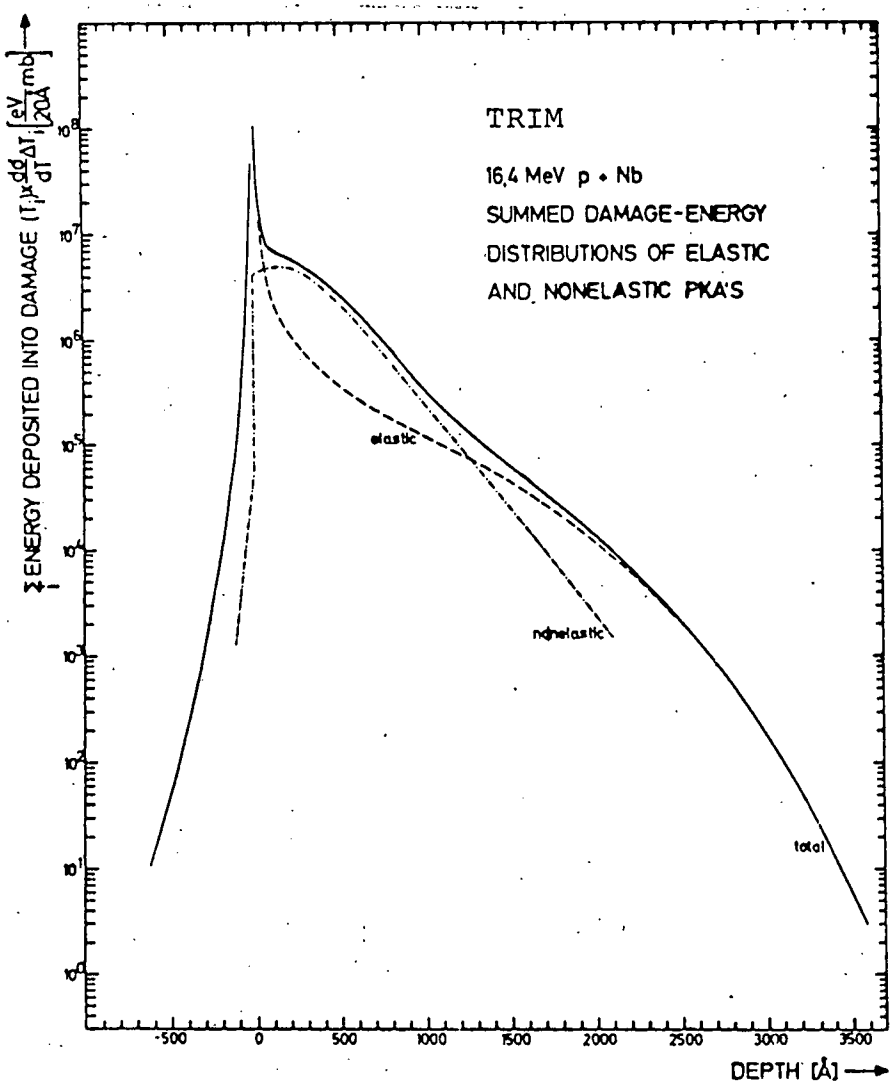
TRIM
16,4 MeV p + Nb
SUMMED DAMAGE-ENERGY
DISTRIBUTIONS OF ELASTIC
AND NONELASTIC PKA'S
elastic
nonelastic
total
DEPTH [Å]

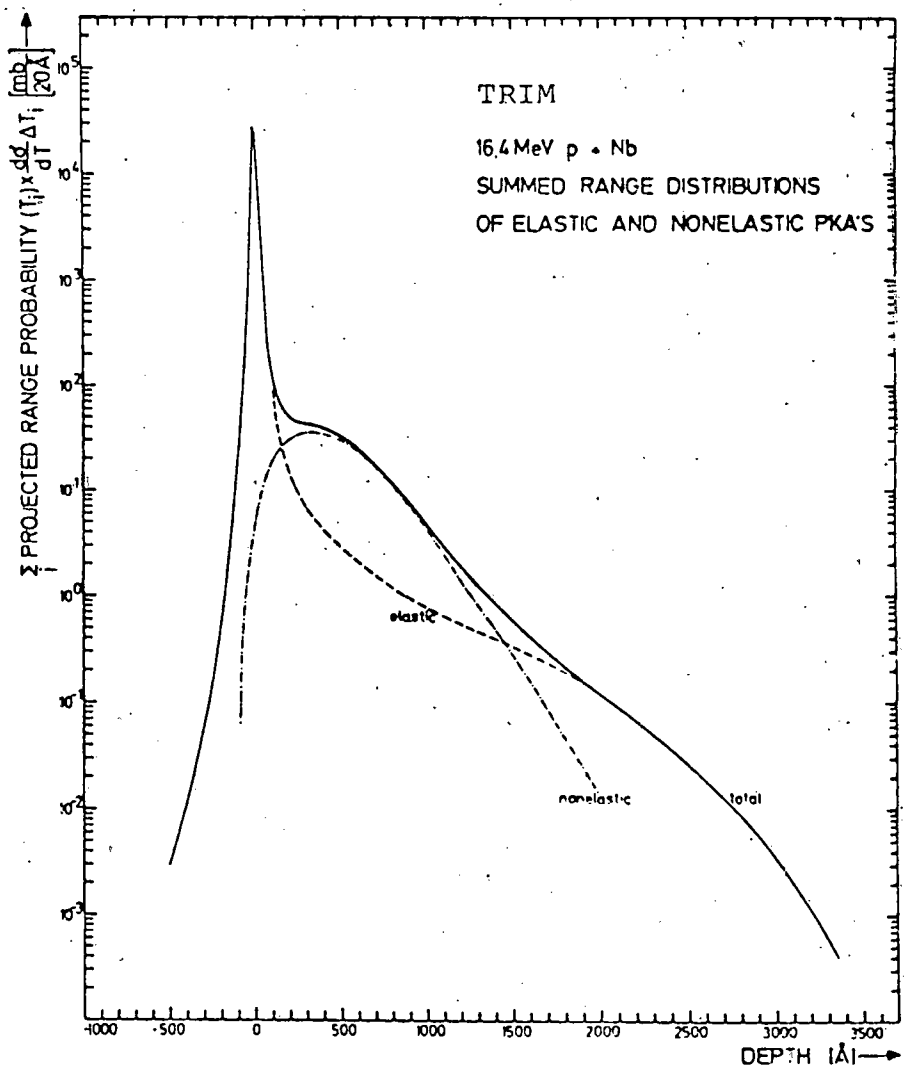
TRIM
16,4 MeV p + Nb
SUMMED RANGE DISTRIBUTIONS
OF ELASTIC AND NONELASTIC PKA'S
elastic
nonelastic
total
DEPTH [Å]

Fig. 5.(a)

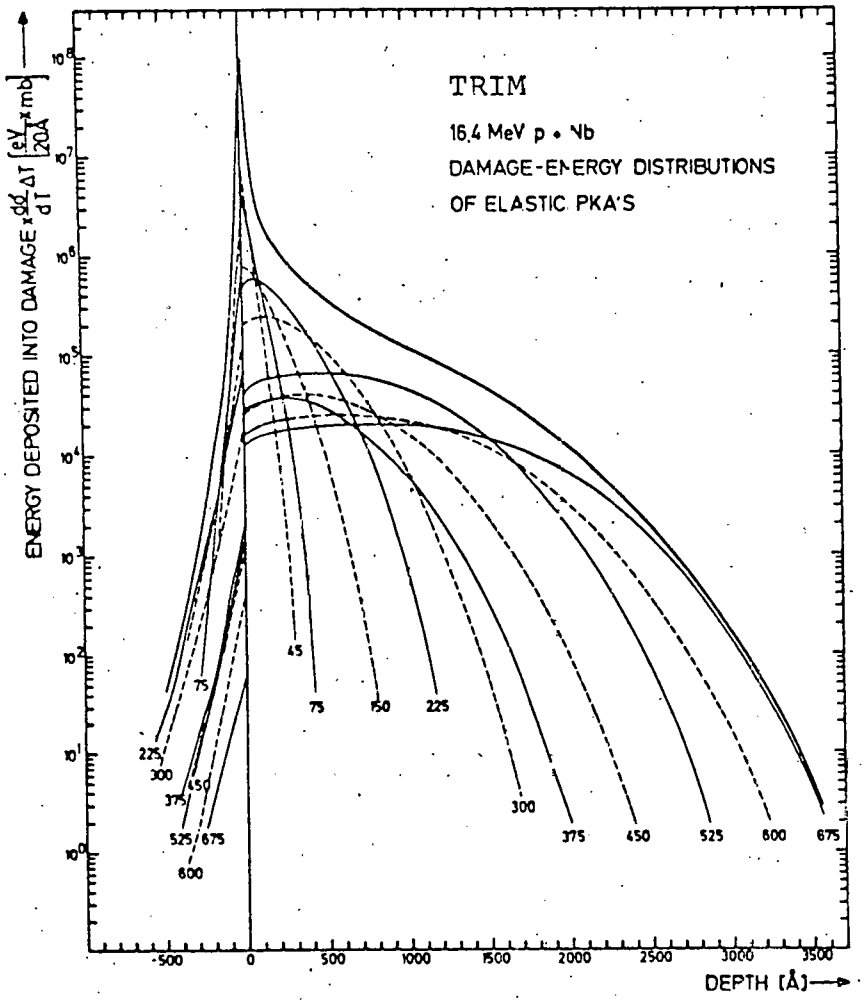

Fig. 5. (b)

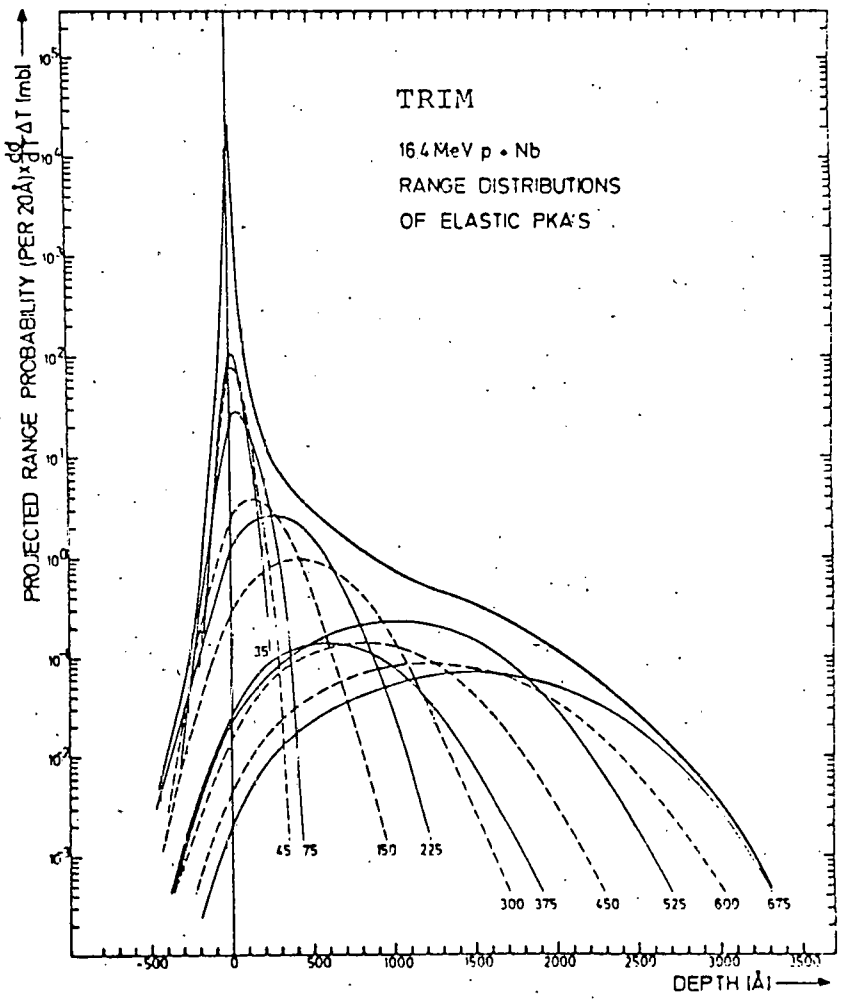

FIGURE 5. The parameter used in Fig. 5(a) and (b) indicates the primary recoil energy in units of keV.. It should be noted that the starting angle of the primary recoil has been accounted for in the calculation.

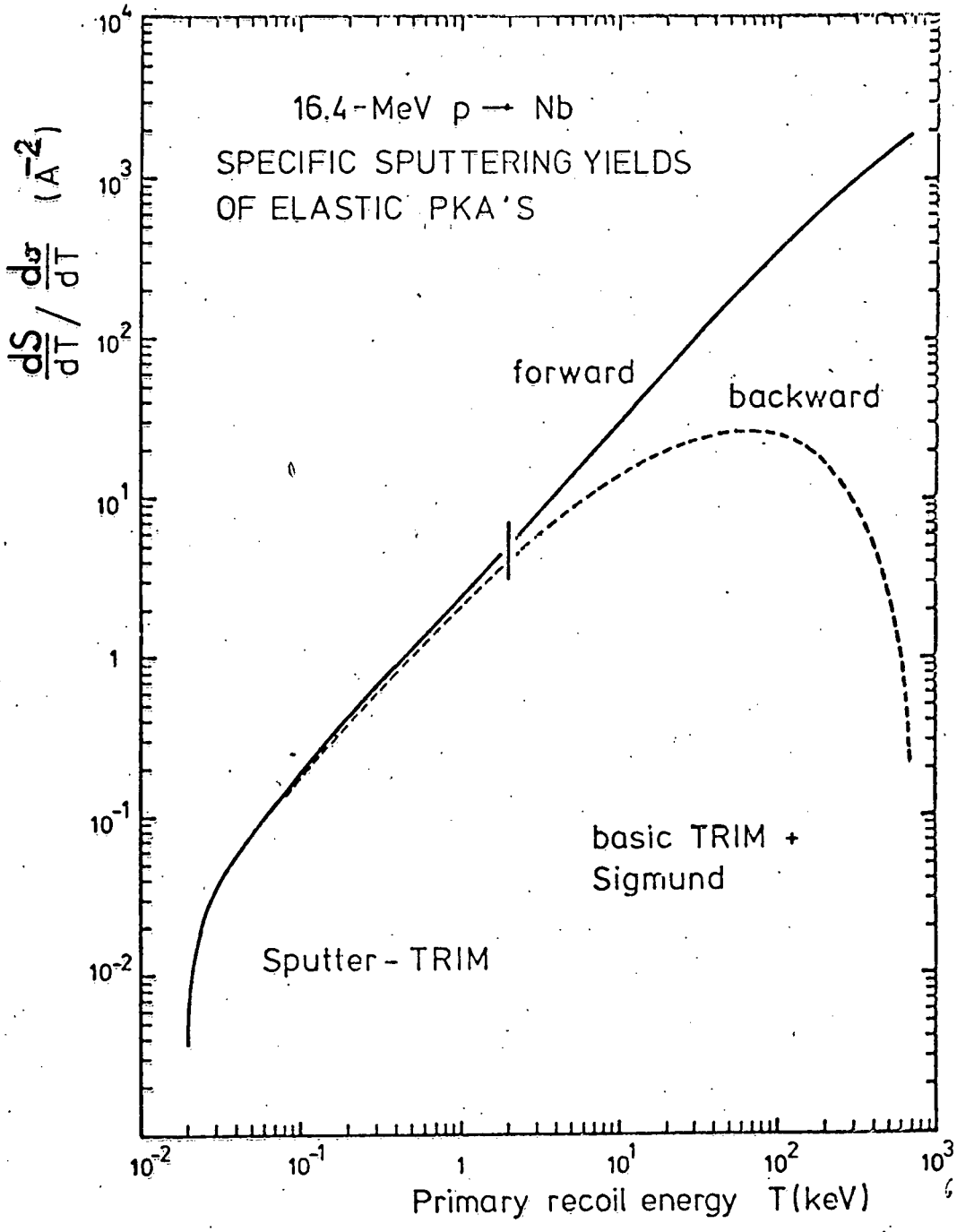

Fig. 6. Spec. sp. yields $\frac{dS}{dT} / \frac{d\sigma}{dT}$ for elastic PKA's (shown here for 16.4 MeV protons; 14.1 MeV neutrons are practically identical).